TOPICS IN MULTI-COMPONENT ULTRACOLD GASES AND GAUGE FIELDS

BY

TOMOKI OZAWA

DISSERTATION

Submitted in partial fulfillment of the requirements
for the degree of Doctor of Philosophy in Physics
in the Graduate College of the
University of Illinois at Urbana-Champaign, 2012

Urbana, Illinois

Doctoral Committee:

Professor Smitha Vishveshwara, Chair
Professor Gordon Baym, Director of Research
Professor Brian DeMarco
Professor Matthew Gilbert

Abstract

In this thesis, we present theoretical studies on three topics related to multi-component ultracold gases and gauge fields.

The first topic that we discuss is artificial gauge fields in ultracold gases. Recently, methods to create artificial gauge fields coupled to neutral ultracold systems using a light-induced Berry's connection have been rapidly developing. These methods are not only capable of creating Abelian gauge fields, such as a conventional magnetic field, but also non-Abelian gauge fields, which opens a way to explore and simulate a wide variety of physical models. In this thesis, we discuss various properties of bosons with Rashba-Dresselhaus spin-orbit coupling, which is a special type of non-Abelian gauge field. We investigate the stability of Bose-Einstein condensates with Rashba-Dresselhaus spin-orbit coupling, and show that the condensates are stable against quantum and thermal fluctuations. We also consider the renormalization of the bare interaction by calculating the t-matrix and its consequence on the ground state phase diagrams.

The second topic discussed here is three-component ultracold fermionic systems. It is known that ferromagnetism and superfluidity can coexist at low enough temperature in three-component ultracold fermions. In this thesis, we elucidate how fermionic pairing and population imbalance enhance each other. We also describe a crossover from Bardeen-Cooper-Schrieffer state of fermionic pairing state to the limit of Bose-Einstein condensate of three weakly interacting species of molecules, as the interaction increases. Furthermore, we find an interesting similarity in the free energies between three-component ultracold fermions and quantum chromodynamics.

The last topic discussed here is Niels Bohr's double-slit interference *gedankenexperiment* with charged particles, which argues that the consistency of elementary quantum mechanics requires that the electromagnetic field must be quantized. In the experiment a particle's path through the slits is determined by measuring the Coulomb field that it produces at large distances. Under these conditions the interference pattern must be suppressed; otherwise quantum mechanics is not consistent. The mechanism for the suppression of the interference pattern is that, as the particle's

trajectory is bent in diffraction by the slits, it must radiate and the radiation must carry away phase information. Thus, the radiation field must be a quantized dynamical degree of freedom. We also consider the related setup in which one attempts to determine the path of a massive particle through an interferometer by measuring the Newtonian gravitational potential the particle produces. In this case, we show that the interference pattern would have to be finer than the Planck length and thus indiscernible. Therefore, unlike for the electromagnetic field, Bohr's argument does not imply that the gravitational field must be quantized.

Acknowledgements

First and foremost, I would like to express my deepest gratitude to my advisor, Gordon Baym, for his guidance, encouragement, and patience. I was so lucky to learn directly from him how to perform physics research, and to see how a mentor should interact with a student.

I must thank Tetsuo Hatsuda, who generously allowed me to stay at the University of Tokyo every winter for the past three years. Some important parts of my research were done in the intellectually stimulating atmosphere of the Theoretical Hadron Physics Group of the University of Tokyo. I also benefited a lot from Kenji Maeda through his extremely critical way of thinking toward physics.

I am grateful to Smitha Vishveshwara for listening to me and helping me in applying for jobs during her extremely busy days. I am deeply indebted to her.

My research could not have been possible without a friendly atmosphere here in the University of Illinois at Urbana-Champaign. Since my days with full of homework in Loomis 390 hallway, I have benefited a lot from various academic discussion with my friends and colleagues. I am especially grateful to Wade DeGottardi, Sarang Gopalakrishnan, Benjamin Hsu, Mingwu Lu, David McKay, Jeremy McMinis, Stephanie Law Toner, and Jitong Yu. I thank John Nichol and Seungmin Hong for being patient roommates for a year, and John for helping me discover the joy of playing guitar. I am also grateful to Juan Jottar for kindly sharing his BibTeX style file with me, which saved me a lot of time from preparing the bibliography in this thesis.

It was a pleasure to share an office, 341 Loomis, with Soheil Baharian and Philip Powell, who often discussed with me not only physics and science but also religion, politics, and other important subjects in the world. I am also extremely thankful to Philip for carefully going through this manuscript.

I would like to thank all the participants of ECT* Doctoral Training Programme 2009, "The physics of strongly correlated systems: from quark matter to ultra cold atoms," which took place in Trento, Italy. They made my three months stay in Italy just impossible to forget.

I am indebted to my friends from the University of Tokyo, whom I studied physics and math together. They have always inspired and encouraged me.

I am grateful to National Science Foundation, which supported me through Grants No. PHY05-00914, PHY07-01611, and PHY09-69790. I also wish to acknowledge the Department of Physics at the University of Illinois for giving me various teaching assistantships. Through teaching, I might have learned as much as I have taught.

Last but not least, I would like to express my sincere gratitude to my parents and family for their love, support, and understanding throughout my study. My special thanks go to Tokiha, who made my last years in doctoral study much more delightful, for her constant support and encouragement.

Table of Contents

List of Figures

Chapter 1

Introduction

We discuss three topics in this thesis. The first topic is artificial gauge fields in ultracold gases, especially ultracold bosons with Rashba-Dresselhaus spin-orbit coupling. The second topic is the Bardeen-Cooper-Shrieffer (BCS) to Bose-Einstein condensate (BEC) crossover of three-component ultracold fermions. The last topic is a double-slit interference problem, which discusses why electromagnetic field must be quantized.

In the following sections, we give brief introductory accounts on the three topics covered in this thesis. Parts of this thesis are based on the author's publications [1, 2, 3, 4, 5].

1.1 Gauge fields and ultracold gases

Ultracold gases are versatile playgrounds to realize, explore, and discover various physical models and phenomena. Indeed, one major reason that ultracold gases are currently attracting so much attention is that it is possible to simulate various physical models using ultracold gases, which are otherwise difficult to solve or realize.

One crucial ingredient which is not present in neutral ultracold gases in their natural forms, but important in many areas in physics, is the coupling with electromagnetic fields, or more generally, gauge fields. A free non-relativistic particle with charge q coupled to a magnetic field $\mathbf{B}$ is described by the Hamiltonian

$$\mathcal{H} = \frac{1}{2m}\left(\mathbf{p} - \frac{q}{c}\mathbf{A}\right)^2, \tag{1.1}$$

where c is the speed of light and the vector potential $\mathbf{A}$ satisfies $\mathbf{B} = \nabla \times \mathbf{A}$. Many of the interesting phenomena in conventional condensed matter physics, such as superconductivity and quantum Hall effects, are the consequence of electrons coupling to electromagnetic fields. On the other hand, since

$q = 0$ for neutral ultracold atoms, these atoms do not naturally couple to electromagnetic fields as in (1.1). Thus, if we wish to simulate the coupling of electrons, or other charged particles, to electromagnetic fields using ultracold gases, we need a method for creating artificial gauge potentials to "trick" neutral particles into behaving as if they are charged particles in electromagnetic fields. There are two major schemes for achieving artificial gauge fields in neutral ultracold gases; the first is to rotate the gas, and the second is to use position-dependent atom-light interaction to create Berry's connection. Our main focus in this thesis is on the latter scheme, but let us first briefly discuss the former method of rotation.

If an ultracold atomic system in a harmonic trap is rotating with an angular velocity $\mathbf{\Omega}$, the Hamiltonian in the rotating frame is

$$\mathcal{H} - \mathbf{\Omega} \cdot \mathbf{L}, \tag{1.2}$$

where $\mathcal{H}$ is the Hamiltonian in the non-rotating frame and $\mathbf{L}$ is the angular momentum operator [6]. The single-particle Hamiltonian in the rotating frame is then

$$\begin{aligned} \mathcal{H} - \mathbf{\Omega} \cdot \mathbf{L} &= \frac{p^2}{2m} + \frac{1}{2} m\omega^2 r^2 - \mathbf{\Omega} \cdot (\mathbf{r} \times \mathbf{p}) \\ &= \frac{1}{2m} \left(\mathbf{p} - m\mathbf{\Omega} \times \mathbf{r}\right)^2 - \frac{1}{2} m(\mathbf{\Omega} \times \mathbf{r})^2 + \frac{1}{2} m\omega^2 r^2, \end{aligned} \tag{1.3}$$

where ω is the trap frequency. If the axis of rotation is in the z direction, such that $\mathbf{\Omega} = (0, 0, \Omega)$, the Hamiltonian in the rotating frame becomes

$$\mathcal{H} - \mathbf{\Omega} \cdot \mathbf{L} = \frac{1}{2m} \left(\mathbf{p} - m\Omega(-y, x, 0)\right)^2 + \frac{1}{2} m(\omega^2 - \Omega^2)(x^2 + y^2) + \frac{1}{2} m\omega^2 z^2. \tag{1.4}$$

This Hamiltonian formally has the form of a particle in a trap coupled to a vector potential

$$\frac{q}{c}\mathbf{A} = m\Omega(-y, x, 0). \tag{1.5}$$

The magnetic field produced by this vector potential is

$$\nabla \times \mathbf{A} = \left(0, 0, \frac{2mc}{q}\Omega\right) = \frac{2mc}{q}\mathbf{\Omega}. \tag{1.6}$$

Thus, the Hamiltonian in the rotating frame takes the same form as that of a charged particle coupled to an external magnetic field, whose magnitude and direction are proportional to the angular velocity of rotation. In other words, ultracold gases under rotation "think" as if they are

charged particles coupled to a magnetic field, even though the particles are neutral. Experiments have shown that the rotation creates quantized vortices in BECs [7, 8]. For fast enough rotation, these vortices form a triangular lattice, as in Fig. 1.1. This formation of a triangular lattice, which was known as an Abrikosov lattice, is originally predicted for magnetic flux lines in type-II superconductors where condensed Cooper pairs are coupled to an external magnetic field.

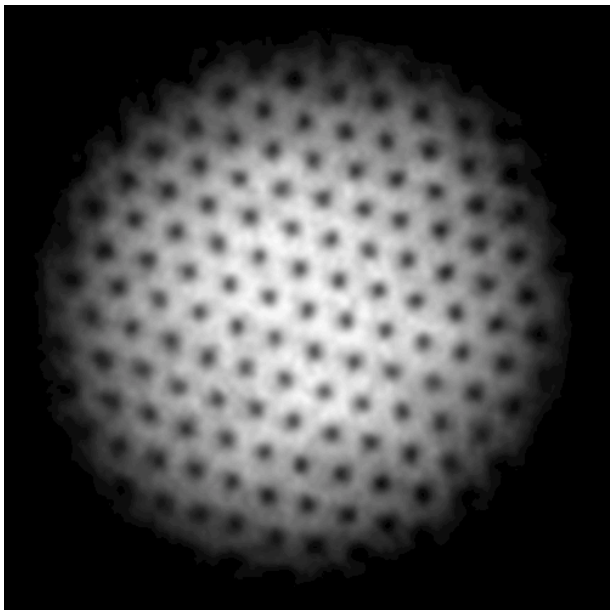

Figure 1.1: Quantized vortices created in a rotating BEC of sodium. © Martin Zwierlein.

Studies in rotating ultracold systems have been successful, both theoretically and experimentally, yielding various novel phenomena such as a prediction of the emergence of highly correlated quantum-Hall like states [9, 10]. However, there are also drawbacks to this method. It is experimentally difficult to achieve very rapid rotation as it requires a fine tuning of the ratio Ω/ω close to 1. Also, the artificial magnetic field produced through rotation is necessarily constant. The second means of creating artificial gauge fields, using a laser-assisted Berry's connection has the prospect of circumventing these shortcomings. Moreover, laser-assisted Berry's connections are capable of simulating more than a simple external magnetic field, and can also model non-Abelian gauge fields in the following way. The Hamiltonian of n-component ultracold gases in the spinor basis is an $n \times n$ matrix. Therefore, generally speaking, each component of the gauge field $\mathbf{A} = (A_x, A_y, A_z)$

is an $n \times n$ matrix, which couples to the momentum as:

$$\frac{1}{2m}\left(\mathbf{p}I_{n\times n} - \mathbf{A}\right)^2, \tag{1.7}$$

where $I_{n\times n}$ is the $n \times n$ identity matrix. (We include the coefficients of $\mathbf{A}$, such as q/c in the case of Abelian vector potential, into $\mathbf{A}$.) When some components of $\mathbf{A}$ do not commute (e.g. $[A_x, A_y] \neq 0$), the gauge field $\mathbf{A}$ is called non-Abelian. (On the other hand, if all the components of $\mathbf{A}$ commute with each other, the gauge field is Abelian. For instance, the conventional magnetic field is produced by 1×1 Abelian gauge fields.) As we will discuss in detail, Berry's connection can also create non-Abelian gauge fields, which significantly broadens the range of physical models which ultracold gases can explore. In this thesis, special attention is given to the Rashba-Dresselahsu spin-orbit coupling, which is a special type of non-Abelian gauge fields of the form $\mathbf{A} \propto (\sigma_x, \sigma_y, 0)$, where σ_x and σ_y are the Pauli matrices. When a particle is coupled to the Rashba-Dresselhaus spin-orbit coupling, the single-particle ground state is doubly (or more) degenerate, which leads to a non-trivial BEC structure. In addition, the renormalization of the interaction needs a careful treatment because of the modified single-particle spectrum, as we will discuss.

1.2 Multi-component ultracold fermions

Another topic of interest in this thesis is three-component ultracold fermionic systems. Here, we briefly review the physics of two-component ultracold fermions to familiarize ourselves with concepts that are common in multi-component ultracold fermions.

Two-component ultracold fermions can be, to a large extent, understood from an analogy with spinfull electrons in metals. Electrons in a metal with a weak attractive interaction are known to exhibit superconductivity at low temperature. If the attractive interaction is independent of angle, the superconductivity is described by BCS theory [11, 12]. In the BCS theory, particles with opposite spins and momenta pair, and the pairs condense into the same state. In other words, a BEC of paired fermions is the origin of BCS superconductivity [1]. The same mechanism applies for two-component ultracold fermions, where the two components are regarded as two pseudospins. In

[1] Strictly speaking, the paired fermions are not bosons in the sense that they do not obey Bose commutation relations. On the other hand, the pairs all have the same wavefunction, so, in this sense, the pairs are condensed into the same state [13]. More precisely, the BCS state is a coherent state of fermion pairs.

the case of two-component ultracold fermions, the fermions with opposite pseudospins and momenta pair, and the pairs condense to form a superfluid. The original BCS theory is applicable only for a weak interaction; however, in ultracold systems the interaction can be tuned and need not be weak. Leggett argued that the physics of weak and strong attraction are continuously connected, and can be described by a variational approach using a single BCS-like ansatz wavefunction at zero temperature [14]. When the attraction is weak, the BCS-like state is composed of pairs whose size is greater than the inter-particle spacing. As the interaction is increased, the size of the pairs becomes smaller and eventually becomes much smaller than the inter-particle spacing, in which case the pairs can be regarded as molecules consisting of two fermions. Thus, in the strong interaction limit, the system at low enough temperature is a BEC of paired fermions. This continuous crossover from the BCS state of weakly interacting fermions to the BEC of paired (molecular) fermions is called the *BCS-BEC crossover*. The fermions remain a superfluid during the BCS-BEC crossover. The BCS-BEC crossover theory can be extended to a finite temperature. At finite temperature, we must include the effects of fluctuations of pairs. Nozières and Schmitt-Rink found that the finite temperature BCS-BEC crossover can be qualitatively described by considering ladder diagrams for the free energy, taking into account the effects of pairing fluctuations [15]. Figure 1.2 is a schematic phase diagram of the BCS-BEC crossover. The horizontal axis is $-1/k_F a$, where k_F is the Fermi momentum and a is the scattering length, which is positive in the BCS region and negative in the BEC region.

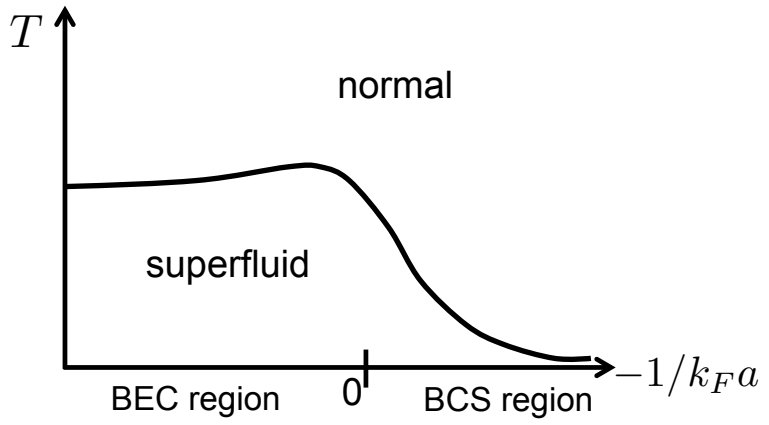

Figure 1.2: A schematic phase diagram of the BCS-BEC crossover in two-component ultracold fermions.

The continuous transition in the BCS-BEC crossover has been experimentally observed [16, 17, 18]. Rotating the two-component fermions below the superfluid transition temperature, quantized vortices have been observed, as shown in the Figure 1.3, and no phase transition has been observed between the BCS region and the BEC region [19].

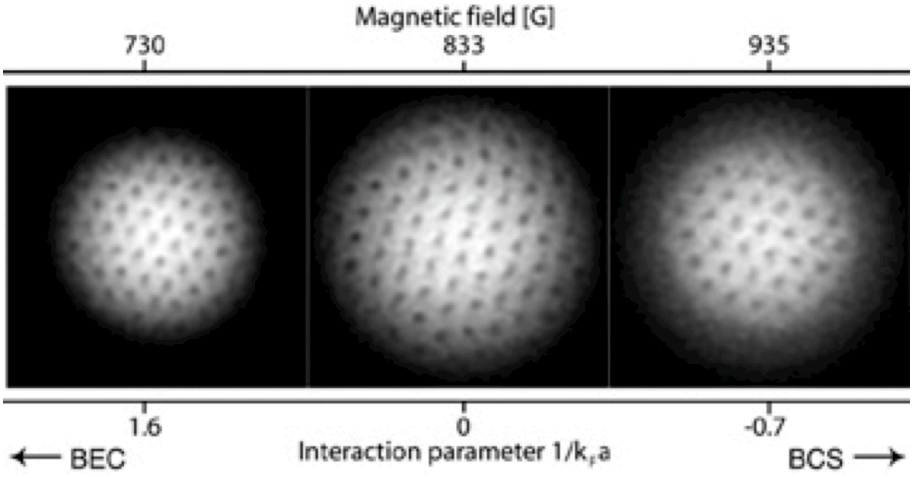

Figure 1.3: The BCS-BEC crossover of quantized vortices in a rotating two-component Fermi gas of ^{6}Li. The right figure is in the BCS region of weak interaction, and the left figure is in the BEC region of strong interaction. The middle figure is in the intermediate region called the unitarity regime. © Martin Zwierlein.

In this thesis, we discuss the BCS-BEC crossover of three-component ultracold fermionic systems. As we will see, both superfluidity and magnetism can coexist in three-component ultracold fermions. Fortunately, basic methods for describing the BCS-BEC crossover in two-component fermions, such as the Leggett's BCS-like ansatz state at zero temperature, and Nozières and Schmitt-Rink's approach at the finite temperature, remain valid for three-component systems. As two-component ultracold fermions can be used to simulate spinfull electrons in metals, three-component systems are expected to be able to simulate an even wider variety of physical models. In particular, there is the prospect of simulating analogs of quantum chromodynamics (QCD) using three-component ultracold fermions, where the three components correspond to the three colors of QCD. We will see that the Ginzburg-Landau free energies of three-components ultracold fermions and QCD have similar structures.

1.3 Should gauge fields be quantized?

In section 1.1, we discussed static gauge fields, in which the gauge fields were not an independent quantum degrees of freedom. In reality, gauge fields are quantized; for example, electromagnetic fields should be quantized and photons must have an independent quantum degree of freedom. There are numerous pieces of experimental evidence to think that the the electromagnetic field should be quantized, such as the spontaneous emission of light, the Lamb shift, etc[2]. In another vein, Niels Bohr conceived an ingenious *gedankenexperiment* that demonstrated that the electromagnetic field must be quantized by requiring the consistency of quantum mechanics. An outline of his argument is as follows. Consider a double-slit interference experiment with charged particles. When the charge is small, such as with electrons, we know that an interference pattern will emerge. If the Coulomb field created by the particles is large enough, it should be possible to detect the path (which slit the particle went through) by measuring the particle's Coulomb field. If the measuring device for the Coulomb field is located far enough from the slit, the measurement process cannot affect the interference pattern, and the interference pattern should remain. However, it would be a contradiction of quantum mechanics if we were able to detect the path of the particles and still observe the interference pattern at the same time. This contradiction arises because we have not treated the electromagnetic field as an independent degree of freedom. If the electromagnetic field is quantized and has an independent quantum degree of freedom, the *bremsstrahlung* produced by the charged particle as they turn the corner at the slits are entangled to the state of the particle. As a result of this entanglement, the particle obtains a random phase information and thus the interference pattern is destroyed. Therefore, if we assume that the electromagnetic field is quantized, quantum mechanics is safe and consistent. In this thesis, we give a detailed analysis of Niels Bohr's *gedankenexperiment* [3] and also consider an extension to discuss if gravity should be quantized.

[2] It is worth noting that while often cited in this regard, the photoelectric effect does not, in fact, require the quantization of the electromagnetic field [20, 21].

[3] This *gedankenexperiment* was told by Aage Petersen to Gordon Baym at Copenhagen ca. 1961. Petersen was Niels Bohr's scientific secretary (amanuensis) from 1952 until Bohr's death in 1962. To the author's knowledge, this experiment is not mentioned in Bohr's published papers, unpublished manuscripts, or letters. Aage Bohr, the son of Niels Bohr, when queried about the experiment, wrote that, "Many ways of observing effects distinguishing between the "paths" of the electron were certainly discussed ... I do not remember any specific scheme exploiting the Coulomb field far away from the electron." (Letter to G. Baym, 6 June 2001.) References to N. Bohr's ideas in this thesis

Let us now briefly review an ordinary double-slit interference experiment, in which electrons go through a double-slit one by one and are detected at the screen. As the number of detected electrons increases, an interference pattern emerges on the screen. Figure 1.4 shows the interference pattern produced from an actual experiment by a Hitachi group (e.g. [23]).

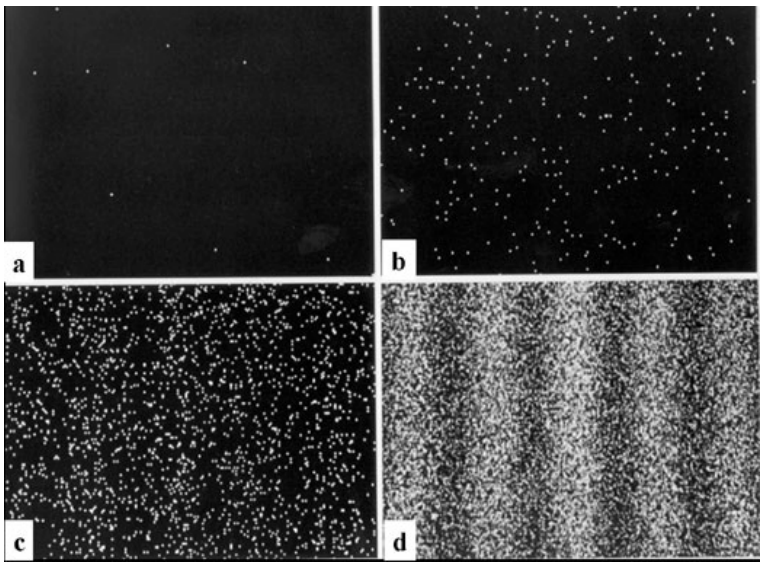

Figure 1.4: Double-slit interference pattern of electrons. As the number of detected electrons increases from (a) to (d), the interference pattern is built up. © Hitachi, Ltd.

We can construct a simple model to explain this experiment. Consider the double-slit setup of Figure 1.5. Let $\mathbf{p}_1(\mathbf{r})$ and $\mathbf{p}_2(\mathbf{r})$ be the momenta of particles which went through the upper and lower slits, respectively, and reached the position $\mathbf{r}$ on the screen. The state of the particle at the screen is

$$|\text{state}\rangle = \int_{\text{screen}} d^2r \left(u_1(\mathbf{r})|\mathbf{p}_1(\mathbf{r})\rangle + u_2(\mathbf{r})|\mathbf{p}_2(\mathbf{r})\rangle \right), \tag{1.8}$$

where $u_1(\mathbf{r})$ and $u_2(\mathbf{r})$ are appropriate weights for the states from the upper and the lower slits, respectively, and $|\mathbf{p}\rangle$ represents the state with momentum $\mathbf{p}$. The probability of measuring a particle at position $\mathbf{r}$ is

$$\langle\text{state}|\psi^\dagger(\mathbf{r})\psi(\mathbf{r})|\text{state}\rangle = \|\psi(\mathbf{r})|\text{state}\rangle\|^2, \tag{1.9}$$

follow Petersen's description of the experiment told by Gordon Baym to the author. A similar *gedankenexperiment* was described in the chapter 15 of [22] as well.

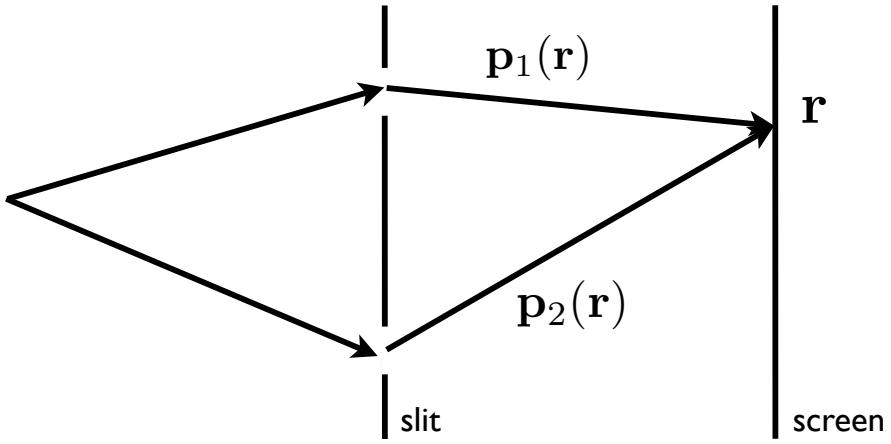

Figure 1.5: A setup of a double-slit experiment.

where

$$\psi(\mathbf{r}) = e^{i\mathbf{p}_1(\mathbf{r})\cdot\mathbf{r}}\psi_{\mathbf{p}_1(\mathbf{r})} + e^{i\mathbf{p}_2(\mathbf{r})\cdot\mathbf{r}}\psi_{\mathbf{p}_2(\mathbf{r})} \tag{1.10}$$

is the particle annihilation operator at $\mathbf{r}$, and $\psi_{\mathbf{p}}$ is the particle annihilation operator of momentum $\mathbf{p}$. Throughout this thesis, we set $\hbar = 1$ unless otherwise stated. When the lower slit is closed, the state is, up to an overall normalization factor,

$$|\text{state}\rangle_{\text{upper}} = \int_{\text{screen}} d^2r \; u_1(\mathbf{r})|\mathbf{p}_1(\mathbf{r})\rangle. \tag{1.11}$$

Then, when the lower slit is closed, the probability of finding a particle at position $\mathbf{r}$ is

$$\|\psi(\mathbf{r})|\text{state}\rangle_{\text{upper}}\|^2 = \left\|e^{i\mathbf{p}_1(\mathbf{r})\cdot\mathbf{r}}u_1(\mathbf{r})|0\rangle\right\|^2 = |u_1(\mathbf{r})|^2, \tag{1.12}$$

where $|0\rangle$ is the vacuum state. This probability is proportional to the intensity of the particle beam at the screen when the lower slit is closed. Thus let us define the intensity by

$$I_u(\mathbf{r}) \equiv |u_1(\mathbf{r})|^2. \tag{1.13}$$

Similarly, the intensity of the particle beam when the upper slit is closed is

$$I_l(\mathbf{r}) \equiv |u_2(\mathbf{r})|^2. \tag{1.14}$$

When both slits are open, probability of finding a particle at position $\mathbf{r}$ is

$$\begin{aligned}\|\psi(\mathbf{r})\rangle\|^2 &= \left|e^{i\mathbf{p}_1(\mathbf{r})\cdot\mathbf{r}}u_1(\mathbf{r}) + e^{i\mathbf{p}_2(\mathbf{r})\cdot\mathbf{r}}u_2(\mathbf{r})\right|^2 \\ &= |u_1(\mathbf{r})|^2 + |u_2(\mathbf{r})|^2 + u_1(\mathbf{r})u_2^*(\mathbf{r})e^{i(\mathbf{p}_1(\mathbf{r})-\mathbf{p}_2(\mathbf{r}))\cdot\mathbf{r}} + c.c. \\ &= I_u(\mathbf{r}) + I_l(\mathbf{r}) + 2\sqrt{I_u(\mathbf{r})I_l(\mathbf{r})}\cos((\mathbf{p}_1(\mathbf{r}) - \mathbf{p}_2(\mathbf{r}))\cdot\mathbf{r} + \phi), \end{aligned} \tag{1.15}$$

where $u_1(\mathbf{r})u_2^*(\mathbf{r}) \equiv |u_1(\mathbf{r})u_2^*(\mathbf{r})|e^{i\phi}$. Thus, at least for a short interval, the intensity sinusoidally oscillates and produces the familiar interference pattern. Upon deriving this expression, we assumed in (1.8) that the state at the screen is a superposition of states produced by a particle going through the upper slit and the lower slit. Thus, if there is a way to find which path the particle took, the interference will not occur, and the interference pattern should not be observed.

In this thesis, we discuss how this argument may be extended for charged particles with quantum electromagnetic degrees of freedom in the context of Niels Bohr's *gedankenexperiment*. We also discuss a similar *gedankenexperiment* with massive particles to see if we can conclude that the gravitational field should be quantized as well. We find that the result is negative; the analogous argument does not require the quantization of the gravitational field.

1.4 Outline of this thesis

The organization of this thesis is as follows:

In chapter 2, we discuss how gauge fields are artificially produced in neutral ultracold systems. We discuss a general theory of Berry's connection and how this tool can be used to create artificial gauge fields in ultracold systems. We then move on to discuss Rashba-Dresselhaus spin-orbit coupling. We explain single-particle properties of a particle with Rashba-Dresselhaus spin-orbit coupling, such as the single-particle spectrum and the possibility of BEC in the absence of interaction.

In chapter 3, we discuss the stability of BEC's in the presence of Rashba-Dresselhaus spin-orbit coupling with an s-wave contact interaction. We show, by first calculating the Green's function, that the BEC's are stable against quantum and thermal fluctuations. Also, comparing free energies of the normal phase and the condensed phase, we infer that generally the system is condensed at zero temperature, and undergoes a transition to normal at non-zero temperature. The content in this chapter is based on [1].

In chapter 4, we discuss how the bare interaction is renormalized in the presence of Rashba-Dresselhaus spin-orbit coupling, and how the renormalized interaction affects the phase diagram. In particular, we derive the exact two-body t-matrix of two bosons or two fermions scattering in an arbitrary mixture of Rashba and Dresselhaus spin-orbit coupling. We describe the phase diagram for bosons within the mean-field approximation using the t-matrix as an effective interaction. The content in this chapter is based on [2, 3].

In chapter 5, we discuss three-component ultracold fermions. We investigate the phase diagram and the BCS-BEC crossover of a homogeneous three-component ultracold Fermi gas with a U(3)-invariant attractive interaction. We show that the system at sufficiently low temperatures exhibits population imbalance as well as fermionic pairing. We describe the crossover in this system, connecting the weakly interacting BCS regime of the partially population-imbalanced fermion pairing state and the BEC limit with three weakly interacting species of molecules, including pairing fluctuations within a t-matrix calculation of the particle self-energies. The content in this chapter is based on [4].

In chapter 6, we discuss our final topic of Niels Bohr's double-slit *gedankenexperiment*. We show how the measurement limit of the path is related to the charge of the particle by first reconstructing the argument of the measurability of small electric fields by Bohr and Rosenfeld. Next, we discuss how the visibility of the interference pattern varies as a function of the charge of the particle, assuming that the electromagnetic radiation has an independent quantum degree of freedom. We then conclude that we cannot efficiently measure the path of the particle without destroying the interference pattern, showing the consistency of the quantum mechanics. We also discuss that a similar argument does not lead to the requirement that the gravitational field be quantized. The content in this chapter is based on [5].

In appendix A, we develop a theory of scattering in both two and three dimensions, emphasizing differences between different dimensions. We explain how the effective interaction and the t-matrix are related, and how the bare interaction can be renormalized in terms of the scattering length.

Appendices from B to G are devoted to lengthy calculations omitted in the main text.

Chapter 2

Artificial gauge fields in ultracold atoms

2.1 Introduction

In most experimental systems, trapped ultracold atoms are neutral and do not naturally couple to gauge fields, such as electromagnetic fields, in a way charged particles are coupled these fields[1]. On the other hand, many interesting phenomena in condensed matter systems are the result of the coupling between charged particles, which are often electrons, and gauge fields, usually electromagnetic fields. Examples of such phenomena include Aharonov-Bohm effects, quantum Hall effects, and the formation of quantum vortices in type-II superconductors.

Roughly speaking, there are two different methods for obtaining a gauge-field like potential in ultracold atomic systems. One method is to rotate the gas. By rotating the gas, the Hamiltonian acquires an effective static Abelian gauge field in the rotating frame, which amounts to coupling the neutral atoms to effective magnetic fields as we saw in the section 1.1.

Another method for creating artificial gauge fields involves using finely tuned and aligned lasers. There have been many proposals for obtaining external (static) gauge fields, both Abelian and non-Abelian, and some are already realized [24, 25, 26, 27, 28, 29, 30, 31]. Such a system is of great interest not only because of the prospect of simulating various models in condensed matter physics in which electrons are coupled to magnetic fields, but also because of the possibility of exploring physical systems which have never been conceived before. For example, in conventional condensed matter physics, the charge carriers are electrons, which are fermions, but using ultracold atoms one

[1] Ultracold atoms do couple to electric and magnetic fields, and it is this coupling which makes magnetic and optical traps possible. However, the coupling structure between ultracold atoms and electromagnetic fields is quite different than that between charged particles and these fields.

can create artificial gauge fields coupled to bosons, which has no analog in conventional condensed matter physics.

In this chapter, we begin by explaining Berry's connection and how this tool is used to create artificial gauge fields in ultracold gases. We then discuss single-particle properties of a particle with Rashba-Dresselhaus spin-orbit coupling, which is a special class of non-Abelian gauge field.

2.2 Berry's connection

Berry's connection is the effective gauge field that arises when the state of the system contains both fast and slowly varying components [32]. While the quickly varying component of the state adiabatically follows the slowly varying component obeying the quantum adiabatic theorem, the slowly varying component acquires Berry's connection.

We first develop a general theory of Berry's connection, and then apply the theory to ultracold gases. In the case of ultracold atoms, the slow component is the translational motion of the atom, and the fast component is the internal state of the atom. An atom moves in the field created by finely aligned lasers, and the translational motion of the atom acquires Berry's connection, which serves as an artificially created gauge field to the atom.

Let $\mathbf{r}$ denote the position involved in the state which is changing slowly[2]. Then, the state whose parameters vary quickly is described by a Hamiltonian with given $\mathbf{r}$. (Now we are treating $\mathbf{r}$ as a classical variable to describe the fast component, although in principle it is not. This is the Born-Oppenheimer approximation.) Let us call the Hamiltonian with fast variables $\mathcal{H}^F(\mathbf{r})$. Note that $\mathcal{H}^F(\mathbf{r})$ may contain a spatial derivative term, but if so, it will not be with respect to $\mathbf{r}$, which is the position of the slowly varying component. When we write $\mathcal{H}^F(\mathbf{r})$, $\mathbf{r}$ is an external parameter which is fixed. Let $\{|\chi_l(\mathbf{r})\rangle\}$ denote a complete set of orthonormal eigenstates for $\mathcal{H}^F(\mathbf{r})$ with the respective eigenvalues E_l. Applying the adiabatic theorem we conclude that when the slow variable is changed, the fast variable follows the change of the slow variable adiabatically. This means that we only need to consider a certain subspace spanned by $\{|\chi_l(\mathbf{r})\rangle\}$ which have the same (or

[2] In this chapter, we need to distinguish between vectors and matrices. We let a capital letter in bold font denote a matrix, and a lower-case letter in bold font denote a vector. A capital letter in bold font with an arrow on its top denote a vector of matrices. For example, $\vec{\mathbf{A}} = (\mathbf{A}_x, \mathbf{A}_y, \mathbf{A}_z)$, where $\mathbf{A}_i$ are matrices. On the other hand, $\mathbf{r} = (x, y, z)$ is a vector in three dimensional space.

similar) energy eigenvalue. Let $\mathfrak{g}$ be the set of indices in the subspace with the same energy. When the subspace is non-degenerate, $\mathfrak{g}$ contains only one element. When the subspace is degenerate, $\mathfrak{g}$ contains several elements.

Let us now begin by writing the overall state of the system as

$$|\Phi(\mathbf{r})\rangle = \sum_{l\in\mathfrak{g}} \psi_l(\mathbf{r})|\chi_l(\mathbf{r})\rangle, \tag{2.1}$$

where $|\Phi(\mathbf{r}),\rangle$ denotes the partial projection of the whole state $|\Phi\rangle$ onto the subspace of slowly varying components with position $\mathbf{r}$. We may now write the total one-particle Hamiltonian as

$$\mathcal{H} = \left(-\frac{\nabla^2}{2m} + U(\mathbf{r})\right)\mathbf{I} + \mathcal{H}^F(\mathbf{r}), \tag{2.2}$$

where $\mathbf{I}$ is the identity operator in the Hilbert space of the quickly varying components. Then, the Schrödinger equation is

$$\begin{aligned} i\frac{\partial}{\partial t}|\Phi(\mathbf{r});t\rangle &= i\frac{\partial}{\partial t}\sum_{l\in\mathfrak{g}}\psi_l(\mathbf{r},t)|\chi_l(\mathbf{r})\rangle \\ &= \mathcal{H}|\Phi(\mathbf{r});t\rangle = \left(-\frac{\nabla^2}{2m} + U(\mathbf{r}) + \mathcal{H}^F(\mathbf{r})\right)\sum_{l\in\mathfrak{g}}\psi_l(\mathbf{r})|\chi_l(\mathbf{r})\rangle \\ &= \sum_{l\in\mathfrak{g}}\left(-\frac{\nabla^2}{2m} + U(\mathbf{r}) + E_l\right)\psi_l(\mathbf{r})|\chi_l(\mathbf{r})\rangle. \end{aligned} \tag{2.3}$$

Applying $\langle\chi_m(\mathbf{r})|$ where $m\in\mathfrak{g}$ from the left, we obtain

$$\begin{aligned} i\frac{\partial}{\partial t}\psi_m(\mathbf{r},t) &= \left(-\frac{\nabla^2}{2m} + U(\mathbf{r}) + E_m\right)\psi_m(\mathbf{r}) - \frac{1}{m}\sum_{l\in\mathfrak{g}}\nabla\psi_l(\mathbf{r})\cdot\langle\chi_m(\mathbf{r})|\nabla|\chi_l(\mathbf{r})\rangle \\ &\qquad - \frac{1}{2m}\sum_{l\in\mathfrak{g}}\psi_l(\mathbf{r})\langle\chi_m(\mathbf{r})|\nabla^2|\chi_l(\mathbf{r})\rangle \\ &= \sum_{n,l\in\mathfrak{g}}\frac{1}{2m}\left(\frac{\nabla}{i}\delta_{mn} - i\langle\chi_m(\mathbf{r})|\nabla|\chi_n(\mathbf{r})\rangle\right)\left(\frac{\nabla}{i}\delta_{nl} - i\langle\chi_n(\mathbf{r})|\nabla|\chi_l(\mathbf{r})\rangle\right)\psi_l(\mathbf{r}) \\ &+ \left(U(\mathbf{r}) + E_m\right)\psi_m(\mathbf{r}) + \sum_{l\in\mathfrak{g}}\frac{1}{2m}\left(\nabla\cdot\langle\chi_m(\mathbf{r})|\nabla|\chi_l(\mathbf{r})\rangle\right)\psi_l(\mathbf{r}) \\ &+ \sum_{n,l\in\mathfrak{g}}\frac{1}{2m}\langle\chi_m(\mathbf{r})|\nabla|\chi_n(\mathbf{r})\rangle\langle\chi_n(\mathbf{r})|\nabla|\chi_l(\mathbf{r})\rangle\psi_l(\mathbf{r}) - \frac{1}{2m}\sum_{l\in\mathfrak{g}}\langle\chi_m(\mathbf{r})|\nabla^2|\chi_l(\mathbf{r})\rangle\psi_l(\mathbf{r}). \end{aligned} \tag{2.4}$$

Defining

$$\vec{A}_{ml}(\mathbf{r}) \equiv i\langle\chi_m(\mathbf{r})|\nabla|\chi_l(\mathbf{r})\rangle, \tag{2.5}$$

the above equation can be written as

$$i\frac{\partial}{\partial t}\psi_m(\mathbf{r},t) = \sum_{n,l\in\mathfrak{g}} \frac{1}{2m}\left(\frac{\nabla}{i}\delta_{mn} - \vec{A}_{mn}(\mathbf{r})\right)\left(\frac{\nabla}{i}\delta_{nl} - \vec{A}_{nl}(\mathbf{r})\right)\psi_l(\mathbf{r}) + (U(\mathbf{r}) + E_m)\,\psi_m(\mathbf{r}) + \sum_{l\in\mathfrak{g}} \frac{1}{2m}\left(\nabla\langle\chi_m(\mathbf{r})|\right)\cdot\left(\nabla|\chi_l(\mathbf{r})\rangle\right)\psi_l(\mathbf{r}) - \sum_{n,l\in\mathfrak{g}} \frac{1}{2m}\vec{A}_{mn}(\mathbf{r})\cdot\vec{A}_{nl}(\mathbf{r})\psi_l(\mathbf{r}). \tag{2.6}$$

This equation can be written in terms of $\vec{\psi}(\mathbf{r})$, which is the vector whose components are $\psi_m(\mathbf{r})$ with $m \in \mathfrak{g}$, and $\vec{\mathbf{A}}(\mathbf{r})$, which is a matrix whose (m,l) element is $\vec{A}_{ml}(\mathbf{r})$. Then,

$$i\frac{\partial}{\partial t}\vec{\psi}(\mathbf{r},t) = \left(\frac{1}{2m}\left(\frac{\nabla}{i}\mathbf{I} - \vec{\mathbf{A}}(\mathbf{r})\right)^2 + (U(\mathbf{r}) + E_m)\mathbf{I} + \mathbf{V}(\mathbf{r})\right)\vec{\psi}(\mathbf{r},t), \tag{2.7}$$

where (m,l) component of a matrix $\mathbf{V}(\mathbf{r})$ is

$$V_{ml}(\mathbf{r}) \equiv \frac{1}{2m}\left(\nabla\langle\chi_m(\mathbf{r})|\right)\cdot\left(\nabla|\chi_l(\mathbf{r})\rangle\right) - \sum_{n\in\mathfrak{g}} \frac{1}{2m}\vec{A}_{mn}(\mathbf{r})\cdot\vec{A}_{nl}(\mathbf{r}). \tag{2.8}$$

Now the effective Schrödinger equation (2.7) for the wavefunction of the slow component looks as if the particle is traveling in the vector potential given by $\vec{\mathbf{A}}(\mathbf{r})$ and the scalar potential $\mathbf{V}(\mathbf{r})$ in addition to the original potential $U(\mathbf{r})$. The emergent effective vector potential $A(\mathbf{r})$ is called the Berry's connection. If there is only one component in $\mathfrak{g}$, the wavefunction $\psi(\mathbf{r})$ has only one component, and so does the Berry's connection. In this case, the vector potential is called Abelian. On the other hand, if there are more than one element in $\mathfrak{g}$, the wavefunction is a vector with more than one component, and the Berry's connection becomes a matrix with more than one dimension. When the Berry's connection is noncommutative, the vector potential is non-Abelian.

We can rewrite the scalar potential in a more compact way, by using a relation derived by taking the derivative of $\langle\chi_l(\mathbf{r})|\chi_m(\mathbf{r})\rangle = \delta_{l,m}$, which is

$$\left(\nabla\langle\chi_l(\mathbf{r})|\right)|\chi_m(\mathbf{r})\rangle = -\langle\chi_l(\mathbf{r})|\nabla|\chi_m(\mathbf{r})\rangle. \tag{2.9}$$

Then,

$$\begin{aligned} V_{ml}(\mathbf{r}) &= \sum_n \frac{1}{2m}\left(\nabla\langle\chi_m(\mathbf{r})|\right)\cdot|\chi_n(\mathbf{r})\rangle\langle\chi_n(\mathbf{r})|\nabla|\chi_l(\mathbf{r})\rangle - \sum_{n\in\mathfrak{g}} \frac{1}{2m}\vec{A}_{mn}(\mathbf{r})\cdot\vec{A}_{nl}(\mathbf{r}) \\ &= -\sum_n \frac{1}{2m}\langle\chi_m(\mathbf{r})|\nabla|\chi_n(\mathbf{r})\rangle\cdot\langle\chi_n(\mathbf{r})|\nabla|\chi_l(\mathbf{r})\rangle - \sum_{n\in\mathfrak{g}} \frac{1}{2m}\vec{A}_{mn}(\mathbf{r})\cdot\vec{A}_{nl}(\mathbf{r}) \\ &= \sum_n \frac{1}{2m}\vec{A}_{mn}(\mathbf{r})\cdot\vec{A}_{nl}(\mathbf{r}) - \sum_{n\in\mathfrak{g}} \frac{1}{2m}\vec{A}_{mn}(\mathbf{r})\cdot\vec{A}_{nl}(\mathbf{r}) \\ &= \sum_{n\notin\mathfrak{g}} \frac{1}{2m}\vec{A}_{mn}(\mathbf{r})\cdot\vec{A}_{nl}(\mathbf{r}), \end{aligned} \tag{2.10}$$

which is an expression found in [33].

Finally, we note that the matrix $\vec{\mathbf{A}}(\mathbf{r})$ is a vector of Hermitian matrices:

$$\vec{A}_{ml}(\mathbf{r}) = i\langle\chi_m(\mathbf{r})|\nabla|\chi_l(\mathbf{r})\rangle = -i\left(\nabla\langle\chi_m(\mathbf{r})|\right)|\chi_l(\mathbf{r})\rangle = \left(i\langle\chi_l(\mathbf{r})|\nabla|\chi_m(\mathbf{r})\rangle\right)^* = \vec{A}_{lm}(\mathbf{r})^*. \tag{2.11}$$

So far we have developed a general theory of the Berry's connection. Now, let us look at some specific examples of the use of Berry's connections to realize artificial gauge fields in ultracold gases.

2.3 Creating artificial gauge fields

There are many proposals to create artificial gauge fields using Berry's connection. Here we describe a scheme which was used in the first experimental realization of an artificial gauge field in [24, 25][3].

Consider a system of ultracold ^{87}Rb atoms, focusing on the three hyperfine levels with $F = 1$. Two of the states $|g_1\rangle$ and $|g_2\rangle$, are coupled to the third state $|e\rangle$, with space dependent complex Rabi frequencies κ_1 and κ_2. The Hamiltonian of the three internal states in $\{|g_1\rangle, |e\rangle, |g_2\rangle\}$ basis is

$$\mathcal{H} = \frac{1}{2}\begin{pmatrix} -2\delta & \kappa_1^* & 0 \\ \kappa_1 & 0 & \kappa_2 \\ 0 & \kappa_2^* & 2\delta \end{pmatrix}, \tag{2.12}$$

where 2δ is the detuning of Raman excitation between the states $|g_1\rangle$ and $|g_2\rangle$. Choosing the laser configuration so that the difference of the wave vectors of two coupling lasers is directed in the x direction and $\kappa_1 = \kappa_2^* = \kappa e^{-ik_d x}$, the Hamiltonian becomes

$$\mathcal{H} = \delta\begin{pmatrix} -1 & \frac{\kappa}{2\delta}e^{ik_d x} & 0 \\ \frac{\kappa}{2\delta}e^{-ik_d x} & 0 & \frac{\kappa}{2\delta}e^{ik_d x} \\ 0 & \frac{\kappa}{2\delta}e^{-ik_d x} & 1 \end{pmatrix} \equiv \delta\begin{pmatrix} -1 & \frac{\tan\theta}{\sqrt{2}}e^{ik_d x} & 0 \\ \frac{\tan\theta}{\sqrt{2}}e^{-ik_d x} & 0 & \frac{\tan\theta}{\sqrt{2}}e^{ik_d x} \\ 0 & \frac{\tan\theta}{\sqrt{2}}e^{-ik_d x} & 1 \end{pmatrix}, \tag{2.13}$$

where $\tan\theta \equiv \kappa/\sqrt{2}\delta$. The eigenstates of this Hamiltonian are 0 and $\pm\delta/\cos\theta = \pm\sqrt{\delta^2 + \kappa^2/2}$. The normalized eigenvectors corresponding to the eigenvectors $-\sqrt{\delta^2 + \kappa^2/2}$, 0, and $\sqrt{\delta^2 + \kappa^2/2}$

[3] The analysis of the scheme we describe here is based on [33], which makes explicit use of the Berry's connection. On the other hand, the original analysis of the setup, which is given in [34], does not directly use the Berry's connection. The two analyses yield the same result in the parameter regime where they are both valid. However, the analysis given in [34] applies to a wider parameter regime.

are

$$|-\rangle \equiv \begin{pmatrix} e^{ik_d x}\cos^2(\theta/2) \\ -\frac{1}{\sqrt{2}}\sin\theta \\ e^{-ik_d x}\sin^2(\theta/2) \end{pmatrix}, \quad |0\rangle \equiv \begin{pmatrix} e^{ik_d x}\frac{\sin\theta}{\sqrt{2}} \\ \cos\theta \\ -e^{-ik_d x}\frac{\sin\theta}{\sqrt{2}} \end{pmatrix}, \quad |+\rangle \equiv \begin{pmatrix} e^{ik_d x}\sin^2(\theta/2) \\ \frac{1}{\sqrt{2}}\sin\theta \\ e^{-ik_d x}\cos^2(\theta/2) \end{pmatrix}, \tag{2.14}$$

respectively. Assuming the energy $-\sqrt{\delta^2+\kappa^2/2}$ is lower than the other two states, we can use an adiabatic approximation in which the system follows the lowest energy eigenstate throughout the system's evolution. In this approximation, the artificial gauge field created is an Abelian gauge field, which is:

$$\vec{A} = i\langle -|\nabla|-\rangle = -\cos\theta\nabla(k_d x) = (-k_d\cos\theta, 0, 0), \tag{2.15}$$

and the artificial magnetic field is

$$\vec{B} = \nabla\times\vec{A} = (0, -k_d\partial_z\cos\theta, k_d\partial_y\cos\theta), \tag{2.16}$$

where $\cos\theta$ depends on position through the position dependence of δ. The first experimental realization of the artificial gauge field was with a constant δ, which leads to non-zero vector field, but zero artificial magnetic field [24]. Later the same group realized a non-zero artificial magnetic field utilizing a δ with spatial variation in the y direction [25]. The artificial magnetic field was thus in the z direction and they observed quantized vortices in the BEC as shown in the Figure 2.1.

In a similar manner, a non-Abelian gauge field can be artificially created in ultracold gases. In the next section, we turn our attention to the Rashba-Dresselhaus spin-orbit coupling, which is a special kind of non-Abelian gauge fields.

2.4 Rashba-Dresselhaus spin-orbit coupling

2.4.1 Hamiltonian

Among the many possible configurations of non-Abelian gauge fields in ultracold atoms, special interest has been given to a certain type of non-Abelian gauge field which is known as Rashba-Dresselhaus spin-orbit coupling.

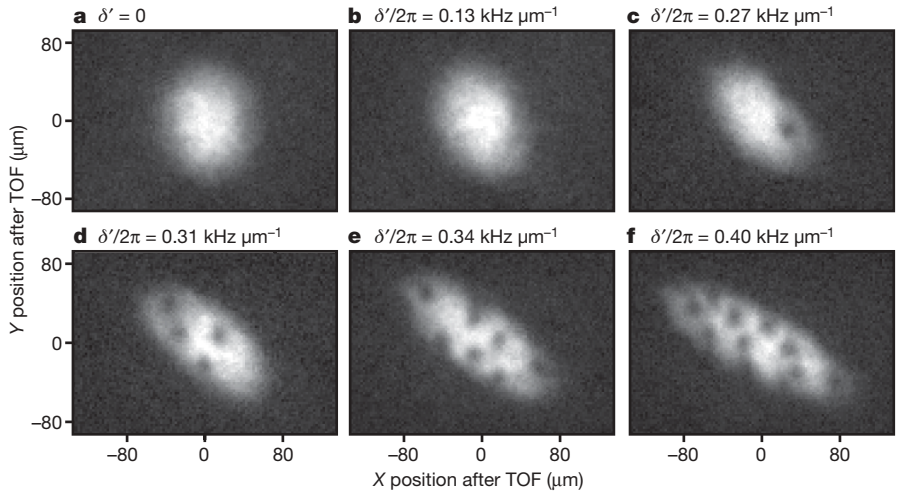

Figure 2.1: Vortices created in a BEC of ^{87}Rb coupled to an artificial magnetic field. δ' is the gradient of the detuning δ. As δ' increases, the number of vortices increases because the artificial magnetic field becomes larger. The asymmetry in the shape of the cloud is from a shear force due to the Raman lasers. Adapted by permission from Macmillan Publishers Ltd: *Nature* **462**, 628-632, copyright 2009 [25].

The theory of Rashba-Dresselhaus spin-orbit coupling was originally developed in the context of two-dimensional semiconductors [35, 36]. The Rashba spin-orbit coupling and the Dresselhaus spin-orbit coupling both couple the momentum $\mathbf{p}$ and the spin $\boldsymbol{\sigma}$, but their origins are different. The Rashba spin-orbit coupling is the result of the inversion asymmetry of the confining potential (or the structure), whereas the Dresselhaus spin-orbit coupling is the result of the inversion asymmetry of the bulk [37, 38]. The overall spin-orbit coupling is the result of an interplay between the Rashba and the Dresselhaus spin-orbit couplings.

The Rashba spin-orbit coupling is given by the Hamiltonian

$$\mathcal{H}_R = c_R \left(p_x \sigma_y - p_y \sigma_x \right), \tag{2.17}$$

and the Dresselhaus spin-orbit coupling is

$$\mathcal{H}_D = c_D \left(p_x \sigma_x - p_y \sigma_y \right), \tag{2.18}$$

where c_R and c_D are respective coupling strengths. In order to facilitate our analysis let us first

transform the Hamiltonians by performing a pseudospin rotation given by a unitary matrix

$$\begin{pmatrix} e^{-i\pi/8} & 0 \\ 0 & e^{i\pi/8} \end{pmatrix}. \tag{2.19}$$

Under this transformation, the Pauli matrices transform to

$$\begin{aligned} \sigma_x &\to \begin{pmatrix} e^{i\pi/8} & 0 \\ 0 & e^{-i\pi/8} \end{pmatrix} \sigma_x \begin{pmatrix} e^{-i\pi/8} & 0 \\ 0 & e^{i\pi/8} \end{pmatrix} = \frac{\sigma_x - \sigma_y}{\sqrt{2}}, \\ \sigma_y &\to \begin{pmatrix} e^{i\pi/8} & 0 \\ 0 & e^{-i\pi/8} \end{pmatrix} \sigma_y \begin{pmatrix} e^{-i\pi/8} & 0 \\ 0 & e^{i\pi/8} \end{pmatrix} = \frac{\sigma_x + \sigma_y}{\sqrt{2}}. \end{aligned} \tag{2.20}$$

Then, the Rashba and Dresselhaus Hamiltonians transform as

$$\mathcal{H}_R \to c_R \left(p_x \frac{\sigma_x + \sigma_y}{\sqrt{2}} - p_y \frac{\sigma_x - \sigma_y}{\sqrt{2}} \right) = c_R \left(\frac{p_x - p_y}{\sqrt{2}} \sigma_x + \frac{p_x + p_y}{\sqrt{2}} \sigma_y \right) \tag{2.21}$$

$$\mathcal{H}_D \to c_D \left(p_x \frac{\sigma_x - \sigma_y}{\sqrt{2}} - p_y \frac{\sigma_x + \sigma_y}{\sqrt{2}} \right) = c_D \left(\frac{p_x - p_y}{\sqrt{2}} \sigma_x - \frac{p_x + p_y}{\sqrt{2}} \sigma_y \right). \tag{2.22}$$

Finally, let us rename the axes in the momentum space so that

$$\frac{p_x - p_y}{\sqrt{2}} \to p_x, \qquad \frac{p_x + p_y}{\sqrt{2}} \to p_y. \tag{2.23}$$

Thus, we obtain

$$\mathcal{H}_R \to c_R \left(p_x \sigma_x + p_y \sigma_y \right), \tag{2.24}$$

$$\mathcal{H}_D \to c_D \left(p_x \sigma_x - p_y \sigma_y \right). \tag{2.25}$$

The sum of the two spin-orbit coupling Hamiltonians give

$$\mathcal{H}_R + \mathcal{H}_D \to (c_R + c_D) p_x \sigma_x + (c_R - c_D) p_y \sigma_y \equiv \frac{\kappa}{m} p_x \sigma_x + \frac{\eta \kappa}{m} p_y \sigma_y, \tag{2.26}$$

where $\kappa \equiv m(c_R + c_D)$ and $\eta \equiv (c_R - c_D)/(c_R + c_D)$. The parameter κ measures the overall strength of the Rashba-Dresselhaus spin-orbit coupling, while η is a measure of the relative strength of the Rashba-Dresselhaus spin-orbit couplings. Without a loss of generality, we can assume $\kappa > 0$ and $0 \leq \eta \leq 1$ [4]. In the case of pure Rashba spin-orbit coupling, we have $\eta = 1$, and in the case of an

[4] When $\kappa < 0$ or $\eta < 0$ or $1 < \eta$, we can always flip the signs of p_x or p_y and redefine the axis of momenta to satisfy $\kappa > 0$ and $0 \leq \eta \leq 1$.

equal mixture of the Rasbha and the Dresselhaus spin-orbit coupling ($c_R = c_D$), we have $\eta = 0$. Since η also sets the anisotropy of the spin-orbit coupling in x and y directions in the rotated basis, we will call η the anisotropy of the spin-orbit coupling. In what follows, we consider the Rashba-Dresselhaus spin-orbit coupling in the rotated basis and use

$$\mathcal{H}_{RD} \equiv \frac{\kappa}{m} p_x \sigma_x + \frac{\eta\kappa}{m} p_y \sigma_y, \tag{2.27}$$

as the Rashba-Dresselhaus spin-orbit interaction.

2.4.2 Proposed scheme

There have been a several proposals to realize Rashba-Dresselhaus spin-orbit coupling in ultracold gases [39, 40, 41, 42, 43]. Here we describe one scheme utilizing "dark states" following the argument in [33]. This scheme utilizes a multipod configuration, where N (almost) degenerate levels $|g_j\rangle$, where $j = 1, \cdots, N$ are coupled to one excited state $|e\rangle$ with position dependent complex Rabi frequencies $\kappa_j(\mathbf{r})$, described by an internal Hamiltonian

$$\mathcal{H} = \sum_{j=1}^{N} \left(\frac{\kappa_j(\mathbf{r})}{2} |e\rangle\langle g_j| + h.c. \right). \tag{2.28}$$

Eventually we take $N = 3$, but for the moment, we proceed with the general case of N states. We choose the coupling lasers so that

$$\kappa_j(\mathbf{r}) = \frac{\kappa}{\sqrt{N}} e^{i\mathbf{k}_j \cdot \mathbf{r}}, \tag{2.29}$$

where $\mathbf{k}_j \equiv k(-\cos\alpha_j, \sin\alpha_j, 0)$ and $\alpha \equiv 2\pi j/N$. Then,

$$\mathcal{H} = \frac{\kappa}{2} |e\rangle \left(\sum_{j=1}^{N} \langle g_j | \frac{e^{i\mathbf{k}_j \cdot \mathbf{r}}}{\sqrt{N}} \right) + h.c. \equiv \frac{\kappa}{2} |e\rangle\langle B| + h.c. \tag{2.30}$$

Thus, among the N degenerate states, only $|B\rangle$, which is called the *bright state*, is coupled to the excited state. The $N-1$ states which are not coupled to the excited state are called *dark states*. We consider the situation where the atoms stay adiabatically in the dark states. We can take the basis of the dark states to be

$$|D_n\rangle \equiv \sum_{j=1}^{N} |g_j\rangle \frac{e^{i\alpha_j n - i\mathbf{k}_j \cdot \mathbf{r}}}{\sqrt{N}}, \tag{2.31}$$

where $n = 1, \cdots, N-1$. One can prove that $|e\rangle$, $|B\rangle$, and $|D_n\rangle$ form an orthonormal basis. We note here that eigenstates of the Hamiltonian (2.30) with non-zero energies are $|\pm\rangle \equiv (|e\rangle \pm |B\rangle)/\sqrt{2}$ with energies $\pm\kappa/2$. Thus, although the dark states do not couple to the excited states, there is a lower energy state than the dark states. The artificial gauge field created in the dark states is

$$\begin{aligned}
\vec{A}_{nm} &= i\langle D_n|\nabla|D_m\rangle = i\frac{1}{N}\sum_{j,l=1}^{N}\langle g_j|e^{-i\alpha_j n+i\mathbf{k}_j\cdot\mathbf{r}}\nabla e^{i\alpha_l m-i\mathbf{k}_l\cdot\mathbf{r}}|g_l\rangle \\
&= i\frac{1}{N}\sum_{j=1}^{N}(-i\mathbf{k}_j)e^{-i\alpha_j(n-m)} \\
&= -\frac{k}{N}\sum_{j=1}^{N}(\cos\alpha_j, -\sin\alpha_j, 0)e^{-i\alpha_j(n-m)} \\
&= -\frac{k}{N}\sum_{j=1}^{N}\frac{1}{2}(e^{i\alpha_j}+e^{-i\alpha_j}, ie^{i\alpha_j}-ie^{-i\alpha_j}, 0)e^{-i\alpha_j(n-m)} \\
&= -\frac{k}{2}(\delta_{n,m+1}+\delta_{n,m-1}, i\delta_{n,m+1}-i\delta_{n,m-1}, 0),
\end{aligned} \tag{2.32}$$

where $n, m = 1, \cdots, N-1$, and the artificial scalar potential is

$$\begin{aligned}
V_{nm} &= -\frac{1}{2m}\left(\langle D_n|\nabla|-\rangle\langle -|\nabla|D_m\rangle + \langle D_n|\nabla|+\rangle\langle +|\nabla|D_m\rangle\right) \\
&= -\frac{1}{2m}\langle D_n|\nabla|B\rangle\langle B|\nabla|D_m\rangle \\
&= -\frac{1}{2m}\frac{1}{N}\sum_{j=1}^{N}(-i\mathbf{k}_j)e^{-i\alpha_j n}\cdot\frac{1}{N}\sum_{l=1}^{N}(-i\mathbf{k}_l)e^{i\alpha_l m} \\
&= \frac{k^2}{2m}\frac{1}{N}\sum_{j=1}^{N}(\cos\alpha_j, -\sin\alpha_j, 0)e^{-i\alpha_j n}\cdot\frac{1}{N}\sum_{l=1}^{N}(\cos\alpha_l, -\sin\alpha_l, 0)e^{i\alpha_l m} \\
&= \frac{k^2}{8m}(\delta_{n,1}+\delta_{n,N-1}, i\delta_{n,1}-i\delta_{n,N-1}, 0)\cdot(\delta_{m,N-1}+\delta_{m,1}, i\delta_{m,N-1}-i\delta_{m,1}, 0) \\
&= \frac{k^2}{4m}\left(\delta_{n,1}\delta_{m,1}+\delta_{n,N-1}\delta_{m,N-1}\right).
\end{aligned} \tag{2.33}$$

Choosing $N = 3$, the the artificial gauge field is a vector of 2×2 matrices,

$$\vec{\mathbf{A}} = -\frac{k}{2}\left(\sigma_x, \sigma_y, 0\right), \tag{2.34}$$

which is exactly the pure Rashba spin-orbit coupling, and the artificial scalar potential is

$$V = \frac{k^2}{4m}\mathbf{I}_{2\times 2}, \tag{2.35}$$

which is proportional to the identity matrix and simply moves the zero of the energy.

Experimentally, the pure Rashba spin-orbit coupling has not been realized yet. The scheme described above utilizing dark states is, although in principle possible, technically difficult due to the short lifetime of particles which is the result of collisions which initiate transitions from dark states to the lower energy state. A scheme to overcome this problem has been proposed [43].

The equal mixture of the Rashba and the Dresselhaus spin-orbit couplings is experimentally realized in [27]. There, the experimenters use a setup similar to the one used to create an artificial Abelian gauge field described in the section 2.3, but they decouple one state by means of a large detuning and create an effective 2×2 Hamiltonian, which after a proper rotation of a basis has the form of an equal mixture of Rashba-Dresselhaus spin-orbit coupling (i.e. zero anisotropy $\eta = 0$). The vector potential itself is then Abelian since only one component is non-zero, but the scalar potential is also a 2×2 matrix, and the artificial gauge field is non-Abelian in the sense that the vector potential and the scalar potential do not commute. A theoretical analysis of this system is given by Ho and Zhang in [44].

2.4.3 Single particle motion

It is well known that a charged particle moving in a constant magnetic field, which is a U(1) Abelian field, makes a circular trajectory in the plane perpendicular to the magnetic field. Now that we have an access to non-Abelian gauge fields, it is natural to ask a question: "what is the motion of a particle moving in an external non-Abelian gauge field?" In this subsection, we start with the motion of a particle in a general non-Abelian gauge field, and then choose Rashba-Dresselhaus spin-orbit coupling as a specific example to investigate the details[5].

The Hamiltonian of the system is

$$\mathcal{H} = \frac{1}{2m}\left(p_x\mathbf{I} - \mathbf{A}_x\right)^2 + \frac{1}{2m}\left(p_y\mathbf{I} - \mathbf{A}_y\right)^2 + \frac{1}{2m}\left(p_z\mathbf{I} - \mathbf{A}_z\right)^2 \tag{2.36}$$

where $\mathbf{I}$ is the 2 by 2 identity matrix, and $(\mathbf{A}_x, \mathbf{A}_y, \mathbf{A}_z)$ is the vector of SU(2) non-Abelian vector fields. In the following, we may omit writing $\mathbf{I}$ when there is no ambiguity. The magnetic field $\mathbf{B}$ is defined through the field strength tensor $\mathbf{F}_{ij}$, which is defined as

$$\mathbf{F}_{ij} = \partial_i \mathbf{A}_j - \partial_j \mathbf{A}_i - i[\mathbf{A}_i, \mathbf{A}_j]. \tag{2.37}$$

[5] A similar analysis is given in [45].

The magnetic field is then defined by

$$\mathbf{B}_i = \frac{\epsilon_{ijk}\mathbf{F}_{jk}}{2}, \tag{2.38}$$

where ϵ_{ijk} is a completely anti-symmetric unit tensor with $\epsilon_{xyz} = 1$. For example, since $\mathbf{F}_{ij}$ is anti-symmetric,

$$\mathbf{B}_z = \mathbf{F}_{xy} = (\nabla \times \vec{\mathbf{A}})_z + \frac{1}{i}[\mathbf{A}_x, \mathbf{A}_y]. \tag{2.39}$$

Note that this magnetic field is still a 2 by 2 matrix. From this expression, we can see that we can have non-zero magnetic field even when the vector potential is constant due to the non-Abelian nature of the vector potential.

To obtain a constant SU(2) magnetic field in z-direction, we can assume a vector potential of the form

$$\vec{\mathbf{A}} = (\mathbf{A}_x, \mathbf{A}_y, 0), \tag{2.40}$$

where $\mathbf{A}_x$ and $\mathbf{A}_y$ do not depend on position. Then, the magnetic field is

$$\vec{\mathbf{B}} = \left(0, 0, \frac{1}{i}[\mathbf{A}_x, \mathbf{A}_y]\right). \tag{2.41}$$

Next, we solve the Heisenberg equations of motion for the Hamiltonian.

Heisenberg equations of motion

In the presence of the magnetic field (2.40), the Hamiltonian of our system is

$$\mathcal{H} = \frac{1}{2m}\left(p_x\mathbf{I} - \mathbf{A}_x\right)^2 + \frac{1}{2m}\left(p_y\mathbf{I} - \mathbf{A}_y\right)^2 + \frac{1}{2m}p_z^2\mathbf{I}. \tag{2.42}$$

Let us define the time evolution operator U by

$$U = \exp\left(-i\mathcal{H}t\right). \tag{2.43}$$

Then, operator $\mathcal{O}$ in the Heisenberg representation is

$$\mathcal{O}(t) = U^\dagger \mathcal{O} U, \tag{2.44}$$

whose time evolution is determined by

$$i\frac{d}{dt}\mathcal{O}(t) = U^\dagger[\mathcal{O}, \mathcal{H}]U \tag{2.45}$$

Since there is no explicit position dependence in the Hamiltonian, we have

$$i\frac{d}{dt}p_x(t)\mathbf{I} = i\frac{d}{dt}p_y(t)\mathbf{I} = i\frac{d}{dt}p_y(t)\mathbf{I} = 0. \tag{2.46}$$

Therefore, the momentum is a constant of motion and we may write

$$p_x(t) = p_x, \qquad p_y(t) = p_y, \qquad p_z(t) = p_z. \tag{2.47}$$

The time dependence of position is more complicated. The z-component is the simplest, and we have

$$i\frac{d}{dt}z(t)\mathbf{I} = U^\dagger[z,\mathcal{H}]U = U^\dagger\frac{ip_z}{m}U = i\frac{p_z(t)}{m}\mathbf{I} = i\frac{p_z}{m}\mathbf{I}. \tag{2.48}$$

Therefore, integrating yields

$$z(t) = \frac{p_z}{m}t + z(0). \tag{2.49}$$

Omitting the obvious $\mathbf{I}$, the time dependence of x is given by

$$i\frac{d}{dt}x(t) = U^\dagger[x,\mathcal{H}]U = \frac{1}{2m}U^\dagger[x,(p_x-\mathbf{A}_x)^2]U = \frac{i}{m}U^\dagger\left(p_x-\mathbf{A}_x\right)U = i\frac{p_x(t)-\mathbf{A}_x(t)}{m}. \tag{2.50}$$

Note that the vector potential $\mathbf{A}_x$ also evolves with time in the Heisenberg representation according to $\mathbf{A}_x(t) = U^\dagger\mathbf{A}_xU$, due to the non-Abelian nature of the potential. A similar equation of motion holds for $y(t)$, and we obtain

$$\frac{d}{dt}x(t) = \frac{p_x(t)-\mathbf{A}_x(t)}{m}, \qquad \frac{d}{dt}y(t) = \frac{p_y(t)-\mathbf{A}_y(t)}{m}. \tag{2.51}$$

Next, we need to look at the time evolution of the vector potential in the Heisenberg representation. From the Heisenberg equations of motion, we obtain

$$\begin{aligned} i\frac{d}{dt}\mathbf{A}_x(t) &= U^\dagger[\mathbf{A}_x,\mathcal{H}]U = \frac{1}{2m}U^\dagger[\mathbf{A}_x,(p_y-\mathbf{A}_y)^2]U \\ &= -\frac{1}{2m}U^\dagger\left([\mathbf{A}_x,\mathbf{A}_y]\left(p_y-\mathbf{A}_y\right)+\left(p_y-\mathbf{A}_y\right)[\mathbf{A}_x,\mathbf{A}_y]\right)U \\ &= -\frac{i}{2m}U^\dagger\left(\mathbf{B}_z\left(p_y-\mathbf{A}_y\right)+\left(p_y-\mathbf{A}_y\right)\mathbf{B}_z\right)U. \end{aligned} \tag{2.52}$$

Therefore, we have

$$\frac{d}{dt}\mathbf{A}_x(t) = -\frac{1}{2m}\left(2p_y\mathbf{B}_z(t)-\mathbf{B}_z(t)\mathbf{A}_y(t)-\mathbf{A}_y(t)\mathbf{B}_z(t)\right). \tag{2.53}$$

Similarly, for $\mathbf{A}_y(t)$, we have

$$\frac{d}{dt}\mathbf{A}_y(t) = \frac{1}{2m}\left(2p_x\mathbf{B}_z(t) - \mathbf{B}_z(t)\mathbf{A}_x(t) - \mathbf{A}_x(t)\mathbf{B}_z(t)\right). \tag{2.54}$$

Finally, we need an equation of motion for $\mathbf{B}_z(t)$, which is

$$\begin{aligned}\frac{d}{dt}\mathbf{B}_z(t) &= \frac{1}{i}\frac{d}{dt}[\mathbf{A}_x(t), \mathbf{A}_y(t)] = -U^\dagger[[\mathbf{A}_x, \mathbf{A}_y], \mathcal{H}]U \\ &= -\frac{1}{2m}U^\dagger[[\mathbf{A}_x, \mathbf{A}_y], (p_x - \mathbf{A}_x)^2 + (p_y - \mathbf{A}_y)^2]U.\end{aligned} \tag{2.55}$$

Before choosing a particular vector potential, let us see how the change in species, which corresponds to the change in hyperfine species in ultracold gases, occur in this setup. For example, suppose the system is originally prepared in the first species, whose state can be written as $(1, 0)^t$, apart from the center-of-mass wavefunction. Then, at a later time t, the probability of finding the particle in the first species is given by

$$\begin{pmatrix}1 & 0\end{pmatrix} U^\dagger \begin{pmatrix}1 & 0\\ 0 & 0\end{pmatrix} U \begin{pmatrix}1\\ 0\end{pmatrix}. \tag{2.56}$$

Then, defining

$$\mathbf{P}_1 = \begin{pmatrix}1 & 0\\ 0 & 0\end{pmatrix}, \tag{2.57}$$

the probability of finding the particle in the first species can be calculated through the Heisenberg representation of $\mathbf{P}_1$, whose time evolution is

$$\begin{aligned}i\frac{d}{dt}\mathbf{P}_1(t) &= U^\dagger[\mathbf{P}_1, \mathcal{H}]U \\ &= \frac{1}{2m}U^\dagger[\mathbf{P}_1, (p_x - \mathbf{A}_x)^2 + (p_y - \mathbf{A}_y)^2]U.\end{aligned} \tag{2.58}$$

To simplify further, we need a specific choice of the vector potential, which we will do in the next section.

Rashba-Dresselhaus

Now, for the sake of concreteness, we consider a Rashba-Dresselhaus-type of non-Abelian gauge field: $\mathbf{A}_x = -\kappa\sigma_x$, $\mathbf{A}_y = -\kappa\sigma_y$, and $\mathbf{A}_z = 0$ with κ being a constant. For this vector potential, the

magnetic field is $\mathbf{B}_z = [\mathbf{A}_x, \mathbf{A}_y]/i = 2\kappa^2\sigma_z$. Then, the equation of motion for $\mathbf{B}_z(t)$ is

$$\begin{aligned}\frac{d}{dt}\mathbf{B}_z(t) &= -\frac{1}{2m}U^\dagger[[\mathbf{A}_x, \mathbf{A}_y], (p_x - \mathbf{A}_x)^2 + (p_y - \mathbf{A}_y)^2]U \\ &= \frac{2\kappa^2}{i}\frac{1}{2m}U^\dagger[\sigma_z, (p_x - \mathbf{A}_x)^2 + (p_y - \mathbf{A}_y)^2]U \\ &= \frac{\kappa^2}{im}U^\dagger[\sigma_z, -2p_x\mathbf{A}_x - 2p_y\mathbf{A}_y]]U \\ &= \frac{\kappa^3}{im}U^\dagger(4ip_x\sigma_y - 4ip_y\sigma_x)U \\ &= \frac{4\kappa^2}{m}\left(p_y\mathbf{A}_x(t) - p_x\mathbf{A}_y(t)\right). \end{aligned} \tag{2.59}$$

Meanwhile, the equations of motion for $\mathbf{A}_x$ and $\mathbf{A}_y$ are

$$\begin{aligned}\frac{d}{dt}\mathbf{A}_x(t) &= -\frac{1}{2m}U^\dagger\left(2p_y\mathbf{B}_z - \mathbf{B}_z\mathbf{A}_y - \mathbf{A}_y\mathbf{B}_z\right)U \\ &= -\frac{1}{2m}U^\dagger\left(4\kappa^2 p_y\sigma_z + 2\kappa^3\sigma_z\sigma_y + 2\kappa^3\sigma_y\sigma_z\right)U \\ &= -\frac{1}{2m}U^\dagger 4\kappa^2 p_y\sigma_z U \\ &= -\frac{p_y}{m}\mathbf{B}_z(t) \end{aligned} \tag{2.60}$$

$$\begin{aligned}\frac{d}{dt}\mathbf{A}_y(t) &= \frac{1}{2m}\left(2p_x\mathbf{B}_z(t) - \mathbf{B}_z(t)\mathbf{A}_x(t) - \mathbf{A}_x(t)\mathbf{B}_z(t)\right) \\ &= \frac{p_x}{m}\mathbf{B}_z(t). \end{aligned} \tag{2.61}$$

Therefore, we can write

$$\begin{aligned}\frac{d^2}{dt^2}\left(p_y\mathbf{A}_x(t) - p_x\mathbf{A}_y(t)\right) &= -\frac{p_y^2}{m}\frac{d}{dt}\mathbf{B}_z(t) - \frac{p_x^2}{m}\frac{d}{dt}\mathbf{B}_z(t) \\ &= -\frac{p_x^2 + p_y^2}{m}\frac{4\kappa^2}{m}\left(p_y\mathbf{A}_x(t) - p_x\mathbf{A}_y(t)\right). \end{aligned} \tag{2.62}$$

For convenience, define $p_\perp = \sqrt{p_x^2 + p_y^2}$. Then, the solution to the above differential equation is

$$p_y\mathbf{A}_x(t) - p_x\mathbf{A}_y(t) = \mathbf{C}\sin\left(\frac{2\kappa p_\perp}{m}t\right) + \mathbf{D}\cos\left(\frac{2\kappa p_\perp}{m}t\right), \tag{2.63}$$

where, setting $t = 0$, we see

$$\mathbf{D} = p_y\mathbf{A}_x - p_x\mathbf{A}_y. \tag{2.64}$$

$\mathbf{C}$ is determined by taking the derivative of (2.63):

$$\begin{aligned}\frac{d}{dt}\left(p_y\mathbf{A}_x(t) - p_x\mathbf{A}_y(t)\right) &= -\frac{p_y^2}{m}\mathbf{B}_z(t) - \frac{p_x^2}{m}\mathbf{B}_z(t) = -\frac{p_\perp^2}{m}\mathbf{B}_z(t) \\ &= \frac{2\kappa p_\perp}{m}\mathbf{C}\cos\left(\frac{2\kappa p_\perp}{m}t\right) - \frac{2\kappa p_\perp}{m}\mathbf{D}\sin\left(\frac{2\kappa p_\perp}{m}t\right), \end{aligned} \tag{2.65}$$

from which we see

$$\mathbf{B}_z(t) = -\frac{2\kappa}{p_\perp}\mathbf{C}\cos\left(\frac{2\kappa p_\perp}{m}t\right) + \frac{2\kappa}{p_\perp}\mathbf{D}\sin\left(\frac{2\kappa p_\perp}{m}t\right). \tag{2.66}$$

Taking $t = 0$, we may conclude that

$$\mathbf{C} = -\frac{p_\perp}{2\kappa}\mathbf{B}_z = -p_\perp\kappa\sigma_z. \tag{2.67}$$

Now, we can find $\mathbf{A}_x(t)$ and $\mathbf{A}_y(t)$.

$$\frac{d}{dt}\mathbf{A}_x(t) = -\frac{p_y}{m}\mathbf{B}_z(t) = \frac{2\kappa p_y}{mp_\perp}\mathbf{C}\cos\left(\frac{2\kappa p_\perp}{m}t\right) - \frac{2\kappa p_y}{mp_\perp}\mathbf{D}\sin\left(\frac{2\kappa p_\perp}{m}t\right) \tag{2.68}$$

$$\frac{d}{dt}\mathbf{A}_y(t) = \frac{p_x}{m}\mathbf{B}_z(t) = -\frac{2\kappa p_x}{mp_\perp}\mathbf{C}\cos\left(\frac{2\kappa p_\perp}{m}t\right) + \frac{2\kappa p_x}{mp_\perp}\mathbf{D}\sin\left(\frac{2\kappa p_\perp}{m}t\right). \tag{2.69}$$

These equations can be integrated to give

$$\mathbf{A}_x(t) = \frac{p_y}{p_\perp^2}\left(\mathbf{C}\sin\left(\frac{2\kappa p_\perp}{m}t\right) + \mathbf{D}\cos\left(\frac{2\kappa p_\perp}{m}t\right) - \mathbf{D}\right) + \mathbf{A}_x \tag{2.70}$$

$$\mathbf{A}_y(t) = -\frac{p_x}{p_\perp^2}\left(\mathbf{C}\sin\left(\frac{2\kappa p_\perp}{m}t\right) + \mathbf{D}\cos\left(\frac{2\kappa p_\perp}{m}t\right) - \mathbf{D}\right) + \mathbf{A}_y. \tag{2.71}$$

Note that they give the correct values at $t = 0$.

We can now finally write down $x(t)$ and $y(t)$. The equations of motion were

$$\begin{aligned}\frac{d}{dt}x(t) &= \frac{p_x(t) - \mathbf{A}_x(t)}{m} \\ &= \frac{p_x - \mathbf{A}_x}{m} - \frac{p_y}{mp_\perp^2}\left(\mathbf{C}\sin\left(\frac{2\kappa p_\perp}{m}t\right) + \mathbf{D}\cos\left(\frac{2\kappa p_\perp}{m}t\right) - \mathbf{D}\right)\end{aligned} \tag{2.72}$$

$$\begin{aligned}\frac{d}{dt}y(t) &= \frac{p_y(t) - \mathbf{A}_y(t)}{m} \\ &= \frac{p_y - \mathbf{A}_y}{m} + \frac{p_x}{mp_\perp^2}\left(\mathbf{C}\sin\left(\frac{2\kappa p_\perp}{m}t\right) + \mathbf{D}\cos\left(\frac{2\kappa p_\perp}{m}t\right) - \mathbf{D}\right).\end{aligned} \tag{2.73}$$

Integrating yields

$$x(t) = \frac{p_x - \mathbf{A}_x}{m}t - \frac{p_y}{2\kappa p_\perp^3}\left(\mathbf{C} - \mathbf{C}\cos\left(\frac{2\kappa p_\perp}{m}t\right) + \mathbf{D}\sin\left(\frac{2\kappa p_\perp}{m}t\right) - \frac{2\kappa p_\perp}{m}Dt\right) + x(0) \tag{2.74}$$

$$y(t) = \frac{p_y - \mathbf{A}_y}{m}t + \frac{p_x}{2\kappa p_\perp^3}\left(\mathbf{C} - \mathbf{C}\cos\left(\frac{2\kappa p_\perp}{m}t\right) + \mathbf{D}\sin\left(\frac{2\kappa p_\perp}{m}t\right) - \frac{2\kappa p_\perp}{m}Dt\right) + y(0), \tag{2.75}$$

with

$$\mathbf{C} = -\frac{p_\perp}{2\kappa}\mathbf{B}_z = -p_\perp\kappa\sigma_z \tag{2.76}$$

$$\mathbf{D} = p_y\mathbf{A}_x - p_x\mathbf{A}_y. \tag{2.77}$$

At this point, $x(t)$ and $y(t)$ are 2×2 matrices. To obtain the motion of a particle, we need to take the expectation values with respect to the initial state we want to consider. We can also calculate the probability of being in the first (hyperfine) species $\mathbf{P}_1(t)$.

$$\begin{aligned} i\frac{d}{dt}\mathbf{P}_1(t) &= \frac{1}{2m}U^\dagger[\mathbf{P}_1, (p_x - \mathbf{A}_x)^2 + (p_y - \mathbf{A}_y)^2]U \\ &= -\frac{1}{m}U^\dagger[\mathbf{P}_1, p_x\mathbf{A}_x + p_y\mathbf{A}_y]U \\ &= \frac{\kappa}{m}U^\dagger(p_x[\mathbf{P}_1, \sigma_x] + p_y[\mathbf{P}_1, \sigma_y])U \\ &= \frac{\kappa}{m}U^\dagger(p_x i\sigma_y - p_y i\sigma_x)U \\ &= i\frac{1}{m}(p_y\mathbf{A}_x(t) - p_x\mathbf{A}_y(t)), \\ &= i\frac{1}{m}\left(\mathbf{C}\sin\left(\frac{2\kappa p_\perp}{m}t\right) + \mathbf{D}\cos\left(\frac{2\kappa p_\perp}{m}t\right)\right). \end{aligned} \tag{2.78}$$

Therefore,

$$\begin{aligned} \mathbf{P}_1(t) &= \frac{1}{2\kappa p_\perp}\left(\mathbf{C} - \mathbf{C}\cos\left(\frac{2\kappa p_\perp}{m}t\right) + \mathbf{D}\sin\left(\frac{2\kappa p_\perp}{m}t\right)\right) + \mathbf{P}_1 \\ &= -\frac{\sigma_z}{2}\left(1 - \cos\left(\frac{2\kappa p_\perp}{m}t\right)\right) - \frac{p_y\sigma_x - p_x\sigma_y}{2p_\perp}\sin\left(\frac{2\kappa p_\perp}{m}t\right) + \mathbf{P}_1. \end{aligned} \tag{2.79}$$

Thus, we solved the Heisenberg equations of motion for the particle moving in a non-Abelian field with $\vec{\mathbf{A}} = -\kappa(\sigma_x, \sigma_y, 0)$. After taking the expectation values with respect to the initial state of interest, we see that if the particle does not have a momentum in z direction, the particle will move in the xy plane forming circular orbit with the center of the circular motion moving linearly. Additionally, we find that the probability of being in the first species oscillates with time.

In the next subsection, we discuss the unique dispersion of Rashba-Dresselhaus spin-orbit coupling.

2.4.4 Single particle spectrum

The single particle Hamiltonian of Rashba-Dresselhaus spin-orbit coupling can be exactly diagonalized. Here, we consider anisotropic Rashba-Dresselhaus spin-orbit coupling described by the following Hamiltonian in 2×2 spinor basis

$$\mathcal{H} = \frac{(\mathbf{p}I - \vec{\mathbf{A}})^2}{2m} - \frac{\eta^2\kappa^2}{2m}\mathbf{I} \tag{2.80}$$

with

$$\vec{\mathbf{A}} = (\mathbf{A}_x, \mathbf{A}_y, \mathbf{A}_z) = -\kappa(\sigma_x, \eta\sigma_y, 0), \tag{2.81}$$

where $0 \leq \eta \leq 1$ sets the anisotropy. When $\eta = 1$, the spin-orbit interaction is isotropic. The last term $-\eta^2\kappa^2 I/2m$ in the Hamiltonian is added so that the system's ground state has zero energy. Then, diagonalizing

$$\mathcal{H} = \frac{p^2+\kappa^2}{2m}\mathbf{I} + \frac{\kappa}{m}(p_x\sigma_x + \eta p_y\sigma_y) = \frac{1}{2m}\begin{pmatrix} p^2+\kappa^2 & 2\kappa(p_x - i\eta p_y) \\ 2\kappa(p_x + i\eta p_y) & p^2+\kappa^2 \end{pmatrix}, \tag{2.82}$$

we obtain the single particle energy spectrum

$$\epsilon_\pm(\mathbf{p}) = \frac{(p_\perp \pm \kappa)^2 + (1-\eta^2)p_y^2 + p_z^2}{2m}. \tag{2.83}$$

where we defined $p^2 \equiv p_x^2 + p_y^2 + p_z^2$ and $p_\perp e^{i\phi} \equiv p_x + i\eta p_y$. There are two branches $\epsilon_-(\mathbf{p})$ and $\epsilon_+(\mathbf{p})$ in the dispersion. The corresponding eigenvectors are

$$\mathbf{v}_\pm(\mathbf{p}) = \frac{1}{\sqrt{2}}\begin{pmatrix} 1 \\ \pm e^{i\phi} \end{pmatrix}, \tag{2.84}$$

which implies that the eigenstates of the Hamiltonian are

$$\Psi_{\pm,\mathbf{p}}(\mathbf{r}) = \frac{e^{i\mathbf{p}\cdot\mathbf{r}}}{\sqrt{2}}\begin{pmatrix} 1 \\ \pm e^{i\phi} \end{pmatrix} \tag{2.85}$$

in the position-space basis.

In the second quantized basis, the original Hamiltonian is

$$\mathcal{H} = \sum_{\mathbf{p}} \begin{pmatrix} a_{\mathbf{p}}^\dagger & b_{\mathbf{p}}^\dagger \end{pmatrix} \frac{(\mathbf{p}\mathbf{I} - \vec{\mathbf{A}})^2 - \eta^2\kappa^2 I}{2m} \begin{pmatrix} a_{\mathbf{p}} \\ b_{\mathbf{p}} \end{pmatrix}, \tag{2.86}$$

where $a_{\mathbf{p}}$ and $b_{\mathbf{p}}$ are the annihilation operators of particles with momentum $\mathbf{p}$ in pseudospin species a and b, respectively. Defining the new operators $\alpha_{\mathbf{p}}$ and $\beta_{\mathbf{p}}$ by

$$\begin{pmatrix} \alpha_{\mathbf{p}} \\ \beta_{\mathbf{p}} \end{pmatrix} \equiv \frac{1}{\sqrt{2}}\begin{pmatrix} 1 & -e^{-i\phi} \\ 1 & e^{-i\phi} \end{pmatrix}\begin{pmatrix} a_{\mathbf{p}} \\ b_{\mathbf{p}} \end{pmatrix}, \tag{2.87}$$

the Hamiltonian is diagonalized as

$$\mathcal{H} = \sum_{\mathbf{p}} \left(\epsilon_-(\mathbf{p})\alpha_{\mathbf{p}}^\dagger\alpha_{\mathbf{p}} + \epsilon_+(\mathbf{p})\beta_{\mathbf{p}}^\dagger\beta_{\mathbf{p}} \right). \tag{2.88}$$

It is worth noting that the transformation from (a-b) basis to (α-β) basis depends on the momentum, as one can see from (2.87). It is this momentum dependence of the transformation that causes the momentum dependence of the interaction, as we will see in the following chapters.

The single particle energy spectrum (2.83) is drastically modified from the free case, which is just $p^2/2m$. The energy spectrum with spin-orbit coupling is plotted in Figure 2.2.

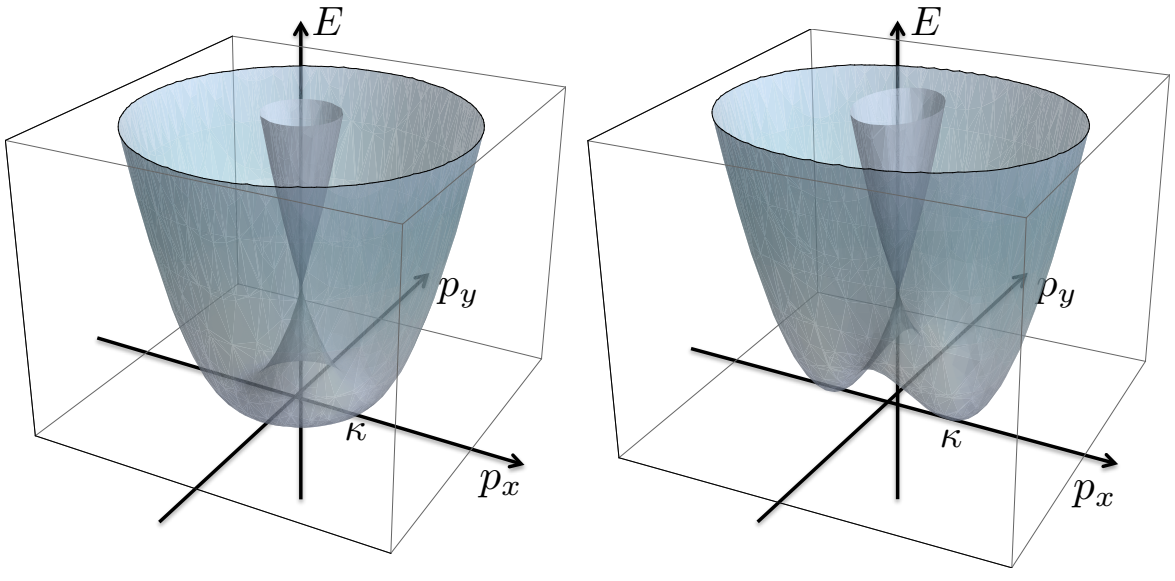

(a) (b)

Figure 2.2: Dispersion of a particle with Rashba-Dresselahsu spin-orbit coupling (2.83). The dispersion in z-direction, which is just $p_z^2/2m$, is not drawn. (a) Pure Rashba spin-orbit coupling ($\eta = 1$) with degeneracy along $(p_\perp, p_z) = (\kappa, 0)$. (b) Rashba-Dresselhaus mixture ($\eta = 0.7$) with two-fold degeneracy at $\mathbf{p} = (\pm\kappa, 0, 0)$.

When $0 \leq \eta < 1$, the energy spectrum has doubly degenerate minima at $\mathbf{p} = (\pm\kappa, 0, 0)$. On the other hand, when $\eta = 1$, the energy spectrum is circularly degenerate along $p_\perp = \kappa$. These degenerate single-particle ground states have nontrivial consequences in many-body Bose systems and many researchers have analyzed the properties of ultracold bosonic systems with Rashba-Dresselhaus spin-orbit coupling [46, 47, 48, 49, 50, 51, 52, 53, 54].

Before introducing the interaction, let us consider the possibility of BEC in the ideal Bose gas with Rashba-Dresselhaus spin-orbit coupling.

2.4.5 Bose-Einstein Condensation without interaction

Introducing the chemical potential μ, the number density of excited particles at temperature $T = 1/\beta$ is given by

$$n_{ex} = \frac{1}{V}\sum_{\mathbf{p}}\left(\frac{1}{e^{\beta(\epsilon_-(\mathbf{p})-\mu)}-1}+\frac{1}{e^{\beta(\epsilon_+(\mathbf{p})-\mu)}-1}\right). \tag{2.89}$$

Since the minimum value of $\epsilon_\pm(\mathbf{p})$ is zero, the chemical potential must be negative, as usual. The right hand side of (2.89) is an increasing function of the chemical potential, and the BEC is formed at a temperature where the right hand side equals the total number of particles when $\mu = 0$. Then, at the critical temperature T_c,

$$\begin{aligned} n &= \int \frac{d^3p}{(2\pi)^3}\left(\frac{1}{e^{\beta_c\epsilon_-(\mathbf{p})}-1}+\frac{1}{e^{\beta_c\epsilon_+(\mathbf{p})}-1}\right) \\ &= (2mT_c)^{3/2}\int\frac{d^3p}{(2\pi)^3}\left(\frac{1}{e^{(\sqrt{p_x^2+\eta^2p_y^2}-\kappa/\sqrt{2mT_c})^2+(1-\eta^2)p_y^2+p_z^2}-1}\right. \\ &\qquad\left.+\frac{1}{e^{(\sqrt{p_x^2+\eta^2p_y^2}+\kappa/\sqrt{2mT_c})^2+(1-\eta^2)p_y^2+p_z^2}-1}\right), \end{aligned} \tag{2.90}$$

where we have rescaled the variable of integration in the second line. For $0 \le \eta < 1$, for a given κ there always exists $T_c > 0$ which satisfies the above equation. However, for $\eta = 1$, the right hand side diverges and there is no $T_c > 0$ which can satisfy the equation. This means that for $\eta = 1$ there is no BEC transition at a finite temperature for an ideal Bose gas with Rashba-Dresselhaus spin-orbit coupling. Physically, this absence of BEC for $\eta = 1$ is due to the fact that because of the infinitely degenerate single-particle ground states the low-energy density of states becomes two-dimensional; focusing on the low-energy, the density of states is

$$\begin{aligned} D(E) &= \int\frac{d^3p}{(2\pi)^3}\delta(E-\epsilon_-(\mathbf{p})) = \int\frac{d^3p}{(2\pi)^3}\delta\left(E-\frac{(p_\perp-\kappa)^2+p_z^2}{2m}\right) \\ &= 2m\int\frac{p_\perp dp_\perp dp_z}{(2\pi)^2}\delta\left(2mE-(p_\perp-\kappa)^2-p_z^2\right) \\ &\approx 2m\kappa\int\frac{dp_\perp dp_z}{(2\pi)^2}\delta\left(2mE-p_\perp^2-p_z^2\right) \\ &= \frac{m\kappa}{2\pi}, \end{aligned} \tag{2.91}$$

which is constant as in two dimensional free Bose gas. Thus just as the ideal Bose gas in two dimensions does not form a BEC at finite temperatures (although superfluidity can appear through

a Kosterlitz-Thouless mechanism in the presence of interactions), the same mechanism leads to the absence of BEC at finite temperature in Bose gases with Rashba-Dresselhaus spin-orbit coupling in the absence of interactions.

Chapter 3

Stability of spin-orbit coupled BEC's against fluctuations

3.1 Introduction

Condensates of ultracold bosons in three dimensions with Rashba spin-orbit coupling differ from usual Bose-Einstein condensates (BEC's) in several important ways. In the absence of interparticle interactions, the low-lying density of states is two-dimensional [47], and thus condensation is destroyed by thermal fluctuations at any non-zero temperature. With interparticle interactions present, fluctuations around mean-field states lead at finite temperature to an instability of the plane-wave state in two dimensions [50]. In this chapter, we consider three-dimensional ultracold bosons with Rashba-Dresselhaus coupling, to investigate the effects of quantum and thermal fluctuations on a plane-wave Bose-Einstein condensation, and show that interactions in fact stabilize the condensate in 3D. This interaction-induced BEC is a unique feature of bosons with Rashba-Dresselhaus spin-orbit coupling, with no analogous system yet found. However, unlike in usual BEC's, a non-condensed state is not, as we show, kinematically forbidden at any non-zero temperature. Condensation, while favored at very low temperature, should disappear at high temperature. As in a BCS superconductor, where both a normal and condensed state are allowed at low temperature, the system should undergo a similar phase transition at a critical temperature. The materials in this chapter is based on [1].

We consider bosons with Rashba-Dresselhaus spin-orbit coupling in three dimensions with s-

wave contact interactions, described by the Hamiltonian

$$\begin{aligned}\mathcal{H} &= \sum_{\mathbf{p}} \begin{pmatrix} a_{\mathbf{p}}^\dagger & b_{\mathbf{p}}^\dagger \end{pmatrix} \left(\frac{p^2+\kappa^2}{2m} I + \frac{\kappa}{m} \left(p_x \sigma_x + \eta p_y \sigma_y \right) \right) \begin{pmatrix} a_{\mathbf{p}} \\ b_{\mathbf{p}} \end{pmatrix} \\ &\quad + \frac{1}{2V} \sum_{\mathbf{p}_1+\mathbf{p}_2=\mathbf{p}_3+\mathbf{p}_4} \left(g_{aa}\ a_{\mathbf{p}_4}^\dagger a_{\mathbf{p}_3}^\dagger a_{\mathbf{p}_2} a_{\mathbf{p}_1} + g_{bb}\ b_{\mathbf{p}_4}^\dagger b_{\mathbf{p}_3}^\dagger b_{\mathbf{p}_2} b_{\mathbf{p}_1} + 2 g_{ab}\ a_{\mathbf{p}_4}^\dagger b_{\mathbf{p}_3}^\dagger b_{\mathbf{p}_2} a_{\mathbf{p}_1} \right) \\ &\equiv \mathcal{H}_{\mathrm{kin}} + \mathcal{H}_{\mathrm{int}}. \end{aligned} \tag{3.1}$$

In this chapter, we use the (constant) mean-field couplings g_{ij}; effects of higher order corrections and the renormalization of the effective interaction are considered in the next chapter.

We first discuss the ground state phase diagram within mean-field theory for both anisotropic and isotropic spin-orbit couplings. Then, focusing on an isotropic spin-orbit coupling, we consider the quantum and thermal fluctuations upon the mean-field ground state and investigate the stability of BECs against these fluctuations.

3.2 Mean-field ground state

3.2.1 Anisotropic case

We begin by considering the ground state of the anisotropic case ($0 \le \eta < 1$). When the spin-orbit coupling is anisotropic, the single-particle spectrum has two-fold degenerate minima at $\mathbf{p} = (\pm\kappa, 0, 0) \equiv \pm\boldsymbol{\kappa}$. Apart from quantum depletion of condensates, we expect that the condensate is formed on these two minima. We begin, therefore, by positing the ansatz state[1]

$$|\Psi\rangle = \frac{1}{\sqrt{N!}} \left(c_{\boldsymbol{\kappa}} \alpha_{\boldsymbol{\kappa}}^\dagger + c_{-\boldsymbol{\kappa}} \alpha_{-\boldsymbol{\kappa}}^\dagger \right)^N |0\rangle, \tag{3.2}$$

where $|0\rangle$ is a vacuum state with no particle, the operator α is defined by (2.87), and the normalization requires $|c_{\boldsymbol{\kappa}}|^2 + |c_{-\boldsymbol{\kappa}}|^2 = 1$.

We wish to determine the coefficients $c_{\boldsymbol{\kappa}}$ and $c_{-\boldsymbol{\kappa}}$ which minimize the energy of the system. By an explicit calculation, we obtain

$$\langle\Psi|\mathcal{H}|\Psi\rangle = \langle\Psi|\mathcal{H}_{\mathrm{int}}|\Psi\rangle = \frac{N(N-1)}{8V} \left(g_{aa} + g_{bb} + 2g_{ab} + 2|c_{\boldsymbol{\kappa}}|^2 |c_{-\boldsymbol{\kappa}}|^2 \left(g_{aa} + g_{bb} - 2g_{ab} \right) \right). \tag{3.3}$$

[1]Note that we can also consider fragmented condensate states as a possible ground state. However, as described in [55], the fragmented condensate states are quite fragile against external perturbations, so considering realistic situations we do not worry about the possibility of fragmented condensates

Thus, if $g_{aa}+g_{bb} > 2g_{ab}$, $(c_{\boldsymbol{\kappa}}, c_{-\boldsymbol{\kappa}}) = (1,0)$ or $(0,1)$ is preferred, and if $g_{aa}+g_{bb} < 2g_{ab}$, $(|c_{\boldsymbol{\kappa}}|, |c_{-\boldsymbol{\kappa}}|) = (1/\sqrt{2}, 1/\sqrt{2})$ is preferred.

The former case, $(c_{\boldsymbol{\kappa}}, c_{-\boldsymbol{\kappa}}) = (1,0)$ or $(0,1)$, is a BEC made of particles with a single momentum, and is called a *plane wave state*. The latter case $(|c_{\boldsymbol{\kappa}}|, |c_{-\boldsymbol{\kappa}}|) = (1/\sqrt{2}, 1/\sqrt{2})$ is a BEC made of two different momenta, forming a standing wave, and is called a *striped state*.

3.2.2 Isotropic case

When the spin-orbit coupling is isotropic ($\eta = 1$), the single-particle ground state is highly degenerate. Defining $\alpha_\theta \equiv \alpha_{(\kappa\cos\theta, \kappa\sin\theta, 0)}$, a BEC ansatz generally takes the following form:

$$|\Psi\rangle = \frac{1}{\sqrt{N}} \left(\sum_{0\le\theta<2\pi} c_\theta \alpha_\theta^\dagger \right)^N |0\rangle = \frac{1}{\sqrt{N}} \left(\sum_{0\le\theta<2\pi} c_\theta \frac{a_\theta^\dagger - e^{-i\theta} b_\theta^\dagger}{\sqrt{2}} \right)^N |0\rangle \tag{3.4}$$

with the normalization $\sum_\theta |c_\theta|^2 = 1$. One can prove

$$\langle\Psi|\mathcal{H}|\Psi\rangle = \frac{N(N-1)}{8V} \sum_{\mathbf{p}_1+\mathbf{p}_2=\mathbf{p}_3+\mathbf{p}_4} \left(g_{aa} + g_{bb} e^{i(\theta_4+\theta_3-\theta_2-\theta_1)} + 2g_{ab} e^{i(\theta_3-\theta_2)} \right) c_{\mathbf{p}_4}^* c_{\mathbf{p}_3}^* c_{\mathbf{p}_2} c_{\mathbf{p}_1}. \tag{3.5}$$

The combinations of $(\mathbf{p}_1, \mathbf{p}_2, \mathbf{p}_3, \mathbf{p}_4)$ which are on the single-particle ground states and conserve the momentum are

$$(\mathbf{p}, \mathbf{p}, \mathbf{p}, \mathbf{p}) \tag{3.6}$$

$$(\mathbf{p}, -\mathbf{p}, \mathbf{p}', -\mathbf{p}') \tag{3.7}$$

$$(\mathbf{p}, \mathbf{p}', \mathbf{p}, \mathbf{p}') \text{ and } (\mathbf{p}, \mathbf{p}', \mathbf{p}', \mathbf{p}) \text{ with } \mathbf{p} \neq \pm\mathbf{p}', \tag{3.8}$$

where $\mathbf{p}$ and $\mathbf{p}'$ satisfy $p_\perp = p'_\perp = \kappa$. Then,

$$\begin{aligned}\langle\Psi|\mathcal{H}|\Psi\rangle = \frac{N(N-1)}{8V} \Bigg[& 2(g_{aa}+g_{bb}+g_{ab}) - (g_{aa}+g_{bb}+2g_{ab}) \sum_\theta |c_\theta|^4 + 2g_{ab} \left(\sum_\theta e^{-i\theta} |c_\theta|^2 \right)^2 \\ & -2(g_{aa}+g_{bb}) \sum_\theta |c_{\theta+\pi}|^2 |c_\theta|^2 + g_{aa} \left| \sum_\theta c_{\theta+\pi} c_\theta \right|^2 + g_{bb} \left| \sum_\theta e^{-2i\theta} c_{\theta+\pi} c_\theta \right|^2 \Bigg]. \end{aligned} \tag{3.9}$$

We wish to find values of c_θ which minimize the energy of the system. However, finding a general condition for c_θ is difficult, so here we estimate the energy for several configurations of c_θ and discuss which state plausibly has the lowest energy.

Case I : $c_0 = 1$ (plane wave state)

$$\langle\Psi|\mathcal{H}|\Psi\rangle = \frac{N(N-1)}{8V}\left[2(g_{aa}+g_{bb}+g_{ab})-(g_{aa}+g_{bb})\right] \tag{3.10}$$

Case II : $c_0 = c_\pi = 1/\sqrt{2}$ (striped state)

$$\langle\Psi|\mathcal{H}|\Psi\rangle = \frac{N(N-1)}{8V}\left[2(g_{aa}+g_{bb}+g_{ab})-\frac{g_{aa}+g_{bb}+2g_{ab}}{2}\right] \tag{3.11}$$

Case III : $c_{2\pi n/M} = 1/\sqrt{M}$ with $n = 0, 1, \cdots M-1$, and $M \geq 3$ is an odd integer

$$\langle\Psi|\mathcal{H}|\Psi\rangle = \frac{N(N-1)}{8V}\left[2(g_{aa}+g_{bb}+g_{ab})-\frac{g_{aa}+g_{bb}+2g_{ab}}{M}\right] \tag{3.12}$$

Case IV : $c_{2\pi n/M} = 1/\sqrt{M}$ with $n = 0, 1, \cdots M-1$, and $M \geq 4$ is an even integer

$$\langle\Psi|\mathcal{H}|\Psi\rangle = \frac{N(N-1)}{8V}\left[2(g_{aa}+g_{bb}+g_{ab})-\frac{g_{aa}+g_{bb}+2g_{ab}}{M}-\frac{2(g_{aa}+g_{bb})}{M}+g_{aa}\right] \tag{3.13}$$

Comparing these four cases, we see that if $g_{aa}+g_{bb} > 2g_{ab}$, case I (plane wave state) wins, and if $g_{aa}+g_{bb} < 2g_{ab}$, case II (striped state) wins. In fact, a numerical calculation also gives the same result [49], which is exactly the same as the anisotropic case. Thus we find that, in Rashba-Dresselhaus coupled Bose systems, the plane wave state and the striped state are the two states which are preferred as the ground state within mean-field theory with the bare couplings. Figure 3.1 is the mean-field phase diagram which is valid for both anisotropic and isotropic cases.

In the following section, we consider the effects of fluctuations upon the mean-field ground state and discuss the stability of the condensates.

3.3 Effects of fluctuations

In this section, we focus on the isotropic spin-orbit coupling $\eta = 1$ with isotropic interaction $g \equiv g_{aa} = g_{bb} = g_{ab}$. The plane wave state and the striped state are degenerate ground states within mean-field theory with the bare couplings, but a study including quantum and thermal fluctuations within the bare couplings shows that the plane wave state is favored [54]. Therefore here we consider a plane wave ground state with wave vector $\boldsymbol{\kappa} \equiv (\kappa, 0, 0)$, with macroscopic occupation, above which quantum and thermal fluctuation will be applied.

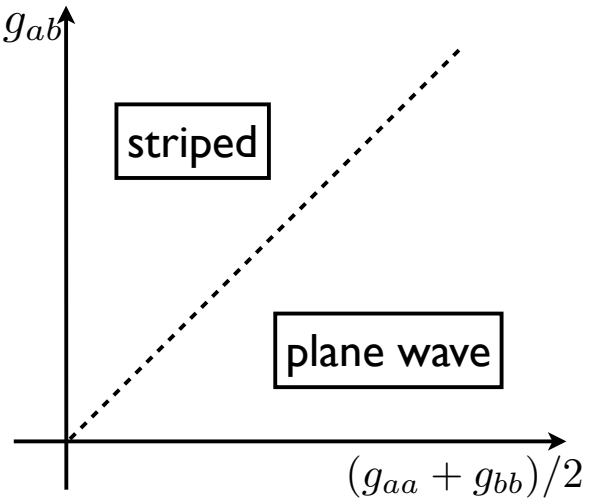

Figure 3.1: The mean-field phase diagram of bosons with Rashba-Dresselhaus spin-orbit coupling with mean-field (bare) interparticle interactions.

Since the operator $(a^\dagger_{\boldsymbol{\kappa}} - b^\dagger_{\boldsymbol{\kappa}})/\sqrt{2}$ creates a particle in the single-particle ground state with momentum $\boldsymbol{\kappa}$, it is easier to work in the following $(-,+)$ basis:

$$\begin{pmatrix} \psi_{-,\mathbf{p}} \\ \psi_{+,\mathbf{p}} \end{pmatrix} = \frac{1}{\sqrt{2}} \begin{pmatrix} 1 & -1 \\ 1 & 1 \end{pmatrix} \begin{pmatrix} a_{\mathbf{p}} \\ b_{\mathbf{p}} \end{pmatrix}. \tag{3.14}$$

The state created by $\psi^\dagger_{-,\boldsymbol{\kappa}}$ is macroscopically occupied. In terms of this $(-,+)$ basis, the original Hamiltonian becomes

$$\begin{aligned} \mathcal{H}' = &\sum_{\mathbf{p}} \begin{pmatrix} \psi^\dagger_{-,\mathbf{p}} & \psi^\dagger_{+,\mathbf{p}} \end{pmatrix} \left[\left(\frac{p^2+\kappa^2}{2m} - \mu \right) I + \frac{\kappa}{m} \left(-p_x \sigma_z + p_y \sigma_y \right) \right] \begin{pmatrix} \psi_{-,\mathbf{p}} \\ \psi_{+,\mathbf{p}} \end{pmatrix} \\ &+ \frac{g}{2V} \sum_{\mathbf{p}_1+\mathbf{p}_2=\mathbf{p}_3+\mathbf{p}_4} \left(\psi^\dagger_{-,\mathbf{p}_4} \psi^\dagger_{-,\mathbf{p}_3} \psi_{-,\mathbf{p}_2} \psi_{-,\mathbf{p}_1} + \psi^\dagger_{+,\mathbf{p}_4} \psi^\dagger_{+,\mathbf{p}_3} \psi_{+,\mathbf{p}_2} \psi_{+,\mathbf{p}_1} + 2\psi^\dagger_{-,\mathbf{p}_4} \psi^\dagger_{+,\mathbf{p}_3} \psi_{+,\mathbf{p}_2} \psi_{-,\mathbf{p}_1} \right). \end{aligned} \tag{3.15}$$

In the following, we derive the fluctuations of the system in terms of the single particle matrix Green ' s functions. We estimate the quantum depletion of the number of particles in the excited state, and also the lowest order correction to the energy due to quantum fluctuations. We then look at the infrared structure of the Green's functions to discuss the stability of condensate at finite temperature. We also obtain the free energy of a normal state and compare the states with and without condensates to discuss the phase transition at finite temperature.

3.3.1 Green's functions

We use the Bogoliubov approximation, where the operators $\psi^\dagger_{-,\boldsymbol{\kappa}}$ and $\psi_{-,\boldsymbol{\kappa}}$ in the Hamiltonian are replaced by $\sqrt{N_0}$, where N_0 is the number of condensate particles. Then the Hamiltonian becomes

$$\begin{aligned}
\mathcal{H}' \sim & -\mu N_0 + \frac{g}{2V}N_0^2 + \sum_{\mathbf{p}\neq\boldsymbol{\kappa}} \begin{pmatrix}\psi^\dagger_{-,\mathbf{p}} & \psi^\dagger_{+,\mathbf{p}}\end{pmatrix} \left[\left(\frac{p^2+\kappa^2}{2m}-\mu\right) I + \frac{\kappa}{m}\left(-p_x\sigma_z + p_y\sigma_y\right)\right] \begin{pmatrix}\psi_{-,\mathbf{p}} \\ \psi_{+,\mathbf{p}}\end{pmatrix} \\
& + \frac{g}{2V}\sqrt{N_0} \sum_{\substack{\boldsymbol{\kappa}+\mathbf{p}_2=\mathbf{p}_3+\mathbf{p}_4 \\ \mathbf{p}_i\neq\boldsymbol{\kappa}}} \left(2\psi^\dagger_{-,\mathbf{p}_4}\psi^\dagger_{-,\mathbf{p}_3}\psi_{-,\mathbf{p}_2} + 2\psi^\dagger_{-,\mathbf{p}_4}\psi^\dagger_{+,\mathbf{p}_3}\psi_{+,\mathbf{p}_2}\right) \\
& + \frac{g}{2V}\sqrt{N_0} \sum_{\substack{\mathbf{p}_1+\mathbf{p}_2=\mathbf{p}_3+\boldsymbol{\kappa} \\ \mathbf{p}_i\neq\boldsymbol{\kappa}}} \left(2\psi^\dagger_{-,\mathbf{p}_3}\psi_{-,\mathbf{p}_2}\psi_{-,\mathbf{p}_1} + 2\psi^\dagger_{+,\mathbf{p}_3}\psi_{+,\mathbf{p}_2}\psi_{-,\mathbf{p}_1}\right) \\
& + \frac{g}{2V}N_0 \sum_{\mathbf{p}\neq\boldsymbol{\kappa}} \left(4\psi^\dagger_{-,\mathbf{p}}\psi_{-,\mathbf{p}} + \psi^\dagger_{-,2\boldsymbol{\kappa}-\mathbf{p}}\psi^\dagger_{-,\mathbf{p}} + \psi_{-,2\boldsymbol{\kappa}-\mathbf{p}}\psi_{-,\mathbf{p}} + 2\psi^\dagger_{+,\mathbf{p}}\psi_{+,\mathbf{p}}\right) \\
& + \frac{g}{2V} \sum_{\substack{\mathbf{p}_1+\mathbf{p}_2=\mathbf{p}_3+\mathbf{p}_4 \\ \mathbf{p}_i\neq\boldsymbol{\kappa}}} \left(\psi^\dagger_{-,\mathbf{p}_4}\psi^\dagger_{-,\mathbf{p}_3}\psi_{-,\mathbf{p}_2}\psi_{-,\mathbf{p}_1} + \psi^\dagger_{+,\mathbf{p}_4}\psi^\dagger_{+,\mathbf{p}_3}\psi_{+,\mathbf{p}_2}\psi_{+,\mathbf{p}_1} + 2\psi^\dagger_{-,\mathbf{p}_4}\psi^\dagger_{+,\mathbf{p}_3}\psi_{+,\mathbf{p}_2}\psi_{-,\mathbf{p}_1}\right).
\end{aligned} \tag{3.16}$$

The chemical potential with the Hartree-Fock energy, which we call μ_0, is

$$\begin{aligned}
\mu_0 = \frac{\partial}{\partial N_0}\langle\mathcal{H}\rangle &= \left\langle \frac{g}{V}N_0 + \frac{g}{2V}\sum_{\mathbf{p}\neq\boldsymbol{\kappa}} \left(4\psi^\dagger_{-,\mathbf{p}}\psi_{-,\mathbf{p}} + \psi^\dagger_{-,2\boldsymbol{\kappa}-\mathbf{p}}\psi^\dagger_{-,\mathbf{p}} + \psi_{-,2\boldsymbol{\kappa}-\mathbf{p}}\psi_{-,\mathbf{p}} + 2\psi^\dagger_{+,\mathbf{p}}\psi_{+,\mathbf{p}}\right)\right\rangle \\
&= gn_0 + 2gn_- + gn_+.
\end{aligned} \tag{3.17}$$

From the approximated Hamiltonian (3.16), we would like to construct an equation of motion for Green's functions with Hartree-Fock energy included. In the Hartree-Fock approximation, the terms proportional to $\sqrt{N_0}$ in (3.16) do not contribute, thus, we can ignore these terms.

In terms of the following vector in Nambu-Gorkov representation

$$\begin{aligned}
\Psi_{\mathbf{p}}(t) &\equiv \begin{pmatrix}\psi_{-,\mathbf{p}}(t) & \psi^\dagger_{-,2\boldsymbol{\kappa}-\mathbf{p}}(t) & \psi_{+,\mathbf{p}}(t) & \psi^\dagger_{+,2\boldsymbol{\kappa}-\mathbf{p}}(t)\end{pmatrix}^t \\
&\equiv \begin{pmatrix}\psi_{-,\mathbf{p}}(t) & \psi^\dagger_{-,\mathbf{p}'}(t) & \psi_{+,\mathbf{p}}(t) & \psi^\dagger_{+,\mathbf{p}'}(t)\end{pmatrix}^t,
\end{aligned} \tag{3.18}$$

where t is the tranposition and $\mathbf{p}' \equiv 2\boldsymbol{\kappa} - \mathbf{p}$, we define the matrix Greens's function by

$$\begin{aligned}
&\mathbf{G}(\mathbf{p}; t_1, t_2) \equiv -i\langle T\Psi_{\mathbf{p}}(t_1)\Psi_{\mathbf{p}}(t_2)^\dagger\rangle \\
&= -i\left\langle T\begin{pmatrix}
\psi_{-,\mathbf{p}}(t_1)\psi^\dagger_{-,\mathbf{p}}(t_2) & \psi_{-,\mathbf{p}}(t_1)\psi_{-,\mathbf{p}'}(t_2) & \psi_{-,\mathbf{p}}(t_1)\psi^\dagger_{+,\mathbf{p}}(t_2) & \psi_{-,\mathbf{p}}(t_1)\psi_{+,\mathbf{p}'}(t_2) \\
\psi^\dagger_{-,\mathbf{p}'}(t_1)\psi^\dagger_{-,\mathbf{p}}(t_2) & \psi^\dagger_{-,\mathbf{p}'}(t_1)\psi_{-,\mathbf{p}'}(t_2) & \psi^\dagger_{-,\mathbf{p}'}(t_1)\psi^\dagger_{+,\mathbf{p}}(t_2) & \psi^\dagger_{-,\mathbf{p}'}(t_1)\psi_{+,\mathbf{p}'}(t_2) \\
\psi_{+,\mathbf{p}}(t_1)\psi^\dagger_{-,\mathbf{p}}(t_2) & \psi_{+,\mathbf{p}}(t_1)\psi_{-,\mathbf{p}'}(t_2) & \psi_{+,\mathbf{p}}(t_1)\psi^\dagger_{+,\mathbf{p}}(t_2) & \psi_{+,\mathbf{p}}(t_1)\psi_{+,\mathbf{p}'}(t_2) \\
\psi^\dagger_{+,\mathbf{p}'}(t_1)\psi^\dagger_{-,\mathbf{p}}(t_2) & \psi^\dagger_{+,\mathbf{p}'}(t_1)\psi_{-,\mathbf{p}'}(t_2) & \psi^\dagger_{+,\mathbf{p}'}(t_1)\psi^\dagger_{+,\mathbf{p}}(t_2) & \psi^\dagger_{+,\mathbf{p}'}(t_1)\psi_{+,\mathbf{p}'}(t_2)
\end{pmatrix}\right\rangle.
\end{aligned} \tag{3.19}$$

Writing down the Heisenberg equations of motion for $\psi_{-,\mathbf{p}}$ and $\psi_{+,\mathbf{p}}$, we can derive the equations of motion for the Green's function. The detailed derivation is given in the Appendix B, and the Green's function is

$$\mathbf{G}(\mathbf{p}, z) = \begin{pmatrix}
z - A & -gn_0 & i\frac{\kappa}{m}p_y & 0 \\
-gn_0 & -z - C & 0 & -i\frac{\kappa}{m}p'_y \\
-i\frac{\kappa}{m}p_y & 0 & z - B & 0 \\
0 & i\frac{\kappa}{m}p'_y & 0 & -z - D
\end{pmatrix}^{-1}, \tag{3.20}$$

where $\mathbf{G}(\mathbf{p}, z)$ is the Fourier transform of $\mathbf{G}(\mathbf{p}; t_1, t_2)$ defined in (B.15), and

$$A = \frac{p^2 - 2\kappa p_x + \kappa^2}{2m} - \mu + g(2n_0 + 2n_- + n_+) = \frac{(\mathbf{p} - \boldsymbol{\kappa})^2}{2m} - \mu + g(2n_0 + 2n_- + n_+) \tag{3.21}$$

$$B = \frac{p^2 + 2\kappa p_x + \kappa^2}{2m} - \mu + g(n_0 + n_- + 2n_+) = \frac{(\mathbf{p} + \boldsymbol{\kappa})^2}{2m} - \mu + g(n_0 + n_- + 2n_+) \tag{3.22}$$

$$C = \frac{p'^2 - 2\kappa p'_x + \kappa^2}{2m} - \mu + g(2n_0 + 2n_- + n_+) = \frac{(\mathbf{p}' - \boldsymbol{\kappa})^2}{2m} - \mu + g(2n_0 + 2n_- + n_+) \tag{3.23}$$

$$D = \frac{p'^2 + 2\kappa p'_x + \kappa^2}{2m} - \mu + g(n_0 + n_- + 2n_+) = \frac{(\mathbf{p}' + \boldsymbol{\kappa})^2}{2m} - \mu + g(n_0 + n_- + 2n_+). \tag{3.24}$$

Explicitly calculating the inverse, we obtain

$$\begin{aligned}
&\mathbf{G}(\mathbf{p}, z) = \frac{1}{\det \mathbf{G}^{-1}(\mathbf{p}, z)} \\
&\begin{pmatrix}
(z - B)\left((z + C)(z + D) - \frac{\kappa^2}{m^2}p'^2_y\right) & -gn_0(z - B)(z + D) & \cdots \\
-gn_0(z - B)(z + D) & -(z + D)\left((z - A)(z - B) - \frac{\kappa^2}{m^2}p^2_y\right) & \cdots \\
\vdots & \vdots & \ddots
\end{pmatrix},
\end{aligned} \tag{3.25}$$

where

$$\det \mathbf{G}^{-1}(\mathbf{p},z) = \left((z-A)(z-B) - \frac{\kappa^2 p_y^2}{m^2}\right)\left((z+C)(z+D) - \frac{\kappa^2 p_y'^2}{m^2}\right) + (gn_0)^2(z-B)(z+D). \tag{3.26}$$

We have thus obtained an expression for the Green's function. In the following, we investigate the stability of the system using the Green's function.

3.3.2 Low momentum excitations

Let us now look at the low momentum excitations of our system. The excitations are determined by the poles of the Green's function in frequency space, which are the solutions to the equation $\det \mathbf{G}^{-1}(\mathbf{p},z) = 0$. Since $\det \mathbf{G}^{-1}(\mathbf{p},z) = \det \mathbf{G}^{-1}(2\boldsymbol{\kappa}-\mathbf{p},-z)$, the roots of $\det \mathbf{G}^{-1}(\mathbf{p},z) = 0$ come in pairs: two positive and two negative, corresponding to two excitations, for each $\mathbf{p}$. One of the two excitations is gapless in the limit $\mathbf{p} \to \boldsymbol{\kappa}$, and the other is gapless in the limit $\mathbf{p} \to -\boldsymbol{\kappa}$. In the following, we investigate them one by one.

Excitation gapless in the limit $\mathbf{p} \to \boldsymbol{\kappa}$

Since our condensate is sitting at a momentum $\boldsymbol{\kappa} = (\kappa, 0, 0)$, it is convenient to introduce a shifted momentum $\mathbf{q}$ by writing $\mathbf{p} = \boldsymbol{\kappa} + \mathbf{q}$ and look at small $\mathbf{q}$. Then, $\mathbf{p}' = 2\boldsymbol{\kappa} - \mathbf{p} = \boldsymbol{\kappa} - \mathbf{q}$. Also, for notational convenience, we write $n = n_0 + n_- + n_+$. Then,

$$A = \frac{q^2}{2m} - \mu + ng + g(n_0 + n_-) = C \tag{3.27}$$

$$B = \frac{(\mathbf{q}+2\boldsymbol{\kappa})^2}{2m} - \mu + ng + gn_+ \tag{3.28}$$

$$D = \frac{(\mathbf{q}-2\boldsymbol{\kappa})^2}{2m} - \mu + ng + gn_+. \tag{3.29}$$

At this point, we would like to use μ_0 as a chemical potential. Defining $\Delta n \equiv n_+ - n_-$, we obtain

$$A = C = \frac{q^2}{2m} + gn_0, \qquad B = \frac{(\mathbf{q}+2\boldsymbol{\kappa})^2}{2m} + g\Delta n, \qquad D = \frac{(\mathbf{q}-2\boldsymbol{\kappa})^2}{2m} + g\Delta n. \tag{3.30}$$

Focusing on the low momentum excitations, we assume $|\mathbf{q}| \ll 2\kappa$, so that Thus,

$$A = C = \frac{q^2}{2m} + gn_0 \qquad\qquad B \approx D \approx \frac{2\kappa^2}{m} + g\Delta n. \tag{3.31}$$

Then, the low-momentum excitations are determined by

$$\det \mathbf{G}^{-1}(\boldsymbol{\kappa}+\mathbf{q},z) \approx z^4 - \left(A^2+B^2-(gn_0)^2+2\frac{\kappa^2 q_y^2}{m^2}\right)z^2 + \left(AB-\frac{\kappa^2 q_y^2}{m^2}\right)^2 - (gn_0)^2B^2 = 0. \tag{3.32}$$

Solving for z, we obtain

$$z^2 = \frac{A^2+B^2-(gn_0)^2}{2} + \frac{\kappa^2 q_y^2}{m^2} \pm \sqrt{\left(\frac{A^2+B^2-(gn_0)^2}{2}+\frac{\kappa^2 q_y^2}{m^2}\right)^2 - \left(AB-\frac{\kappa^2 q_y^2}{m^2}\right)^2 + (gn_0)^2B^2}. \tag{3.33}$$

Thus, among two positive roots of $\det \mathbf{G}^{-1}(\boldsymbol{\kappa}+\mathbf{q},z)=0$, the one given by the positive sign in (3.33) is gapped, and the one with negative sign in (3.33) is gapless in the limit $\mathbf{q}\to 0$. The spectrum gapped at $\mathbf{q}=0$ is, as we see below, gapless in the limit $\mathbf{p}\to -\boldsymbol{\kappa}$ (namely $\mathbf{q}\to -2\boldsymbol{\kappa}$). Thus, the low-energy excitation spectrum gapless in the limit $\mathbf{q}\to 0$ is

$$\epsilon_1(\mathbf{q}) \approx \sqrt{2gn_0\left(\frac{q_x^2+q_z^2}{2m}+\frac{q_y^2}{2m}\frac{m}{2\kappa^2}\left(g\Delta n+\frac{q_y^2}{2m}\right)\right)}. \tag{3.34}$$

The dispersion relation for $q_y=0$ is linear at low momenta, as in the usual Bogoliubov spectrum. Since $q_y^2/2m$ is generally larger than $g|\Delta n|$ in typical experimental setups, the dispersion is essentially quadratic for $q_x=q_z=0$[2], and thus

$$\epsilon_1(\mathbf{q}) \approx \sqrt{2gn_0\left(\frac{q_x^2+q_z^2}{2m}+\frac{1}{4\kappa^2}\frac{q_y^4}{2m}\right)}. \tag{3.35}$$

Excitation gapless in the limit $\mathbf{p}\to -\boldsymbol{\kappa}$

To consider a gapless excitation in the limit $\mathbf{p}\to -\boldsymbol{\kappa}$, we define $\mathbf{q}'\equiv \mathbf{p}+\boldsymbol{\kappa}$. The excitation corresponds to the positive root of $\det \mathbf{G}^{-1}(\mathbf{p},z)=0$ for a given $\mathbf{p}$ which becomes gapless in the limit $\mathbf{q}'\to 0$. Ignoring n_- and n_+ as small, as we discuss below, one finds that the excitation is

$$\epsilon_2(\mathbf{q}') = \frac{q_x'^2+q_y'^2}{2m} + \frac{gn_0}{\kappa^2/m+gn_0}\frac{q_y'^2}{4m}. \tag{3.36}$$

This excitation is quadratic and free particle-like in all directions, unlike the other excitation. The spectra of the two excitations agree with the result of [54].

[2] As discussed below, Δn is of order $n_0\sqrt{(mg)^3 n_0}$, and $n_0\sim N/L^3$, where N is the total number of particles, and L is the linear size of the system, and the smallest q_y is $\sim \pi/L$. Then naively writing $g\sim 4\pi a/m$ where a is the scattering length, we obtain $|g\Delta n|/q_y^2/2m \sim 10^2 N^{3/2}(a/L)^{5/2}$. Taking typical experimental parameters from [27], $N\sim 10^5$, $L\sim 10^{-2}$cm, and $a\sim$5nm we estimate $|g\Delta n|<0.1q_y^2/2m$.

3.3.3 Condensate depletion

We now consider the condensate depletion of the system due to quantum fluctuations. The number of particles in $(-)$ state is given by

$$n_- = \frac{i}{(2\pi)^4}\int d^3q dz \frac{(z-B)\left((z+C)(z+D)-\frac{\kappa^2}{m^2}q_y^2\right)}{\left((z-A)(z-B)-\frac{\kappa^2}{m^2}q_y^2\right)\left((z+C)(z+D)-\frac{\kappa^2}{m^2}q_y^2\right)+(gn_0)^2(z-B)(z+D)}, \tag{3.37}$$

where only the negative poles in the z integral are taken upon integration. Similarly, the number of particles in $(+)$ state is

$$n_+ = \frac{i}{(2\pi)^4}\int d^3q dz \frac{(z-A)\left((z+C)(z+D)-\frac{\kappa^2}{m^2}q_y^2\right)+(gn_0)^2(z+D)}{\left((z-A)(z-B)-\frac{\kappa^2}{m^2}q_y^2\right)\left((z+C)(z+D)-\frac{\kappa^2}{m^2}q_y^2\right)+(gn_0)^2(z-B)(z+D)}. \tag{3.38}$$

The poles in z at large $\mathbf{q}$ behave as $-q^2/2m$, and since at large q, $A \sim B \sim C \sim D \sim q^2/2m$, naive power counting would indicate that the integrand after the z integration behaves as q^{-1}, which combined with three q-integrals yields a quadratic ultraviolet divergence. In fact, cancellations in the integrand lead to convergence, which we now show. Since the Green's function has two negative and two positive poles, let us factor the denominator in the form

$$\begin{aligned}\det \mathbf{G}^{-1}(\mathbf{p},z) &= \left((z-A)(z-B)-\frac{\kappa^2}{m^2}q_y^2\right)\left((z+C)(z+D)-\frac{\kappa^2}{m^2}q_y^2\right)+(gn_0)^2(z-B)(z+D)\\ &= (z-E_1)(z-E_2)(z-E_3)(z-E_4),\end{aligned} \tag{3.39}$$

where $E_1 < E_2 < 0 < E_3 < E_4$. Asymptotically at large q, $E_1 \sim E_2 \sim -q^2$ and $E_3 \sim E_4 \sim q^2$. Then,

$$\begin{aligned} n_- &= \frac{i}{(2\pi)^4}\int d^3q dz \frac{(z-B)\left((z+C)(z+D)-\frac{\kappa^2}{m^2}q_y^2\right)}{(z-E_1)(z-E_2)(z-E_3)(z-E_4)}\\ &= \frac{i}{(2\pi)^4}(2\pi i)\int d^3q \left(\frac{(E_1-B)\left((E_1+C)(E_1+D)-\frac{\kappa^2}{m^2}q_y^2\right)}{(E_1-E_2)(E_1-E_3)(E_1-E_4)}\right.\\ &\qquad\left.+\frac{(E_2-B)\left((E_2+C)(E_2+D)-\frac{\kappa^2}{m^2}q_y^2\right)}{(E_2-E_1)(E_2-E_3)(E_2-E_4)}\right). \end{aligned} \tag{3.40}$$

On the other hand, since

$$\left((E_1 - A)(E_1 - B) - \frac{\kappa^2}{m^2}q_y^2\right)\left((E_1 + C)(E_1 + D) - \frac{\kappa^2}{m^2}q_y^2\right) + (gn_0)^2(E_1 - B)(E_1 + D) = 0, \tag{3.41}$$

we can write

$$(E_1 + C)(E_1 + D) - \frac{\kappa^2}{m^2}q_y^2 = -\frac{(gn_0)^2(E_1 - B)(E_1 + D)}{(E_1 - A)(E_1 - B) - \frac{\kappa^2}{m^2}q_y^2} \tag{3.42}$$

and similarly for $E_1 \to E_2$. Thus, we can rewrite (3.40) as

$$n_- = \frac{i}{(2\pi)^4}(2\pi i)\int d^3q \left(\frac{-(E_1 - B)}{(E_1 - E_2)(E_1 - E_3)(E_1 - E_4)}\frac{(gn_0)^2(E_1 - B)(E_1 + D)}{(E_1 - A)(E_1 - B) - \frac{\kappa^2}{m^2}q_y^2} + (E_1 \leftrightarrow E_2)\right). \tag{3.43}$$

As $E_1 - E_2 \sim q$ and $E_1 - E_3 \sim E_1 - E_4 \sim E_1 - A \sim E_1 - B \sim q^2$, the denominator of the integral goes as $\sim q^9$. On the other hand, as $E_1 + D \sim q$, the numerator goes as q^5. Therefore, the overall integrand goes as q^{-4}, which combined with the integral over d^3q does not result in an ultraviolet divergence. We can also rewrite the integral as

$$n_- = \frac{i}{(2\pi)^4}\int d^3q dz \frac{-(gn_0)^2(z - B)^2(z + D)}{\det \mathbf{G}^{-1}(\mathbf{p}, z)\left((z - A)(z - B) - \frac{\kappa^2}{m^2}q_y^2\right)}, \tag{3.44}$$

which is easier to evaluate numerically.

We can similarly see that n_+ is not ultraviolet divergent:

$$n_+ = \frac{i}{(2\pi)^4}\int d^3q dz \frac{-(gn_0)^2(z + D)\frac{\kappa^2}{m^2}q_y^2}{\det \mathbf{G}^{-1}(\mathbf{p}, z)\left((z - A)(z - B) - \frac{\kappa^2}{m^2}q_y^2\right)}. \tag{3.45}$$

Since the integrand itself contains n_- and n_+ through Δn, these equations should be solved self-consistently. To a first approximation (which is equivalent to Bogoliubov approximation), we can ignore Δn in the integrand and evaluate n_- and n_+ directly. Having done so, we must then check the consistency of our calculation by computing $\Delta n/n_0$ and observing whether it is small enough so that the approximation is justified.

Equations (3.44) and (3.45) can be evaluated numerically as a function of $\kappa/\sqrt{2mgn_0}$. The number of excited particles $n_{ex} = n_- + n_+$ is plotted in Fig. 3.2[3]. Generally, $n_- \gg n_+$, and the contribution of n_+ to the number of excited particles is negligible. As the figure shows, the condensate depletion increases with $\kappa/\sqrt{2mgn_0}$, and is of order $n_0\sqrt{(2mg)^3 n_0} \ll n$, thus justifying our use of the Bogoliubov approximation.

[3] Thanks to numerical assistance from Philip Powell.

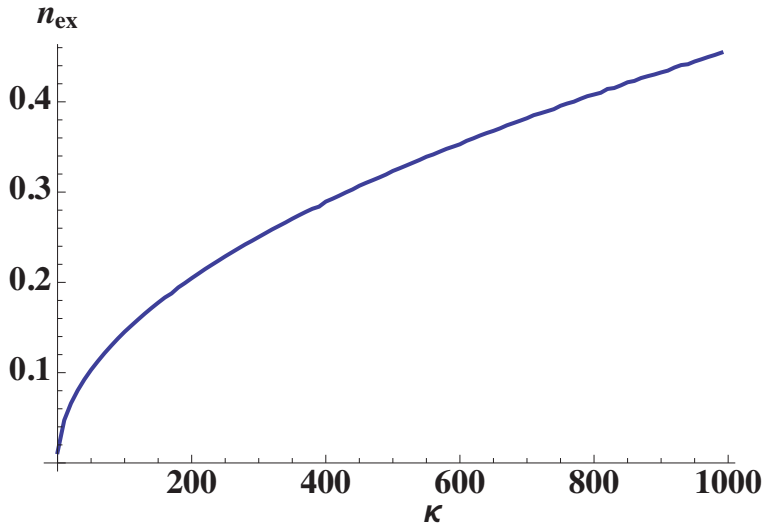

Figure 3.2: The number of excited particles, in units of $(2mgn_0)^{3/2}$ as a function of the spin-orbit coupling strength κ in units of $\sqrt{2mgn_0}$. Generally $n_- \gg n_+$ and $n_{ex} \approx n_-$.

3.3.4 Ground state energy corrections

We can similarly evaluate the correction to the ground state energy from the quantum fluctuation. The ground state energy density in terms of Green's functions is

$$\frac{E}{V} = \frac{\mu n}{2} - g\left(n_-^2 + n_+^2 + n_- n_+\right) + \frac{1}{2}\frac{i}{(2\pi)^3}\int d^3p dz \mathrm{Tr}\left[\left(\left(z + \frac{p^2+\kappa^2}{2m}\right) I + \frac{\kappa}{m}\left(-p_x\sigma_z + p_y\sigma_y\right)\right)\begin{pmatrix} G_{11}(\mathbf{p},z) & G_{13}(\mathbf{p},z) \\ G_{31}(\mathbf{p},z) & G_{33}(\mathbf{p},z)\end{pmatrix}\right], \tag{3.46}$$

where the second term takes care of the double-counting issue of Hartree-Fock approximation, and the term in braces is z plus the single-particle Hamiltonian in the $(-,+)$ basis. As before, assuming n_- and n_+ to be much smaller than n_0, which is appropriate at the dilute limit, we ignore the contribution from Hartree-Fock terms. The integral equals $gn_0(2mgn_0)^{3/2}$ times a dimensionless function X of μ/gn_0 and $\kappa/\sqrt{2mgn_0}$. Since the chemical potential in mean-field is $\mu = gn_0$ and n_{ex} is $\mathcal{O}((2mgn_0)^{3/2})$, the energy density is

$$\frac{E}{V} = \frac{\mu n}{2} + Xgn(2mgn)^{3/2}, \tag{3.47}$$

where X is, explicitly,

$$Xgn_0(2mgn_0)^{3/2} = \frac{1}{2}\frac{i}{(2\pi)^4}\int d^3p dz \frac{1}{\det \mathbf{G}^{-1}(\mathbf{p},z)}\left[\left(z+\frac{p^2+2\kappa p_x+\kappa^2}{2m}\right)(z+D)(gn_0)^2\right.$$
$$\left.+\left((z+A)(z+D)-\frac{\kappa^2}{m^2}p_y^2\right)\left(\left(z+\frac{p^2+\kappa^2}{2m}\right)(2z-A-B)-\frac{\kappa}{m}p_x(A-B)-2\frac{\kappa^2}{m^2}p_y^2\right)\right]. \quad (3.48)$$

Then, we write the chemical potential similarly as (c.f. [56]),

$$\mu = gn\left(1+Y\sqrt{(2mg)^3 n}\right). \quad (3.49)$$

Since

$$\mu = \frac{\partial E}{\partial N} \approx \frac{\partial}{\partial n}\left(\frac{E}{V}\right) = \frac{1}{2}\mu + \frac{n}{2}\frac{\partial \mu}{\partial n} + \frac{\partial}{\partial n}\left(Xgn(2mgn)^{3/2}\right)$$
$$= \frac{1}{2}\mu + \frac{1}{2}gn\left(1+\frac{3}{2}Y\sqrt{(2mg)^3 n}\right) + \frac{5}{2}Xgn(2mgn)^{3/2}, \quad (3.50)$$

we find

$$\mu = gn\left(1+Y\sqrt{(2mg)^3 n}\right) = gn\left(1+\frac{3}{2}Y\sqrt{(2mg)^3 n}\right) + 5Xgn(2mgn)^{3/2}, \quad (3.51)$$

which implies

$$Y = -10X. \quad (3.52)$$

Thus the ground state energy is

$$\frac{E}{V} \approx \frac{gn^2}{2}\left(1-8X\sqrt{(2mg)^3 n}\right), \quad (3.53)$$

In calculating X, we take $\mu = gn_0$; deviations of μ from gn_0 result in higher order corrections.

For $\kappa \to 0$, one finds $X = -1/15\sqrt{2}\pi^2$, which leads to

$$\frac{E}{V}(\kappa = 0) = \frac{gn^2}{2}\left(1+\frac{8}{15\sqrt{2}\pi^2}\sqrt{(2mg)^3 n}\right), \quad (3.54)$$

which is the ground state energy derived by Lee and Yang [57, 58]. As we tune κ away from 0, we need to evaluate the integral numerically. Figure 3.3 shows the shift in the ground state energy, $\Delta E \equiv E/V - gn^2/2$, in units of $(\sqrt{(2mg)^3 n})gn^2/2$, as a function of $\kappa/\sqrt{2mgn_0}$. The energy decreases with increasing κ, and ΔE changes from positive to negative at $\kappa \sim 0.6\sqrt{2mgn_0}$, an effect too small to see in the figure.

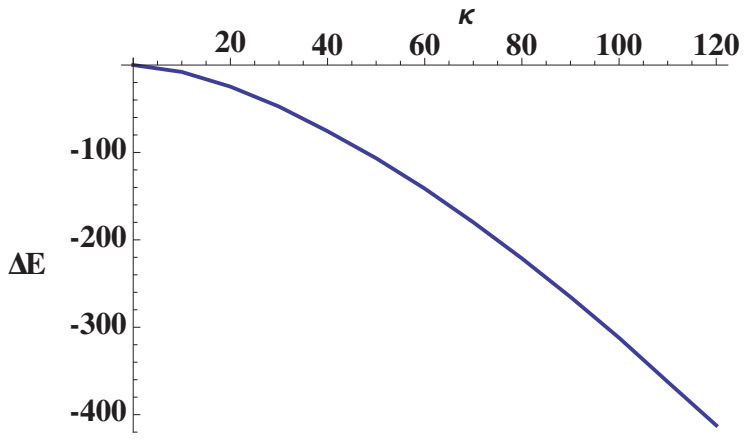

Figure 3.3: The shift in the ground state energy density, ΔE, in units of $(\sqrt{(2mg)^3 n})gn^2/2$, as a function of the spin-orbit coupling strength κ in units of $\sqrt{2mgn_0}$.

3.3.5 Finite temperature BEC

In the absence of interactions, bosons with Rashba spin-orbit coupling do not have a finite temperature transition to a BEC because the density of states becomes two-dimensional at low energy. However, in the presence of interactions, the density of states is modified and, as we will see soon, it is possible to have a BEC at finite temperature.

The number of excited particles at temperature T is

$$n_- + n_+ = -\frac{T}{(2\pi)^3} \sum_\nu \int d^3p \left(G_{11}(\mathbf{p}, z_\nu) + G_{22}(\mathbf{p}, z_\nu) \right), \tag{3.55}$$

where the ν sum is over bosonic Matsubara frequencies.

The system forms a BEC at a given temperature when n_{ex} converges in the infrared, and the total particle density exceeds n_{ex}. The infrared structure is captured by the $z_\nu = 0$ component of the Matsubara sum. Since there are two gapless excitations $\epsilon_1(\mathbf{q})$ and $\epsilon_2(\mathbf{q}')$, we need to add infrared contributions from two limits $\mathbf{q} \to 0$ and $\mathbf{q}' \to 0$. In the limit of small q and q' and using $\mu = \mu_0$, one finds from inverting

$$\begin{aligned} G_{11}(\boldsymbol{\kappa} + \mathbf{q}, 0) + G_{33}(\boldsymbol{\kappa} + \mathbf{q}, 0) &= -\frac{gn_0}{\epsilon_1(\mathbf{q})^2}, \\ G_{11}(-\boldsymbol{\kappa} + \mathbf{q}', 0) + G_{33}(-\boldsymbol{\kappa} + \mathbf{q}', 0) &= -\frac{1}{\epsilon_2(\mathbf{q}')}, \end{aligned} \tag{3.56}$$

respectively, and thus,

$$\begin{aligned} n_- + n_+ &\sim -\frac{T}{(2\pi)^3}\int d^3p\,(G_{11}(\mathbf{p},0)+G_{33}(\mathbf{q},0)) \\ &\sim T\int\frac{d^3q}{(2\pi)^3}\left(\frac{gn_0}{\epsilon_1(\mathbf{q})^2}+\frac{1}{\epsilon_2(\mathbf{q})}+C\right) \\ &\sim T\int\frac{d^3q}{(2\pi)^3}\left(\frac{m}{q_x^2+q_z^2+q_y^4/4\kappa^2}+\frac{2m}{q_x^2+q_z^2+q_y^2\dfrac{gn_0}{2\kappa^2/m+2gn_0}}+C\right), \end{aligned} \tag{3.57}$$

where C is a constant as $\mathbf{q}\to 0$. The integral converges in the infrared, and thus a BEC can form at finite temperature.

Equivalently, the number of excited particles is given in terms of the fluctuations of the condensate by $n_{ex} = \langle\delta\psi_-^\dagger(\mathbf{r})\delta\psi_-(\mathbf{r})\rangle$. To illustrate the connection we evaluate the fluctuations in terms of the deviation of the free energy with respect to small variations of $\langle\psi_-\rangle$ neglecting the free particle-like excitations ϵ_2. The mean-field condensate wavefunction is $\langle\psi(\mathbf{r})\rangle_0 = \sqrt{n_0}e^{i\boldsymbol{\kappa}\cdot\mathbf{r}}$. Then, defining $\langle\Psi_-(\mathbf{r})\rangle \equiv (e^{-i\boldsymbol{\kappa}\cdot\mathbf{r}}\langle\psi_-(\mathbf{r})\rangle, e^{i\boldsymbol{\kappa}\cdot\mathbf{r}}\langle\psi_-(\mathbf{r})\rangle^*)$, the following relation holds (cf. Eq. (18) of [59])

$$\delta F = -\frac{1}{2}\int\frac{d^3q}{(2\pi)^3}\delta\langle\Psi_-(\mathbf{q})\rangle^\dagger\mathbf{G}_{--}^{-1}(\boldsymbol{\kappa}+\mathbf{q},0)\delta\langle\Psi_-(\mathbf{q})\rangle, \tag{3.58}$$

where $\mathbf{G}_{--}(\mathbf{p};,t_1,t_2) \equiv -i\langle T(\Psi_-(\mathbf{p},t_1)\Psi_-^\dagger(\mathbf{p},t_2)\rangle$ is the upper left 4 components of $\mathbf{G}(\mathbf{p};t_1,t_2)$, and $\delta\langle\Psi_-(\mathbf{q})\rangle$ is the small variation of the Fourier transform of $\langle\Psi_-(\mathbf{r})\rangle$. Explicitly, from (3.20) one finds,

$$\mathbf{G}_{--}^{-1}(\boldsymbol{\kappa}+\mathbf{q},0) = -\begin{pmatrix} A(\boldsymbol{\kappa}+\mathbf{q})-\frac{(\kappa q_y/m)^2}{B(\boldsymbol{\kappa}+\mathbf{q})} & gn_0 \\ gn_0 & A(\boldsymbol{\kappa}+\mathbf{q})-\frac{(\kappa q_y/m)^2}{D(\boldsymbol{\kappa}+\mathbf{q})}\end{pmatrix}. \tag{3.59}$$

Since phase fluctuations are important in low energy, let us define the phase $\theta(\mathbf{r})$ by $\langle\Psi_-(\mathbf{r})\rangle = (\sqrt{n_0}e^{i\theta(\mathbf{r})}, \sqrt{n_0}e^{-i\theta(\mathbf{r})})$, and then in terms of its Fourier transform $\theta(\mathbf{q})$ we have

$$\delta F = \frac{n_0}{2}\int\frac{d^3q}{(2\pi)^3}|\theta(\mathbf{q})|^2\left(q^2-2\kappa^2q_y^2\left(\frac{1}{(2\boldsymbol{\kappa}-\mathbf{q})^2}+\frac{1}{(2\boldsymbol{\kappa}+\mathbf{q})^2}\right)\right). \tag{3.60}$$

Thus

$$\overline{|\delta\langle\psi_-(\mathbf{q})\rangle|^2} = \frac{n_0\int d\{\theta(\mathbf{q})\}|\theta(\mathbf{q})|^2e^{-\beta\delta F}}{\int d\{\theta(\mathbf{q})\rangle\}e^{-\beta\delta F}} = mT\left(q^2-2\kappa^2q_y^2\left(\frac{1}{(2\boldsymbol{\kappa}-\mathbf{q})^2}+\frac{1}{(2\boldsymbol{\kappa}+\mathbf{q})^2}\right)\right)^{-1}. \tag{3.61}$$

Approximating the final term by its small q limit, we find

$$\overline{|\delta\langle\psi_-(\mathbf{q})\rangle|^2} \approx \frac{mT}{q_x^2 + q_z^2 + q_y^4/4\kappa^2}, \tag{3.62}$$

from which we find

$$n_{ex} = \int \frac{d^3q}{(2\pi)^3} \overline{|\delta\langle\psi_-(\mathbf{q})\rangle|^2} \sim T \int \frac{d^3q}{(2\pi)^3} \frac{m}{q_x^2 + q_z^2 + q_y^4/4\kappa^2}, \tag{3.63}$$

in agreement with the first term, the leading term, of (3.57). This result is consistent with Jian and Zhai's effective field theory approach to calculate phase fluctuations [50], applied in three dimensions.

3.4 Normal state

So far, we have assumed the existence of condensate, and proved that the condensate is not destroyed by thermal fluctuations. We should also ask whether a non-condensed state is favorable at finite temperature. Here we obtain the free energy of the normal state within the Hartree-Fock approximation and compare the free energies with and without a condensate.

The Green's functions of a normal state within the Hartree-Fock approximation can be obtained by setting $n_0 = 0$ in (3.20), which yields

$$\begin{pmatrix} G_{11}(\mathbf{p}, z) & G_{13}(\mathbf{p}, z) \\ G_{31}(\mathbf{p}, z) & G_{33}(\mathbf{p}, z) \end{pmatrix}^{-1} = \begin{pmatrix} z - A & i\frac{\kappa}{m}p_y \\ -i\frac{\kappa}{m}p_y & z - B \end{pmatrix}, \tag{3.64}$$

where

$$A = \frac{(\mathbf{p} - \boldsymbol{\kappa})^2}{2m} - \mu + g(2n_- + n_+), \qquad B = \frac{(\mathbf{p} + \boldsymbol{\kappa})^2}{2m} - \mu + g(n_- + 2n_+). \tag{3.65}$$

Then, the reduced Hamiltonian within the Hartree-Fock approximation is

$$\mathcal{H}_{\mathrm{HF}} = -Vg\left(n_-^2 + n_+^2 + n_- n_+\right) + \sum_{\mathbf{p}\neq\boldsymbol{\kappa}} \begin{pmatrix} \psi_{-,\mathbf{p}}^\dagger & \psi_{+,\mathbf{p}}^\dagger \end{pmatrix} \begin{pmatrix} A & -i\frac{\kappa}{m}p_y \\ i\frac{\kappa}{m}p_y & B \end{pmatrix} \begin{pmatrix} \psi_{-,\mathbf{p}} \\ \psi_{+,\mathbf{p}} \end{pmatrix}. \tag{3.66}$$

In fact, $n_- = n_+ = n/2$, where n is the total number density of particles; namely there is no spontaneous imbalance of population in each pseudospin species. One one can prove this by introducing independent chemical potentials for each species, and seeing that the second derivative

of the Ginzburg-Landau free energy with respect to the population imbalance is positive. The derivation is outlined in Appendix C.

Setting $n_- = n_+ = n/2$, the Helmholtz free energy density is

$$\mathcal{F} = \mu n - \frac{3}{4} g n^2 + \frac{1}{\beta V} \sum_{\mathbf{p}} \ln\left(1 - e^{-\beta \xi_\alpha(\mathbf{p})}\right) + \frac{1}{\beta V} \sum_{\mathbf{p}} \ln\left(1 - e^{-\beta \xi_\beta(\mathbf{p})}\right), \tag{3.67}$$

where

$$\xi_\alpha(\mathbf{p}) = \frac{(p_\perp - \kappa)^2 + p_z^2}{2m} - \mu + \frac{3}{2} g n, \qquad \xi_\beta(\mathbf{p}) = \frac{(p_\perp + \kappa)^2 + p_z^2}{2m} - \mu + \frac{3}{2} g n. \tag{3.68}$$

The number equation, which determines the chemical potential for a given temperature, is

$$\frac{n}{2} = \frac{1}{V} \sum_{\mathbf{p}} \left(\frac{f_B(\xi_\alpha(\mathbf{p}))}{2} + \frac{f_B(\xi_\beta(\mathbf{p}))}{2} \right). \tag{3.69}$$

An important feature of this number equation is that there is always a value of μ which satisfies this equation for a given temperature, thus the state without condensate is not kinematically forbidden at any non-zero temperature.

As $T \to 0$ in the absence of a condensate, $\mu \to 3gn/2$, and

$$\mathcal{F} \to \frac{3}{4} g n^2. \tag{3.70}$$

This energy is larger than the ground state energy with condensate

$$\frac{1}{2} g n^2 \left(1 + \mathcal{O}(\sqrt{(2mg)^3 n})\right). \tag{3.71}$$

Therefore, at sufficiently low temperature, a condensate is energetically preferred. At low temperature $F(\mu, n_0) < F(\mu, 0)$, so $n_0 > 0$. The condensate density decreases with temperature, and the transition to the normal state, if second order, occurs when $\partial F(\mu, n_0)/\partial n_0 = 0$ at $n_0 = 0$. Determination of the order of the transition, the transition temperature, and possible critical exponents at the transition is left to the future[4].

[4] At the mean field level, the transition is (spuriously) first order, as in the Bogoliubov approximation to the finite temperature Bose gas [60].

Chapter 4

Renormalized interaction in spin-orbit coupled BEC's

4.1 Introduction

In this chapter we consider the effects of the renormalized interaction in ultracold atoms with Rashba-Dresselhaus spin-orbit coupling. Although our main concern is bosons, we also derive the renormalized interaction for fermions. The material in this chapter is based on papers [2, 3].

When the inter-particle potential is described by an s-wave contact interaction, the relation between the bare interaction and the effective interaction is non-trivial, because the scattering t-matrix, which serves as an effective interaction, depends on the large momentum cutoff, as explained in Appendix A.6, and the proper renormalization of the momentum cutoff is required. For Bose gases in the absence of Rashba-Dresselhaus spin-orbit coupling, the low energy t-matrix is proportional to the scattering length, in terms of which the momentum cutoff is renormalized, and thus the effective interaction is proportional to the scattering length. However, for Bose gases with Rashba-Dresselhaus interaction, as we see below, this simple relation between the bare interaction and the scattering length does not hold.

For a contact interaction with strength g, in the absence of Rashba-Dresselhaus spin-orbit coupling, the integral equation for the zero-energy T-matrix is, from (A.151),

$$\frac{1}{T_0(0,0)} = \frac{m}{4\pi a} = \frac{1}{g} + \int^{\Lambda} \frac{d^3k}{(2\pi)^3} \frac{1}{2\epsilon_0(\mathbf{k})}, \tag{4.1}$$

where $\epsilon_0(\mathbf{k}) \equiv k^2/2m$ is the free particle dispersion and a is the scattering length in free space. We have written the free t-matrix T_0 to distinguish from the t-matrix with spin-orbit coupling. After

introducing the Rashba-Dresselhaus spin-orbit coupling, the dispersion is altered, and the relation (4.1) is no longer valid [53]. To obtain the effective interaction in terms of the physical observables, we must first obtain the correct t-matrix.

Naively replacing $\epsilon_0(\mathbf{k})$ by the dispersion of the lower branch, $\epsilon_-(\mathbf{k}) = \{(k_\perp - \kappa)^2 + k_z^2\}/(2m)$, demonstrates the apparent difficulty in obtaining the relation between bare coupling and the t-matrix. For the zero-energy t-matrix, one may write

$$\frac{1}{T} \sim \frac{1}{g} + \int^{\Lambda} \frac{d^3k}{(2\pi)^3} \frac{m}{(k_\perp - \kappa)^2 + k_z^2} \sim \frac{1}{g} + \frac{m}{2\pi^2}\left(\Lambda + \frac{\pi\kappa}{2}\ln\Lambda + \cdots\right). \tag{4.2}$$

The integral is ultraviolet divergent. Even after renormalizing the linear divergence using (4.1), we are still left with the logarithmic divergence.

As we will see in the following section, the logarithmic divergences do indeed vanish if we include the contributions from the both lower and upper energy branches when calculating the t-matrix. Thus, in the end, the t-matrix can be written solely in terms of low energy parameters which do not depend on either the ultraviolet cutoff or the short distance behavior of the interaction.

4.2 T-matrix

4.2.1 Bethe-Salpeter equations

The starting Hamiltonian for both isotropic and anisotropic spin-orbit coupling is the same as the previous chapter, Eq. (3.1), which is

$$\begin{aligned}\mathcal{H} = &\sum_{\mathbf{p}} \begin{pmatrix} a_{\mathbf{p}}^\dagger & b_{\mathbf{p}}^\dagger \end{pmatrix} \left(\frac{p^2+\kappa^2}{2m} I + \frac{\kappa}{m}\left(p_x\sigma_x + \eta p_y \sigma_y\right)\right) \begin{pmatrix} a_{\mathbf{p}} \\ b_{\mathbf{p}} \end{pmatrix} \\ &+ \frac{1}{2V} \sum_{\mathbf{p}_1+\mathbf{p}_2=\mathbf{p}_3+\mathbf{p}_4} \left(g_{aa}\ a_{\mathbf{p}_4}^\dagger a_{\mathbf{p}_3}^\dagger a_{\mathbf{p}_2} a_{\mathbf{p}_1} + g_{bb}\ b_{\mathbf{p}_4}^\dagger b_{\mathbf{p}_3}^\dagger b_{\mathbf{p}_2} b_{\mathbf{p}_1} + 2g_{ab}\ a_{\mathbf{p}_4}^\dagger b_{\mathbf{p}_3}^\dagger b_{\mathbf{p}_2} a_{\mathbf{p}_1}\right) \\ \equiv &\ \mathcal{H}_{\text{kin}} + \mathcal{H}_{\text{int}},\end{aligned} \tag{4.3}$$

with $0 \le \eta \le 1$. We consider both bosons and fermions. For fermions, $g_{aa} = g_{bb} = 0$. We are interested in the low-energy scattering, especially the zero-energy scattering of particles in the single-particle ground states. In this case, it is convenient to move to the (α, β) basis introduced

in (2.87), in terms of which the Hamiltonian becomes

$$\mathcal{H} = \sum_{\mathbf{p}} \left[\epsilon_-(\mathbf{p}) \alpha^\dagger_{\mathbf{p}} \alpha_{\mathbf{p}} + \epsilon_+(\mathbf{p}) \beta^\dagger_{\mathbf{p}} \beta_{\mathbf{p}} \right] + \mathcal{H}_{\text{int}}, \tag{4.4}$$

where the interaction part of the Hamiltonian is of the form

$$\begin{aligned}
\mathcal{H}_{\text{int}} = \frac{1}{V} \sum_{\mathbf{p}_1+\mathbf{p}_2=\mathbf{p}_3+\mathbf{p}_4} \Bigg[& \frac{1}{2} \mathcal{V}^{(1)}_{\phi_1,\phi_2;\phi_3,\phi_4} \left(\alpha^\dagger_{\mathbf{p}_4} \alpha^\dagger_{\mathbf{p}_3} \alpha_{\mathbf{p}_2} \alpha_{\mathbf{p}_1} + \beta^\dagger_{\mathbf{p}_4} \beta^\dagger_{\mathbf{p}_3} \beta_{\mathbf{p}_2} \beta_{\mathbf{p}_1} \right) \\
& + \frac{1}{2} \mathcal{V}^{(2)}_{\phi_1,\phi_2;\phi_3,\phi_4} \left(\beta^\dagger_{\mathbf{p}_4} \beta^\dagger_{\mathbf{p}_3} \alpha_{\mathbf{p}_2} \alpha_{\mathbf{p}_1} + \alpha^\dagger_{\mathbf{p}_4} \alpha^\dagger_{\mathbf{p}_3} \beta_{\mathbf{p}_2} \beta_{\mathbf{p}_1} \right) + \frac{1}{\sqrt{2}} \mathcal{V}^{(3)}_{\phi_1,\phi_2;\phi_3,\phi_4} \left(\alpha^\dagger_{\mathbf{p}_4} \beta^\dagger_{\mathbf{p}_3} \beta_{\mathbf{p}_2} \beta_{\mathbf{p}_1} + \beta^\dagger_{\mathbf{p}_4} \alpha^\dagger_{\mathbf{p}_3} \alpha_{\mathbf{p}_2} \alpha_{\mathbf{p}_1} \right) \\
& + \frac{1}{\sqrt{2}} \mathcal{V}^{(4)}_{\phi_1,\phi_2;\phi_3,\phi_4} \left(\alpha^\dagger_{\mathbf{p}_4} \alpha^\dagger_{\mathbf{p}_3} \beta_{\mathbf{p}_2} \alpha_{\mathbf{p}_1} + \beta^\dagger_{\mathbf{p}_4} \beta^\dagger_{\mathbf{p}_3} \alpha_{\mathbf{p}_2} \beta_{\mathbf{p}_1} \right) + \mathcal{V}^{(5)}_{\phi_1,\phi_2;\phi_3,\phi_4} \alpha^\dagger_{\mathbf{p}_4} \beta^\dagger_{\mathbf{p}_3} \beta_{\mathbf{p}_2} \alpha_{\mathbf{p}_1} \Bigg].
\end{aligned} \tag{4.5}$$

The coefficients $V^{(i)}$ are defined by

$$\begin{aligned}
\mathcal{V}^{(1)}_{\phi_1,\phi_2;\phi_3,\phi_4} &= \frac{g_{aa}}{4} + \frac{g_{bb}}{4} e^{i(\phi_1+\phi_2-\phi_3-\phi_4)} \pm \frac{g_{ab}}{8} \left(e^{i\phi_1} \pm e^{i\phi_2} \right) \left(e^{-i\phi_3} \pm e^{-i\phi_4} \right), \\
\mathcal{V}^{(2)}_{\phi_1,\phi_2;\phi_3,\phi_4} &= \frac{g_{aa}}{4} + \frac{g_{bb}}{4} e^{i(\phi_1+\phi_2-\phi_3-\phi_4)} \mp \frac{g_{ab}}{8} \left(e^{i\phi_1} \pm e^{i\phi_2} \right) \left(e^{-i\phi_3} \pm e^{-i\phi_4} \right), \\
\frac{1}{\sqrt{2}} \mathcal{V}^{(3)}_{\phi_1,\phi_2;\phi_3,\phi_4} &= \frac{g_{aa}}{4} - \frac{g_{bb}}{4} e^{i(\phi_1+\phi_2-\phi_3-\phi_4)} \pm \frac{g_{ab}}{8} \left(e^{i\phi_1} \pm e^{i\phi_2} \right) \left(e^{-i\phi_3} \mp e^{-i\phi_4} \right), \\
\frac{1}{\sqrt{2}} \mathcal{V}^{(4)}_{\phi_1,\phi_2;\phi_3,\phi_4} &= \frac{g_{aa}}{4} - \frac{g_{bb}}{4} e^{i(\phi_1+\phi_2-\phi_3-\phi_4)} \pm \frac{g_{ab}}{8} \left(e^{i\phi_1} \mp e^{i\phi_2} \right) \left(e^{-i\phi_3} \pm e^{-i\phi_4} \right), \\
\frac{1}{2} \mathcal{V}^{(5)}_{\phi_1,\phi_2;\phi_3,\phi_4} &= \frac{g_{aa}}{4} + \frac{g_{bb}}{4} e^{i(\phi_1+\phi_2-\phi_3-\phi_4)} \mp \frac{g_{ab}}{8} \left(e^{i\phi_1} \mp e^{i\phi_2} \right) \left(e^{-i\phi_3} \mp e^{-i\phi_4} \right),
\end{aligned} \tag{4.6}$$

where the upper signs are for bosons and the lower signs are for fermions. The angles ϕ_i are defined by $p_{i,x} + i\eta p_{i,y} \equiv e^{i\phi_i} \sqrt{p^2_{i,x} + \eta^2 p^2_{i,y}}$. As we can see, the interaction mixes different species in the (α, β) basis. The coefficients of each term are chosen so that the Feynman rules for vertices in the (α, β) basis are just $\mathcal{V}^{(i)}$s.

We now calculate the t-matrix describing the collision of two atoms in the α-branch with incoming momenta $\mathbf{q}/2 + \mathbf{p}$ and $\mathbf{q}/2 - \mathbf{p}$ and outgoing momenta $\mathbf{q}/2 + \mathbf{p}'$ and $\mathbf{q}/2 - \mathbf{p}'$. The momentum of each particle is on the degenerate ground-state circle for $\eta = 1$ and either $\mathbf{p}_0$ or $-\mathbf{p}_0$ for $0 \leq \eta < 1$. The single particle propagators are $1/(\omega - \epsilon_\pm(\mathbf{p}))$, and characteristically, the interactions in the (α, β) basis are dependent on angle. The t-matrix is the sum of ladder diagrams (Fig. 4.1). We denote the momenta of particles in the intermediate off-shell states by $\mathbf{q}/2 + \mathbf{k}$ and $\mathbf{q}/2 - \mathbf{k}$ and label angles of the momenta ϕ_i as in the Fig. 4.1. The Bethe-Salpeter equation for the

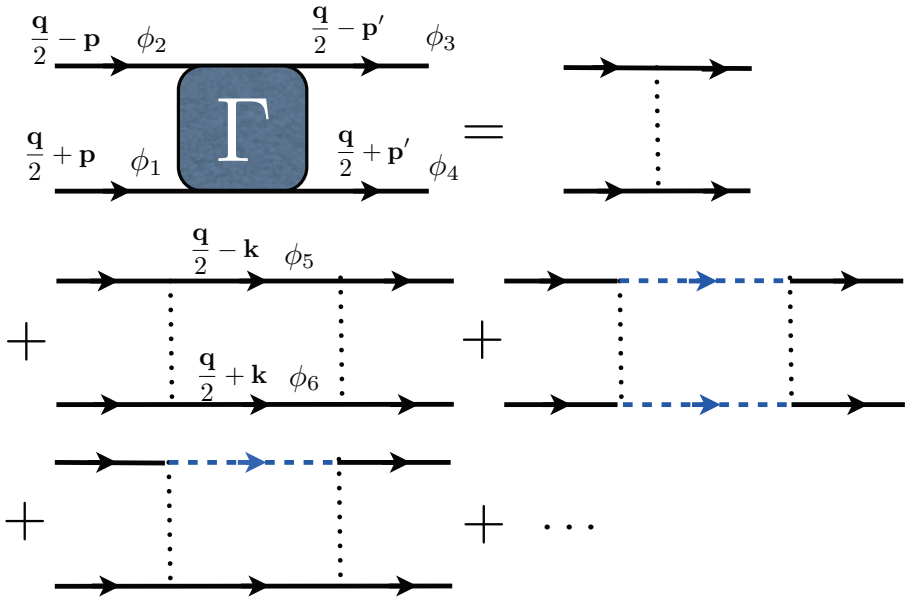

Figure 4.1: The scattering t-matrix for two particles in the α-branch. The solid lines denote particles in α-branch, and the dashed lines are particles in the β-branch. The ϕ_i are the angles of the corresponding momenta in the x-y plane.

zero-energy vertex function $\Gamma^{\alpha\alpha}_{\alpha\alpha}$ with incoming and outgoing α-α particles is

$$\begin{aligned}
\Gamma^{\alpha\alpha}_{\alpha\alpha}(\mathbf{p},\mathbf{p}';\mathbf{q}) &= \mathcal{V}^{(1)}_{\phi_1,\phi_2;\phi_3,\phi_4} \\
&- \int \frac{d^3k}{(2\pi)^3}\left[\frac{\mathcal{V}^{(1)}_{\phi_1,\phi_2;\phi_5,\phi_6}\Gamma^{\alpha\alpha}_{\alpha\alpha}(\mathbf{k},\mathbf{p}';\mathbf{q})}{\epsilon_-(\frac{\mathbf{q}}{2}-\mathbf{k})+\epsilon_-(\frac{\mathbf{q}}{2}+\mathbf{k})} + \frac{\mathcal{V}^{(2)}_{\phi_1,\phi_2;\phi_5,\phi_6}\Gamma^{\alpha\alpha}_{\beta\beta}(\mathbf{k},\mathbf{p}';\mathbf{q})}{\epsilon_+(\frac{\mathbf{q}}{2}-\mathbf{k})+\epsilon_+(\frac{\mathbf{q}}{2}+\mathbf{k})} \pm \frac{\mathcal{V}^{(3)}_{\phi_1,\phi_2;\phi_6,\phi_5}\Gamma^{\alpha\alpha}_{\alpha\beta}(\mathbf{k},\mathbf{p}';\mathbf{q})}{\epsilon_+(\frac{\mathbf{q}}{2}-\mathbf{k})+\epsilon_-(\frac{\mathbf{q}}{2}+\mathbf{k})}\right], \\
\Gamma^{\alpha\alpha}_{\beta\beta}(\mathbf{p},\mathbf{p}';\mathbf{q}) &= \mathcal{V}^{(2)}_{\phi_1,\phi_2;\phi_3,\phi_4} \\
&- \int \frac{d^3k}{(2\pi)^3}\left[\frac{\mathcal{V}^{(2)}_{\phi_1,\phi_2;\phi_5,\phi_6}\Gamma^{\alpha\alpha}_{\alpha\alpha}(\mathbf{k},\mathbf{p}';\mathbf{q})}{\epsilon_-(\frac{\mathbf{q}}{2}-\mathbf{k})+\epsilon_-(\frac{\mathbf{q}}{2}+\mathbf{k})} + \frac{\mathcal{V}^{(1)}_{\phi_1,\phi_2;\phi_5,\phi_6}\Gamma^{\alpha\alpha}_{\beta\beta}(\mathbf{k},\mathbf{p}';\mathbf{q})}{\epsilon_+(\frac{\mathbf{q}}{2}-\mathbf{k})+\epsilon_+(\frac{\mathbf{q}}{2}+\mathbf{k})} + \frac{\mathcal{V}^{(3)}_{\phi_1,\phi_2;\phi_5,\phi_6}\Gamma^{\alpha\alpha}_{\alpha\beta}(\mathbf{k},\mathbf{p}';\mathbf{q})}{\epsilon_+(\frac{\mathbf{q}}{2}-\mathbf{k})+\epsilon_-(\frac{\mathbf{q}}{2}+\mathbf{k})}\right], \\
\Gamma^{\alpha\alpha}_{\alpha\beta}(\mathbf{p},\mathbf{p}';\mathbf{q}) &= \mathcal{V}^{(4)}_{\phi_1,\phi_2;\phi_3,\phi_4} \\
&- \int \frac{d^3k}{(2\pi)^3}\left[\frac{\mathcal{V}^{(4)}_{\phi_1,\phi_2;\phi_5,\phi_6}\Gamma^{\alpha\alpha}_{\alpha\alpha}(\mathbf{k},\mathbf{p}';\mathbf{q})}{\epsilon_-(\frac{\mathbf{q}}{2}-\mathbf{k})+\epsilon_-(\frac{\mathbf{q}}{2}+\mathbf{k})} \pm \frac{\mathcal{V}^{(4)}_{\phi_2,\phi_1;\phi_5,\phi_6}\Gamma^{\alpha\alpha}_{\beta\beta}(\mathbf{k},\mathbf{p}';\mathbf{q})}{\epsilon_+(\frac{\mathbf{q}}{2}-\mathbf{k})+\epsilon_+(\frac{\mathbf{q}}{2}+\mathbf{k})} + \frac{\mathcal{V}^{(5)}_{\phi_1,\phi_2;\phi_6,\phi_5}\Gamma^{\alpha\alpha}_{\alpha\beta}(\mathbf{k},\mathbf{p}';\mathbf{q})}{\epsilon_+(\frac{\mathbf{q}}{2}-\mathbf{k})+\epsilon_-(\frac{\mathbf{q}}{2}+\mathbf{k})}\right],
\end{aligned} \tag{4.7}$$

where $\Gamma^{\rho\tau}_{\mu\nu}(\mathbf{p},\mathbf{p}';\mathbf{q})$ is the t-matrix for scattering of particles in the branches μ,ν with momenta $\mathbf{q}/2\pm\mathbf{p}$ to branches ρ,τ with final momenta $\mathbf{q}/2\pm\mathbf{p}'$. The angles ϕ_5 and ϕ_6 are the angles of $\mathbf{q}/2-\mathbf{k}$ and $\mathbf{q}/2+\mathbf{k}$ in the x-y plane with y components multiplied by η. As before, the upper signs

are for bosons and the lower signs are for fermions. We obtain the t-matrices by solving this set of Bethe-Salpeter equations. We consider fermions and bosons separately in the following subsections.

4.2.2 Fermions

Solving for the t-matrices for fermions is easier than bosons, because for fermions $g_{aa} = g_{bb} = 0$. Looking at (4.7), we can observe

$$\Gamma^{\alpha\alpha}_{\alpha\alpha}(\mathbf{p},\mathbf{p}';\mathbf{q}) = -\Gamma^{\beta\beta}_{\alpha\alpha}(\mathbf{p},\mathbf{p}';\mathbf{q}), \qquad \frac{\Gamma^{\alpha\alpha}_{\alpha\alpha}(\mathbf{p},\mathbf{p}';\mathbf{q})}{e^{i\phi_1}-e^{i\phi_2}} = \frac{1}{\sqrt{2}}\frac{\Gamma^{\alpha\beta}_{\alpha\alpha}(\mathbf{p},\mathbf{p}';\mathbf{q})}{e^{i\phi_1}+e^{i\phi_2}}. \tag{4.8}$$

Then, the set of Bethe-Salpeter equations reduces to

$$\begin{aligned}\frac{\Gamma^{\alpha\alpha}_{\alpha\alpha}(\mathbf{p},\mathbf{p}';\mathbf{q})}{e^{i\phi_1}-e^{i\phi_2}} &= -\frac{g_{ab}}{8}\left(e^{-i\phi_3}-e^{-i\phi_4}\right) + \frac{g_{ab}}{8}\int\frac{d^3k}{(2\pi)^3}\left[\frac{\left(e^{-i\phi_5}-e^{-i\phi_6}\right)}{\epsilon_-(\frac{\mathbf{q}}{2}-\mathbf{k})+\epsilon_-(\frac{\mathbf{q}}{2}+\mathbf{k})}\right.\\ &\left.+\frac{\left(e^{-i\phi_5}-e^{-i\phi_6}\right)}{\epsilon_+(\frac{\mathbf{q}}{2}-\mathbf{k})+\epsilon_+(\frac{\mathbf{q}}{2}+\mathbf{k})} - \frac{2\left(e^{-i\phi_5}+e^{-i\phi_6}\right)}{\epsilon_+(\frac{\mathbf{q}}{2}-\mathbf{k})+\epsilon_-(\frac{\mathbf{q}}{2}+\mathbf{k})}\frac{e^{i\phi_5}+e^{i\phi_6}}{e^{i\phi_6}-e^{i\phi_5}}\right]\Gamma^{\alpha\alpha}_{\alpha\alpha}(\mathbf{k},\mathbf{p}';\mathbf{q}).\end{aligned} \tag{4.9}$$

Rearranging terms, we have

$$\begin{aligned}\frac{\Gamma^{\alpha\alpha}_{\alpha\alpha}(\mathbf{p},\mathbf{p}';\mathbf{q})}{(e^{i\phi_1}-e^{i\phi_2})(e^{-i\phi_3}-e^{-i\phi_4})} &= -\frac{g_{ab}}{8} - \frac{g_{ab}}{8}\int\frac{d^3k}{(2\pi)^3}\left[\frac{|e^{i\phi_5}-e^{i\phi_6}|^2}{\epsilon_-(\frac{\mathbf{q}}{2}-\mathbf{k})+\epsilon_-(\frac{\mathbf{q}}{2}+\mathbf{k})}\right.\\ &\left.+\frac{|e^{i\phi_5}-e^{i\phi_6}|^2}{\epsilon_+(\frac{\mathbf{q}}{2}-\mathbf{k})+\epsilon_+(\frac{\mathbf{q}}{2}+\mathbf{k})} + \frac{2|e^{i\phi_5}+e^{i\phi_6}|^2}{\epsilon_+(\frac{\mathbf{q}}{2}-\mathbf{k})+\epsilon_-(\frac{\mathbf{q}}{2}+\mathbf{k})}\right]\frac{\Gamma^{\alpha\alpha}_{\alpha\alpha}(\mathbf{k},\mathbf{p}';\mathbf{q})}{(e^{i\phi_6}-e^{i\phi_5})(e^{-i\phi_3}-e^{-i\phi_4})}.\end{aligned} \tag{4.10}$$

Defining

$$\tilde{\Gamma}^{\alpha\alpha}_{\alpha\alpha}(\mathbf{p},\mathbf{p}';\mathbf{q}) \equiv \frac{\Gamma^{\alpha\alpha}_{\alpha\alpha}(\mathbf{p},\mathbf{p}';\mathbf{q})}{(e^{i\phi_1}-e^{i\phi_2})(e^{-i\phi_3}-e^{-i\phi_4})}, \tag{4.11}$$

equation (4.10) can be regarded as a self-consistent equation for $\tilde{\Gamma}$:

$$\begin{aligned}\tilde{\Gamma}^{\alpha\alpha}_{\alpha\alpha}(\mathbf{p},\mathbf{p}';\mathbf{q}) &= -\frac{g_{ab}}{8} - \frac{g_{ab}}{8}\int\frac{d^3k}{(2\pi)^3}\left[\frac{|e^{i\phi_5}-e^{i\phi_6}|^2}{\epsilon_-(\frac{\mathbf{q}}{2}-\mathbf{k})+\epsilon_-(\frac{\mathbf{q}}{2}+\mathbf{k})}\right.\\ &\left.+\frac{|e^{i\phi_5}-e^{i\phi_6}|^2}{\epsilon_+(\frac{\mathbf{q}}{2}-\mathbf{k})+\epsilon_+(\frac{\mathbf{q}}{2}+\mathbf{k})} + \frac{2|e^{i\phi_5}+e^{i\phi_6}|^2}{\epsilon_+(\frac{\mathbf{q}}{2}-\mathbf{k})+\epsilon_-(\frac{\mathbf{q}}{2}+\mathbf{k})}\right]\tilde{\Gamma}^{\alpha\alpha}_{\alpha\alpha}(\mathbf{k},\mathbf{p}';\mathbf{q}).\end{aligned} \tag{4.12}$$

Since the right hand side does not depend on $\mathbf{p}$, $\tilde{\Gamma}^{\alpha\alpha}_{\alpha\alpha}(\mathbf{p},\mathbf{p}';\mathbf{q})$ does not depend on $\mathbf{p}$. Then,

$$\begin{aligned}&\left(1+\frac{g_{ab}}{8}\int\frac{d^3k}{(2\pi)^3}\left[\frac{|e^{i\phi_5}-e^{i\phi_6}|^2}{\epsilon_-(\frac{\mathbf{q}}{2}-\mathbf{k})+\epsilon_-(\frac{\mathbf{q}}{2}+\mathbf{k})} + \frac{|e^{i\phi_5}-e^{i\phi_6}|^2}{\epsilon_+(\frac{\mathbf{q}}{2}-\mathbf{k})+\epsilon_+(\frac{\mathbf{q}}{2}+\mathbf{k})} + \frac{2|e^{i\phi_5}+e^{i\phi_6}|^2}{\epsilon_+(\frac{\mathbf{q}}{2}-\mathbf{k})+\epsilon_-(\frac{\mathbf{q}}{2}+\mathbf{k})}\right]\right)\\ &\times\tilde{\Gamma}^{\alpha\alpha}_{\alpha\alpha}(\mathbf{p},\mathbf{p}';\mathbf{q}) = -\frac{g_{ab}}{8},\end{aligned} \tag{4.13}$$

which implies

$$\Gamma^{\alpha\alpha}_{\alpha\alpha}(\mathbf{p},\mathbf{p}';\mathbf{q}) = -(e^{i\phi_1}-e^{i\phi_2})(e^{-i\phi_3}-e^{-i\phi_4})\times$$
$$\left(\frac{8}{g_{ab}}+\int\frac{d^3k}{(2\pi)^3}\left[\frac{|e^{i\phi_5}-e^{i\phi_6}|^2}{\epsilon_-(\frac{\mathbf{q}}{2}-\mathbf{k})+\epsilon_-(\frac{\mathbf{q}}{2}+\mathbf{k})}+\frac{|e^{i\phi_5}-e^{i\phi_6}|^2}{\epsilon_+(\frac{\mathbf{q}}{2}-\mathbf{k})+\epsilon_+(\frac{\mathbf{q}}{2}+\mathbf{k})}+\frac{2|e^{i\phi_5}+e^{i\phi_6}|^2}{\epsilon_+(\frac{\mathbf{q}}{2}-\mathbf{k})+\epsilon_-(\frac{\mathbf{q}}{2}+\mathbf{k})}\right]\right)^{-1}. \tag{4.14}$$

This is the t-matrix for fermions in the lower dispersion branch. To determine if this t-matrix depends on the ultraviolet cutoff, we define the dimensionless functions

$$f(\tilde{q}/2)\equiv$$
$$\frac{\pi}{m\kappa}\int\frac{d^3k}{(2\pi)^3}\left[\frac{1}{\epsilon_-(\frac{\mathbf{q}}{2}-\mathbf{k})+\epsilon_-(\frac{\mathbf{q}}{2}+\mathbf{k})}+\frac{1}{\epsilon_+(\frac{\mathbf{q}}{2}-\mathbf{k})+\epsilon_+(\frac{\mathbf{q}}{2}+\mathbf{k})}+\frac{2}{\epsilon_+(\frac{\mathbf{q}}{2}-\mathbf{k})+\epsilon_-(\frac{\mathbf{q}}{2}+\mathbf{k})}-\frac{4m}{k^2}\right], \tag{4.15}$$

$$g(\tilde{q}/2)\equiv$$
$$-\frac{\pi}{m\kappa}\int\frac{d^3k}{(2\pi)^3}\left[\frac{\cos(\phi_5-\phi_6)}{\epsilon_-(\frac{\mathbf{q}}{2}-\mathbf{k})+\epsilon_-(\frac{\mathbf{q}}{2}+\mathbf{k})}+\frac{\cos(\phi_5-\phi_6)}{\epsilon_+(\frac{\mathbf{q}}{2}-\mathbf{k})+\epsilon_+(\frac{\mathbf{q}}{2}+\mathbf{k})}-\frac{2\cos(\phi_5-\phi_6)}{\epsilon_+(\frac{\mathbf{q}}{2}-\mathbf{k})+\epsilon_-(\frac{\mathbf{q}}{2}+\mathbf{k})}\right], \tag{4.16}$$

where $\tilde{q}\equiv|\mathbf{q}|/\kappa$. One can prove that $f(x)$ and $g(x)$ do not diverge in the ultraviolet. Then,

$$\Gamma^{\alpha\alpha}_{\alpha\alpha}(\mathbf{p},\mathbf{p}';\mathbf{q}) = -(e^{i\phi_1}-e^{i\phi_2})(e^{-i\phi_3}-e^{-i\phi_4})\left(\frac{8}{g_{ab}}+\int\frac{d^3k}{(2\pi)^3}\frac{8m}{k^2}+\frac{2m\kappa}{\pi}[f(\tilde{q}/2)+g(\tilde{q}/2)]\right)^{-1}. \tag{4.17}$$

The relation between the scattering length a_{ab} in the absence of the spin-orbit coupling and the bare coupling g_{ab} is (4.1)

$$\frac{1}{g_{ab}} = \frac{m}{4\pi a_{ab}} - \int\frac{d^3k}{(2\pi)^3}\frac{m}{k^2}. \tag{4.18}$$

Then,

$$\begin{aligned}\Gamma^{\alpha\alpha}_{\alpha\alpha}(\mathbf{p},\mathbf{p}';\mathbf{q}) &= -(e^{i\phi_1}-e^{i\phi_2})(e^{-i\phi_3}-e^{-i\phi_4})\left(\frac{2m}{\pi a_{ab}}+\frac{2m\kappa}{\pi}[f(\tilde{q}/2)+g(\tilde{q}/2)]\right)^{-1}\\ &= -\frac{\pi a_{ab}}{2m}\frac{(e^{i\phi_1}-e^{i\phi_2})(e^{-i\phi_3}-e^{-i\phi_4})}{1+a_{ab}\kappa[f(\tilde{q}/2)+g(\tilde{q}/2)]}.\end{aligned} \tag{4.19}$$

This t-matrix is explicitly free of the ultraviolet divergence, and written solely in terms of physical observables. Similarly, logarithmic ultraviolet divergences do not appear in the gap equation

for fermions in paired states, and linear divergences can again be renormalized away in favor of scattering lengths, as discussed in [61, 62, 63, 64, 65, 66].

The functions $f(x)$ and $g(x)$ depend on the anisotropy η. In the isotropic case of $\eta = 1$, the functions behave as in Fig. 4.2. The functions diverges logarithmically at the infrared as $x \to 0$,

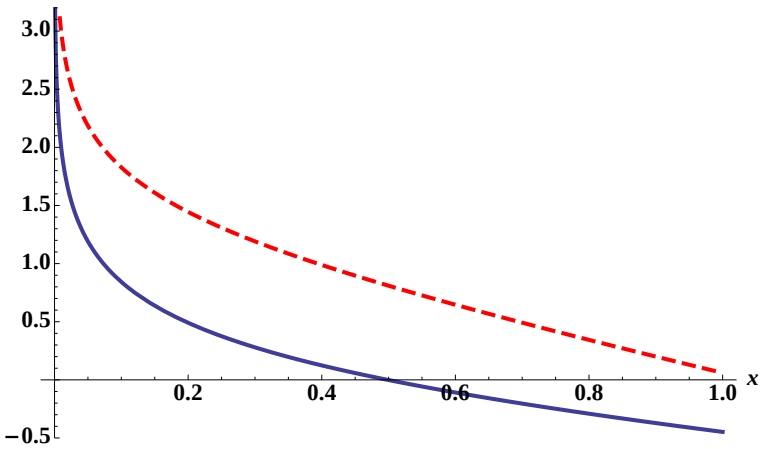

Figure 4.2: The center-of-mass momentum dependence of $f(x)$ (solid line) and $g(x)$ (dashed line) when $\eta = 1$ as defined in Eq. (4.15) and (4.16).

which leads to the conclusion

$$\Gamma^{\alpha\alpha}_{\alpha\alpha}(\mathbf{p}, \mathbf{p}'; 0) = 0, \tag{4.20}$$

namely, there is no interaction if the center of mass momentum of the two colliding particles is zero. In other words, if the colliding particles have opposite momenta, the particles do not feel the interaction. This infrared divergence for $\eta = 1$ arises from the existence of infinitely many pairs of zero-energy single-particle states with $q = 0$. For $\mathbf{q} \neq 0$, there is only one pair of zero-energy states and, thus, no infrared divergence. A similar mechanism for the infrared divergence occurs in Bose systems as well, as we discuss next.

4.2.3 Bosons

As for fermions, the t-matrix for bosons does not contain any ultraviolet divergences. However, the bosonic t-matrix is much more difficult to obtain. The detailed derivation is given in Appendix D.

The result is

$$\Gamma^{\alpha\alpha}_{\alpha\alpha}(\mathbf{p},\mathbf{p}';\mathbf{q}) = \frac{\pi}{m\kappa}\begin{pmatrix} 1 & e^{i(\phi_1+\phi_2)} & \dfrac{e^{i\phi_1}+e^{i\phi_2}}{2}\end{pmatrix} M^{-1} \begin{pmatrix} 1 \\ e^{-i(\phi_3+\phi_4)} \\ \dfrac{e^{-i\phi_3}+e^{-i\phi_4}}{2}\end{pmatrix}, \tag{4.21}$$

where

$$M = \begin{pmatrix} f(\frac{\tilde{q}}{2})+\frac{1}{\kappa a_{aa}} & h_1(\tilde{\mathbf{q}}/2) & h_2(\tilde{\mathbf{q}}/2) \\ h_1^*(\tilde{\mathbf{q}}/2) & f(\frac{\tilde{q}}{2})+\frac{1}{\kappa a_{bb}} & h_2^*(\tilde{\mathbf{q}}/2) \\ h_2^*(\tilde{\mathbf{q}}/2) & h_2(\tilde{\mathbf{q}}/2) & \frac{1}{2}\left(f(\frac{\tilde{q}}{2})-g(\frac{\tilde{q}}{2})+\frac{1}{\kappa a_{ab}}\right)\end{pmatrix}, \tag{4.22}$$

with $\tilde{\mathbf{q}} \equiv \mathbf{q}/\kappa$ and $\tilde{q} \equiv q/\kappa$. The dimensionless functions $f(\tilde{q}/2)$ and $g(\tilde{q}/2)$ are the same as in the previous subsection:

$$\begin{aligned} &f(\tilde{q}/2) \equiv \\ &\frac{\pi}{m\kappa}\int \frac{d^3k}{(2\pi)^3}\left[\frac{1}{\epsilon_-(\frac{\mathbf{q}}{2}+\mathbf{k})+\epsilon_-(\frac{\mathbf{q}}{2}-\mathbf{k})}+\frac{1}{\epsilon_+(\frac{\mathbf{q}}{2}+\mathbf{k})+\epsilon_+(\frac{\mathbf{q}}{2}-\mathbf{k})}+\frac{2}{\epsilon_-(\frac{\mathbf{q}}{2}+\mathbf{k})+\epsilon_+(\frac{\mathbf{q}}{2}-\mathbf{k})}-\frac{4m}{k^2}\right] \\ &g(\tilde{q}/2) \equiv \\ &-\frac{\pi}{m\kappa}\int \frac{d^3k}{(2\pi)^3}\left[\frac{\cos(\phi_5-\phi_6)}{\epsilon_-(\frac{\mathbf{q}}{2}+\mathbf{k})+\epsilon_-(\frac{\mathbf{q}}{2}-\mathbf{k})}+\frac{\cos(\phi_5-\phi_6)}{\epsilon_+(\frac{\mathbf{q}}{2}+\mathbf{k})+\epsilon_+(\frac{\mathbf{q}}{2}-\mathbf{k})}-\frac{2\cos(\phi_5-\phi_6)}{\epsilon_-(\frac{\mathbf{q}}{2}+\mathbf{k})+\epsilon_+(\frac{\mathbf{q}}{2}-\mathbf{k})}\right]. \end{aligned} \tag{4.23}$$

The dimensionless functions $h_1(\tilde{\mathbf{q}}/2)$, and $h_2(\tilde{\mathbf{q}}/2)$ are defined by

$$\begin{aligned} &h_1(\tilde{\mathbf{q}}/2) \equiv \\ &\frac{\pi}{m\kappa}\int \frac{d^3k}{(2\pi)^3}\left[\frac{e^{i(\phi_5+\phi_6)}}{\epsilon_-(\frac{\mathbf{q}}{2}+\mathbf{k})+\epsilon_-(\frac{\mathbf{q}}{2}-\mathbf{k})}+\frac{e^{i(\phi_5+\phi_6)}}{\epsilon_+(\frac{\mathbf{q}}{2}+\mathbf{k})+\epsilon_+(\frac{\mathbf{q}}{2}-\mathbf{k})}-\frac{2e^{i(\phi_5+\phi_6)}}{\epsilon_-(\frac{\mathbf{q}}{2}+\mathbf{k})+\epsilon_+(\frac{\mathbf{q}}{2}-\mathbf{k})}\right] \\ &h_2(\tilde{\mathbf{q}}/2) \equiv \\ &\frac{\pi}{2m\kappa}\int \frac{d^3k}{(2\pi)^3}\left[\frac{e^{i\phi_5}+e^{i\phi_6}}{\epsilon_-(\frac{\mathbf{q}}{2}+\mathbf{k})+\epsilon_-(\frac{\mathbf{q}}{2}-\mathbf{k})}-\frac{e^{i\phi_5}+e^{i\phi_6}}{\epsilon_+(\frac{\mathbf{q}}{2}+\mathbf{k})+\epsilon_+(\frac{\mathbf{q}}{2}-\mathbf{k})}-\frac{2(e^{i\phi_5}-e^{i\phi_6})}{\epsilon_-(\frac{\mathbf{q}}{2}+\mathbf{k})+\epsilon_+(\frac{\mathbf{q}}{2}-\mathbf{k})}\right]. \end{aligned} \tag{4.24}$$

Note that changing the angle of $\mathbf{q}$ in the x-y plane only changes the overall phases of $h_1(\tilde{\mathbf{q}}/2)$ and $h_2(\tilde{\mathbf{q}}/2)$. In addition, these four functions are everywhere finite except for the logarithmic divergence of $f(\tilde{q}/2)$ at $\tilde{q}=0$.

4.3 Ground state phases

We now determine the many-body ground state via mean-field theory using the t-matrix derived above as the effective interaction, an approximation valid as long as the na_{ij}^3 are all $\ll 1$, where n is the particle density. In mean field, we assume that all particles are in the single-particle ground states $(\kappa, 0, 0)$ or $(-\kappa, 0, 0)$, and thus ignore possible occupation of excited states as a consequence of the interaction. In this case the system is described essentially by the Nozières model [67]. The issues of going beyond mean field, (e.g., via Bogoliubov theory) as well as including possible effects of the condensate on the effective interaction, are beyond the scope of this thesis and are left for the future. For $0 \leq \eta < 1$, we take the particles to be either at $\mathbf{p} = (\kappa, 0, 0)$ or $(-\kappa, 0, 0)$; the relevant interactions are those between particles of either the same momentum or opposite momenta. We denote the interaction with same momentum by $\Gamma_0 \equiv \Gamma_{\alpha\alpha}^{\alpha\alpha}(0, 0; \pm 2\boldsymbol{\kappa})$ and that with opposite momenta by $\Gamma_\pi \equiv \Gamma_{\alpha\alpha}^{\alpha\alpha}(\pm\boldsymbol{\kappa}, \mp\boldsymbol{\kappa}, 0)$, where $\boldsymbol{\kappa} \equiv (\kappa, 0, 0)$ as in the previous chapter.

The relevant terms in the interaction are then equivalent to the Nozières model [67]

$$\mathcal{H}_{\rm int} \sim \frac{1}{2V}\Gamma_0 N(N+1) \; + \frac{1}{V}(2\Gamma_\pi - \Gamma_0) N_\pi N_0, \tag{4.25}$$

where $N_0 \equiv \alpha^\dagger_{(\kappa,0,0)}\alpha_{(\kappa,0,0)}$ and $N_\pi \equiv \alpha^\dagger_{(-\kappa,0,0)}\alpha_{(-\kappa,0,0)}$. The total number of particles, $N = N_0 + N_\pi$, is fixed. For $\Gamma_0 < 2\Gamma_\pi$, the ground state is a single BEC with either all the particles in $(\kappa, 0, 0)$ or $(-\kappa, 0, 0)$, while, for $\Gamma_0 > 2\Gamma_\pi$, the condensate is nominally fragmented with half of the atoms forming a BEC in one state and the other half forming a BEC in the other state. However, as shown in Ref. [55], such a fragmented state is expected to be unstable against formation of a coherent condensate with a condensate wave function that is a coherent superposition of the two momenta. Following the conventions of Refs. [49, 50], we call the single BEC phase "plane wave," and the BEC phase with two different momenta "striped." The difference of the present calculation from earlier studies with mean-field couplings [49, 50], is that here the bare couplings, $\mathcal{V}^{(1)}_{0,0;0,0}$ and $\mathcal{V}^{(1)}_{0,\pi;0,\pi}$, are replaced by Γ_0 and Γ_π, respectively.

While there is no difficulty in deriving the phase diagrams for general scattering lengths, we assume here for simplicity that the intraspecies scattering lengths are equal, $a_{aa} = a_{bb}$. Then,

$$\begin{aligned}
\Gamma_0 &= \frac{2\pi}{m\kappa}\frac{1/\kappa a_{aa} + 1/\kappa a_{ab} + 2f(1) - g(1) + h_1(1) - 4h_2(1)}{(1/\kappa a_{ab} + f(1) - g(1))(1/\kappa a_{aa} + f(1) + h_1(1)) - 4h_2(1)^2}, \\
\Gamma_\pi &= \frac{2\pi}{m\kappa}\frac{1}{1/\kappa a_{aa} + f(0) - h_1(0)},
\end{aligned} \tag{4.26}$$

where $h_1(0) \equiv h_1(\tilde{\mathbf{q}} = (0,0,0))$, $h_1(1) \equiv h_1(\tilde{\mathbf{q}} = (1,0,0))$, etc. The quantities $f(0)$, $h_1(0)$, $f(1)$, $g(1)$, $h_1(1)$, and $h_2(1)$, which depend on η, can be calculated numerically. The interaction between different momenta Γ_π is independent of a_{ab}, and is a monotonically increasing nonnegative function of κa_{aa}, equal to 0 at $\kappa a_{aa} = 0$ and reaching $2\pi/\left[m\kappa(f(0) - h_1(0))\right]$ at $\kappa a_{aa} = \infty$. The dependence of Γ_0 on κa_{aa} and κa_{ab} is more complicated. We plot Γ_0 and Γ_π, both scaled by $2\pi/(m\kappa)$, for $\eta = 0.5$ in Fig. 4.3. Now we discuss the ground-state phases from $\eta = 0$ to 1.

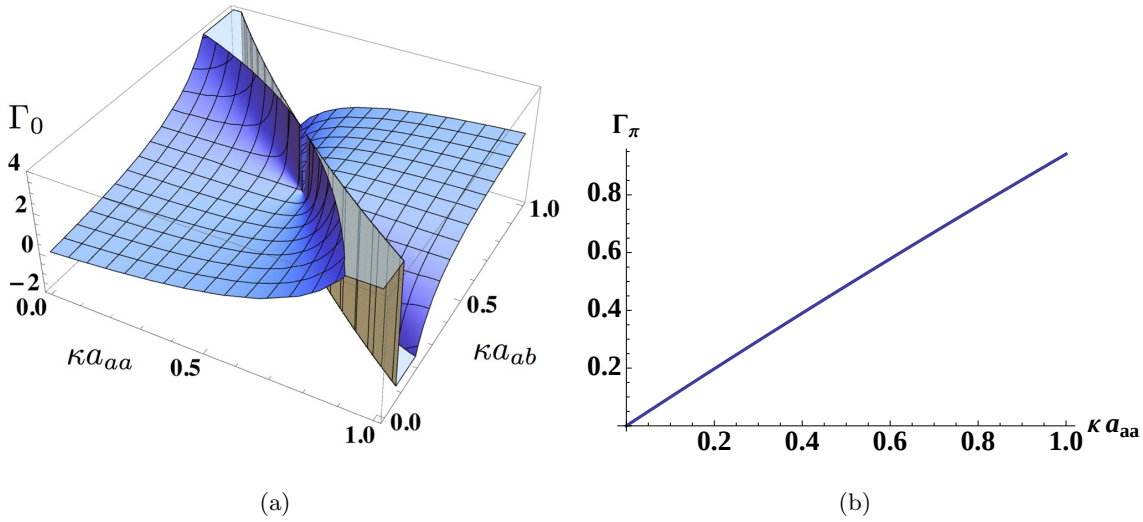

(a) (b)

Figure 4.3: (a) Γ_0 as a function of κa_{aa} and κa_{ab}, and (b) Γ_π as a function of κa_{aa}, both scaled by $2\pi/(m\kappa)$, for $\eta = 0.5$. The vertical plane in the middle of panel (a) indicates the resonance where, from left to right, Γ_0 diverges to positive infinity and comes back from negative infinity.

When $\eta = 0$, the effective interactions are relatively simple. It can be shown that $f(0) = h_1(0)$ for $\eta = 0$; hence $\Gamma_\pi = 2\pi a_{aa}/m$, and the effective interaction in the $\mathbf{q} = 0$ channel does not depend on the spin-orbit coupling strength κ. In the $\mathbf{q}/2 = (\kappa, 0, 0)$ channel, $f(1) = -1, g(1) = 0, h_1(1) = 0$, and $h_2(1) = 1/2$, so,

$$\Gamma_0 = \frac{2\pi}{m\kappa} \frac{\kappa a_{aa} + \kappa a_{ab} - 4\kappa a_{aa}\kappa a_{ab}}{1 - \kappa a_{aa} - \kappa a_{ab}} \tag{4.27}$$

for $\eta = 0$. The effective interaction at small κa_{aa} and κa_{ab} is positive, and diverges when $\kappa a_{aa} + \kappa a_{ab}$ approaches unity. As one crosses the line $\kappa a_{aa} + \kappa a_{ab} = 1$, Γ_0 starts at negative infinity and remains negative until $\kappa a_{aa} + \kappa a_{ab} = 4\kappa a_{aa}\kappa a_{ab}$, after which Γ_0 is positive. When Γ_0 is negative, we expect the BEC in bulk to be unstable against collapse, as in ordinary BEC's with negative

scattering length in the absence of spin-orbit couplings. We call the phase with an attractive interaction "unstable." The three possible ground-state phases, plane wave, striped, and unstable, are determined by the sign of Γ_0 and the interplay between Γ_0 and Γ_π.

As η increases from 0, the basic structure of Γ_0 does not change; Γ_0 remains positive at small κa_{aa} and κa_{ab}, and as these variables increase, Γ_0 again diverges at a line in the κa_{aa}-κa_{ab} plane, beyond which it is negative up to a second line, after which Γ_0 is positive. Since the denominator of Γ_0 is quadratic in $1/(\kappa a)$ [Eq. (4.26)], it has in fact two zeros, one for positive scattering lengths, as shown, and a second for negative scattering lengths, which is discussed at the end of this section. The structure for positive scattering lengths is illustrated in Fig. 4.3, for $\eta = 0.5$.

The ground-state phase diagrams for various η are plotted in Fig. 4.4. In the panels, the plane-wave phase is labeled "P," the striped phase "S," and the unstable phase "U." The plane-wave phase occurs when $0 < \Gamma_0 < 2\Gamma_\pi$, the striped phase when $2\Gamma_\pi < \Gamma_0$, and the unstable phase when $\Gamma_0 < 0$. Note the overall tendency of the phase diagrams as η increases; the upper striped region detaches from the resonant critical point, where the resonant line (between S and U) and the line with $\Gamma_0 = 0$ (between U and P) touch, and the region is pushed upward as η is increased. Meanwhile, the shapes of the resonant line and the boundaries of plane-wave regions change but, with the exception of the upper striped region, the overall topology does not change. The dashed lines $a_{aa} = a_{ab}$ in the figures are the phase-separation lines obtained earlier [49] using mean-field couplings $4\pi a_{aa}/m$ and $4\pi a_{ab}/m$; there the striped phase is preferred above the dashed lines and the plane-wave phase is preferred below the dashed lines. Use of mean-field couplings is accurate for small κa_{aa} and κa_{ab} but, as these variables increase, the deviation from the mean-field-coupling prediction becomes significant and the phase diagrams exhibit qualitatively new and rich structures.

This overall tendency continues to around $\eta \sim 0.99$. With further increase of η toward isotropy, $\eta = 1$, we start to observe qualitatively new behavior of the phase diagrams. The phase diagrams close to $\eta = 1$ are plotted in Fig. 4.5. As one sees, the striped region comes back from above and touches the resonant critical point, and at the same time the lower plane-wave region detaches from the critical point. In the limit $\eta = 1$, the plane-wave region vanishes.

The behavior around $\eta \simeq 1$ is in fact logarithmic in the deviations of the anisotropy η from unity. We write $\delta = 1 - \eta^2$; as $\delta \to 0$, $h_1(0)$, $f(1)$, $g(1)$, $h_1(1)$, and $h_2(1)$ approach finite values, but, in leading order for small δ, $f(0) \sim |\ln \delta|/4$. Setting, for small δ, $h_1(0)$, $f(1)$, $g(1)$, $h_1(1)$, and

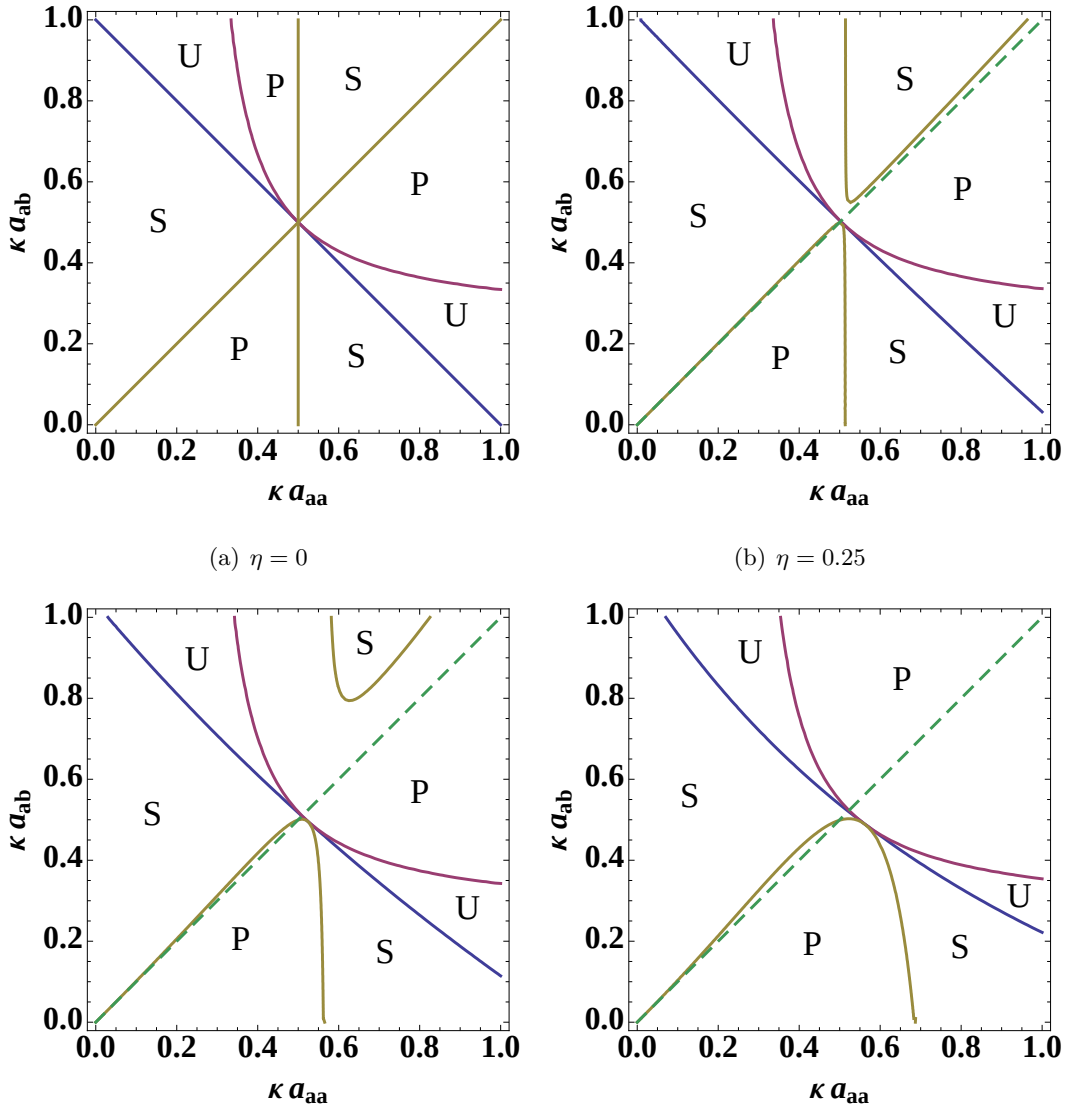

(a) $\eta = 0$

(b) $\eta = 0.25$

(c) $\eta = 0.50$

(d) $\eta = 0.75$

Figure 4.4: Ground state phase diagrams in the κa_{aa} - κa_{ab} plane for anisotropies $\eta = 0$, 0.25, 0.5, and 0.75. The regions P are the plane-wave phase with a BEC of a single momentum. The regions S are the striped phase with a BEC of a coherent superposition of two different momenta. The phase in the regions U are unstable, with the effective interaction Γ_0 negative. Along the line between S and U, Γ_0 diverges, and along the line between U and P, Γ_0 vanishes. The intersection of these two lines is a critical point. The dashed lines indicate the phase diagram derived using mean-field coupling, in which the plane is separated into an upper striped region and a lower plane wave region.

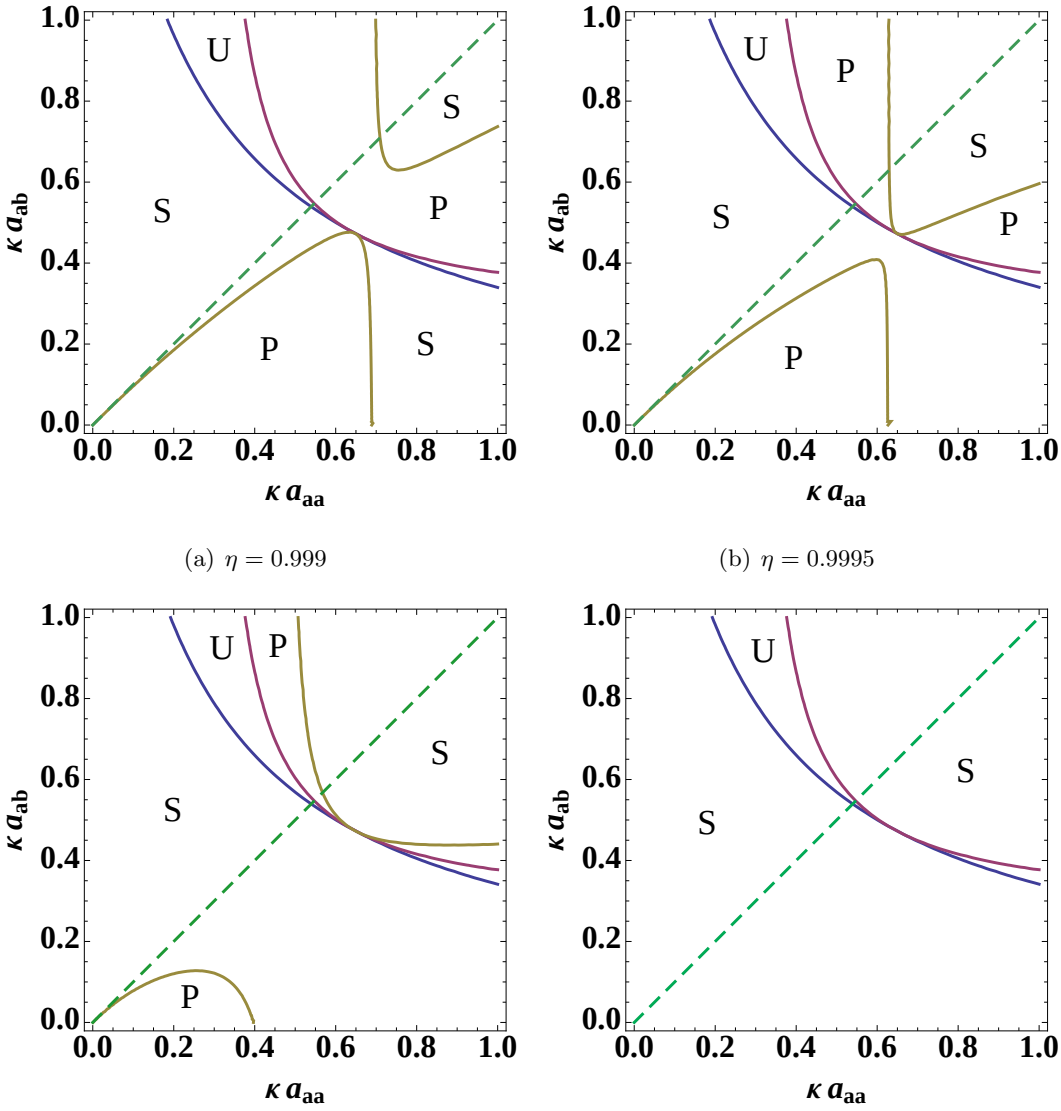

(a) $\eta = 0.999$

(b) $\eta = 0.9995$

(c) $\eta = 0.99999$

(d) $\eta = 1$

Figure 4.5: Ground-state phase diagrams for η close to unity.

$h_2(1)$, to their values at $\delta = 0$ and approximating $f(0)$ by $|\ln\delta|/4$, corresponds to fixing Γ_0 and varying the slope of Γ_π. In the isotropic limit $\delta = 0$, $\Gamma_\pi = 0$ and thus a plane-wave region is not allowed [cf. Eq. (4.25)]. With small anisotropy, Γ_π can be positive, and small plane-wave regions appear.

We now briefly consider tuning the scattering lengths to negative values. In the absence of spin-orbit couplings, negative scattering lengths lead to an instability in large systems. On the other hand, as we see from Eq. (4.26), tuning the inverse scattering lengths to just below 0 does not immediately lead to an attractive interaction; in the presence of the spin-orbit coupling fields, Rashba-Dresselhaus couplings can stabilize BEC's with negative scattering lengths if the inverse scattering lengths are small. Even when Γ_0 is negative, systems with small particle number can be metastable in the presence of an attractive interaction [1]. For illustration, we plot the phase diagram for $\eta = 0.5$, extended to negative scattering lengths in Fig. 4.6. In the regions marked "Stable," $\Gamma_0 > 0$ and the ground state is either a plane-wave or striped phase. As seen in the figure, when both scattering lengths a_{aa} and a_{ab} are negative and large, another stable region appears in the phase diagram, in which the ground state is in the striped phase. The line between the lower-left striped phase and the unstable phase is a second resonant line along which Γ_0 diverges. A stable region with negative scattering lengths generally exists for all $0 < \eta \leq 1$; as η increases, the stable region in the phase diagram becomes larger.

4.4 Conclusion

Proposed schemes to realize Rashba-Dresselhaus spin-orbit couplings in ultracold atomic experiments [39, 40, 41, 42, 43] use Raman lasers to couple atoms in different hyperfine states. In general as one transforms the original basis to one in which the coupling has the Rashba-Dresselhaus spin-orbit structure, the interaction Hamiltonian acquires terms such as $a^\dagger_{\mathbf{p}_4} a^\dagger_{\mathbf{p}_3} a_{\mathbf{p}_2} b_{\mathbf{p}_1}$ which do not conserve the number of particles in each pseudospin state (a-like and b-like). Our analysis, which

[1] Assuming bosons trapped in an isotropic harmonic potential, we can roughly estimate the particle number below which the condensate is stable with $\Gamma_0 < 0$. In the absence of spin-orbit coupling, the critical number of bosons is $N_c \sim 0.6 a_{\rm osc}/|a|$, where $a_{\rm osc}$ is the oscillator length of a trap $\sqrt{\hbar/(m\omega)}$ [68]. For spin-orbit coupled bosons, the scattering length is replaced by $m\Gamma_0/(4\pi)$. Introducing a scaled effective coupling $\tilde{\Gamma}_0 = m\kappa\Gamma_0/(2\pi)$ (the scale used in Fig. 4.3), we estimate a critical number $N_c \sim 0.3\kappa a_{\rm osc}/|\tilde{\Gamma}_0|$. Using realistic values of $\kappa \sim \sqrt{2}\pi/804$ nm [27] and $a_{\rm osc} \sim 1\mu$m, we obtain $N_c \sim 2/|\tilde{\Gamma}_0|$, which implies that stabilization occurs only quite close to the line $\Gamma_0 = 0$.

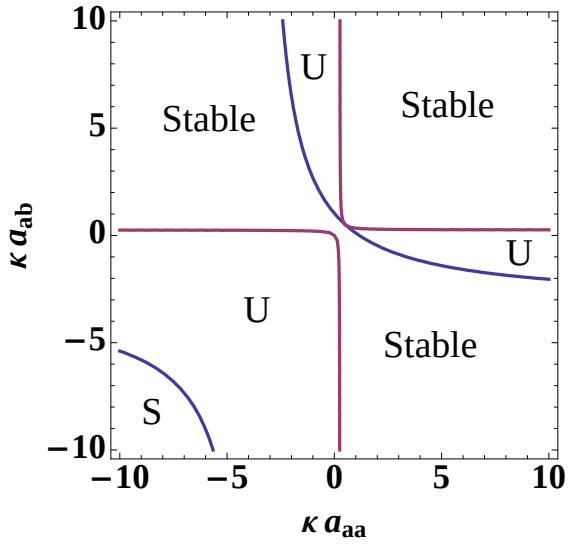

Figure 4.6: Ground-state phase diagram for $\eta = 0.5$ extended to negative values of scattering lengths. The regions marked U and S are unstable and striped phases, as before. The region marked "Stable" is either a plane-wave or striped phase. Note the appearance of a stable (striped) phase when both scattering lengths are large and negative.

did not take such terms into account, can be directly compared with proposed experiments when the interaction is independent of species ($g_{aa} = g_{bb} = g_{ab}$), in which case the interaction is independent of the choice of basis. This condition is a good approximation for the three hyperfine states of ^{87}Rb in the lowest $F = 1$ state. The assumption that $g_{aa} = g_{bb} = g_{ab}$ corresponds to the (dashed) diagonal lines in Figs. 4.4 and 4.5. Figure 4.7 shows the phase diagram in the η-κa plane, where a is the assumed common scattering length.

For $0 \leq \eta \leq 0.99$, the system, with increasing κa, experiences transitions from plane-wave to striped, then to unstable, and finally to the plane-wave phase again, as seen in Fig. 4.7(a). Looking more closely at the region $0.9 \leq \eta \leq 1$, as drawn on a logarithmic scale in Fig. 4.7(b), we find that the line separating the lower plane-wave and striped regions terminates and another line starts from positive infinity above which the striped phase is preferred. This new line touches the uppermost line (below the upper P phase) in the figure in the $\eta \to 1$ limit, and thus no plane-wave region exists for isotropic spin-orbit coupling[2].

[2]While one can achieve large scattering lengths experimentally with Feshbach resonances, the general $m_F, m_{F'}$ dependence of the resonances leads to differences of the scattering lengths near the resonances, a complicating feature requiring analysis beyond the scope of this thesis.

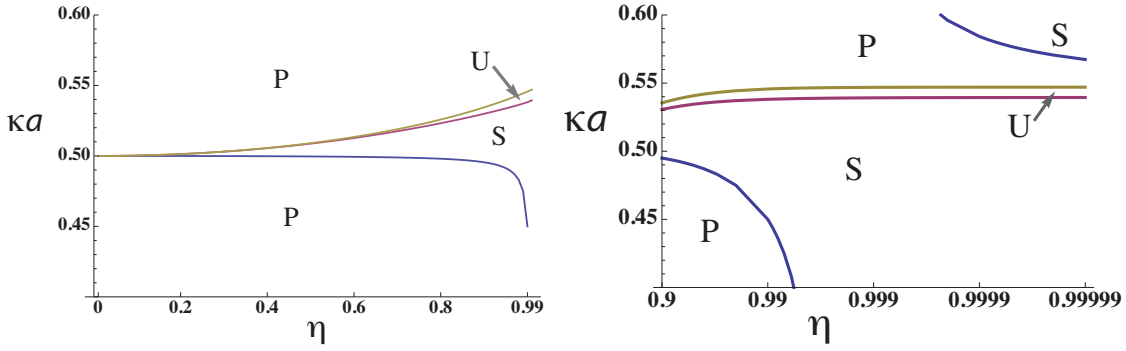

(a) (b)

Figure 4.7: Ground-state phase diagram when $a_{aa} = a_{bb} = a_{ab} = a$ in the η-κa plane for (a) anisotropies less than 0.99 and (b) anisotropies close to unity. The horizontal axis of panel (b) is a logarithmic scale.

Chapter 5

Three-component ultracold fermions

5.1 Introduction

In this chapter, we turn our attention to the three-component ultracold fermions. The content in this chapter is based on [4].

Multi-component ultracold atomic systems have recently been the focus of both experiment and theory, motivated in part by the prospect of simulating a wider range of many-body models, such as lattice SU(N) models [69, 70, 71, 72, 73] and quantum chromodynamics (QCD) analogs [74, 75, 76, 77], than is possible with single- or two-component systems. The possibility of creating analogs of color superfluid states and the formation of hadronic states in multicomponent systems [74, 75, 76] is especially interesting since the regime of cold dense QCD matter is not directly achievable in current nuclear experiments or in lattice QCD.

When three species of fermions weakly attract each other, two species form Cooper pairs and the third remains a Fermi liquid [78, 79, 80, 81, 82, 83, 84, 85]. Which two species pair depends on anisotropies in the interactions and mass differences between different species. If there is no anisotropy, the Hamiltonian of the system possesses global U(3) symmetry with respect to rotation in species space, and the pairing breaks this symmetry. An important feature of the three-component fermion system is spontaneous population imbalance, first noted in the continuum in Ref. [84] at $T = 0$. In addition, BCS superfluidity and population imbalance (magnetism), with two independent order parameters, can coexist, an intrinsic feature of a multicomponent Fermi systems, as shown by Cherng et al. [85] in the weak-coupling BCS regime.

We consider here U(3) invariant three-component ultracold Fermi gases in three-dimensional free space with varying interaction, with a focus on spontaneous population imbalance and superfluidity

at finite temperature at general interaction strength; we study the phase diagram in general and the BCS-BEC crossover of the system, fixing only the total number of particles and allowing spontaneous population imbalance to occur. With a fixed total number of particles, population imbalance is accompanied by spatial inhomogeneities, such as, domain formation. In this chapter, we first analyze the system at zero temperature in BCS mean field to show that the fermion pairing gap and population imbalance both develop with increasing bare attractive interaction between the fermions. Then we discuss non-zero temperature, starting from the BCS region where the scattering length is small and negative. We calculate the population imbalance as well as the BCS transition temperature as a function of interaction strength and temperature, to lowest order in the interaction. The thermodynamic potential derived here agrees with previous calculations [79, 80, 81, 82, 83] when the chemical potentials of the three species are equal. We also derive the Ginzburg-Landau free energy as a function of the two order parameter–the pairing gap and the population imbalanc–and discuss a possible analogy between dense QCD and three-component ultracold fermions. We then turn to the BEC limit of three-component ultracold fermions, where the scattering length is small and positive, a regime described by three different weakly interacting species of molecules made of different combinations of fermions. We show that Bose condensation of the molecules is accompanied by population imbalance. Finally, we discuss the BCS-BEC crossover connecting BCS and BEC limits, following the procedure of Nozières and Schmitt-Rink [15] to include pairing fluctuations (or non-condensed pairs), here in a summation of ladder diagrams for the self-energies; this calculation yields a transition temperature to the condensate phase that reduces to the BCS and BEC limits.

Degenerate three-component gases have been experimentally realized using the three lowest hyperfine states of ^{6}Li [86, 87]; at high magnetic fields, well beyond unitarity, the scattering lengths between the three hyperfine states are negative and sufficiently close that the system is approximately U(3) invariant. In addition, ultracold gases of alkaline-earth-metal atoms possess good SU(N) invariance (with N up to 10) [71, 72, 73], and are good candidates to observe the physics discussed here. Ytterbium has an SU(6) symmetry due to the nuclear spin; an SU(3) invariant mixture can be obtained by using only three spin components. In ^{6}Li as well as in ^{171}Yb and ^{173}Yb, the temperatures currently achieved experimentally are around $T \gtrsim 0.3T_F$ [73, 86, 87]. With a factor of ~ 3 decrease in temperature, phase separation due to the formation of population-imbalanced

domains could be observed.

Around the unitarity point, $1/a = 0$, in a U(3) invariant system (where a is the s-wave scattering length), three-body Efimov bound states can exist [88, 89, 90, 91, 92, 93, 94, 95, 96, 97]. Efimov states have been experimentally observed in a trap through an increase of the particle loss rate, mediated by these states [86, 87, 98]. In this thesis, we analyze the system on time scales long enough to see the two-body interaction physics but short enough that Efimov states, or three-body collisions, can be neglected; such an intermediate thermalized regime can exist in a trap at sufficiently low densities, since the two-body collision rate is proportional to the particle density squared whereas the three-body collision rate is proportional to the density cubed [1]. As we show, the homogeneous state is unstable against the formation of inhomogeneous structures with population imbalance; population imbalance suppresses the formation of Efimov states, tending to stabilize the inhomogeneous three-component system.

5.2 Three-component U(3) invariant fermions

We consider a three-component fermion system in free space with equal masses and the same scattering length between different species. We label the three species by "colors" in analogy with QCD, "red (r)," "green (g)," and "blue (b)." At low temperature, the interaction is dominated by s-wave scattering, and the Hamiltonian is

$$\mathcal{H}' \equiv \mathcal{H} - \mu\mathcal{N} = \sum_{\mathbf{k},\alpha} \left(\frac{k^2}{2m} - \mu \right) \psi^\dagger_{\alpha,\mathbf{k}} \psi_{\alpha,\mathbf{k}} + \frac{U}{2V} \sum_{\alpha,\beta} \sum_{\mathbf{k},\mathbf{k}',\mathbf{q}} \psi^\dagger_{\beta,\mathbf{k}'-\mathbf{q}} \psi^\dagger_{\alpha,\mathbf{k}+\mathbf{q}} \psi_{\alpha,\mathbf{k}} \psi_{\beta,\mathbf{k}'}, \tag{5.1}$$

where $\psi^\dagger_{\alpha,\mathbf{k}}$ is the creation operator of a particle with color α = r, g, b with momentum $\mathbf{k}$; V is the volume, and we take $\hbar = 1$ throughout. We assume an attractive bare contact interaction of strength $U < 0$. Although we take a common chemical potential μ for all three species, the numbers of each species in the state of lowest free energy can be different as a consequence of interactions, an effect that would be observable in an experiment that starts with equal numbers, as an inhomogeneous state. The Hamiltonian is invariant under global U(3) rotations of the species.

The attractive interaction leads to pairing of fermions at low temperature. The pairing order

[1] Huckans et al. [87] argue that strong interactions with a long lifetime (> 0.1s) can in fact be achieved in a low-density gas.

parameter is antisymmetric in color, and thus has the form

$$\Delta_\alpha(\mathbf{r}) \propto \epsilon_{\alpha\beta\gamma}\langle\psi_\beta(\mathbf{r})\psi_\gamma(\mathbf{r})\rangle, \tag{5.2}$$

where $\epsilon_{\alpha\beta\gamma}$ is a completely anti-symmetric unit tensor. Since under a global U(3) rotation,

$$\psi_{\alpha,\mathbf{k}} \to U_{\alpha\beta}\psi_{\beta,\mathbf{k}}, \tag{5.3}$$

where $U_{\alpha\beta} \in \mathrm{U}(3)$ (we use the convention that repeated indices are summed over), Δ_α transforms as

$$\Delta_\alpha(\mathbf{r}) \propto \frac{\epsilon_{\alpha\beta\gamma}}{2}\langle\psi_\beta(\mathbf{r})\psi_\gamma(\mathbf{r})\rangle \to (\det U)U^*_{\alpha\beta}\Delta_\beta(\mathbf{r}), \tag{5.4}$$

where $\psi_\alpha(\mathbf{r})$ is the Fourier transform of $\psi_{\alpha,\mathbf{k}}$.

To prove Eq. (5.4), we consider the operator $\hat{\Delta}_\alpha = \epsilon_{\alpha\beta\gamma}\psi_\beta\psi_\gamma$, whose expectation value is proportional to Δ_α. The combination $\psi_\alpha\hat{\Delta}_\alpha$ transforms as

$$\begin{aligned}\psi^T\hat{\Delta} \equiv \psi_\alpha\hat{\Delta}_\alpha &= \epsilon_{\alpha\beta\gamma}\psi_\alpha\psi_\beta\psi_\gamma \\ &\to \epsilon_{\alpha\beta\gamma}U_{\alpha\zeta}U_{\beta\eta}U_{\gamma\xi}\psi_\zeta\psi_\eta\psi_\xi = \det U\epsilon_{\zeta\eta\xi}\psi_\zeta\psi_\eta\psi_\xi = \det U\epsilon_{\alpha\beta\gamma}\psi_\alpha\psi_\beta\psi_\gamma = \det U\psi^T\hat{\Delta}.\end{aligned} \tag{5.5}$$

On the other hand, $\psi^T \to \psi^T U^T$. Therefore, $\hat{\Delta} \to \det U(U^T)^{-1} = \det UU^*$.

As a consequence of the transformation (5.4), we can – when the order parameter is independent of position – always choose appropriate axes of colors to transform the pairing order parameter into the form $\vec{\Delta} = (0, 0, \Delta)$, that is, by taking appropriate linear combinations of the species, we find that only two colors are paired and one is left unpaired. By applying a Bogoliubov-Valatin transformation, we can see that there are two gapped fermionic excitations corresponding to the quasiparticles of the paired fermions, and one ungapped excitation due to the unpaired fermions. In the following, we assume, without loss of generality, that the red and green particles are paired and the blue are not paired.

5.3 BCS Mean Field at $T = 0$

In this section, we consider the ground state of the system within mean-field BCS theory. We describe the pairing between r and g particles and unpaired b particles with the BCS-like ansatz,

$$|\Psi\rangle = \prod_{\mathbf{k}}\left(u_{\mathbf{k}} + v_{\mathbf{k}}\psi^\dagger_{r,\mathbf{k}}\psi^\dagger_{g,-\mathbf{k}}\right)\prod_{|\mathbf{k}|\le k^b_F}\psi^\dagger_{b,\mathbf{k}}|\mathrm{vac}\rangle, \tag{5.6}$$

where $|u_{\mathbf{k}}|^2+|v_{\mathbf{k}}|^2 = 1$ and k_F^b is the b Fermi momentum. The parameters $u_{\mathbf{k}}$ and $v_{\mathbf{k}}$ are determined by minimizing $\langle\Psi|\mathcal{H}-\mu\mathcal{N}|\Psi\rangle$ at fixed μ. Following the standard procedure, we obtain

$$u_{\mathbf{k}}^2 = \frac{1}{2}\left(1+\frac{\xi_{\mathbf{k}}}{\sqrt{\xi_{\mathbf{k}}^2+\Delta^2}}\right),\ v_{\mathbf{k}}^2 = \frac{1}{2}\left(1-\frac{\xi_{\mathbf{k}}}{\sqrt{\xi_{\mathbf{k}}^2+\Delta^2}}\right), \tag{5.7}$$

where $\xi_{\mathbf{k}} = k^2/2m-\mu$ and the gap $\Delta = -(U/V)\sum_{\mathbf{k}} u_{\mathbf{k}}v_{\mathbf{k}}$ is determined by

$$\Delta = -\frac{U}{V}\sum_{\mathbf{k}}\frac{1}{2}\frac{\Delta}{\sqrt{\xi_{\mathbf{k}}^2+\Delta^2}}. \tag{5.8}$$

We use the relation of the bare coupling U and the scattering length a [14, 99],

$$\frac{1}{U} = \frac{m}{4\pi a}-\frac{1}{V}\sum_{\mathbf{k}}\frac{m}{k^2}, \tag{5.9}$$

to rewrite the gap equation for $\Delta\neq 0$ in terms of a as

$$\frac{m}{4\pi a} = \frac{1}{V}\sum_{\mathbf{k}}\left(\frac{m}{k^2}-\frac{1}{2}\frac{1}{\sqrt{\xi_{\mathbf{k}}^2+\Delta^2}}\right). \tag{5.10}$$

The chemical potential is determined by fixing the total number of particles N:

$$N = \langle\Psi|\sum_{\alpha,\mathbf{k}}\psi_{\alpha,\mathbf{k}}^\dagger\psi_{\alpha,\mathbf{k}}|\Psi\rangle = \sum_{\mathbf{k}}\left(1-\frac{\xi_{\mathbf{k}}}{\sqrt{\xi_{\mathbf{k}}^2+|\Delta|^2}}\right)+V\frac{(k_F^b)^3}{6\pi^2}. \tag{5.11}$$

The same gap and number equations were derived in Ref. [84] using path-integral techniques. We solve the gap equation (5.10) and the number equation (5.11) simultaneously to calculate the pairing gap and the number imbalance in terms of the scattering length.

In Fig. 5.1, we plot the pairing gap Δ, measured in units of $\epsilon_F = k_F^2/2m$, and the number of r particles N_r divided by the total number of particles N, against $-1/k_Fa$, where $k_F = (6\pi^2N/3V)^{1/3}$. The right side of the figure corresponds to the weak-coupling regime (BCS region); the bare coupling becomes stronger toward the left side (BEC region) of the figure. As we see, $|\Delta|$ and the fraction of red particles, N_r/N, increase with stronger interaction. The N_r/N axis ranges from 1/3 to 1/2; when $N_r/N = 1/3$, all three species are equally populated, but for $N_r/N = 1/2$, only r and g particles are present. In general, N_r/N is greater than 1/3 in the interacting system, and it approaches 1/2 as the interaction becomes stronger. Thus the ground state of the interacting system always exhibits population imbalance, or magnetization (in analogy with a spin system).

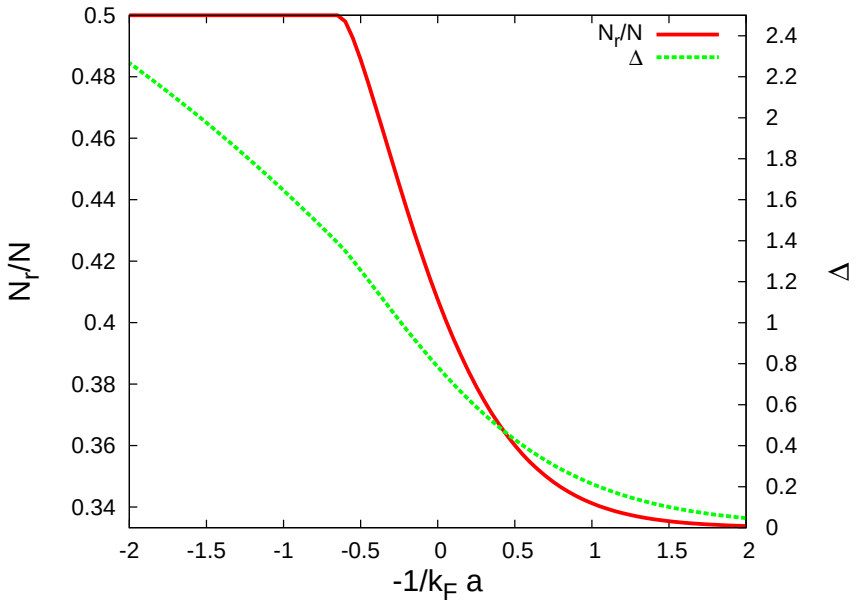

Figure 5.1: The number of red particles divided by the number of total particles N_r/N and the pairing gap Δ, in units of ϵ_F, at zero temperature, vs. $-1/k_F a$. The solid line shows N_r/N (left vertical axis) and the dotted line Δ (right vertical axis).

The magnetization arises physically through the gain of pairing energy when there are more particles in r and g states, and as remarked earlier, it would reveal itself in experiment as an inhomogeneous distribution of particle numbers.

With this basic picture in mind, we turn now to non-zero temperature.

5.4 BCS region

In the BCS region, where the scattering length a is negative and small, perturbation theory in terms of the scattering length describes the system well. We first derive the phase diagram in this region, and then we derive the corresponding Ginzburg-Landau free energy.

5.4.1 Mean-field phase diagram

The mean-field Hamiltonian $\mathcal{H}_M$ is

$$\begin{aligned}\mathcal{H}_M - \mu\mathcal{N} = &\sum_{\mathbf{k},\alpha}\left(\xi_{\mathbf{k}} + \frac{U_H}{V}(N - N_\alpha)\right)\psi^\dagger_{\alpha,\mathbf{k}}\psi_{\alpha,\mathbf{k}} - \Delta^*\sum_{\mathbf{k}}\psi_{r,\mathbf{k}}\psi_{g,-\mathbf{k}} - \Delta\sum_{\mathbf{k}}\psi^\dagger_{g,-\mathbf{k}}\psi^\dagger_{r,\mathbf{k}} \\ &- \frac{V}{U}|\Delta|^2 - \frac{U_H}{V}\left(N_rN_g + N_gN_b + N_bN_r\right), \end{aligned} \tag{5.12}$$

where

$$\Delta = -\frac{U}{V}\sum_{\mathbf{k}}\langle\psi_{r,\mathbf{k}}\psi_{g,-\mathbf{k}}\rangle. \tag{5.13}$$

As was done earlier, we assume equal numbers of red and green particles, $N_r = N_g$. Also, we now include the Hartree energy, $U_H = 4\pi a/m$. Defining

$$\xi_{r,\mathbf{k}} = \xi_{\mathbf{k}} + \frac{U_H}{V}(N_r + N_b), \tag{5.14}$$

$$\xi_{b,\mathbf{k}} = \xi_{\mathbf{k}} + \frac{U_H}{V}2N_r, \tag{5.15}$$

we rewrite the mean-field Hamiltonian as

$$\begin{aligned}\mathcal{H}_M - \mu\mathcal{N} = &\sum_{\mathbf{k}}\xi_{r,\mathbf{k}}\left(\psi^\dagger_{r,\mathbf{k}}\psi_{r,\mathbf{k}} + \psi^\dagger_{g,\mathbf{k}}\psi_{g,\mathbf{k}}\right) + \sum_{\mathbf{k}}\xi_{b,\mathbf{k}}\psi^\dagger_{b,\mathbf{k}}\psi_{b,\mathbf{k}} \\ &- \Delta^*\sum_{\mathbf{k}}\psi_{r,\mathbf{k}}\psi_{g,-\mathbf{k}} - \Delta\sum_{\mathbf{k}}\psi^\dagger_{g,-\mathbf{k}}\psi^\dagger_{r,\mathbf{k}} - \frac{V}{U}|\Delta|^2 - \frac{U_H}{V}\left(N_r^2 + 2N_rN_b\right), \end{aligned} \tag{5.16}$$

which is essentially the BCS mean-field Hamiltonian for paired red and green particles plus normal blue particles. Diagonalizing by a Bogoliubov-Valatin transformation, we find the thermodynamic potential

$$\begin{aligned}\Omega(T,\mu) = &-\frac{2}{\beta}\sum_{\mathbf{k}}\ln\left[1 + e^{-\beta\epsilon_k}\right] - \frac{1}{\beta}\sum_{\mathbf{k}}\ln\left[1 + e^{-\beta\xi_{b,\mathbf{k}}}\right] \\ &- \sum_{\mathbf{k}}\left(\varepsilon_k - \xi_{r,\mathbf{k}}\right) - \frac{V}{U}|\Delta|^2 - \frac{U_H}{V}\left(N_r^2 + 2N_rN_b\right), \end{aligned} \tag{5.17}$$

where $\varepsilon_k \equiv \sqrt{\xi^2_{r,\mathbf{k}} + |\Delta|^2}$. The condition $\partial\Omega/\partial|\Delta|^2 = 0$ gives the gap equation

$$\frac{1}{V}\sum_{\mathbf{k}}\frac{1 - 2f\left(\varepsilon_k\right)}{2\varepsilon_k} = -\frac{1}{U}, \tag{5.18}$$

where $f(x) = 1/(e^{\beta x}+1)$ is the Fermi distribution function. Again, μ is determined by the number equations

$$N_r = \sum_{\mathbf{k}} \frac{1}{2}\left(1 - \xi_{r,\mathbf{k}} \frac{\tanh \beta\varepsilon_k/2}{\varepsilon_k}\right), \tag{5.19}$$

$$N_b = \sum_{\mathbf{k}} f(\xi_{b,\mathbf{k}}) \tag{5.20}$$

with

$$N = 2N_r + N_b. \tag{5.21}$$

Numerically solving the gap equation (5.18) with the number equation (5.21), we obtain the gap and number imbalance at given temperature and scattering length, shown in Fig. 5.2. The figure

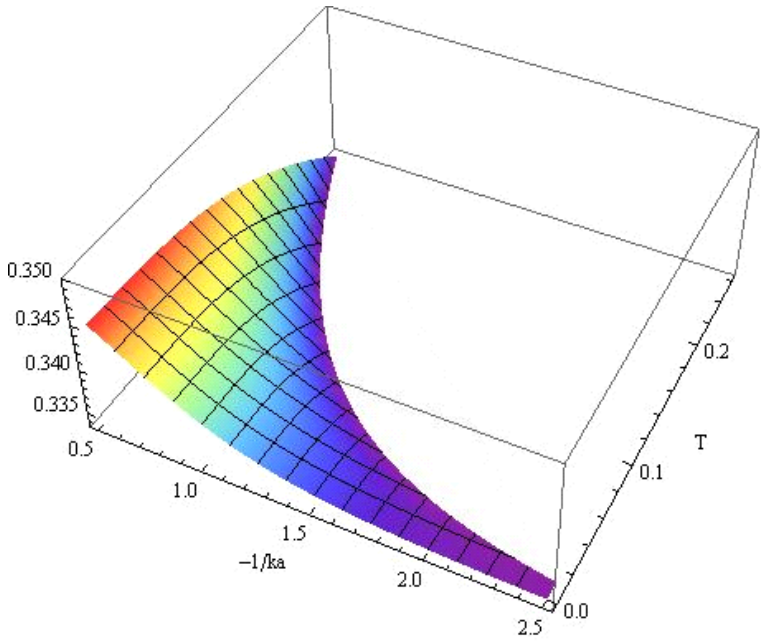

Figure 5.2: Phase diagram of the BCS region: N_r/N vs. $-1/k_F a$ and temperature, in units of ϵ_F. The z-axis ranges from 1/3 to 0.35. The intersection of the surface and the bottom plane toward higher T is the transition line between the ordered and normal phases.

plots N_r/N as a function of $-1/k_F a$ and T. The normal phase is the unshaded region at higher T; here $\Delta = 0$ and $N_r/N = 1/3$. In the shaded region, $\Delta \neq 0$ and $N_r/N > 1/3$, a small number imbalance. We show in the next subsection using the Ginzburg-Landau free energy that $\Delta \neq 0$

implies $N_r/N > 1/3$ and vice versa. To extend the theory to the unitarity and BEC regimes, we take pair fluctuations into account [2], in Sec. VI.

In the next subsection, we derive the Ginzburg-Landau free energy of the system in the BCS regime, and derive the relations between the pairing gap and the number imbalance.

5.4.2 Ginzburg-Landau free energy

The interplay between pairing and number imbalance is most easily seen from the Ginzburg-Landau free energy, the expansion of the free energy in terms of the corresponding order parameters around the transition temperature. We define the order parameter for number imbalance, ϕ, by

$$\phi = \frac{N_r}{V} - \frac{N}{3V}, \tag{5.22}$$

Fixing the total number of particles $N = 2N_r + N_b$, we have equivalently

$$\phi = -\frac{1}{2}\left(\frac{N_b}{V} - \frac{N}{3V}\right). \tag{5.23}$$

To derive the Ginzburg-Landau free energy it is convenient (in the derivation only) to let the chemical potential μ_b for b be different from the chemical potential μ_r for r and g. The thermodynamic potential $\Omega(T, \mu_r, \mu_b)$ can be derived as in the previous subsection. The Helmholtz free energy is then

$$F(\Delta, \phi) = \Omega + 2\mu_r N_r + \mu_b N_b, \tag{5.24}$$

in terms of which the Ginzburg-Landau (GL) free-energy density can be obtained by expanding

$$\mathcal{F}_{\rm GL}(\Delta, \phi) \equiv \frac{1}{V}\left(F(\Delta, \phi) - F(0, 0)\right). \tag{5.25}$$

We define

$$\tilde{\xi}_{r,\mathbf{k}} = \frac{k^2}{2m} - \mu_r + \frac{U_H}{V}(N_r + N_b) \tag{5.26}$$

$$\tilde{\xi}_{b,\mathbf{k}} = \frac{k^2}{2m} - \mu_b + \frac{U_H}{V}2N_r, \tag{5.27}$$

[2] We have so far assumed that the blue particles do not pair. However, the blue particles feel an effective attractive interaction with each other mediated by the existence of the red and green particles [100] , which can lead to p-wave pairing state of the blue particles. However, as shown by Kagan and Chubukov [101], the transition temperature to such p-wave pairing is too low ($T_c \sim 10^{-7} T_F$) to be observed in experiment, and we ignore it here.

and $\tilde{\varepsilon}_k \equiv \sqrt{\tilde{\xi}_{r,\mathbf{k}}^2 + \Delta^2}$, and the chemical potential of the normal phase μ_0 implicitly through

$$\frac{N}{3} = \sum_{\mathbf{k}} \frac{1}{e^{\beta\xi_{\mathbf{k}}^0} + 1}, \tag{5.28}$$

where $\xi_{\mathbf{k}}^0 = k^2/2m - \mu_0 + 2U_H N/3V$. In terms of these quantities, the Ginzburg-Landau free-energy density is

$$\begin{aligned}\mathcal{F}_{\mathrm{GL}}(\Delta,\phi) = &-\frac{2}{\beta V}\sum_{\mathbf{k}} \ln\left[1 + e^{-\beta\tilde{\varepsilon}_k}\right] - \frac{1}{\beta V}\sum_{\mathbf{k}} \ln\left[1 + e^{-\beta\tilde{\xi}_{b,\mathbf{k}}}\right] + \frac{3}{\beta V}\sum_{\mathbf{k}} \ln\left[1 + e^{-\beta\tilde{\xi}_{\mathbf{k}}^0}\right] \\ &- \frac{1}{V}\sum_{\mathbf{k}}\left(\tilde{\varepsilon}_k - \tilde{\xi}_{r,\mathbf{k}}\right) - \frac{\Delta^2}{U} + 3U_H\phi^2 + 2(\mu_r - \mu_b)\phi + \frac{N}{3V}\left(2\mu_r + \mu_b - 3\mu_0\right); \end{aligned} \tag{5.29}$$

in the expansion in ϕ and Δ, we keep in mind that μ_r and μ_b are implicit functions of Δ and ϕ through the number equations

$$\phi = \frac{1}{V}\sum_{\mathbf{k}} \frac{1}{2}\left(1 - \xi_{r,\mathbf{k}} \frac{\tanh \beta\tilde{\varepsilon}_k/2}{\tilde{\varepsilon}_k}\right) - \frac{N}{3V} \tag{5.30}$$

and

$$-2\phi = \frac{1}{V}\sum_{\mathbf{k}} \frac{1}{e^{\beta\tilde{\xi}_{b,\mathbf{k}}} + 1} - \frac{N}{3V}. \tag{5.31}$$

The Ginzburg-Landau free energy up to fourth order in the order parameters is

$$\mathcal{F}_{GL}(\Delta,\phi) = a\Delta^2 + \left(b + \frac{(c_2)^2}{c_1}\right)\Delta^4 + 3\left(\frac{1}{c_1} - U_H\right)\phi^2 + c_3\phi^3 + c_4\phi^4 - 2\frac{c_2}{c_1}\Delta^2\phi + c_5\Delta^2\phi^2, \tag{5.32}$$

where $c_1 \sim c_5$ and b are all positive, but the sign of a depends on temperature. The detailed coefficients are given in Appendix E.

The physically realized values of the order parameters minimize the Ginzburg-Landau energy; to leading order in the order parameters, we then have

$$\frac{\partial \mathcal{F}_{GL}}{\partial \phi} = 6\left(\frac{1}{c_1} - U_H\right)\phi - 2\frac{c_2}{c_1}\Delta^2 = 0, \tag{5.33}$$

$$\frac{\partial \mathcal{F}_{GL}}{\partial \Delta} = 2\Delta\left[a + 2\left(b + \frac{(c_2)^2}{c_1}\right)\Delta^2 - 2\frac{c_2}{c_1}\phi\right] = 0. \tag{5.34}$$

The first condition implies

$$\phi = \frac{c_2}{3(1 - c_1 U_H)}\Delta^2, \tag{5.35}$$

indicating that if the pairing gap is non-zero, the number imbalance is non-zero, and vice versa. The second condition, combined with Eq. (5.35), implies

$$\Delta \left[a + 2 \left(b + 2\frac{(c_2)^2}{c_1} - \frac{(c_2)^2}{3c_1(1 - c_1 U_H)} \right) \Delta^2 \right] = 0. \tag{5.36}$$

In addition to the solution $\Delta = 0$, when $a < 0$ this equation has a second solution, with lower free energy,

$$\Delta^2 = \frac{|a|}{2(b + {c_2}^2/c_1 - {c_2}^2/(3c_1(1 - c_1 U_H)))}. \tag{5.37}$$

The transition to fermion pairing is at the temperature at which $a = 0$.

The Ginzburg-Landau free energy of three-component ultracold fermions has certain similarities to the Ginzburg-Landau free energy of dense QCD derived in Refs. [102, 103, 104], which makes multicomponent ultracold atoms a promising analog of dense QCD. The Ginzburg-Landau free energy of dense QCD has the form

$$\Omega_{QCD}(d, \sigma) = \frac{\alpha'}{2}|d|^2 + \frac{\beta'}{4}|d|^4 + \frac{a'}{2}\sigma^2 - \frac{c'}{3}\sigma^3 + \frac{b'}{4}\sigma^4 - \gamma'|d|^2\sigma + \lambda'|d|^2\sigma^2, \tag{5.38}$$

where d is the quark-quark pairing order parameter and σ is the chiral symmetry breaking order parameter. We attach primes to the coefficients to avoid possible confusion with similarly labeled quantities used earlier. The signs of α' and a' depend on the temperature and the strength of the couplings. As argued in Refs. [102, 103, 104], β', c', γ', and λ' are positive.

With the correspondence between the present system and the dense QCD system, $\Delta \leftrightarrow d$ and $\phi \leftrightarrow \sigma$, we see that the two Ginzburg-Landau free energies have a similar structure. Although the original QCD Lagrangian has a local SU(3) gauge symmetry, the Ginzburg-Landau free energy (5.38), which does not take the gluonic degrees of freedom explicitly into account, possesses only global SU(3) symmetry. To this extent, one can construct an analogy with ultracold atomic fermions. Similarly, Nambu–Jona-Lasinio models of QCD [105, 106, 107, 108] also have only global SU(3) symmetry. Differences between the QCD free energy and that of ultracold fermions are that the sign of a' becomes negative at low temperature whereas the coefficient of ϕ^2 is always positive, and in addition the coefficients of σ^3 and ϕ^3 are opposite in sign. These differences are due to the fact that the dense QCD system can undergo chiral symmetry breaking without quark-quark pairing, but the three-component ultracold fermion system, beginning with equal populations, cannot

spontaneously develop local number imbalance without fermion pairing; with the symmetric interaction we are assuming, number imbalance arises from the gain of pairing energy with an increasing number of paired particles. It would be interesting to see how the analogy can be sharpened in multi-component atomic systems where spontaneous number imbalance and fermion pairing occur independently, for example, with increased numbers of species or with deviations from fully symmetric interactions.

5.5 BEC limit

We turn now to the BEC limit, where the scattering length between fermions is small and positive. We can regard the system here as a collection of three types of weakly interacting bound Bose molecules, each made of two fermions, which can be red-green, green-blue, or blue-red. The molecules Bose-condense at sufficiently low temperature. The condensate of molecules can be reduced to a condensate of one type of molecule by appropriately choosing the color axes, as with pairing in the BCS regime. The condensate in the BEC limit is composed of the same two colors that are paired in the BCS limit.

At high temperature, the system is not condensed, but is simply a gas of thermally excited molecules. Unlike in the condensate, one cannot exclude the existence of three types of thermally excited molecules. Whether the high-temperature system develops a number imbalance depends upon the intermolecular interactions. For the same type of molecules, the effective scattering length is $0.6a$ [109], where a is the scattering length of the constituent fermions. Between different molecules, as we show later, the effective scattering length is still $0.6a$. Thus, above the condensation temperature, the system is described by three kinds of thermally excited molecules with the same interaction between all molecules. As we show in Appendix F, the uncondensed Bose system does not develop a spontaneous number imbalance as long as the interaction between the same types of bosons is greater than half of the interaction between the different bosons. Thus the present system does not exhibit number imbalance above the condensate transition temperature.

We have, therefore, the following picture of the BEC limit. At high temperature the system is a homogeneous mixture of three types of molecules. The Bose-Einstein condensation temperature

is that of noninteracting bosons of mass $2m$ and density $N/6V$,

$$T_{\rm BEC} = \frac{\pi}{m[\zeta(3/2)]^{2/3}} \left(\frac{N}{6V}\right)^{2/3} \approx 0.137\, T_F. \tag{5.39}$$

Below $T_{\rm BEC}$, the system is a mixture of the condensate of one type of molecule and a cloud of thermal molecules of three types, which vanishes at $T = 0$.

We now show that the scattering length between different molecules is the same as that, $0.6a$, between like molecules. The derivation of Ref. [109] of the scattering length between similar molecules depended on the symmetry of the four-particle scattering wave function. Since, as we show, the wave function for scattering of different molecules has the same symmetry, the arguments of Ref. [109] lead to the same scattering length. We write the four-particle scattering wave function between similar molecules, for example, red-green on red-green, as $\Psi_s(\mathbf{r}_1, \mathbf{r}_2; \mathbf{r}_3, \mathbf{r}_4)$, where $\mathbf{r}_1$ denotes the position of the red fermion of the first molecule, $\mathbf{r}_2$ is the position of the green fermion of the first molecule, $\mathbf{r}_3$ is the red fermion of the second molecule, and $\mathbf{r}_4$ is the green fermion of the second molecule. The symmetries due to Fermi statistics are

$$\Psi_s(\mathbf{r}_1, \mathbf{r}_2; \mathbf{r}_3, \mathbf{r}_4) = -\Psi_s(\mathbf{r}_3, \mathbf{r}_2; \mathbf{r}_1, \mathbf{r}_4) = -\Psi_s(\mathbf{r}_1, \mathbf{r}_4; \mathbf{r}_3, \mathbf{r}_2). \tag{5.40}$$

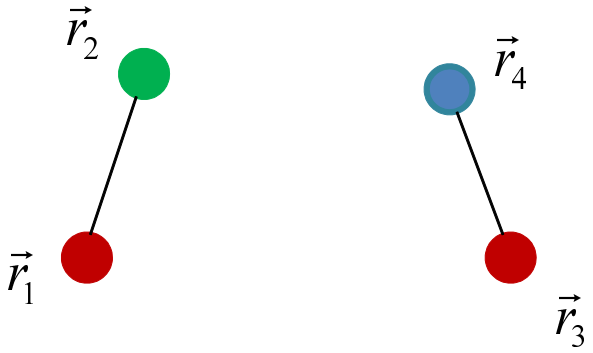

Figure 5.3: Two different molecules colliding.

On the other hand, scattering between different molecules, for example, red-green and red-blue shown in Fig. 5.3, described by the four-particle scattering wavefunction $\Psi_d(\mathbf{r}_1, \mathbf{r}_2; \mathbf{r}_3, \mathbf{r}_4)$ (where $\mathbf{r}_4$ now denotes the position of the blue fermion), has only a single symmetry due to Fermi statistics,

$$\Psi_d(\mathbf{r}_1, \mathbf{r}_2; \mathbf{r}_3, \mathbf{r}_4) = -\Psi_d(\mathbf{r}_3, \mathbf{r}_2; \mathbf{r}_1, \mathbf{r}_4). \tag{5.41}$$

However, for s-wave scattering, the wave function is symmetric with respect to the interchange of molecules, so that

$$\Psi_d(\mathbf{r}_1, \mathbf{r}_2; \mathbf{r}_3, \mathbf{r}_4) = \Psi_d(\mathbf{r}_3, \mathbf{r}_4; \mathbf{r}_1, \mathbf{r}_2). \tag{5.42}$$

Conditions (5.41) and (5.42) imply that

$$\Psi_d(\mathbf{r}_1, \mathbf{r}_2; \mathbf{r}_3, \mathbf{r}_4) = -\Psi_d(\mathbf{r}_1, \mathbf{r}_4; \mathbf{r}_3, \mathbf{r}_2), \tag{5.43}$$

which is exactly the same symmetry that was present due to the exchange of green fermions in Ψ_s.

The Schrödinger equation in the two cases has one apparent difference, that is, the delta-function interaction between the green and blue fermions. However, the antisymmetry (5.43) for exchange of green and blue fermions implies that the product of the green-blue potential and the wave function in the Schrödinger equation vanishes, so that the Schrödinger equation is the same as for identical molecules, and the scattering length is also the same. This argument depends crucially on the two molecules having one color (here red) in common.

5.6 Crossover theory

The crossover, in a two-component system, from BCS pairing in the weak-coupling region to a BEC of weakly interacting molecules in the strong-coupling region is continuous, as seen in experiment [16, 17, 18] and understood theoretically [14, 15, 110, 111, 112, 112, 113, 114, 115]. A common feature of theories of the BCS-BEC crossover at non-zero temperature is the incorporation of pairing fluctuations, which allow thermally excited Cooper pairs to exist above the condensate transition temperature. We now apply this idea to develop a theory of the crossover, at non-zero temperature, in the three-component system to connect the BCS and BEC regimes discussed earlier, and see that the crossover is also continuous.[3] We incorporate pairing fluctuations through a self-consistent summation of ladder diagrams, and then numerically solve for the transition temperature between the condensate and noncondensate phases.

[3] At sufficiently low temperature Efimov states can lower the energy around unitarity, producing a discontinuous transition from the BCS to the BEC regimes [92] .

5.6.1 Self-consistent summation of ladder diagrams

We construct the crossover theory in terms of the finite temperature normal and anomalous Green's functions:

$$\mathcal{G}_\alpha(\mathbf{r}-\mathbf{r}',t-t') = -i\left\langle T\left(\psi_\alpha(\mathbf{r},t)\psi_\alpha^\dagger(\mathbf{r}',t')\right)\right\rangle$$
$$\mathcal{F}(\mathbf{r}-\mathbf{r}',t-t') = -i\left\langle T\left(\psi_r(\mathbf{r},t)\psi_g(\mathbf{r}',t')\right)\right\rangle, \tag{5.44}$$

where T denotes time ordering. We assume still that pairing takes place between r and g particles. The pairing gap is given in terms of the Fourier transform of $\mathcal{F}(\mathbf{r}-\mathbf{r}',t-t')$ by

$$\Delta = -U\int\frac{d^3k}{(2\pi)^3}\mathcal{F}(\mathbf{k},t=0) = -\frac{U}{\beta}\int\frac{d^3k}{(2\pi)^3}\sum_{\omega_k}\mathcal{F}(k), \tag{5.45}$$

where k denotes $(\mathbf{k},\omega_k)$; the summation is over the fermionic Matsubara frequencies $\omega_k = i\pi\nu_k/\beta$ with odd integer ν_k. The Schwinger-Dyson equations for the Green's functions, illustrated in Fig. 5.4, are

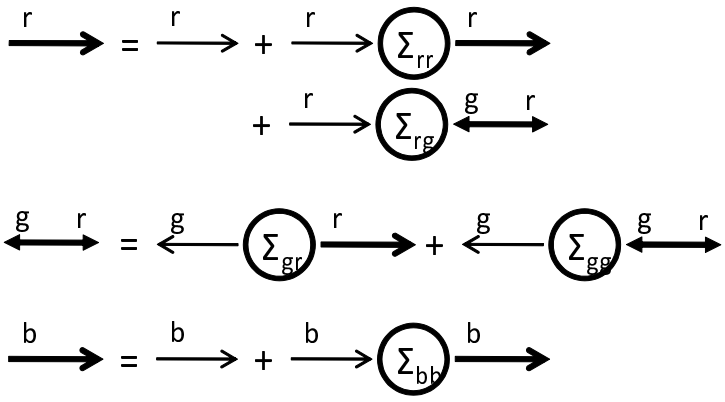

Figure 5.4: The Schwinger-Dyson equations for the normal and anomalous Green's functions.

$$\mathcal{G}_r(k) = \mathcal{G}_0(k) + \mathcal{G}_0(k)\left(\Sigma_{rr}(k)\mathcal{G}_r(k) + \Sigma_{rg}(k)\mathcal{F}^\dagger(k)\right),$$
$$\mathcal{F}^\dagger(k) = \mathcal{G}_0(-k)\left(-\Sigma_{gr}(k)\mathcal{G}_r(k) + \Sigma_{gg}(-k)\mathcal{F}^\dagger(k)\right),$$
$$\mathcal{G}_b(k) = \mathcal{G}_0(k) + \mathcal{G}_0(k)\Sigma_{bb}(k)\mathcal{G}_b(k), \tag{5.46}$$

where $\mathcal{G}_0(k)^{-1} = \omega_k - \xi_{\mathbf{k}}$ is the free-particle Green's function, and $\Sigma_{\alpha\beta}$ are self-energies with an incoming α particle and an outgoing β particle. Solving this system of equations, we obtain

$$\begin{aligned}
\mathcal{G}_r(k) &= \left(\mathcal{G}_0(k)^{-1} - \Sigma_{rr}(k) + \frac{\Sigma_{rg}(k)\Sigma_{gr}(k)}{\mathcal{G}_0(-k)^{-1} - \Sigma_{gg}(-k)}\right)^{-1}, \\
\mathcal{G}_b(k) &= \frac{1}{\mathcal{G}_0(k)^{-1} - \Sigma_{bb}(k)}, \\
\mathcal{F}^\dagger(k) &= -\Sigma_{gr}(k) \cdot \left\{\Sigma_{rg}(k)\Sigma_{gr}(k) + (\mathcal{G}_0(k)^{-1} - \Sigma_{rr}(k))(\mathcal{G}_0(-k)^{-1} - \Sigma_{gg}(-k))\right\}^{-1}.
\end{aligned} \tag{5.47}$$

The main contribution to the off-diagonal self-energies is the gap:

$$\Sigma_{rg}(k) = \frac{U}{\beta}\int \frac{d^3k'}{(2\pi)^3}\sum_{\omega_{k'}} \mathcal{F}(k') = \Sigma_{gr}(k) = -\Delta, \tag{5.48}$$

where we assume without loss of generality that Δ is real. Then the r-particle self-energy, for example, is given by

$$\Sigma_{rr}(k) = -\int \frac{d^3q}{(2\pi)^3}\frac{1}{\beta}\sum_{\omega_q} \left[\Gamma_{rg}(k,k;q)\mathcal{G}_g(-k+q) + \Gamma_{rb}(k,k;q)\mathcal{G}_b(-k+q)\right], \tag{5.49}$$

where $\Gamma_{\alpha\beta}(k,k';q)$, is the two-particle t-matrix for incoming particles of color α with momenta k and β with $-k+q$, and outgoing with momenta k' and $-k'+q$, respectively; the ω_q are bosonic Matsubara frequencies. The corresponding diagram is Fig. 5.5. Including the t-matrix in the

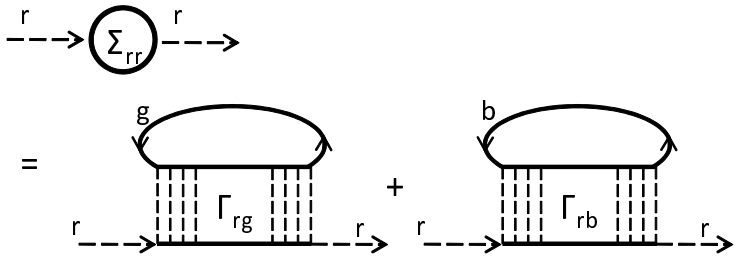

Figure 5.5: Self-energy written in terms of t matrices.

self-energy takes pairing fluctuations into account, and as shown in Ref. [15], encompasses thermal fluctuations of paired molecules in the BEC limit and the Hartree approximation in the BCS limit [15], thus connecting both limits continuously. Note that there is no process of this form in which the top line is anomalous since such a process would involve scattering between two r particles, either initially or finally, which is forbidden by the Pauli principle; the internal lines can, however, be anomalous.

On the other hand, in the self-energy of b particles, the top line can in principle be anomalous; however, this process would involve particle-hole scatterings either initially or finally, which is negligible for short-range interactions [56]; the self-energy involves only a sum of rb and gb particle-particle scatterings. The Bethe-Salpeter equation for the rb t-matrix becomes

$$\Gamma_{rb}(k,k';q) = -U - U\int \frac{d^3p}{(2\pi)^3}\frac{1}{\beta}\sum_{\omega_p}\mathcal{G}_r(p)\mathcal{G}_b(-p+q)\Gamma_{rb}(p,k';q). \tag{5.50}$$

As one sees by iterating this equation, $\Gamma_{rb}(k,k';q)$ is independent of k and k'; we write $\Gamma(k,k';q) = \Gamma(q)$. Solving Eq. (5.50), we obtain

$$\Gamma_{rb}(q) = -\left(\frac{1}{U} + \int \frac{d^3p}{(2\pi)^3}\frac{1}{\beta}\sum_{\omega_p}\mathcal{G}_r(p)\mathcal{G}_b(-p+q)\right)^{-1}; \tag{5.51}$$

Γ_{gb} takes the same form *mutatis mutandis*.

In Γ_{rg} we must take the rg anomalous Green's functions into account, as illustrated in Fig. 5.6. Solving the Bethe-Salpeter equation in Nambu matrix notation, we have

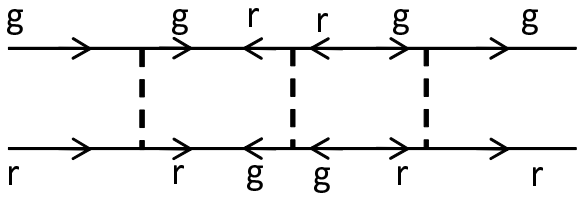

Figure 5.6: An anomalous contribution to the rg t-matrix.

$$\Gamma_{rg}(q) = \frac{\chi_{11}(-q)}{\chi_{11}(q)\chi_{11}(-q) - \chi_{12}(q)^2}, \tag{5.52}$$

where

$$\chi_{11}(q) = -\frac{1}{U} - \int \frac{d^3p}{(2\pi)^3}\frac{1}{\beta}\sum_{\omega_p}\mathcal{G}_r(p)\mathcal{G}_g(q-p), \tag{5.53}$$

$$\chi_{12}(q) = \int \frac{d^3p}{(2\pi)^3}\frac{1}{\beta}\sum_{\omega_p}\mathcal{F}(p)\mathcal{F}^\dagger(q-p). \tag{5.54}$$

To determine the gap and the number imbalance as a function of temperature and scattering length involves self-consistently solving the gap equation (5.47), which can be rewritten as

$$-\frac{1}{U} = \int \frac{d^3k}{(2\pi)^3}\frac{1}{\beta}\sum_{\omega_k}\frac{1}{(\mathcal{G}_0(k)^{-1} - \Sigma_{rr}(k))(\mathcal{G}_0(-k)^{-1} - \Sigma_{gg}(-k)) + \Delta^2}, \tag{5.55}$$

together with the number equations

$$\frac{N_r}{V} = \lim_{\eta\to+0}\int \frac{d^3k}{(2\pi)^3}\frac{1}{\beta}\sum_{\omega_k} e^{i\omega_k\eta}\mathcal{G}_r(k), \tag{5.56}$$

$$\frac{N_b}{V} = \lim_{\eta\to+0}\int \frac{d^3k}{(2\pi)^3}\frac{1}{\beta}\sum_{\omega_k} e^{i\omega_k\eta}\mathcal{G}_b(k). \tag{5.57}$$

However in this thesis we focus only on calculating the transition temperature.

5.6.2 Evaluation of T_c

We now use the formalism of the previous subsection to evaluate the transition temperature, where the pairing gap Δ becomes zero. The gap equation at T_c is equivalent to the condition that $\Gamma_{rg}(q)$ diverges at $q = 0$. Therefore, at T_c, we can make the approximations,

$$\begin{aligned}\Sigma_{rr}(k) &= -\int \frac{d^3q}{(2\pi)^3}\frac{1}{\beta_c}\sum_{\omega_q}\left(\Gamma_{rg}(q)\mathcal{G}_g(q-k) + \Gamma_{rb}(q)\mathcal{G}_b(q-k)\right)\\ &\approx -\int \frac{d^3q}{(2\pi)^3}\frac{1}{\beta_c}\sum_{\omega_q}\left(\Gamma_{rg}(q)\mathcal{G}_g(-k) + \Gamma_{rb}(q)\mathcal{G}_b(-k)\right),\end{aligned} \tag{5.58}$$

and

$$\Sigma_{bb}(k) = -\int \frac{d^3q}{(2\pi)^3}\frac{2}{\beta_c}\sum_{\omega_q}\Gamma_{br}(q)\mathcal{G}_r(q-k) - \int \frac{d^3q}{(2\pi)^3}\frac{2}{\beta_c}\sum_{\omega_q}\Gamma_{br}(q)\mathcal{G}_r(-k). \tag{5.59}$$

For $T \geq T_c$, the t-matrices do not depend on the color indices. Then, using the final line of Eq. (5.58) we see that the Green's function for r particles becomes

$$\mathcal{G}_r(k) = \left(\mathcal{G}_0^{-1}(k) - \Sigma_{rr}(k)\right)^{-1} \approx \left(\mathcal{G}_0^{-1}(k) + \mathcal{G}_0(-k)\Delta_{pg}^2\right)^{-1} = -\frac{\omega_k + \xi_{\mathbf{k}}}{|\omega_k|^2 + \xi_{\mathbf{k}}^2 + \Delta_{pg}^2}, \tag{5.60}$$

where we introduce a "pseudogap" Δ_{pg} at T_c by writing

$$\Delta_{pg}^2 = \frac{2}{\beta_c}\int \frac{d^3q}{(2\pi)^3}\sum_{\omega_q}\Gamma(q), \tag{5.61}$$

with $\Gamma = \Gamma_{rg} = \Gamma_{rb} = \Gamma_{br}$. The final line of Eq. (5.60) is just a BCS Green's function with the gap replaced by the pseudogap. We write $E_{\mathbf{k}} = \sqrt{\xi_{\mathbf{k}}^2 + \Delta_{pg}^2}$ for convenience. Similarly $\mathcal{G}_b(k)$ has the same form at $T = T_c$.

The number equations then reduce to

$$\frac{N}{3V} = \frac{1}{2}\int \frac{d^3k}{(2\pi)^3}\left(1 - \frac{\xi_{\mathbf{k}}}{E_{\mathbf{k}}}\tanh\frac{\beta_c E_{\mathbf{k}}}{2}\right), \tag{5.62}$$

while the equation for the pseudogap is

$$\begin{aligned} -\frac{1}{U} &= \int \frac{d^3k}{(2\pi)^3} \frac{1}{\beta_c} \sum_{\omega_k} \mathcal{G}_r(k)\mathcal{G}_g(-k) \\ &= \int \frac{d^3k}{(2\pi)^3} \left\{ \left(1 + \frac{\xi_{\mathbf{k}}^2}{E_{\mathbf{k}}^2}\right) \frac{\tanh(\beta_c E_{\mathbf{k}}/2)}{4E_{\mathbf{k}}} - \frac{\Delta_{pg}^2}{E_{\mathbf{k}}^2} \frac{f'(E_{\mathbf{k}})}{2} \right\}; \end{aligned} \tag{5.63}$$

as before, the bare coupling U is related to the scattering length a through Eq. (5.9).

In the BCS limit, $k_F a \to 0^-$, Δ_{pg}^2 tends to zero, as we can see by considering the BCS gap equation at T_c (not the mean-field BCS transition temperature, but the same T_c that we are using here) with a gap Δ

$$-\frac{1}{U} = \int \frac{d^3k}{(2\pi)^3} \left\{ \frac{\tanh(\beta_c \sqrt{\xi_{\mathbf{k}}^2 + \Delta^2}/2)}{2\sqrt{\xi_{\mathbf{k}}^2 + \Delta^2}} \right\}. \tag{5.64}$$

Expanding the right sides of (5.63) and (5.64) in terms of Δ_{pg}^2 and Δ^2, we see that the zeroth order terms are identical. Also, since the final line of Eq. (5.63) decreases monotonically with Δ_{pg}^2, the limit $\Delta^2 \to 0$, as in weak-coupling BCS, implies $\Delta_{pg}^2 \to 0$.

Determining T_c requires estimating Δ_{pg}^2, which we do by expanding $\Gamma_{rg}(q)^{-1}$ around $q = 0$, recalling that $\Gamma_{rg}(0)^{-1} = 0$ at T_c:

$$\begin{aligned} -\Gamma_{rg}(\mathbf{q}, \omega_q)^{-1} &= \frac{1}{U} + \int \frac{d^3p}{(2\pi)^3} \frac{1}{\beta_c} \sum_{\omega_p} \mathcal{G}_r(p)\mathcal{G}_g(q-p) \\ &\approx \int \frac{d^3p}{(2\pi)^3} \frac{1}{\beta_c} \sum_{\omega_p} \mathcal{G}_r(p) \left\{ \frac{\partial}{\partial\omega} \mathcal{G}_g(\mathbf{k}, \omega)\Big|_{k=-p} \omega_q + \frac{1}{6} \nabla^2 \mathcal{G}_g(\mathbf{k}, \omega)\big|_{k=-p} q^2 \right\} \\ &\equiv Z\omega_q - \gamma q^2. \end{aligned} \tag{5.65}$$

Explicit forms for Z and γ are given in Appendix G. The pseudogap then becomes

$$\Delta_{pg}^2 = -2 \int \frac{d^3q}{(2\pi)^3} \frac{1}{\beta_c} \sum_{\omega_q} \frac{1}{Z\omega_q - \gamma q^2} = 2\frac{1}{Z} \int \frac{d^3q}{(2\pi)^3} \frac{1}{e^{\beta_c \gamma q^2/Z} - 1} = \frac{\zeta(3/2)}{4Z} \left(\frac{Z}{\pi \beta_c \gamma} \right)^{3/2}. \tag{5.66}$$

Solving the number equation (5.62), the gap equation (5.63), and the expression for the pseudogap (5.66) self-consistently, we obtain the transition temperature, plotted against $-1/k_F a$ in Fig. 5.7. The solid line in the figure is the transition temperature calculated with the ladder summation formalism described here, and the dotted line is the result from mean-field BCS theory. The ladder summation line approaches the mean-field line in the BCS limit. On the other hand, in the BEC

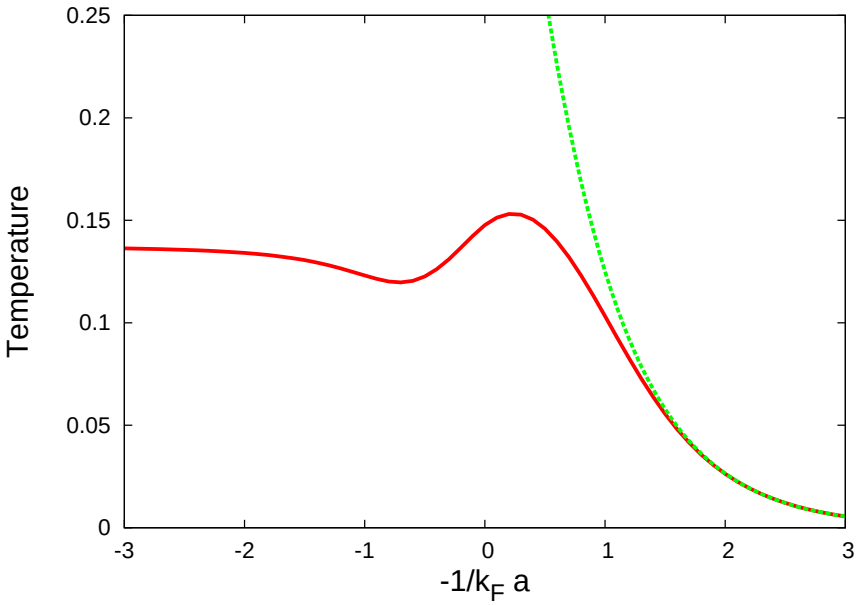

Figure 5.7: The phase diagram of three-component ultracold Fermi gas. The temperature is in units of T_F. The solid line is the transition temperature calculated with pairing fluctuations incorporated through the summation of ladder diagrams. The dotted line is the transition temperature calculated from mean-field BCS theory. The mean-field line corresponds roughly to the temperature at which fermions start to form (noncondensed) pairs. The line calculated from the ladder summation is where the Cooper pairs start to condense. Toward the left end of the figure, the transition temperature approaches the BEC limiting value $T_c \sim 0.137\, T_F$.

limit, the ladder summation correctly yields $T_c \to 0.137\,T_F$. The crossover theory presented here connects both limits continuously.

Throughout, we have kept a common chemical potential for the different species, and found that below T_c the number of b particles becomes smaller than the number of r or g particles. In ultracold atomic experiments, the number of the particles in each species is usually fixed at the start, and thus the simplest scenario that may occur experimentally is that the number imbalance appears through the formation of population-imbalanced domains. The formation of population-imbalanced domains leads to a gain of condensation energy of order $E_c V/2$ for the fully imbalanced state, where E_c is the condensate energy density in a balanced system; the factor $1/2 = 3/2 - 1$ is the increase in the relative number of Cooper pairs in the imbalanced state over that in the balanced state. On the other hand, the formation of a single domain wall costs a net surface energy E_{surf} of order $E_c V \xi_c/L$, where ξ_c is the coherence length and L is the linear size of the system. The condition that the formation of the domain is beneficial for the system is $E_c V/2 > E_{surf}$, or roughly $L/\xi_c \gtrsim 1$, which typically holds well. Domain formation is expected to decrease the free energy from that of the homogeneous state at low temperature. Other possible realizations of population imbalance include the formation of a "color density" wave or the formation of an inhomogeneous (Fulde-Ferrell-Larkin-Ovchinnikov) superfluid; we leave analysis of these states as future study. Also to apply the present theory quantitatively under realistic experimental conditions it will be necessary to investigate the effects of Efimov states.

Chapter 6

Bohr's gedankenexperiment on double-slit interference

6.1 Introduction

In this chapter, we discuss Niels Bohr's double-slit *gedankenexperiment*. The content in this chapter is based on [5].

Niels Bohr once suggested a very simple *gedankenexperiment* to prove that, in order to preserve the consistency of elementary quantum mechanics, the radiation field must be quantized as photons. In the experiment one carries out conventional two-slit diffraction with electrons (or other charged particles), building up the diffraction pattern one electron at a time (as in the experiment of Ref. [23]). One then tries to determine which slit the electron went through by measuring far away, in the plane of the slits, the Coulomb field of the electron as it passes through the slits. See Fig. 6.1. If the electron passes through the upper slit it produces a stronger field than if it passes through lower slit. Thus if one can measure the field sufficiently accurately one gains "which-path" information, posing the possibility of seeing interference while at the same time knowing the path the electron takes, a fundamental violation of the principles of quantum mechanics.

In an experiment with ordinary electrons of charge e the uncertainty principle prevents measurement of the Coulomb field to the required accuracy, as we shall see below, following the prescription of Bohr and Rosenfeld for measuring electromagnetic fields [116, 117]. However, as Bohr pointed out, one can imagine carrying out the same experiment with (*super*) electrons of arbitrarily large charge, Ze, and indeed, for sufficiently large Z, one can determine which slit each electron went through. However, elementary quantum mechanics requires that once one has the capability of ob-

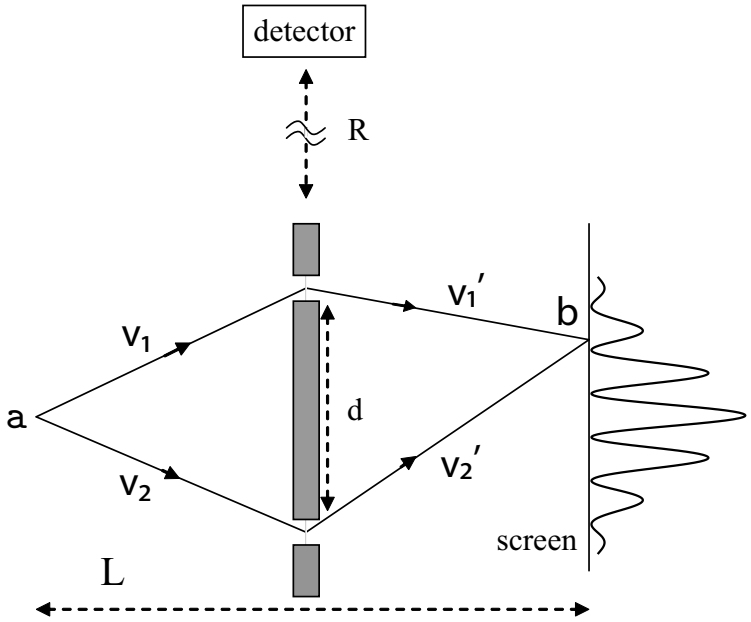

Figure 6.1: Two slit diffraction with single electrons, in which one measures the Coulomb field produced by the electrons at the far-away detector.

taining "which-path" information, even in principle, the interference pattern must be suppressed, independent of whether one actually performs the measurement.

Underlying the loss of the pattern is that the electron not only carries a Coulomb field, produces a radiation field as it "turns the corner" when passing through the slits, The larger the charge the stronger is the radiation produced. This radiation must introduce a random phase to the electron in order to destroy the pattern, and so itself must carry phase information; thus the electromagnetic field must have independent quantum degrees of freedom. Were the quantum mechanical electrons to emit classical radiation, the emission would produce a well-defined phase shift of the electron amplitudes along the path, which while possibly shifting the pattern, as in the Aharonov-Bohm effect [118], would not destroy it. In a sense the suppression of the pattern is an extension of the Aharonov-Bohm effect to fluctuating electromagnetic potentials (discussed by Aharonov and Popescu[1]).

Our object in this chapter is to carry out a detailed analysis of the physics implicit in Bohr's suggested experiment. After describing the experiment more fully, we determine the strength of charge needed to measure the Coulomb field at large distances sufficiently accurately. We then

[1]Aharonov Y and Popescu S, unpublished; P. Kwiat, private communication.

analyze how coupling of the particle to the quantized electromagnetic field in diffraction suppresses the interference pattern, with increasing charge, before Coulomb measurements can yield "which-path" information.

The first experiment that revealed effects of quantization of the electromagnetic field in interference is that of Grangier et al. [119], which showed how interference of single photons differs from classical interference. The loss of particle coherence in interferometry due to photon emission was first demonstrated by Pfau et al. [120], and due to photon scattering by Chapman et al [121]. Various works, both theoretical and experimental, have discussed determining the path of charged particles in the double-slit problem, but none, it seems, in connection with Bohr's proposed experiment. The theoretical possibility of distinguishing paths by measurement of photon field is discussed in Ref. [122], while Refs. [123] and [124] discuss determining the path through detection of the electric field inside the loop of the paths. See also Stern et al. [125] on decoherence due to the interaction of charged particles with the gauge field. Experimental attempts to measure "which-path" information using interferometers fabricated in high-mobility two-dimensional electron gases include Refs. [126, 127, 128].

A natural question to ask is whether by measuring the Newtonian gravitational field produced by the mass of a particle as it diffracts, one can similarly gain "which-path" information; as we show, the answer is that one can, for sufficiently large mass. However, one cannot conclude in this case that the gravitational field must also be quantized, since for masses for which one can measure the path, the fringe separation in the diffraction pattern would shrink to below the Planck length, $\ell_{\rm pl} = (G\hbar/c^3)^{1/2}$, where G is Newton's gravitational constant and c is the speed of light. In this chapter, we explicitly write $\hbar$. However, position measurements are fundamentally limited in accuracy to scales $\gtrsim \ell_{\rm pl}$ [129], and therefore distinguishing so a fine pattern cannot be carried out. Unlike in the electromagnetic case, where the interference pattern is suppressed due to decoherence caused by the radiated photons, the pattern in the gravitational case becomes immeasurably fine, not because the particles radiate quantized gravitons.

6.2 Measurement of the Coulomb field

In the experiment sketched in Fig. 6.1 a charged particle enters the apparatus from the left side, goes through a double slit, and hits the screen (b). The spacing of the slits is d, and L is the

distance from the particle emitter (a) to the screen. The Coulomb field of the electron is measured at distance $\sim R$ in the plane of the slits, sufficiently far away from the apparatus that there can be no back-reaction from the distant measurement of the electromagnetic field. Thus $R \gtrsim cT$, where T is the time of the flight of the particle, $\simeq L/v$, with v the particle velocity. We consider only non-relativistic particles, in which case the longitudinal Coulomb field of the electron at distance $R \sim cT$ is larger than the transverse radiation field by a factor $\sim c/v$. We assume that the Coulomb field is determined by the charge in the usual manner.

To distinguish whether the particle goes through the upper or lower slit one needs to measure the electric field to at least an accuracy $Ze(1/R^2 - 1/(R+d)^2) \sim Zed/R^3$ (with $d \ll R$). The quantum limit on the measurability of a weak electric field E was obtained by Bohr and Rosenfeld [116, 117]. In an early discussion of such a quantum measurement, Landau and Peierls [130] noted that if one attempts to measure the field by its effect on a point charge, radiation recoil introduces uncertainties in the measurement that diverge for short measuring times, and concluded that "in the quantum range ... the field strengths are not measurable quantities." To avoid this problem, Bohr and Rosenfeld envisioned measuring the average of the electric field over a region of space-time, using an extended apparatus consisting of an object A of mass M and volume V_A with extended charge Q, tethered by Coulomb forces to a similar object B with background charge $-Q$. See Fig. 6.2. The background charge is fixed in space, but A is displaced by an electric field from its

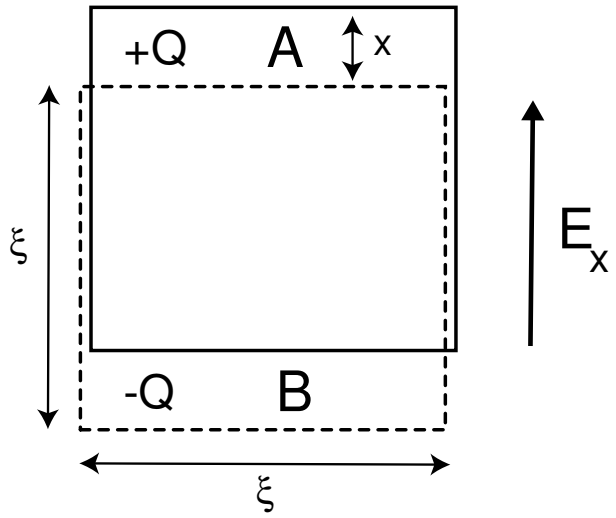

Figure 6.2: Bohr-Rosenfeld apparatus for measuring the electric field. The positively charged object A slides on the negatively charged fixed object B.

equilibrium position. The apparatus measures the field by detecting the deflection of A from its equilibrium position. The net equilibrium charge density of the apparatus is zero in the absence of an external field that displaces the object from the background. In their analysis they first assume quantization of the electromagnetic field, and show how vacuum fluctuations of the field in the region limit the accuracy of field measurements. They then go on to show that the accuracy of the measurement of a single field is limited by the uncertainty principle applied to the apparatus, without the need to invoke field quantization. We give a schematic derivation of this result (see also the recent discussions in Refs. [131, 132, 133].)

The relative motion of A and B is a harmonic oscillator whose frequency ω is readily derived from the familiar expression for the plasma frequency ($\omega_p^2 = 4\pi ne^2/m$), namely $\omega^2 = 4\pi Q^2/MV_A$. When A is displaced relative to B by a distance x, the restoring force acting between them is

$$F = -M\omega^2 x = -4\pi Q^2 x/V_A. \tag{6.1}$$

Thus, an external field E_x acting on A for time T' changes the momentum of A by $p_x = (E_x Q - 4\pi Q^2 x/V_A)T'$, from which one would deduce an electric field,

$$E_x = 4\pi Qx/V_A + p_x/QT'. \tag{6.2}$$

Since p_x and x obey the uncertainty relation, $\delta x \delta p_x \gtrsim \hbar$, we see from minimizing the right side of Eq. (6.2) with respect to δx that the uncertainty in the measurement of E_x is independent of Q, and given by the Bohr-Rosenfeld relation, $\delta E_x \sim \sqrt{\hbar/V_A T'}$. For simplicity we assume cubic geometry of A and B, with $V_A = \xi^3$, The measurement time T' is at most the time of flight, T, since further increasing the measurement time does not help to distinguish the paths; thus we take $T' = T$. In addition the length ξ of interest is at most the Coulomb pulse width, cT, since neither does a longer size help to distinguish the paths. With $\xi = cT$, we obtain the limit of accuracy of the measurement of the Coulomb field:

$$\delta E_x \sim \sqrt{\frac{\hbar}{\xi^3 T}}\ . \tag{6.3}$$

To estimate the critical scale of charge of particles above which one begins to be able to distinguish the path, we take the measuring apparatus to be located from R to $R + \xi$ above the upper slit. Then, when a particle with charge Ze passes through the upper slit, the average Coulomb

field in the apparatus is

$$\frac{1}{\xi}\int_0^{\xi}\frac{Ze}{(R+x)^2}dx=\frac{Ze}{R(R+\xi)}. \tag{6.4}$$

Similarly, the average electric field when the particle passes through the lower slit is $Ze/(R+d)(R+d+\xi)$, where d is the slit interval. Hence to distinguish the paths the apparatus needs to distinguish an electric field difference

$$\Delta E=\frac{Ze(2R+\xi)}{R^2(R+\xi)^2}d, \tag{6.5}$$

a decreasing function of ξ. Since to measure the path, one needs $\Delta E > \delta E$ (the measurement uncertainty), or

$$Ze\gtrsim\frac{R^2(R+\xi)^2}{d(2R+d)}\sqrt{\frac{\hbar}{\xi^3 T}}. \tag{6.6}$$

With $\xi\sim R\sim cT$ we find that the scale of critical charge Z_1 above which one can begin to distinguish the path is

$$Z_1\simeq\frac{1}{\sqrt{\alpha}}\frac{cT}{d}, \tag{6.7}$$

where $\alpha=e^2/\hbar c$ is the fine structure constant. Note that $Z_1\gg 1$, so that one could never detect the path with ordinary electrons or other particles of charge $\sim |e|$. For illustration, from the parameters corresponding to the experiment of Ref. [23]: $d\sim 1$ μm, and $cT\approx 6$ cm, we estimate $Z_1\simeq 7\times 10^5$.

One can in fact, for general Z, determine partial information on the paths, the amount of information increasing with Z. Writing $p(D_u,l)$ as the probability of the particle having taken the lower path and the detector detecting it to have taken the upper path, $p(D_u,u)$ as the probability of the particle having taken the upper path and the detector detecting it to have taken the upper path, etc., one can quantify the information in terms of the *distinguishability* $\mathcal{D}$ [134, 135, 136, 137]

$$\mathcal{D}=|p(D_u,u)-p(D_l,u)|+|p(D_l,l)-p(D_u,l)|\,. \tag{6.8}$$

Since $p(D_u,u)+p(D_l,u)+p(D_l,l)+p(D_u,l)=1$, $\mathcal{D}\leq 1$.

To calculate $\mathcal{D}$ we note that the detector determines the electric field through simultaneous measurement of the position and momentum, which leads to a Gaussian uncertainty of width δE

in the measured value of the electric field from the expected value. For the particle taking the upper path, producing an expected (averaged) electric field E_u at the detector, the probability distribution of the measured electric field is

$$P_u(E) = \frac{1}{\sqrt{2\pi}\delta E} e^{-(E-E_u)^2/2\delta E^2}, \tag{6.9}$$

with a similar expression for the field distribution $P_l(E)$ for the lower path in terms of the expected E_l. Since $E_u > E_l$, we can for simplicity regard the detector as having detected the particle taking the upper path if the measured value of the electric field is greater than $(E_u + E_l)/2$, and as having taken the lower path otherwise.

With the assumption that the amplitudes for the particle taking the upper and the lower paths are equal in magnitude, which is true if the two slits are located symmetrically, then

$$p(D_u, u) = \frac{1}{2} \int_{(E_u+E_l)/2}^{\infty} P_u(E) dE = \frac{1}{2} - p(D_l, u), \tag{6.10}$$

with similar equations for $p(D_l, l)$ and $p(D_u, l)$. With $\Delta E = E_u - E_l$, the distinguishability becomes

$$\mathcal{D} = \frac{1}{\sqrt{\pi}} \int_{-\Delta E/2\sqrt{2}\delta E}^{\Delta E/2\sqrt{2}\delta E} e^{-x^2} dx = \mathrm{erf}(Z/2\sqrt{2}Z_1), \tag{6.11}$$

where $\mathrm{erf}(x)$ is the error function. We plot $\mathcal{D}$ in Fig. 3 below for the parameters of Ref. [23].

6.3 Loss of interference

We turn now to the question of how for sufficiently large charge (which should be $\lesssim Z_1$) the interference pattern must disappear. The basic physics is that the particle radiates when being accelerated by the slits, and undergoes a random change in its phase because it is coupled to a dynamical degree of freedom, the quantized radiation field. We do not take into account any quantum degrees of freedom associated with the slits, i.e., we assume that they act effectively as a potential on the electron. The pattern on the screen is proportional to $\sum_f \left(|\beta_u(b,f) + \beta_l(b,f)|^2\right)$ where $\beta_u(b,f)$ is the amplitude for the particle to go through the upper slit to point b on the screen, with the electromagnetic field going from its initial state $|0\rangle$ (the vacuum) to final multi-photon state $|f\rangle$, and $\beta_l(b,f)$ is the amplitude for the particle to take the lower trajectory.

The interference pattern thus has the relative intensity,

$$I(b) = \frac{2\mathrm{Re}\sum_f \left(\beta_l(b,f)^* \beta_u(b,f)\right)}{\sum_f \left(|\beta_u(b,f)|^2 + |\beta_l(b,f)|^2\right)}. \tag{6.12}$$

While it is possible to carry out a full quantum calculation of the radiation emitted in diffraction, its essential features are brought out if we make the simplifying assumption that the charged particle follows a single straight trajectory along either the upper or lower path from the emission point a to a given point b on the screen (see Fig. 6.1). and thus the emitted radiation has only the effect of changing the phase of the electron amplitude. Then

$$\beta_u(b,f) \simeq \langle f|U_u|0\rangle \beta_u^0, \tag{6.13}$$

where β_u^0 is the simple quantum amplitude in the absence of the electromagnetic field, and

$$U_u = \left(e^{(iZe/\hbar c)\int d\vec{\ell}\cdot\vec{A}(\vec{r},t)}\right)_+, \tag{6.14}$$

where $\vec{A}(\vec{r},t)$ is the electromagnetic field operator, and the the integral is time ordered (denoted by the subscript "+") along the path. From Eq. (6.13),

$$\sum_f |\beta_u(b,f)|^2 = \langle U_u^\dagger U_u\rangle |\beta_u^0|^2 = |\beta_u^0|^2, \tag{6.15}$$

$$\sum_f |\beta_l(b,f)|^2 = |\beta_l^0|^2, \tag{6.16}$$

and

$$\sum_f \beta_l(b,f)^* \beta_u(b,f) = \langle U_l^\dagger U_u\rangle \beta_l^0(b)^* \beta_u^0(b), \tag{6.17}$$

where the brackets denote the electromagnetic vacuum expectation value. Thus

$$\langle U_l^\dagger U_u\rangle = \langle \left(e^{(iZe/\hbar c)\int d\vec{\ell}\cdot\vec{A}(\vec{r},t)}\right)_c \rangle, \tag{6.18}$$

where the subscript c denotes the time ordering of the contour integral from emission to the screen along the upper path and then negatively time-ordered from the screen back to the emission point along the lower path. This expression is the expectation value of the Wilson loop around the path $u-l$ [138]. Since the free quantum electromagnetic field is Gaussianly distributed in the vacuum,

$$\langle U_l^\dagger U_u\rangle = e^{-(Z^2\alpha/2\hbar c)\Phi_{u-l}}, \tag{6.19}$$

where

$$\Phi_{u-l} = \langle \left(\oint_{u-l} d\vec{\ell}\cdot\vec{A}(\vec{r},t)\right)_c^2 \rangle. \tag{6.20}$$

Writing

$$\langle U_l^\dagger U_u \rangle = \mathcal{V} e^{-i\zeta}, \tag{6.21}$$

where the *visibility* $\mathcal{V} = |\langle U_l^\dagger U_u \rangle|$ is ≤ 1, and the phase shift ζ is real, we have

$$I(b) = \frac{2\mathrm{Re}\left(\beta_l^0(b)^* \beta_u^0(b) e^{-i\zeta}\right)}{\left(|\beta_u^0(b)|^2 + |\beta_l^0(b)|^2\right)} \mathcal{V}. \tag{6.22}$$

The coupling to the radiation field reduces the intensity of the interference pattern by $\mathcal{V}$, as well shifting it via ζ. By symmetry, the shift vanishes at the center point on the screen (and is otherwise not relevant to the present discussion.) Since the Coulomb field does not enter the states of the radiation field in $\mathcal{V}$, Eq. (6.22) gives a valid description of the interference pattern whether or not an attempt is made to distinguish paths by detecting the Coulomb field at large distances.

The real part of Φ_{u-l}, entering the visibility, is given by the same integrals as in Eq. (6.20) without time ordering along the contour, since $\vec{j}(\vec{r},t) \cdot \vec{A}(\vec{r},t)$ is Hermitian [139]:

$$\mathrm{Re}\,\Phi_{u-l} = \langle \left(\oint_{u-l} d\vec{\ell} \cdot \vec{A}(\vec{r},t) \right)^2 \rangle. \tag{6.23}$$

To estimate the visibility we write the free electromagnetic field operator in terms of photon annihilation and creation operators: $\vec{A}(r,t) \simeq \sum_k \sum_{\lambda_k} (2\pi\hbar c/k\Omega)^{1/2} (a_k \vec{\lambda}_k e^{i(\vec{k}\cdot\vec{r}-\omega t)} + h.c.)$, where the $\vec{\lambda}$ are the photon polarization vectors, $\omega = ck$, and Ω is the quantization volume. For non-relativistic motion ($v \ll c$) along a classical trajectory,

$$\mathrm{Re}\,\Phi_{u-l} = \int \frac{\hbar c d^3k}{(2\pi)^2 k} \sum_{\lambda_k} \left| \oint_{u-l} dt e^{-i\omega t} \vec{\lambda}_k \cdot v(t) \right|^2 = \frac{2\hbar c}{3\pi} \int k dk \left| \oint_{u-l} dt e^{-i\omega t} \vec{v}(t) \right|^2. \tag{6.24}$$

With the simplifying assumption that on the upper path the velocity undergoes a sudden change at the slits, from $\vec{v}_1$ to $\vec{v}_1\,'$ (see Fig. 1), and from $\vec{v}_2$ to $\vec{v}_2\,'$ through the lower slit, then in the limit of large time of passage, $\omega T \gg 1$,

$$\oint_{u-l} dt e^{-i\omega t} \vec{v}(t) = \frac{i}{\omega} (\vec{v}_1 - \vec{v}_1\,' - \vec{v}_2 + \vec{v}_2\,'), \tag{6.25}$$

For $\omega \lesssim 1/T$, the integral is proportional to T. Near the center of the pattern, $\vec{v}_2\,' \simeq \vec{v}_1$ and $\vec{v}_1\,' \simeq \vec{v}_2$, so that

$$\left| \oint_{u-l} dt e^{-i\omega t} \vec{v}(t) \right|^2 \simeq \frac{4}{\omega^2} (\vec{v}_1 - \vec{v}_2)^2, \tag{6.26}$$

and

$$\log \mathcal{V} \simeq -\frac{4Z^2\alpha}{3\pi c^2}(\vec{v}_1 - \vec{v}_2)^2 \int_{1/T}^{\omega_{\max}} d\omega \frac{1}{\omega}. \tag{6.27}$$

The integral over ω, nominally logarithmically divergent at large ω, is physically cut off by $\omega_{\max}$, the maximum frequency of emitted photons, which from energy conservation cannot exceed $mv^2/2\hbar = \pi v/\lambda$, where λ is the de Broglie wavelength of the interfering particle. The lower cutoff is effectively $1/T$; hence

$$\log \mathcal{V} \simeq -\frac{4Z^2\alpha}{3\pi c^2}(\vec{v}_1 - \vec{v}_2)^2 \log(\pi L/\lambda). \tag{6.28}$$

Equation (6.28) is essentially the non-relativistic limit of the result of Ref. [140]. For $L \gg d$, $(\vec{v}_1 - \vec{v}_2)^2 \simeq (2d/T)^2$, and finally,[2]

$$\mathcal{V} \simeq \exp\left\{-Z^2 \frac{16\alpha}{3\pi} \frac{d^2}{(cT)^2} \log(\pi L/\lambda)\right\}, \tag{6.29}$$

Since the path length must be many de Broglie wavelengths, the charge above which the visibility becomes less than $1/e^2$ obeys,

$$Z_2 \lesssim \frac{cT}{d\sqrt{\alpha}} \frac{1}{[\log(\pi L/\lambda)]^{1/2}} < \frac{cT}{d\sqrt{\alpha}} \lesssim Z_1. \tag{6.30}$$

The visibility and distinguishability are closely related; as Z increases the interference pattern fades away on the scale Z_2, while the distinguishability of the paths by measurement of the Coulomb field grows on the scale Z_1. Quantitatively,

$$\begin{aligned} \mathcal{V}^2 + \mathcal{D}^2 &= \exp\left(-\frac{32}{3\pi}\left(\frac{Z}{Z_2}\right)^2\right) + \operatorname{erf}\left(\frac{Z}{2\sqrt{2}Z_1}\right)^2 \\ &\equiv f(Z). \end{aligned} \tag{6.31}$$

Since $f(0) = f(\infty) = 1$, and for $Z_2 < 8Z_1/\sqrt{3}$ and $0 < Z < \infty$, $f(Z) < 1$

$$\mathcal{V}^2 + \mathcal{D}^2 \leq 1, \tag{6.32}$$

[2]Note that emission of photons with wavelengths λ larger than the slit width d contributes to the decrease in visibility, even though such photons give little or no information about the path. The reason is that photon emission leads to fragmentation of the total amplitude, $\sum_n \sum_{f_n} \left(C^u_{f_n}|u, f_n\rangle + C^l_{f_n}|l, f_n\rangle\right)$, among photon states f_n with various numbers of photons, n. Here $\sum_n \sum_{f_n} |C^u_{f_n}|^2 = \sum_n \sum_{f_n} |C^l_{f_n}|^2 = 1$. Only states $|u, f_n\rangle$ and $|l, f_n\rangle$ with the same photon state can interfere; the total weight of the interfering terms $|\sum_n \sum_{f_n} C^{l*}_{f_n} C^u_{f_n}|$ must be ≤ 1.

in agreement with the inequality derived by Jaeger et al. [135] and Englert [136]. Figure 6.3 shows the visibility and distinguishability as functions of Z, as well as $\mathcal{V}^2+\mathcal{D}^2$, for the parameters of the experiment of Ref. [23], given above. With these parameters, $\log(\pi L/\lambda)\sim 20$.

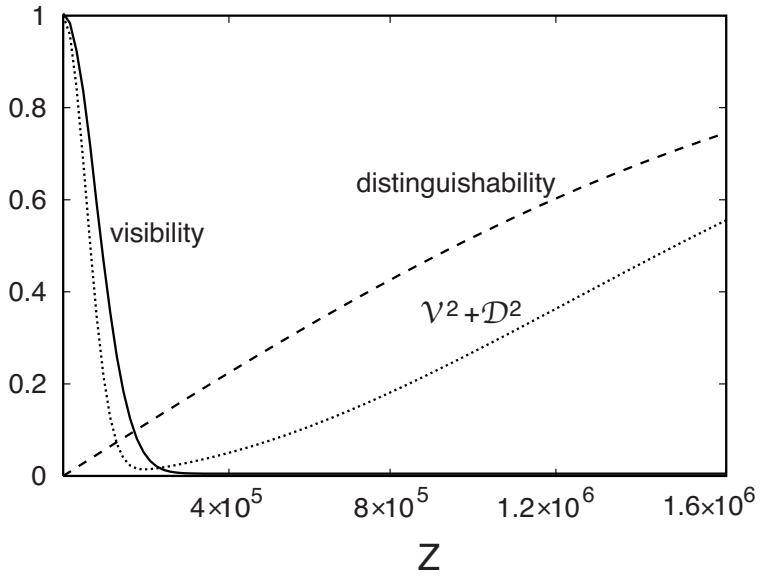

Figure 6.3: Visibility (solid line) and distingishability (dashed line) vs charge for the parameters of Ref. [23], for which the characteristic charge Z_1 for distinguishing paths by measuring the Coulomb field is $\sim 7\times 10^5$, and the characteristic charge Z_2 for loss of interference is $\sim 1.5\times 10^5$. Also shown is $\mathcal{V}^2+\mathcal{D}^2$ (dotted line).

A simple interpretation of the decrease in visibility, in terms of the Aharonov-Bohm effect [118], is that the closed electron loop, $u-l$, encircles a fluctuating electromagnetic field which shifts the interference pattern randomly, thus tending to wash it out. The interpretation of the reduction of the pattern in terms of a random flux requires photon emission processes, and is equivalent to the present discussion. Indeed for the subset of processes in which there is no photon emission, the modification of the interference pattern is given by $\langle U_l^\dagger\rangle\langle U_u\rangle$ [cf. (6.17)], where the brackets denote states with zero photons. Now

$$\mathrm{Re}\log\langle U_u\rangle = -\frac{Z^2\alpha}{3\pi}\int kdk\left|\oint_u e^{-i\omega t}\vec{v}(t)\right|^2 \simeq \frac{1}{4}\log\mathcal{V}; \tag{6.33}$$

the reduction reflects the loss of forward-scattering amplitude owing to photon emission processes. Thus the zero-photon emission pattern is multiplied by a factor $\mathcal{V}^{1/2}$; the suppression of the zero-photon pattern at charge $\sqrt{2}Z$ equals the suppression of the total visibility at charge Z. The phase

of $\langle U_l^\dagger \rangle \langle U_u \rangle$ is essentially proportional to the difference of real parts of the electron self-energy corrections on the upper and lower paths, corrections that do not contribute to the diminution of the interference pattern.

6.4 Measuring the path by gravity

Finally, we ask if it is possible to detect the path by measuring the fluctuations in the (Newtonian) gravitational potential at large distance as a particle of sufficiently large mass passes through the slits. In this scenario, the Newtonian gravitational field plays the role of the Coulomb field for charged particles. We consider detecting the change of the Newtonian gravitational field by using a modern gravity wave detector, e.g., a highly sensitive laser interferometer [141] (a measurement not equivalent to detecting possible gravitational radiation produced by the mass going through the slits.) Figure 6.4 sketches such a detector. As before, the x-axis lies in the plane of the slits. We assume that the mirrors in the detector are tied down in the lab frame; to a first approximation, the distance between the mirrors (or equivalently the ends of a Weber bar) is a harmonic degree of freedom, with oscillator frequency, ω (which includes the gravitational attraction of the two mirrors).

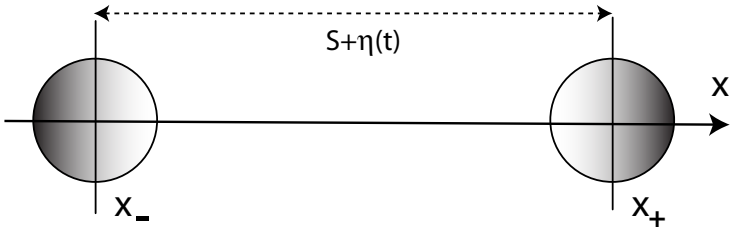

Figure 6.4: Gravitational field detector

We derive schematically the response of the detector to a Newtonian gravitational potential $\phi(x,t)$. In the presence of ϕ, the positions of the mirrors, $x_\pm$, obey the Newtonian equations of motion,

$$\frac{\partial^2 x_\pm}{\partial t^2} = \mp\frac{1}{2}\omega^2[x_+(t) - x_-(t) - S] - \phi'(x_\pm) \tag{6.34}$$

with S the equilibrium distance between the mirrors, and the prime denoting differentiation with

respect to x. We write $x_\pm = x_0 \pm (S+\eta)/2$, where x_0 is the midpoint between the mirrors in equilibrium, and η is the relative displacement of the mirrors caused by the gravitational pulse. Then linearizing in η and ϕ'' we have

$$\frac{\partial^2 \eta(t)}{\partial t^2} = -\omega\eta(t) - \phi''(x_0)S. \tag{6.35}$$

For simplicity we assume that ϕ is zero before the gravitational pulse reaches the detector, and is constant in time during the detection. With initial conditions $\eta(0) = \eta'(0) = 0$, we obtain

$$\eta(t) = -\phi''(x_0)S\frac{1-\cos\omega t}{\omega^2}. \tag{6.36}$$

The accuracy required for the measurement of $\phi''(x_0)$ is

$$\Delta\phi''(x_0) = 2Gm\left(\frac{1}{R^3} - \frac{1}{(R+d)^3}\right) \sim \frac{Gmd}{R^4}, \tag{6.37}$$

where m is the mass of the particle, and the measuring apparatus, as before, is at a distance R from the slits. Thus, since $1-\cos\omega t \le (\omega t)^2/2$, one needs to measure η to an accuracy,

$$\Delta\eta \lesssim \frac{GmdST^2}{R^4} < \frac{Gmd}{Rc^2}. \tag{6.38}$$

which implies that the mass scale for which one can begin to distinguish the path obeys,

$$\frac{Gm^2}{\hbar c} \gtrsim \left(\frac{\Delta\eta}{\ell_{\rm pl}}\right)^2 \left(\frac{R}{d}\right)^2. \tag{6.39}$$

Physically the uncertainty $\Delta\eta$ must exceed the Planck length,[3] and thus

$$\frac{Gm^2}{\hbar c} \gtrsim \left(\frac{R}{d}\right)^2; \tag{6.40}$$

the mass scale must be a factor R/d larger than the Planck mass, $\sqrt{\hbar c/G} \sim 2\times10^{-5}$ g. For $R/d \sim 6\times10^4$ [23], the scale would have to be of order 1 g.

[3]When the displacement is measured by the difference of measured relative positions of the mirrors at times 0 and T, a first estimate of the accuracy of the measurement of η is the *standard quantum limit* $\delta\eta \gtrsim \sqrt{\hbar T/M}$, where M is the mass of each mirror, The mirrors cannot be arbitrarily massive, since the apparatus cannot form a black hole [142], so that $M < Sc^2/4G$, and consequently the standard quantum limit implies, $\delta\eta \gtrsim \ell_{\rm pl}\sqrt{cT/S}$. Various ways to improve on this simple limit using techniques such as contractive states measurements [143, 144], or quantum nondemolition measurements [145, 146] have been proposed. However, our result is independent of these details.

The interference pattern caused by a particle whose mass obeys the condition (6.40) has a fringe separation,

$$\delta_f \sim \frac{L}{d}\frac{\hbar}{mv} \lesssim \ell_{\rm pl}\frac{cT}{R} \lesssim \ell_{\rm pl}, \tag{6.41}$$

which implies that when the mass is large enough to allow "which-path" detection via gravity, the pattern becomes immeasurably fine, of order the Planck length or shorter. This result assures the consistency of quantum mechanics; however, unlike in the electromagnetic case, consistency does not require that the gravitational field be quantized.[4] (While a decrease of the visibility of the pattern would arise were gravity quantized, as in the electromagnetic situation, detailed calculations of the diminution would depend on the detailed theory of quantized gravity assumed, an issue we do not address here.)

In summary, when one can distinguish the path of a particle by measuring the electromagnetic or gravitational field at large distance, interference disappears. For large enough charge on the interfering particle, emission of quantized electromagnetic radiation destroys the interference, while for large enough mass, the pattern becomes too fine to be discerned.

[4] As in the electromagnetic case, one expects a crossover with increasing mass from indistinguishable to distinguishable paths. However, a better understanding of the nature of space-time on the Planck scale is required to determine a quantitivative visibility.

Appendix A

Scattering theory

A.1 Introduction

In this chapter, we consider scattering of two particles in a vacuum, with an interaction which depends on the particles' relative coordinate. We elucidate the role of the dimensionality, discussing both three dimensions and two dimensions in a parallel manner[1]. We start by discussing the general structure of dimension-independent scattering theory, and then go on to define scattering amplitude, phase shift, and scattering length, depending on the dimensionality. We also consider a square well potential as an example and calculate various scattering properties in three dimensions and two dimensions. In two dimensions, we prove that, at least in a square well potential, the low-energy scattering t-matrix vanishes.

A.2 Scattering t-matrix

A.2.1 General theory

The Hamiltonian for a two-particle system with an interaction $\mathcal{V}(\mathbf{r}-\mathbf{r})$ is

$$\mathcal{H}(\mathbf{r}_1,\mathbf{r}_2)=\mathcal{H}_0(\mathbf{r}_1,\mathbf{r}_2)+\mathcal{V}(\mathbf{r}_1-\mathbf{r}_2)=\frac{1}{2m}\left(-\nabla_1^2-\nabla_2^2\right)+\mathcal{V}(\mathbf{r}_1-\mathbf{r}_2), \tag{A.1}$$

[1] The argument given here is influenced by an unpublished note on two dimensional scattering by Baharian [147].

It is conventional to rewrite the Hamiltonian by separating the center of mass coordinate and the relative coordinate[2]. Defining

$$\mathbf{R} = \frac{\mathbf{r}_1 + \mathbf{r}_2}{2}, \qquad \mathbf{r} = \mathbf{r}_1 - \mathbf{r}_2, \tag{A.2}$$

the Hamiltonian now becomes

$$\mathcal{H}(\mathbf{R}, \mathbf{r}) = -\frac{1}{2M}\nabla_R^2 - \frac{1}{2m_r}\nabla_r^2 + \mathcal{V}(\mathbf{r}), \tag{A.3}$$

where $M = 2m$ is the total mass and $m_r = m/2$ is the reduced mass. Thus the Hamiltonian is divided into two parts and the wavefunction can be written as a product of an $\mathbf{R}$-dependent part and an $\mathbf{r}$-dependent part. The relations of the center of mass and relative momenta to the original momenta are

$$\mathbf{P} = \mathbf{p}_1 + \mathbf{p}_2, \qquad \mathbf{p} = \frac{\mathbf{p}_1 - \mathbf{p}_2}{2}. \tag{A.4}$$

Since the $\mathbf{R}$-dependent portion of the Hamiltonian is simply that of a free particle, whose eigenstates are plane waves, we now can focus on the $\mathbf{r}$-dependent part. We begin by writing the Hamiltonian for the relative motion

$$\mathcal{H}(\mathbf{r}) = -\frac{1}{2m_r}\nabla_r^2 + \mathcal{V}(\mathbf{r}). \tag{A.5}$$

The Schrödinger equation for the relative motion is therefore

$$\left(-\frac{1}{2m_r}\nabla_r^2 + \mathcal{V}(\mathbf{r})\right)\Psi(\mathbf{r}) = E\Psi(\mathbf{r}), \tag{A.6}$$

where the energy E is nonnegative throughout this chapter. Let $\psi_0(\mathbf{r})$ denote the wavefunction of the free part of the Hamiltonian with the energy E, i.e.,

$$-\frac{1}{2m_r}\nabla_r^2\psi_0(\mathbf{r}) = E\psi_0(\mathbf{r}). \tag{A.7}$$

A representative solution to this free Schrödinger equation is a plane wave state

$$\psi_0(\mathbf{r}) \propto e^{i\mathbf{k}\cdot\mathbf{r}}, \tag{A.8}$$

[2] We note here that Rashba-Dresselhaus potential, which we discuss in the following chapters, is not separable into the center of mass and relative coordinates.

with $E = k^2/2m_r$, but there are other states, such as a spherical wave states, that satisfy this equation as well.

Defining the Green's function by

$$\left(E + \frac{1}{2m_r}\nabla_r^2\right) G(\mathbf{r} - \mathbf{r}') = \delta(\mathbf{r} - \mathbf{r}'), \tag{A.9}$$

a general solution to the Schrödinger equation obeys the following integral equation:

$$\Psi(\mathbf{r}) = \psi_0(\mathbf{r}) + \int d^d r' G(\mathbf{r} - \mathbf{r}')\mathcal{V}(\mathbf{r}')\Psi(\mathbf{r}'), \tag{A.10}$$

where d is the dimensionality of the space. This equation is the position-space representation of the *Lippmann-Schwinger equation*, although the latter is more commonly written in terms of operators. This integral equation can be solved iteratively as a perturbation series in the interaction, starting from the non-interacting wavefunction $\psi_0(\mathbf{r})$.

We remark here that this Lippmann-Schwinger equation cannot be used for a hard-core potential, since the second term is always identically zero. In order to deal with a hard-core potential, we need a separate treatment, which we do not address further in this thesis.

In many applications, the range of interaction where $\mathcal{V}(\mathbf{r})$ is non-negligible is restricted to a certain region of space, and we observe the wavefunction far away from that region where the interaction is negligible.

The wavefunction itself is not the quantity that is readily measurable. In a typical scattering experiment, particles enter the region of the potential and are scattered in many different directions. One then measures the number of particles scattered into the various directions. Let us imagine that a detector, located at a distance r from the center of the potential, detects the number of scattered particles in a unit solid angle for three dimensions and a unit planar angle for two dimensions. The ratio of the number of detected scattered particles per unit time to the number of incident particles that crosses a unit area per unit time in front of the target is called the *differential cross section*. The *total cross section* is defined by the integral of the differential cross section over all angles. In other words, the total cross section is the number of scattered particles divided by the number of incident particles per unit area per unit time.

To see how the wavefunction behaves far away from the scattering potential, we need to know the asymptotic behavior of the Green's function, which depends on the dimensionality. Before working in a specific dimensionality and solving for the Green's function in the next section, we

introduce the scattering t-matrix and discuss its relation to the effective interaction in the next subsection.

A.2.2 t-matrix and the effective interaction

In many instances, the momentum representation of the Lippmann-Schwinger equation is useful. Let us begin by defining the Fourier transform of the wavefunction and the Green's function by

$$\Psi(\mathbf{r}) = \int \frac{d^d k}{(2\pi)^d} \Psi(\mathbf{k}) e^{i\mathbf{k}\cdot\mathbf{r}}, \qquad G(\mathbf{r}-\mathbf{r}') = \int \frac{d^d k}{(2\pi)^d} G(\mathbf{k}) e^{i\mathbf{k}\cdot(\mathbf{r}-\mathbf{r}')}. \tag{A.11}$$

The Fourier transforms of the free wavefunction $\psi_0(\mathbf{r})$ and the potential $\mathcal{V}(\mathbf{r})$ are defined similarly. Using the definition of the Green's function (A.9), we can see

$$G(\mathbf{k}) = \frac{1}{E - k^2/2m_r}, \tag{A.12}$$

and the Green's function is

$$G(\mathbf{r}-\mathbf{r}') = \int \frac{d^d k}{(2\pi)^d} \frac{1}{E - k^2/2m_r} e^{i\mathbf{k}\cdot(\mathbf{r}-\mathbf{r}')}. \tag{A.13}$$

The Lippmann-Schwinger equation is then

$$\begin{aligned} \int \frac{d^d k}{(2\pi)^d} \Psi(\mathbf{k}) e^{i\mathbf{k}\cdot\mathbf{r}} &= \int \frac{d^d k}{(2\pi)^d} \psi_0(\mathbf{k}) e^{i\mathbf{k}\cdot\mathbf{r}} + \int d^d r' \frac{d^d k}{(2\pi)^d} \frac{d^d k'}{(2\pi)^d} \frac{d^d k''}{(2\pi)^d} \frac{e^{i\mathbf{k}\cdot(\mathbf{r}-\mathbf{r}')} e^{i\mathbf{k}''\cdot\mathbf{r}'} e^{i\mathbf{k}'\cdot\mathbf{r}'}}{E - k^2/2m_r} \mathcal{V}(\mathbf{k}'') \Psi(\mathbf{k}') \\ &= \int \frac{d^d k}{(2\pi)^d} \frac{d^d k'}{(2\pi)^d} \frac{e^{i\mathbf{k}\cdot\mathbf{r}}}{E - k^2/2m_r} \mathcal{V}(\mathbf{k}-\mathbf{k}') \Psi(\mathbf{k}'). \end{aligned} \tag{A.14}$$

Taking the Fourier component with momentum $\mathbf{k}$, we obtain the momentum representation of the Lippmann-Schwinger equation

$$\Psi(\mathbf{k}) = \psi_0(\mathbf{k}) + \frac{1}{E - k^2/2m_r} \int \frac{d^d k'}{(2\pi)^d} \mathcal{V}(\mathbf{k}-\mathbf{k}') \Psi(\mathbf{k}'). \tag{A.15}$$

We are now almost ready to define the scattering t-matrix. The total wavefunction $\Psi(\mathbf{x})$ depends on the choice of our incoming state $\psi_0(\mathbf{k})$. For concreteness, although not entirely necessary, let us choose the incoming state to be the plane wave state with momentum $\mathbf{p}$, which satisfies $E = p^2/2m_r$. Then, $\psi_0(\mathbf{k}) = (2\pi)^d \delta(\mathbf{k}-\mathbf{p})$. Let $\Psi_{\mathbf{p}}(\mathbf{k})$ be the total wavefunction corresponding to this incoming plane wave. Then, the Lippmann-Schwinger equation in the momentum representation is

$$\Psi_{\mathbf{p}}(\mathbf{k}) = (2\pi)^d \delta(\mathbf{k}-\mathbf{p}) + \frac{1}{E - k^2/2m_r} \int \frac{d^d k'}{(2\pi)^d} \mathcal{V}(\mathbf{k}-\mathbf{k}') \Psi_{\mathbf{p}}(\mathbf{k}'). \tag{A.16}$$

We now define the *scattering t-matrix* by

$$T(\mathbf{k},\mathbf{p}) \equiv \int \frac{d^dk'}{(2\pi)^d}\mathcal{V}(\mathbf{k}-\mathbf{k}')\Psi_{\mathbf{p}}(\mathbf{k}') = \int d^dr\ e^{-i\mathbf{k}\cdot\mathbf{r}}\mathcal{V}(\mathbf{r})\Psi_{\mathbf{p}}(\mathbf{r}). \tag{A.17}$$

Note that a commonly used definition of the t-matrix is in terms of operator equations. For the relation between the common approach and our approach, see the end of this section. The Lippmann-Schwinger equation is now concisely expressed as

$$\Psi_{\mathbf{p}}(\mathbf{k}) = (2\pi)^d\delta(\mathbf{k}-\mathbf{p}) + G(\mathbf{k})T(\mathbf{k},\mathbf{p}). \tag{A.18}$$

This equation does not look particularly inspiring, but by multiplying both sides by $\mathcal{V}(\mathbf{p}'-\mathbf{k})$ and integrating over $\mathbf{k}$, we obtain an integral equation for the t-matrix;

$$\begin{aligned} T(\mathbf{p}',\mathbf{p}) &= \mathcal{V}(\mathbf{p}'-\mathbf{p}) + \int \frac{d^dk}{(2\pi)^d}\mathcal{V}(\mathbf{p}'-\mathbf{k})G(\mathbf{k})T(\mathbf{k},\mathbf{p}) \\ &= \mathcal{V}(\mathbf{p}'-\mathbf{p}) + \int \frac{d^dk}{(2\pi)^d}\mathcal{V}(\mathbf{p}'-\mathbf{k})\frac{1}{E-k^2/2m_r}T(\mathbf{k},\mathbf{p}). \end{aligned} \tag{A.19}$$

Let us now make a connection between our definition of the t-matrix and a more commonly used definition in terms of operators (for example in Sakurai [148]). Some useful operator identities that are consistent with the notation in this thesis are

$$\langle\mathbf{x}|\Psi\rangle = \Psi(\mathbf{x}), \quad \langle\mathbf{k}|\Psi\rangle = \Psi(\mathbf{k}), \quad \langle\mathbf{x}|\mathbf{k}\rangle = e^{i\mathbf{k}\cdot\mathbf{x}}, \quad 1 = \int d^dx|\mathbf{x}\rangle\langle\mathbf{x}| = \int \frac{d^dk}{(2\pi)^d}|\mathbf{k}\rangle\langle\mathbf{k}|. \tag{A.20}$$

The t-matrix is often defined by an operator equation

$$\hat{T}|\psi_0\rangle = V|\Psi\rangle. \tag{A.21}$$

Choosing the initial state to be the plane wave state with momentum $\mathbf{p}$, we have

$$\begin{aligned} \langle\mathbf{k}|\hat{T}|\mathbf{p}\rangle = \langle\mathbf{k}|V|\Psi_{\mathbf{p}}\rangle &= \int d^dx\langle\mathbf{k}|\mathbf{x}\rangle\langle\mathbf{x}|V|\Psi_{\mathbf{p}}\rangle = \int d^dx\ e^{-i\mathbf{k}\cdot\mathbf{x}}V(\mathbf{x})\Psi_{\mathbf{p}}(\mathbf{x}) \\ &= \int d^dx\frac{d^dk'}{(2\pi)^d}\frac{d^dk''}{(2\pi)^d}e^{-i\mathbf{k}\cdot\mathbf{x}+i\mathbf{k}'\cdot\mathbf{x}+i\mathbf{k}''\cdot\mathbf{x}}V(\mathbf{k}'')\Psi_{\mathbf{p}}(\mathbf{k}') \\ &= \int \frac{d^dk'}{(2\pi)^d}V(\mathbf{k}-\mathbf{k}')\Psi_{\mathbf{p}}(\mathbf{k}'), \end{aligned} \tag{A.22}$$

which is exactly how we defined $T(\mathbf{p},\mathbf{k})$. Thus, the definition in terms of an operator equation and our definition are equivalent and their relation is

$$\langle\mathbf{k}|\hat{T}|\mathbf{p}\rangle = T(\mathbf{p},\mathbf{k}). \tag{A.23}$$

This equation also implies that the scattering t-matrix is Hermitian satisfying

$$T(\mathbf{p}', \mathbf{p})^* = T(\mathbf{p}, \mathbf{p}'). \tag{A.24}$$

As we show now, the scattering t-matrix turns out to be equal to the vertex function within a ladder approximation in diagrammatic perturbation theory. This relation is crucially exploited in ultracold atomic physics, where the effective interaction and the t-matrix are often used interchangeably.

Suppose two particles are in a vacuum. Consider the vertex function with incoming four momenta $(\mathbf{q}/2+\mathbf{p}, \omega_q/2+\omega_p)$ and $(\mathbf{q}/2-\mathbf{p}, \omega_q/2-\omega_p)$, and outgoing momenta $(\mathbf{q}/2+\mathbf{p}', \omega_q/2+\omega_{p'})$ and $(\mathbf{q}/2-\mathbf{p}', \omega_q/2-\omega_{p'})$. The diagrams for the Bethe-Salpeter equation of the vertex function, approximated by ladder diagrams, are shown in Figure A.1, and the equation is

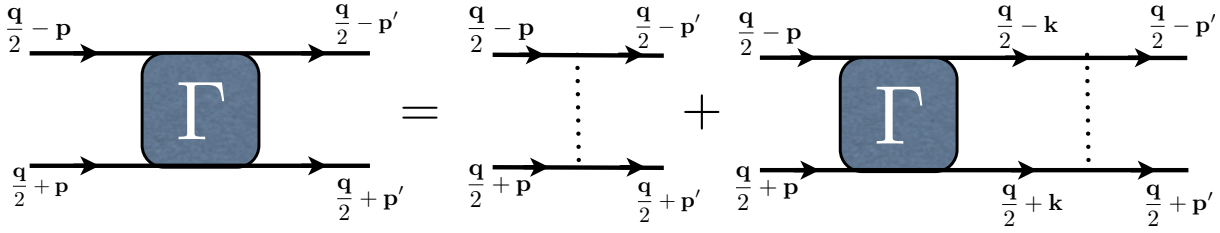

Figure A.1: Bethe-Salpeter equation for the vertex function within ladder approximation

$$\Gamma(\mathbf{p}', \mathbf{p}; \mathbf{q}, \omega_q) = \mathcal{V}(\mathbf{p}' - \mathbf{p}) + i \int \frac{d\omega}{2\pi} \frac{d^d k}{(2\pi)^d} \Gamma(\mathbf{k}, \mathbf{p}; \mathbf{q}, \omega_q) \frac{1}{\omega - \epsilon_0(\mathbf{q}/2 + \mathbf{k}) + i\eta} \times \frac{1}{\omega_q - \omega - \epsilon_0(\mathbf{q}/2 - \mathbf{k}) + i\eta} \mathcal{V}(\mathbf{p}' - \mathbf{k}), \tag{A.25}$$

where $\epsilon_0(\mathbf{x}) = x^2/2m$ with $m = 2m_r$ being the original mass of a particle, not to be confused with a reduced mass, and η is a positive infinitesimal. After decomposing the partial fraction, we have

$$\Gamma(\mathbf{p}', \mathbf{p}; \mathbf{q}, \omega_q) = \mathcal{V}(\mathbf{p}' - \mathbf{p}) + i \int \frac{d\omega}{2\pi} \frac{d^d k}{(2\pi)^d} \Gamma(\mathbf{k}, \mathbf{p}; \mathbf{q}, \omega_q) \frac{1}{\omega_q - \epsilon_0(\mathbf{q}/2 + \mathbf{k}) - \epsilon_0(\mathbf{q}/2 - \mathbf{k}) + i\eta} \times \left(\frac{1}{\omega - \epsilon_0(\mathbf{q}/2 + \mathbf{k}) + i\eta} + \frac{1}{\omega_q - \omega - \epsilon_0(\mathbf{q}/2 - \mathbf{k}) + i\eta} \right) \mathcal{V}(\mathbf{p}' - \mathbf{k}). \tag{A.26}$$

There are two poles in the ω plane, one above the real axis and one below. Thus, whichever way we choose to close the contour in the integral over ω in the complex plane, by introducing a factor

of $e^{i\omega\eta}$ or $e^{-i\omega\eta}$, the result will be the same, and we have

$$\Gamma(\mathbf{p}', \mathbf{p}; \mathbf{q}, \omega_q) = \mathcal{V}(\mathbf{p}' - \mathbf{p}) + \int \frac{d^d k}{(2\pi)^d} \mathcal{V}(\mathbf{p}' - \mathbf{k}) \frac{1}{\omega_q - \epsilon_0(\mathbf{q}/2 + \mathbf{k}) - \epsilon_0(\mathbf{q}/2 - \mathbf{k}) + i\eta} \Gamma(\mathbf{k}, \mathbf{p}; \mathbf{q}, \omega_q). \tag{A.27}$$

If we consider the *on-shell* element of the vertex function by setting $\omega_q = E = \epsilon_0(\mathbf{q}/2 + \mathbf{p}) + \epsilon_0(\mathbf{q}/2 - \mathbf{p})$, we can see that the denominator in the right hand side does not depend on $\mathbf{q}$ and we have

$$\Gamma(\mathbf{p}', \mathbf{p}; \mathbf{q}, E) = \mathcal{V}(\mathbf{p}' - \mathbf{p}) + \int \frac{d^d k}{(2\pi)^d} \mathcal{V}(\mathbf{p}' - \mathbf{k}) \frac{1}{p^2/2m_r - k^2/2m_r + i\eta} \Gamma(\mathbf{k}, \mathbf{p}; \mathbf{q}, E). \tag{A.28}$$

Iterating this equation, we can see that $\Gamma(\mathbf{p}', \mathbf{p}; \mathbf{q}, E)$ does not depend on the center of mass momentum $\mathbf{q}$. Moreover, this integral equation is exactly the same as the equation (A.19) with

$$\Gamma(\mathbf{p}', \mathbf{p}; \mathbf{q}, E) = T(\mathbf{p}', \mathbf{p}). \tag{A.29}$$

Thus we have proven that the t-matrix is equal to the on-shell vertex function within the ladder approximation. Since the vertex function serves as an effective interaction, whenever the ladder approximation is appropriate and the on-shell vertex function is the relevant quantity, the t-matrix can be used as an effective interaction.

Since the on-shell vertex function within the ladder approximation is exactly the same as the scattering t-matrix, the t-matrix is often defined as the ladder approximation of the vertex function.

It is important to take care and note that only the *on-shell* vertex function is equal to the scattering t-matrix. Beliaev and Galitskii found a more general relation between the *off-shell* vertex function within the ladder approximation and the scattering t-matrix, which we will now discuss.

A.2.3 Beliaev-Galitskii relation

A general relation between the vertex function and the t-matrix was found by Beliaev [149] for the case of bosons and Galitskii [99] for the case of fermions. A derivation here is from Chang and Friedberg [150].

An important property of the wavefunctions $\Psi_{\mathbf{p}}(\mathbf{r})$ is that they form a complete orthonormal set. The orthogonality condition is

$$\int \frac{d^d r}{(2\pi)^d} \Psi_{\mathbf{p}}(\mathbf{r}) \Psi^*_{\mathbf{p}'}(\mathbf{r}) = \delta(\mathbf{p} - \mathbf{p}'), \tag{A.30}$$

or equivalently

$$\int \frac{d^dk}{(2\pi)^d}\Psi_{\mathbf{p}}(\mathbf{k})\Psi^*_{\mathbf{p}'}(\mathbf{k}) = \int \frac{d^dk}{(2\pi)^d}\int d^dr \int d^dr' \Psi_{\mathbf{p}}(\mathbf{r})e^{i\mathbf{k}\cdot\mathbf{r}}\Psi^*_{\mathbf{p}'}(\mathbf{r}')e^{-i\mathbf{k}\cdot\mathbf{r}'} = (2\pi)^d\delta(\mathbf{p}-\mathbf{p}'). \quad \text{(A.31)}$$

Recall from (A.27) that the Bethe-Salpeter equation is

$$\Gamma(\mathbf{p}',\mathbf{p};\mathbf{q},\omega_q) = \mathcal{V}(\mathbf{p}'-\mathbf{p}) + \int \frac{d^dk}{(2\pi)^d}\mathcal{V}(\mathbf{p}'-\mathbf{k})\frac{1}{\omega_q - \epsilon_0(\mathbf{q}/2+\mathbf{k}) - \epsilon_0(\mathbf{q}/2-\mathbf{k}) + i\eta}\Gamma(\mathbf{k},\mathbf{p};\mathbf{q},\omega_q). \quad \text{(A.32)}$$

Let us now decompose the vertex function in terms of the full wavefunction-basis as

$$\frac{\Gamma(\mathbf{k},\mathbf{p};\mathbf{q},\omega_q)}{\omega_q - \epsilon_0(\mathbf{q}/2+\mathbf{k}) - \epsilon_0(\mathbf{q}/2-\mathbf{k}) + i\eta} = \int \frac{d^dk'}{(2\pi)^d}c_{\mathbf{k}'}(\mathbf{p};\mathbf{q},\omega_q)\Psi_{\mathbf{k}'}(\mathbf{k}). \quad \text{(A.33)}$$

Then, we have

$$\begin{aligned}
&\left(\omega_q - \epsilon_0(\mathbf{q}/2+\mathbf{p}') - \epsilon_0(\mathbf{q}/2-\mathbf{p}') + i\eta\right)\int \frac{d^dk'}{(2\pi)^d}c_{\mathbf{k}'}(\mathbf{p};\mathbf{q},\omega_q)\Psi_{\mathbf{k}'}(\mathbf{p}') \\
&\quad = \mathcal{V}(\mathbf{p}'-\mathbf{p}) + \int \frac{d^dk}{(2\pi)^d}\int \frac{d^dk'}{(2\pi)^d}c_{\mathbf{k}'}(\mathbf{p};\mathbf{q},\omega_q)\Psi_{\mathbf{k}'}(\mathbf{k})\mathcal{V}(\mathbf{p}'-\mathbf{k}) \\
&\quad = \mathcal{V}(\mathbf{p}'-\mathbf{p}) + \int \frac{d^dk'}{(2\pi)^d}c_{\mathbf{k}'}(\mathbf{p};\mathbf{q},\omega_q)\left(\frac{k'^2}{2m_r} - \frac{p'^2}{2m_r}\right)\left(\Psi_{\mathbf{k}'}(\mathbf{p}') - (2\pi)^d\delta(\mathbf{p}'-\mathbf{k}')\right) \\
&\quad = \mathcal{V}(\mathbf{p}'-\mathbf{p}) + \int \frac{d^dk'}{(2\pi)^d}c_{\mathbf{k}'}(\mathbf{p};\mathbf{q},\omega_q)\left(\frac{k'^2}{2m_r} - \frac{p'^2}{2m_r}\right)\Psi_{\mathbf{k}'}(\mathbf{p}'), \quad \text{(A.34)}
\end{aligned}$$

where we have used (A.16). Writing as

$$\begin{aligned}
\mathcal{V}(\mathbf{p}'-\mathbf{p}) &= \int \frac{d^dk'}{(2\pi)^d}\left(\omega_q - \epsilon_0(\mathbf{q}/2+\mathbf{p}') - \epsilon_0(\mathbf{q}/2-\mathbf{p}') - \frac{k'^2}{2m_r} + \frac{p'^2}{2m_r} + i\eta\right)c_{\mathbf{k}'}(\mathbf{p};\mathbf{q},\omega_q)\Psi_{\mathbf{k}'}(\mathbf{p}') \\
&= \int \frac{d^dk'}{(2\pi)^d}\left(\omega_q - \frac{q^2}{8m_r} - \frac{k'^2}{2m_r} + i\eta\right)c_{\mathbf{k}'}(\mathbf{p};\mathbf{q},\omega_q)\Psi_{\mathbf{k}'}(\mathbf{p}'), \quad \text{(A.35)}
\end{aligned}$$

the complex conjugate of the t-matrix is

$$\begin{aligned}
T^*(\mathbf{p},\mathbf{k}) &= \int \frac{d^dp'}{(2\pi)^d}\mathcal{V}^*(\mathbf{p}-\mathbf{p}')\Psi^*_{\mathbf{k}}(\mathbf{p}') = \int \frac{d^dp'}{(2\pi)^d}\mathcal{V}(\mathbf{p}'-\mathbf{p})\Psi^*_{\mathbf{k}}(\mathbf{p}') \\
&= \int \frac{d^dp'}{(2\pi)^d}\int \frac{d^dk'}{(2\pi)^d}\left(\omega_q - \frac{q^2}{8m_r} - \frac{k'^2}{2m_r} + i\eta\right)c_{\mathbf{k}'}(\mathbf{p};\mathbf{q},\omega_q)\Psi_{\mathbf{k}'}(\mathbf{p}')\Psi^*_{\mathbf{k}}(\mathbf{p}') \\
&= \int \frac{d^dk'}{(2\pi)^d}\left(\omega_q - \frac{q^2}{8m_r} - \frac{k'^2}{2m_r} + i\eta\right)c_{\mathbf{k}'}(\mathbf{p};\mathbf{q},\omega_q)(2\pi)^d\delta(\mathbf{k}'-\mathbf{k}) \\
&= \left(\omega_q - \frac{q^2}{8m_r} - \frac{k^2}{2m_r} + i\eta\right)c_{\mathbf{k}}(\mathbf{p};\mathbf{q},\omega_q). \quad \text{(A.36)}
\end{aligned}$$

Then, going back to (A.33), we have

$$\begin{aligned}
\Gamma(\mathbf{k},\mathbf{p};\mathbf{q},\omega_q) &= \left(\omega_q - \frac{q^2}{8m_r} - \frac{k^2}{2m_r} + i\eta\right)\int \frac{d^dk'}{(2\pi)^d} c_{\mathbf{k}'}(\mathbf{p};\mathbf{q},\omega_q)\Psi_{\mathbf{k}'}(\mathbf{k}) \\
&= \left(\omega_q - \frac{q^2}{8m_r} - \frac{k^2}{2m_r} + i\eta\right)\int \frac{d^dk'}{(2\pi)^d} \frac{T^*(\mathbf{p},\mathbf{k}')}{\omega_q - \dfrac{q^2}{8m_r} - \dfrac{k'^2}{2m_r} + i\eta}\Psi_{\mathbf{k}'}(\mathbf{k}) \\
&= \left(\omega_q - \frac{q^2}{8m_r} - \frac{k^2}{2m_r} + i\eta\right)\int \frac{d^dk'}{(2\pi)^d} \frac{T^*(\mathbf{p},\mathbf{k}')}{\omega_q - \dfrac{q^2}{8m_r} - \dfrac{k'^2}{2m_r} + i\eta} \\
&\qquad\qquad \times \left((2\pi)^d\delta(\mathbf{k}-\mathbf{k}') + \frac{T(\mathbf{k},\mathbf{k}')}{k'^2/2m_r - k^2/2m_r}\right) \\
&= T^*(\mathbf{p},\mathbf{k}) + \left(\omega_q - \frac{q^2}{8m_r} - \frac{k^2}{2m_r} + i\eta\right)\int \frac{d^dk'}{(2\pi)^d} \frac{T^*(\mathbf{p},\mathbf{k}')}{\omega_q - \dfrac{q^2}{8m_r} - \dfrac{k'^2}{2m_r} + i\eta} \frac{T(\mathbf{k},\mathbf{k}')}{k'^2/2m_r - k^2/2m_r} \\
&= T(\mathbf{k},\mathbf{p}) + \int \frac{d^dk'}{(2\pi)^d}\left(\frac{1}{\omega_q - q^2/8m_r - k'^2/2m_r + i\eta} - \frac{1}{k^2/2m_r - k'^2/2m_r}\right) T(\mathbf{k},\mathbf{k}')T(\mathbf{k}',\mathbf{p}).
\end{aligned} \tag{A.37}$$

This last result is the *Beliaev-Galitskii relation* which relates the vertex function within the ladder approximation and the scattering t-matrix.

Now, let us try to understand the low energy behavior of the vertex function. Writing ω_q as a frequency away from the on-shell energy as $\omega_q = E + \delta\omega$, we obtain

$$\begin{aligned}
&\Gamma(\mathbf{k},\mathbf{p};\mathbf{q},\omega_q) \\
&= T(\mathbf{k},\mathbf{p}) + \int \frac{d^dk'}{(2\pi)^d}\left(\frac{1}{\delta\omega + k^2/2m_r - k'^2/2m_r + i\eta} - \frac{1}{k^2/2m_r - k'^2/2m_r}\right) T(\mathbf{k},\mathbf{k}')T(\mathbf{k}',\mathbf{p}) \\
&= T(\mathbf{k},\mathbf{p}) - \int \frac{d^dk'}{(2\pi)^d} \frac{\delta\omega}{(\delta\omega + k^2/2m_r - k'^2/2m_r + i\eta)(k^2/2m_r - k'^2/2m_r)} T(\mathbf{k},\mathbf{k}')T(\mathbf{k}',\mathbf{p}) \\
&= T(\mathbf{k},\mathbf{p}) - \frac{2m_r}{k^2}\int \frac{d^dk'}{(2\pi)^d} \frac{2m_r\delta\omega/k^2}{(2m_r\delta\omega/k^2 + 1 - k'^2/k^2 + i\eta)(1 - k'^2/k^2)} T(\mathbf{k},\mathbf{k}')T(\mathbf{k}',\mathbf{p}).
\end{aligned} \tag{A.38}$$

In three dimensions, as we shall see later in this chapter, the t-matrix approaches a constant value in the low energy limit. Then, the integral in the right hand side is of order $\sim mkT(0,0)^2$. If the energy of the particle we are interested in is low enough that $mkT(0,0) \ll 1$, we can ignore this term and also the deviation of the first term from $T(0,0)$. Then we can approximate

$$\Gamma(\mathbf{k},\mathbf{p};\mathbf{q},\omega_q) \sim T(0,0) \tag{A.39}$$

in the low energy limit. This assumption of $mkT(0,0) \ll 1$ corresponds to the dilute gas limit in the many-body system with the condition $na^3 \ll 1$ where n is the density and a is the scattering length, which is to be defined later in this chapter. Thus we have analyzed only the two-body problem. For the many-body case, it turns out that the many-body correction is of higher order, and to the lowest order, the approximation (A.39) is still valid in the dilute gas limit. Chapter 25 of Abrikosov, Gorkov, and Dzyaloshinski [151] has a detailed treatment of the many-body case.

In two dimensions, the t-matrix approaches zero in the low energy limit, and we should be more careful about the treatment of the low energy effective interaction. To correctly describe the low energy effective interaction in the two dimensional system, we must take the many-body effects into account.

A.3 Green's functions and scattering amplitudes

Let us now come back to our original problem of describing the scattering in three and two dimensional space. In the discussions that follow, the analysis begins to depend on the dimensionality of the system. We will first discuss well-known results from three dimensions and then discuss two dimensions using analogies from three dimensions.

A.3.1 Three dimensions

Referring to (A.13), we see that the Green's function in three spatial dimensions is

$$\begin{aligned} G(\mathbf{r}-\mathbf{r}') &= \int \frac{d^3k}{(2\pi)^3} \frac{1}{E - k^2/2m_r} e^{i\mathbf{k}\cdot(\mathbf{r}-\mathbf{r}')} \\ &= \int_{-1}^{1} d(\cos\theta) \int_0^\infty \frac{dk}{(2\pi)^2} \frac{k^2}{E - k^2/2m_r} e^{ik|\mathbf{r}-\mathbf{r}'|\cos\theta} \\ &= \int_0^\infty \frac{dk}{(2\pi)^2} \frac{k^2}{E - k^2/2m_r} \frac{e^{ik|\mathbf{r}-\mathbf{r}'|} - e^{-ik|\mathbf{r}-\mathbf{r}'|}}{ik|\mathbf{r}-\mathbf{r}'|} \\ &= \int_{-\infty}^\infty \frac{dk}{(2\pi)^2} \frac{k}{E - k^2/2m_r} \cdot \frac{e^{ik|\mathbf{r}-\mathbf{r}'|}}{i|\mathbf{r}-\mathbf{r}'|}. \end{aligned} \tag{A.40}$$

The integral is singular at $k = \pm\sqrt{2m_r E}$, and we need to decide how to deal with these singularities. However we choose to deal with the singularities, we will obtain a function which satisfies the original definition of the Green's function. Therefore, we need to choose a function that physically best describes the problem that we are trying to solve. Particularly useful ways of dealing with the

singularities are to define

$$\begin{aligned} G_{\pm}(\mathbf{r}-\mathbf{r}') &= \lim_{\epsilon\to 0^+}\int_{-\infty}^{\infty}\frac{dk}{(2\pi)^2}\frac{k}{E\pm i\epsilon - k^2/2m_r}\cdot\frac{e^{ik|\mathbf{r}-\mathbf{r}'|}}{i|\mathbf{r}-\mathbf{r}'|} \\ &= \lim_{\epsilon\to 0^+}\int_{-\infty}^{\infty}\frac{dk}{(2\pi)^2}\frac{-2m_r k}{k^2-(2m_r E\pm i\epsilon)}\cdot\frac{e^{ik|\mathbf{r}-\mathbf{r}'|}}{i|\mathbf{r}-\mathbf{r}'|} \\ &= \mp\frac{m_r}{2\pi}\frac{e^{\pm i\sqrt{2m_r E}|\mathbf{r}-\mathbf{r}'|}}{|\mathbf{r}-\mathbf{r}'|}. \end{aligned} \tag{A.41}$$

Plugging this into the integral equation (A.10), we can see that choosing $G_+(\mathbf{r}-\mathbf{r}')$ corresponds to the outgoing wave (we can see this by inserting a factor of e^{-iEt}, which is the time-dependence of the wavefunction), and choosing $G_-(\mathbf{r}-\mathbf{r}')$ corresponds to the incoming wave. To describe a situation in which the incoming wave is a plane wave and the outgoing wave is a scattered wave, we should choose $G_+(\mathbf{r}-\mathbf{r}')$ as the Green's function to use in the equation (A.10).

Now that we have an expression for the Green's function, the integral equation (A.10) becomes

$$\Psi(\mathbf{r}) = \psi_0(\mathbf{r}) - \frac{m_r}{2\pi}\int d^3r'\frac{e^{i\sqrt{2m_r E}|\mathbf{r}-\mathbf{r}'|}}{|\mathbf{r}-\mathbf{r}'|}\mathcal{V}(\mathbf{r}')\Psi(\mathbf{r}'). \tag{A.42}$$

Let us consider the asymptotic behavior of $\Psi(\mathbf{r})$. When r is much larger than the range of interaction, we can write

$$|\mathbf{r}-\mathbf{r}'| \sim r - \hat{r}\cdot\mathbf{r}', \tag{A.43}$$

where $\hat{r}$ is the unit vector in the direction of $\mathbf{r}$, and therefore

$$\begin{aligned} \Psi(\mathbf{r}) &\sim \psi_0(\mathbf{r}) - \frac{m_r}{2\pi}\int d^3r'\frac{e^{i\sqrt{2m_r E}(r-\hat{r}\cdot\mathbf{r}')}}{r-\hat{r}\cdot\mathbf{r}'}\mathcal{V}(\mathbf{r}')\Psi(\mathbf{r}') \\ &= \psi_0(\mathbf{r}) - \frac{m_r}{2\pi}\frac{e^{i\sqrt{2m_r E}r}}{r}\int d^3r' e^{-i\sqrt{2m_r E}\hat{r}\cdot\mathbf{r}'}\mathcal{V}(\mathbf{r}')\Psi(\mathbf{r}') \\ &= \psi_0(\mathbf{r}) + f(E,\hat{r})\frac{e^{i\sqrt{2m_r E}r}}{r}, \end{aligned} \tag{A.44}$$

where

$$f(E,\hat{r}) = -\frac{m_r}{2\pi}\int d^3r' e^{-i\sqrt{2m_r E}r'\cos\theta}\mathcal{V}(\mathbf{r}')\Psi(\mathbf{r}'), \tag{A.45}$$

is called the *scattering amplitude*. This implies that when the position of observation is far away from the potential, the scattered wavefunction behaves as e^{ipr}/r with a coefficient which only depends on the angle ($\hat{r}$) and the energy ($E = p^2/2m_r$). The angular dependence of $f(E,\hat{r})$ enters

since the incident wave $\psi_0(\mathbf{r})$ usually has a certain angular dependence. For instance, if the incident wave is a plane wave, the scattering amplitude depends only on the angle between the incident wave and $\mathbf{r}$, as well as the energy of the incident wave. Notice that it makes sense to talk about the scattering amplitude only at places far enough away from the potential so that the wavefunction can be written as a product of the radial part and the angular part. In other words, the notion of scattering amplitude is only defined asymptotically. The scattering amplitude can be conveniently written in terms of a quantity called *phase shift*, which is the topic of the next section.

By taking the incoming wave to be a plane wave with momentum $\mathbf{p}$ and writing $\mathbf{p} = p\hat{r}$, we can see the relation between the scattering amplitude and the t-matrix:

$$f(E,\hat{r}) = -\frac{m_r}{2\pi}\int d^3r' e^{-i\mathbf{p}'\cdot\mathbf{r}'}\mathcal{V}(\mathbf{r}')\Psi_{\mathbf{p}}(\mathbf{r}') = -\frac{m_r}{2\pi}T(\mathbf{p}',\mathbf{p}). \tag{A.46}$$

The differential cross section is the number of scattered particles per unit time in a unit solid angle divided by the number of particles in the incident beam per unit time per unit area. The number of scattered particles per unit time in a solid angle $d\Omega$ in the direction of $\hat{r}$ is given by

$$\frac{p}{m_r}\cdot\left|f(E,\hat{r})\frac{e^{i\sqrt{2m_rE}r}}{r}\right|^2 r^2 d\Omega = \frac{p}{m_r}\left|f(E,\hat{r})\right|^2 d\Omega. \tag{A.47}$$

On the other hand, the number of particles in the incident beam per unit time per unit area is p/m_r. Therefore, the differential cross section is simply

$$\frac{d\sigma}{d\Omega} = \left|f(E,\Omega_r)\right|^2, \tag{A.48}$$

and the total cross section is

$$\sigma = \int d\Omega \left|f(E,\Omega_r)\right|^2. \tag{A.49}$$

The differential cross section is a measurable quantity, and therefore the absolute value of the scattering amplitude is also a measurable quantity.

A.3.2 Two dimensions

We now turn to the problem of two dimensional scattering. From (A.13) we see that the Green's function in two spatial dimensions is

$$\begin{aligned} G^{(2)}_{\pm}(\mathbf{r}-\mathbf{r}') &= \int \frac{d^2k}{(2\pi)^2}\frac{1}{E-k^2/2m_r \pm i\epsilon}e^{i\mathbf{k}\cdot(\mathbf{r}-\mathbf{r}')} \\ &= \int_0^\infty \frac{dk}{2\pi}\int_0^{2\pi}\frac{d\theta}{2\pi}\frac{k}{E-k^2/2m_r\pm i\epsilon}e^{ik|\mathbf{r}-\mathbf{r}'|\cos\theta}. \end{aligned} \tag{A.50}$$

In terms of the Bessel function of the first kind, which has an integral representation

$$J_0(r) = \int_0^{2\pi} \frac{d\theta}{2\pi} e^{ir\cos\theta}, \tag{A.51}$$

we can rewrite the Green's function in the following way:

$$\begin{aligned} G_{\pm}^{(2)}(\mathbf{r}-\mathbf{r}') &= \int_0^{\infty} \frac{dk}{2\pi} \frac{k}{E - k^2/2m_r \pm i\epsilon} J_0(k|\mathbf{r}-\mathbf{r}'|) \\ &= -2m_r \int_0^{\infty} \frac{dk}{2\pi} \frac{k}{k^2 - (E \pm i\epsilon)} J_0(k|\mathbf{r}-\mathbf{r}'|). \end{aligned} \tag{A.52}$$

Using the following relation between the Bessel function and the Hankel function of the first kind $H_0^{(1)}$:

$$\int_0^{\infty} \frac{x}{x^2 - a} J_0(bx) = \begin{cases} i\frac{\pi}{2} H_0^{(1)}(\sqrt{a}b) & \text{if } \mathrm{Im}(a) > 0 \\ \\ i\frac{\pi}{2} H_0^{(1)}(-\sqrt{a}b) & \text{if } \mathrm{Im}(a) < 0 \end{cases}, \tag{A.53}$$

which is true for $b > 0$, we can write the two dimensional Green's function in the following form:

$$G_{\pm}^{(2)}(\mathbf{r}-\mathbf{r}') = -\frac{im_r}{2} H_0^{(1)}(\pm\sqrt{2m_r E}|\mathbf{r}-\mathbf{r}'|). \tag{A.54}$$

Using the far-field asymptotic behavior of the Hankel function of the first kind

$$H_0^{(1)}(x) \sim \sqrt{\frac{2}{\pi x}} e^{ix - i\pi/4}, \tag{A.55}$$

the Green's function has the asymptotic behavior

$$\begin{aligned} G^{(2)}(\mathbf{r}-\mathbf{r}') &\sim -\frac{im_r}{2} \sqrt{\frac{2}{\pm\pi\sqrt{2m_r E}|\mathbf{r}-\mathbf{r}'|}} e^{\pm i\sqrt{2m_r E}|\mathbf{r}-\mathbf{r}'| - i\pi/4} \\ &= -m\sqrt{\frac{\pm i}{2\pi}} \frac{e^{\pm ip|\mathbf{r}-\mathbf{r}'|}}{\sqrt{p|\mathbf{r}-\mathbf{r}'|}}. \end{aligned} \tag{A.56}$$

As in three dimensional scattering, the plus and minus signs correspond to outgoing and incoming waves, respectively. Taking the outgoing Green's function, the wavefunction has the asymptotic form:

$$\begin{aligned} \Psi(\mathbf{r}) &\sim \psi_0(\mathbf{r}) - m_r \int d^2r' \sqrt{\frac{i}{2\pi}} \frac{e^{ip|\mathbf{r}-\mathbf{r}'|}}{\sqrt{p|\mathbf{r}-\mathbf{r}'|}} \mathcal{V}(\mathbf{r}')\Psi(\mathbf{r}') \\ &= \psi_0(\mathbf{r}) - m_r \sqrt{\frac{i}{2\pi p}} \frac{e^{ipr}}{\sqrt{r}} \int d^2r' e^{-ip\hat{r}\cdot\mathbf{r}'} \mathcal{V}(\mathbf{r}')\Psi(\mathbf{r}') \\ &= \psi_0(\mathbf{r}) + f(E,\hat{r}) \sqrt{\frac{i}{r}} e^{ipr}, \end{aligned} \tag{A.57}$$

where the scattering amplitude in two dimensions is defined by

$$f(E,\hat{r}) = -m_r\sqrt{\frac{1}{2\pi p}}\int d^2r' e^{-ip\hat{r}\cdot\mathbf{r}'}\mathcal{V}(\mathbf{r}')\Psi(\mathbf{r}'). \tag{A.58}$$

Note that while some authors include the factor of $\sqrt{i}$ in the definition of the scattering amplitude, here we follow the notation of the Landau and Lifshitz [152]. In deriving this expression, we used the asymptotic form of the Hankel function, which is only valid when pr is large. We can, of course, always define the scattering amplitude by (A.58), but the expression (A.57) is not valid in the low energy limit $p \to 0$. Thus, the physical meaning of the scattering amplitude as the asymptotic amplitude of the wavefunction is not valid in the low energy limit, which is a characteristic feature of scattering in two dimensions.

Setting $\mathbf{p}' = p\hat{r}$ and assuming that the incoming wave is a plane wave with momentum $\mathbf{p}$, a comparison of (A.17) and (A.58) shows that the scattering amplitude and the t-matrix are related by

$$f(E,\hat{r}) = -m_r\sqrt{\frac{1}{2\pi p}}T(\mathbf{p},\mathbf{p}'). \tag{A.59}$$

The differential cross section is

$$\frac{d\sigma}{d\theta} = \left|f(E,\hat{\theta}_r)\right|^2, \tag{A.60}$$

where $\hat{\theta}_r$ is a unit vector in the direction of the planer angle $d\theta$. The total cross section is

$$\sigma = \int d\theta \left|f(E,\hat{\theta}_r)\right|^2. \tag{A.61}$$

The expressions for the differential and total cross sections are analogous to the expressions for three dimensions; solid angles are replaced by planar angles and everything else stays the same.

A.3.3 One dimension

Although this chapter is mainly concerned with on three and two dimensional scattering, we briefly mention the scattering amplitude in one dimension.

The Green's function in one spatial dimension is

$$G^{(1)}(r-r') = \int_{-\infty}^{\infty}\frac{dk}{2\pi}\frac{1}{E-k^2/2m_r \pm i\epsilon}e^{ik(r-r')} = \mp m_r i\frac{e^{\pm i\sqrt{2m_rE}|r-r'|}}{\sqrt{2m_rE}} = \mp m_r i\frac{e^{\pm ip|r-r'|}}{p}. \tag{A.62}$$

As before, the different signs in $\pm i\epsilon$ correspond to the outgoing and the incoming waves. Taking the outgoing wave, the wavefunction satisfies

$$\Psi(r) = \psi_0(r) - m_r i \int_{-\infty}^{\infty} dr' \frac{e^{ip|r-r'|}}{p} \mathcal{V}(r')\Psi(r'), \tag{A.63}$$

and asymptotically

$$\begin{aligned}\Psi(r) &\sim \psi_0(\mathbf{r}) - m_r i e^{ipr} \int_{-\infty}^{\infty} dr' \frac{e^{iprr'/|r|}}{p} \mathcal{V}(r')\Psi(r') \\ &= \psi_0(\mathbf{r}) + f(E, r/|r|)e^{ipr},\end{aligned} \tag{A.64}$$

where the scattering amplitude in one dimension is defined by

$$f(E, r/|r|) = -m_r i \int_{-\infty}^{\infty} dr' \frac{e^{iprr'/|r|}}{p} \mathcal{V}(r')\Psi(r'). \tag{A.65}$$

Notice that the scattering wavefunction in one dimension does not fall off far away from the target, which is a crucial difference compared to the two or three dimensional case.

A.4 Phase shift and scattering lengths

We have seen the integral equations that determine the scattering wavefunction in three-, two-, and one-dimensions through the Green's functions. Far away from the target, the wavefunctions may be written as the product of a distance -dependent part and an angle-dependent part. The angle dependent part is called the scattering amplitude. In this section, we focus on the properties of the scattering amplitude and introduce the concept of the phase shift which is useful in understanding the physical meaning of the scattering amplitude.

The phase shift is essentially the shift of the phase of the outgoing wave relative to the incoming wave when the scattering wavefunction is expanded in terms of its angular components. In three dimensions, the angular decomposition corresponds to an expansion in terms of the spherical harmonic functions, while in two dimensions, it is in terms of the factors $e^{il\phi}$. In one dimension, the expansion is in the left and right moving waves.

We begin by noting that an incident plane wave may be decomposed into its spherical components as

$$e^{i\mathbf{p}\cdot\mathbf{r}} = e^{ipr\cos\theta} = \sum_{l=0}^{\infty} i^l(2l+1)P_l(\cos\theta)j_l(pr) = \sum_{l=0}^{\infty} i^l(2l+1)P_l(\cos\theta)\frac{h_l(pr) + h_l^*(pr)}{2}, \tag{A.66}$$

where θ is the angle between $\mathbf{p}$ and $\mathbf{r}$, and $P_l(x)$ is the Legendre polynomial. $j_l(x)$ is the spherical Bessel function, and $h_l(x)$ is the spherical Hankel function. Since this incoming wave does not have an angular momentum in the direction of $\mathbf{p}$, the outgoing scattered wavefunction also does not have an angular momentum in the $\mathbf{p}$ direction, thus we can also expand the outgoing scattered wavefunction in terms of Legendre polynomials. Although this expansion is correct in both three dimensions and two dimensions, it is more relevant to use the following expansion in two dimensions:

$$e^{i\mathbf{p}\cdot\mathbf{r}} = e^{ipr\cos\theta} = \sum_{l=-\infty}^{\infty} i^l e^{il\theta} J_l(pr) = \sum_{l=-\infty}^{\infty} i^l e^{il\theta} \frac{H_l(pr) + H_l^*(pr)}{2}, \tag{A.67}$$

where $J_l(pr)$ is the Bessel function of the first kind, and $H_l(pr)$ is the Hankel function of the first kind[3].

When we are far away from the potential, the Schrödinger equation is that of a free particle. In spherical coordinates, the Schrödinger equation reads

$$-\frac{1}{2m_r}\left[\frac{1}{r}\frac{\partial^2}{\partial r^2}r + \frac{1}{r^2\sin\theta}\frac{\partial}{\partial\theta}\left(\sin\theta\frac{\partial}{\partial\theta}\right) + \frac{1}{r^2\sin^2\theta}\frac{\partial^2}{\partial\phi^2}\right]\Psi^{(3)}(\mathbf{r}) = E\Psi^{(3)}(\mathbf{r}) \tag{A.68}$$

in three dimensions and

$$-\frac{1}{2m_r}\left[\frac{1}{r}\frac{\partial}{\partial r}\left(r\frac{\partial}{\partial r}\right) + \frac{1}{r^2}\frac{\partial^2}{\partial\theta^2}\right]\Psi^{(2)}(\mathbf{r}) = E\Psi^{(2)}(\mathbf{r}) \tag{A.69}$$

in two dimensions.

A.4.1 Three dimensions

In three dimensions, we can expand the wavefunction with zero angular momentum in the direction of the incident wave as

$$\Psi^{(3)}(\mathbf{r}) = \sum_{l=0}^{\infty} i^l(2l+1)P_l(\cos\theta)R_l(r), \tag{A.70}$$

where θ is the direction between $\mathbf{r}$ and the direction of the incident wave. The Schrödinger equation then becomes

$$-\frac{1}{2m_r}\left(\frac{d^2}{dr^2} - \frac{l(l+1)}{r^2}\right)rR_l(r) = ErR_l(r). \tag{A.71}$$

[3] Note that in section A.3.2, the Hankel function of the first kind was denoted $H_l^{(1)}$. Henceforth, since there will be no ambiguity, we will omit the superscript.

In terms of $p = \sqrt{2m_r E}$, this equation is

$$\left(\frac{d^2}{dr^2} + p^2 - \frac{l(l+1)}{r^2}\right) rR_l(r) = 0. \tag{A.72}$$

Solutions to this equation are spherical Bessel functions $j_l(pr)$and spherical Neumann functions $n_l(pr)$. Equivalently, through the relation $h_l(x) = j_l(x) + in_l(x)$, the solutions may be written in terms of spherical Hankel functions $h_l(x)$ and their complex conjugates $h_l^*(x)$. Thus, we can write

$$R_l(r) = Ah_l(pr) + Bh_l^*(pr). \tag{A.73}$$

Since the spherical Hankel function has the following asymptotic form as $r \to \infty$

$$h_l(pr) \sim \frac{e^{i(pr - l\pi/2)}}{ipr}, \tag{A.74}$$

we see that $h_l(pr)$ is an outgoing wave and $h_l^*(pr)$ is an incoming wave[4]. Since the potential is neither a source nor a sink of particles, the radial component of the probability current should vanish, namely

$$j_r(r) = \frac{1}{2im_r}\left(R_l^*(r)\frac{\partial}{\partial r}R_l(r) - R_l(r)\frac{\partial}{\partial r}R_l^*(r)\right) = 0. \tag{A.75}$$

Using (A.73), this vanishing condition leads to the constraint

$$j_r(r) = \left(|A|^2 - |B|^2\right)\left(h_l^*(pr)\frac{\partial}{\partial r}h_l(pr) - c.c.\right) = 0. \tag{A.76}$$

For this to be true for any r, we need

$$|A|^2 = |B|^2, \tag{A.77}$$

which is a reasonable result if we want the incoming and the outgoing wave to carry the same number of particles.

Since we are considering a situation in which the incoming wave is a plane wave and the outgoing wave is a scattered wave, the coefficient B of the incoming wave should match that of a plane wave. Looking back at the equation (A.66), we can see that $B = 1/2$. Now, we can write the whole scattering wavefunction as

$$\Psi^{(3)}(\mathbf{r}) = \sum_{l=0}^{\infty} i^l(2l+1)P_l(\cos\theta)\frac{h_l^*(pr) + S_l(p)h_l(pr)}{2}, \tag{A.78}$$

[4] For $l = 0$, $h_0(pr) = e^{ipr}/ipr$.

with a coefficient $S_l(p)$ which depends on the angular momentum and the energy. From (A.77), we know that the coefficients of $h_l(pr)$ and $h_l^*(pr)$ should have the same magnitude, which implies that $|S_l(p)| = 1$. Thus, we can parametrize $S_l(p)$ by a real function $\delta_l(p)$ via

$$S_l(p) = e^{2i\delta_l(p)}. \tag{A.79}$$

The quantity $\delta_l(p)$ is known as the *phase shift* and it is the difference in the phase of the outgoing wave and the incoming plane wave. Notice that if there is no scattering then $S_l(p) = 1$, which is equivalent to $\delta_l(p) = 0$ (no phase shift). Explicitly pulling the plane wave out of the wavefunction, we can write

$$\Psi^{(3)}(\mathbf{r}) = e^{i\mathbf{p}\cdot\mathbf{r}} + \sum_{l=0}^{\infty} i^l(2l+1)P_l(\cos\theta)\frac{\left(e^{2i\delta_l(p)}-1\right)h_l(pr)}{2}. \tag{A.80}$$

Asymptotically this becomes

$$\Psi^{(3)}(\mathbf{r}) \sim e^{i\mathbf{p}\cdot\mathbf{r}} + \sum_{l=0}^{\infty} i^l(2l+1)P_l(\cos\theta)\frac{\left(e^{2i\delta_l(p)}-1\right)}{2}\frac{e^{i(pr-l\pi/2)}}{ipr}. \tag{A.81}$$

Comparing with (A.44) the scattering amplitude can be expressed in terms of the phase shift by writing

$$\begin{aligned} f(p,\theta) &= \sum_{l=0}^{\infty} i^l(2l+1)P_l(\cos\theta)\frac{\left(e^{2i\delta_l(p)}-1\right)}{2}\frac{e^{-il\pi/2}}{ip} \\ &= \sum_{l=0}^{\infty}(2l+1)P_l(\cos\theta)\frac{e^{2i\delta_l(p)}-1}{2ip} \\ &= \sum_{l=0}^{\infty}(2l+1)P_l(\cos\theta)\frac{e^{i\delta_l(p)}\sin\delta_l(p)}{p} \\ &= \sum_{l=0}^{\infty}(2l+1)P_l(\cos\theta)\frac{1}{p}\cdot\frac{1}{\cot\delta_l(p)-i}. \end{aligned} \tag{A.82}$$

Obtaining the scattering wavefunction has been reduced to calculating the phase shifts of the partial waves. One major reason that we have decomposed the wavefunction into its angular components is that, in the low energy limit (which is usually the region of interest in ultracold atomic physics), we can ignore the contributions from the partial waves with $l \geq 1$ and concentrate on $l = 0$, i.e., s-wave scattering. For a proof that s-wave scattering is dominant at low energy, see Baym [153].

At this point, we can prove the optical theorem which relates the imaginary part of the scattering

amplitude and the total cross section. The total cross section is

$$\begin{aligned}\sigma &= 2\pi \int_{-1}^{1} d(\cos\theta)|f(p,\theta)|^2 \\ &= 2\pi \int_{-1}^{1} d(\cos\theta) \sum_{l,l'=0}^{\infty} (2l+1)(2l'+1)P_l(\cos\theta)P_{l'}(\cos\theta)\frac{e^{i\delta_l(p)-i\delta_{l'}(p)}\sin\delta_l(p)\sin\delta_{l'}(p)}{p^2}. \end{aligned} \quad \text{(A.83)}$$

Using the identity

$$\int_{-1}^{1} d(\cos\theta)P_l(\cos\theta)P_{l'}(\cos\theta) = \frac{2}{2l+1}\delta_{ll'} \quad \text{(A.84)}$$

and noticing that $P_l(1) = 1$ for any l, we have

$$\sigma = 4\pi \sum_{l=0}^{\infty}(2l+1)\frac{\sin^2\delta_l(p)}{p^2} = \frac{4\pi}{p}\mathrm{Im}f(p,\theta=0), \quad \text{(A.85)}$$

where the second equality follows from (A.82). This relation is called the *optical theorem*.

For later use, we derive here the asymptotic form of a wavefunction in the low energy. When the energy is low enough so that we can ignore the components with $l \geq 1$, the wavefunction is

$$\Psi^{(3)}_{l=0}(\mathbf{r}) = \frac{h_0^*(pr) + e^{2i\delta_0(p)}h_0(pr)}{2} = \frac{1}{2pr}\left(ie^{-ipr} - ie^{2i\delta_0(p)}e^{ipr}\right) = e^{i\delta_0(p)}\frac{\sin(pr+\delta_0(p))}{pr}. \quad \text{(A.86)}$$

Note that the wavefunction only depends on the distance r, and independent of the angle. It is not hard to confirm that when there is no potential the wavefunction is $\sin(pr)/pr$. Thus the phase shift $\delta_0(p)$ is indeed the phase shift from the wavefunction in the absence of a potential.

Now we are ready to define the scattering length. The *scattering length* is defined as the distance at which the wavefunction $\Psi(\mathbf{r})$ becomes zero when $E = 0$. In other words, the scattering length a satisfies

$$\Psi(a) = 0 \quad \text{(A.87)}$$

for $E \to 0$. As mentioned earlier, at low energy, only s-wave contributes and can neglect direction in defining the scattering length. Taking only the s-wave component, the wavefunction at low energy outside the range of the potential is

$$\Psi^{(3)}(r) = \frac{\sin(pr)}{pr} + \frac{1}{\cot\delta_0(p) - i}\frac{e^{ipr}}{pr}, \quad \text{(A.88)}$$

where the first term is the s-wave component of a plane wave, and the second term is an outgoing scattered wave. As $p \to 0$, the wavefunction becomes

$$\lim_{p\to 0} \Psi^{(3)}(r) = 1 + \lim_{p\to 0} \frac{1}{pr\cot\delta_0(p)}. \tag{A.89}$$

From the definition of the scattering length a,

$$\lim_{p\to 0} \Psi^{(3)}(a) = 1 + \frac{1}{a}\lim_{p\to 0} \frac{1}{p\cot\delta_0(p)} = 0, \tag{A.90}$$

so that we obtain

$$\lim_{p\to 0} p\cot\delta_0(p) = -\frac{1}{a}. \tag{A.91}$$

This equation is often used as the definition of the scattering length.

In terms of the scattering length, the scattering amplitude in the low energy limit is

$$f(p,\theta) \sim \frac{1}{p}\cdot\frac{1}{\cot\delta_0(p) - i} \sim -a. \tag{A.92}$$

A useful relation to keep in mind which follows from this relation is, in the low energy limit, the wavefunction becomes

$$\Psi^{(3)}(\mathbf{r}) \sim 1 - \frac{a}{r}. \tag{A.93}$$

also we find that at low energy, the differential cross section is

$$\frac{d\sigma}{d\Omega} = \lim_{p\to 0} |f(p,\theta)|^2 = a^2, \tag{A.94}$$

and the total cross section is

$$\sigma = 4\pi a^2. \tag{A.95}$$

Finally, from the relation (A.46), we can see that in the low energy limit the t-matrix becomes

$$T(0,0) = \frac{2\pi a}{m_r} = \frac{4\pi a}{m}. \tag{A.96}$$

A.4.2 Two dimensions

In two dimensions, the wavefunction outside the range of potential can be written as

$$\Psi^{(2)}(\mathbf{r}) = \sum_{l=-\infty}^{\infty} i^l R_l(r) e^{il\theta}, \tag{A.97}$$

and the radial wavefunction $R_l(r)$ obeys

$$-\frac{1}{2m}\left[\frac{1}{r}\frac{d}{dr}\left(r\frac{d}{dr}\right) - \frac{l^2}{r^2}\right] R_l(r) = E R_l(r), \tag{A.98}$$

which is equivalent to

$$\left(\frac{d^2}{dr^2} + \frac{1}{r}\frac{d}{dr} + p^2 - \frac{l^2}{r^2}\right) R_l(r) = 0. \tag{A.99}$$

The solutions are the Bessel functions of the first $J_l(pr)$ and the second kind $N_l(pr)$, or equivalently the Hankel function of the first kind $H_l(pr) = J_l(pr) + iN_l(pr)$ and its complex conjugate. The solution is generally

$$R_l(r) = AH_l(pr) + BH_l^*(pr). \tag{A.100}$$

The Hankel function of the first kind has the following asymptotic behavior at large r:

$$H_l(pr) \sim \sqrt{\frac{2}{\pi pr}} e^{i(pr-(2l+1)\pi/4)}, \tag{A.101}$$

thus $H_l(pr)$ is an outgoing wave and $H_l(pr)$ is an incoming wave. Since we want the incoming wave to be a plane wave, comparing with (A.67), we can see that $B = 1/2$. The discussion of the vanishing of probability current in three dimensions holds exactly the same for two dimensions, and the condition implies $|A| = |B| = 1/2$. Now we can define the phase shift in two dimensions analogously to three dimensions by $A = e^{2i\delta_l(p)}/2$.

With this definition of δ_l, the overall wavefunction becomes

$$\Psi^{(2)}(\mathbf{r}) = \sum_{l=-\infty}^{\infty} i^l e^{il\theta} \frac{H_l^*(pr) + e^{2i\delta_l(p)} H_l(pr)}{2}. \tag{A.102}$$

Pulling out the incoming plane wave yields

$$\Psi^{(2)}(\mathbf{r}) = e^{i\mathbf{p}\cdot\mathbf{r}} + \sum_{l=-\infty}^{\infty} i^l e^{il\theta} \frac{e^{2i\delta_l(p)} - 1}{2} H_l(pr). \tag{A.103}$$

Using the asymptotic form of the Hankel function, the asymptotic form of the wavefunction is

$$\Psi^{(2)}(\mathbf{r}) \sim e^{i\mathbf{p}\cdot\mathbf{r}} + \sum_{l=-\infty}^{\infty} i^l e^{il\theta} \frac{e^{2i\delta_l(p)}-1}{2} e^{-i(2l+1)\pi/4} \sqrt{\frac{2}{\pi pr}} e^{ipr}, \tag{A.104}$$

and the scattering amplitude is

$$\begin{aligned} f(p,\theta) &= \sum_{l=-\infty}^{\infty} i^l e^{il\theta} \frac{e^{2i\delta_l(p)}-1}{2} e^{-i(2l+1)\pi/4} \sqrt{\frac{2}{i\pi p}} = \sum_{l=-\infty}^{\infty} e^{il\theta} \sqrt{\frac{2}{\pi p}} \cdot \frac{e^{2i\delta_l(p)}-1}{2i} \\ &= \sum_{l=-\infty}^{\infty} e^{il\theta} \sqrt{\frac{2}{\pi p}} \cdot e^{i\delta_l(p)} \sin\delta_l(p) = \sum_{l=-\infty}^{\infty} e^{il\theta} \sqrt{\frac{2}{\pi p}} \cdot \frac{1}{\cot\delta_l(p) - i}. \end{aligned} \tag{A.105}$$

Just as in three dimensions, in the low energy limit, one can show that the scattering with $l = 0$ is dominant.

Analogously to the three dimensional case, we can prove the optical theorem which relates the total cross section and the imaginary part of the scattering amplitude. The total cross section and the scattering amplitude are related by

$$\begin{aligned} \sigma &= \int_0^{2\pi} d\theta |f(p,\theta)|^2 \\ &= \int_0^{2\pi} d\theta \sum_{l,l'=-\infty}^{\infty} e^{i(l-l')\theta} \frac{2}{\pi p} \cdot e^{i\delta_l(p) - i\delta_{l'}(p)} \sin\delta_l(p) \sin\delta_{l'}(p) \\ &= 2\pi \sum_{l=-\infty}^{\infty} \frac{2}{\pi p} \cdot \sin^2\delta_l(p) \\ &= 2\pi \sqrt{\frac{2}{\pi p}} \mathrm{Im} f(p,\theta=0). \end{aligned} \tag{A.106}$$

Thus, the two dimensional version of the optical theorem can be stated as

$$\mathrm{Im} f(p,\theta=0) = \sqrt{\frac{p}{8\pi}}\sigma. \tag{A.107}$$

The wavefunction with $l = 0$, without any assumptions on pr is

$$\begin{aligned} \Psi^{(2)}_{l=0}(r) &= J_0(pr) + \frac{e^{2i\delta_0(p)}-1}{2} H_0(pr) = e^{i\delta_0(p)} \left(e^{-i\delta_0(p)} J_0(pr) + \frac{e^{i\delta_0(p)} - e^{-i\delta_0(p)}}{2} H_0(pr) \right) \\ &= e^{i\delta_0(p)} \left((\cos\delta_0(p) - i\sin\delta_0(p) J_0(pr) + i\sin\delta_0(p)(J_0(pr) + iN_0(pr)) \right) \\ &= e^{i\delta_0(p)} \left(\cos\delta_0(p) J_0(pr) - \sin\delta_0(p) N_0(pr) \right). \end{aligned} \tag{A.108}$$

Now, assuming $pr \gg 1$ we obtain

$$\begin{aligned}\Psi^{(2)}_{l=0}(r) &\sim e^{i\delta_0(p)}\sqrt{\frac{2}{\pi pr}}\left(\cos\delta_0(p)\cos\left(pr-\frac{\pi}{4}\right)-\sin\delta_0(p)\sin\left(pr-\frac{\pi}{4}\right)\right)\\ &= e^{i\delta_0(p)}\sqrt{\frac{2}{\pi pr}}\cos\left(pr-\frac{\pi}{4}+\delta_0(p)\right).\end{aligned} \tag{A.109}$$

The physical meaning of $\delta_0(p)$ is apparent now; the phase shift is clearly a phase shift.

Let us now define the scattering length in two dimensions as the distance at which the asymptotic wavefunction becomes zero in the zero energy limit, i.e.,

$$\Psi^{(2)}(a) = 0 \tag{A.110}$$

with $E = 0$. We remarked earlier that the scattering amplitude is not well defined in two dimensions, but we can still talk about the wavefunction itself in the low energy limit; thus, the definition of the scattering length has no ambiguity. Evaluating (A.108) at $r = a$, we obtain,

$$\begin{aligned}\Psi^{(2)}_{l=0}(a) &= e^{i\delta_0(p)}\left(\cos\delta_0(p)J_0(pa)-\sin\delta_0(p)N_0(pa)\right)\\ &= e^{i\delta_0(p)}\cos\delta_0(p)\left(J_0(pa)-\tan\delta_0(p)N_0(pa)\right)\\ &= 0.\end{aligned} \tag{A.111}$$

Therefore,

$$\tan\delta_0(p) = \frac{J_0(pa)}{N_0(pa)}. \tag{A.112}$$

In the low energy limit this becomes

$$\lim_{p\to 0}\tan\delta_0(p) = \frac{1+\mathcal{O}(p)}{\frac{2}{\pi}\left(\ln\frac{pa}{2}+\gamma\right)+\mathcal{O}(p)} = \frac{\pi}{2}\cdot\frac{1+\mathcal{O}(p)}{\ln(pa/2)+\gamma}, \tag{A.113}$$

where γ is the Euler-Mascheroni constant. Comparing with the three dimensional result $\tan\delta_0(p) = -ap+\mathcal{O}(p^2)$, we see a different low energy behavior of the phase shift.

From (A.105), the scattering amplitude for $l = 0$ is

$$f(p,\theta) = \sqrt{\frac{2}{\pi p}}\cdot\frac{1}{\cot\delta_0(p)-i}, \tag{A.114}$$

the differential cross section at low energy is

$$\frac{d\sigma}{d\theta} = |f(p,\theta)|^2 = \frac{2}{\pi p}\left|\frac{1}{\cot\delta_0(p)-i}\right|^2 \tag{A.115}$$

Since we have used the asymptotic form of $H_0(pr)$ to derive this result, the relation is only valid when $pr \gg 1$, but the energy is small enough so that the scattering with $l \geq 1$ can be neglected. Using (A.113), the low energy limit of the differential cross section, while keeping $pr \gg 1$, is

$$\frac{d\sigma}{d\theta} = \lim_{p\to 0} \frac{2}{\pi p} \left| \frac{1}{\cot \delta_0(p) - i} \right|^2 = \lim_{p\to 0} \frac{\pi}{2} \frac{1}{p(\ln(pa/2))^2} = \infty. \tag{A.116}$$

Thus, the differential cross section and hence the total cross section tend to diverge in the low energy limit in two dimensions.

When only s-wave scattering is significant, the t-matrix is, from (A.59),

$$T(\mathbf{p}, \mathbf{p}') = -\frac{1}{m_r} \sqrt{2\pi p} f(p, \theta) = -\frac{2}{m_r} \frac{1}{\cot \delta_0(p) - i}. \tag{A.117}$$

In the low energy limit, it is tempting to conclude that

$$\lim_{p,p'\to 0} T(\mathbf{p}, \mathbf{p}') = -\lim_{p\to 0} \frac{2}{m_r} \frac{\pi}{2} \cdot \frac{1}{\ln(pa/2) + \gamma} = 0, \tag{A.118}$$

thus the t-matrix vanishes in the low energy limit in two dimensions. However, this argument is spurious, since the expression (A.59) is not correct in the low energy limit. Although the scattering amplitude is not well defined in two dimensions in the low energy limit unless we keep $pr \gg 1$, the scattering t-matrix is defined for any energy. Thus, deriving any general conclusions regarding the low energy behavior of the two dimensional t-matrix is difficult. In the next section, we consider a specific type of potential (a square well), and we compute the t-matrix explicitly to determine the correct low energy behavior.

A.5 Example: a square well potential

So far, the arguments presented have been quite general and valid for any potential which falls off sufficiently quickly in the far-field[5]. The differential cross section, which is measurable, has been written in terms of the scattering amplitude, which in turn has been written in terms of the phase shifts. To calculate the phase shifts, we need to consider a specific potential. In this section, we consider a spherically symmetric square well potential,

$$\mathcal{V}(r) = \begin{cases} -V_0 & \text{for } r < r_0 \\ 0 & \text{for } r > r_0 \end{cases}, \tag{A.119}$$

and explicitly calculate the low energy scattering properties.

[5] Note that the Coulomb potential is one prominent example of a potential which *does not* satisfy this condition.

A.5.1 Three dimensions

In three dimensions, the radial Schrödinger equation is

$$-\frac{1}{2m_r}\left(\frac{d^2}{dr^2}-\frac{l(l+1)}{r^2}\right)rR_l(r)+\mathcal{V}(r)rR_l(r)=ErR_l(r). \tag{A.120}$$

Since the $l=0$ (s-wave) component dominates at low energy, we take $l=0$, and thereby obtain

$$\left(\frac{d^2}{dr^2}+p^2-2m_r\mathcal{V}(r)\right)rR_0(r)=0, \tag{A.121}$$

where $p=\sqrt{2m_rE}$. At $r<r_0$, the general solution to this differential equation is

$$R_0(r)_{r<r_0}=\frac{A}{pr}\sin\left(\sqrt{p^2+2m_rV_0}\cdot r\right)+\frac{B}{pr}\cos\left(\sqrt{p^2+2m_rV_0}\cdot r\right), \tag{A.122}$$

and at $r>r_0$,

$$R_0(r)_{r>r_0}=\frac{C}{pr}\sin\left(pr\right)+\frac{D}{pr}\cos\left(pr\right), \tag{A.123}$$

where constants A, B, C, and D are to be determined via boundary conditions. Since the wavefunction should be analytic at the origin, we can immediately conclude $B=0$. Remembering (A.86), the wavefunction at $r>r_0$ can be rewritten as

$$R_0(r)_{r>r_0}=\frac{C'}{pr}\sin\left(pr+\delta_0(p)\right). \tag{A.124}$$

If we follow our previous notation, $C'=e^{i\delta_0(p)}$, but since the overall phase of the wavefunction is irrelevant, we can set $C'=1$. Thus the radial wavefunction is

$$R_0(r)=\begin{cases}\dfrac{A}{pr}\sin\left(\sqrt{p^2+2m_rV_0}\cdot r\right) & \text{for } r<r_0\\[2ex] \dfrac{1}{pr}\sin\left(pr+\delta_0(p)\right) & \text{for } r>r_0.\end{cases} \tag{A.125}$$

The wavefunction should connect smoothly at $r=r_0$. Matching the logarithmic derivative at $r=r_0$, we obtain the condition

$$\sqrt{p^2+2m_rV_0}\frac{\cos(\sqrt{p^2+2m_rV_0}\cdot r_0)}{\sin(\sqrt{p^2+2m_rV_0}\cdot r_0)}=p\frac{\cos(pr_0+\delta_0(p))}{\sin(pr_0+\delta_0(p))}. \tag{A.126}$$

It is useful to transform the right hand side into the form

$$\sqrt{p^2+2m_rV_0}\frac{\cos(\sqrt{p^2+2m_rV_0}\cdot r_0)}{\sin(\sqrt{p^2+2m_rV_0}\cdot r_0)}=p\frac{\cos(pr_0)\cos\delta_0(p)-\sin(pr_0)\sin\delta_0(p)}{\sin(pr_0)\cos\delta_0(p)+\cos(pr_0)\sin\delta_0(p)}. \tag{A.127}$$

Solving for $\tan\delta_0(p)$, we obtain

$$\tan\delta_0(p) = -\frac{\sqrt{p^2+2m_rV_0}\frac{\cos(\sqrt{p^2+2m_rV_0}\cdot r_0)}{\sin(\sqrt{p^2+2m_rV_0}\cdot r_0)}\sin(pr_0) - p\cos(pr_0)}{\sqrt{p^2+2m_rV_0}\frac{\cos(\sqrt{p^2+2m_rV_0}\cdot r_0)}{\sin(\sqrt{p^2+2m_rV_0}\cdot r_0)}\cos(pr_0) + p\sin(pr_0)}. \tag{A.128}$$

The scattering amplitude is then

$$f(p,\theta) = \frac{1}{p}\cdot\frac{1}{\cot\delta_0(p) - i} = \frac{\tan\delta_0(p)}{p}\cdot\frac{1}{1 - i\tan\delta_0(p)}. \tag{A.129}$$

In the low energy limit, the phase shift becomes

$$\lim_{p\to 0}\tan\delta_0(p) = -\frac{\sqrt{2m_rV_0}\cot(\sqrt{2m_rV_0}\cdot r_0)(pr_0) - p}{\sqrt{2m_rV_0}\cot(\sqrt{2m_rV_0}\cdot r_0)} = -pr_0\left(1 - \frac{\tan(\sqrt{2m_rV_0}\cdot r_0)}{\sqrt{2m_rV_0}\cdot r_0}\right), \tag{A.130}$$

and the scattering length is

$$a = r_0\left(1 - \frac{\tan(\sqrt{2m_rV_0}\cdot r_0)}{\sqrt{2m_rV_0}\cdot r_0}\right). \tag{A.131}$$

The t-matrix is

$$\begin{aligned}
T(\mathbf{k},\mathbf{p}) &= \int d^3r e^{-i\mathbf{k}\cdot\mathbf{r}}\mathcal{V}(\mathbf{r})\Psi_{\mathbf{p}}(\mathbf{r}) \\
&= -2\pi V_0\int_0^{r_0} dr r^2\int_{-1}^{1} d(\cos\theta)e^{-ikr\cos\theta}\frac{A}{pr}\sin\left(\sqrt{p^2+2m_rV_0}\cdot r\right) \\
&= -2\pi V_0\int_0^{r_0} dr r^2\frac{e^{-ikr}-e^{ikr}}{-ikr}\frac{A}{pr}\sin\left(\sqrt{p^2+2m_rV_0}\cdot r\right) \\
&= -4\pi V_0\frac{A}{p}\int_0^{r_0} dr\frac{\sin(kr)}{k}\sin\left(\sqrt{p^2+2m_rV_0}\cdot r\right) \\
&= -4\pi V_0\frac{A}{pk}\frac{\sqrt{p^2+2m_rV_0}\cos(\sqrt{p^2+2m_rV_0}\cdot r_0)\sin(kr_0) - k\cos(kr_0)\sin(\sqrt{p^2+2m_rV_0}\cdot r_0)}{k^2-p^2-2m_rV_0},
\end{aligned} \tag{A.132}$$

where

$$A = \frac{\sin(pr_0+\delta_0(p))}{\sin(\sqrt{p^2+2m_rV_0}\cdot r_0)}. \tag{A.133}$$

Simplifying further, we obtain

$$T(\mathbf{k},\mathbf{p}) = -4\pi V_0\frac{\sin(pr_0+\delta_0(p))}{pk}\frac{\sqrt{p^2+2m_rV_0}\cot(\sqrt{p^2+2m_rV_0}\cdot r_0)\sin(kr_0) - k\cos(kr_0)}{k^2-p^2-2m_rV_0}. \tag{A.134}$$

The zero energy limit is

$$\begin{aligned}\lim_{k,p\to 0} T(\mathbf{k},\mathbf{p}) &= \frac{2\pi}{m_r}\frac{\sin(pr_0+\delta_0(p))}{p}\left(\sqrt{2m_rV_0}\cdot r_0\cot(\sqrt{2m_rV_0}\cdot r_0)-1\right)\\ &\sim \frac{2\pi}{m_r}r_0\left(1-\frac{\tan(\sqrt{2m_rV_0}\cdot r_0)}{\sqrt{2m_rV_0}\cdot r_0}\right)\\ &= \frac{2\pi a}{m_r},\end{aligned} \tag{A.135}$$

which is exactly what we expect from (A.96).

A.5.2 Two dimensions

In two dimensions, the radial Schrödinger equation is

$$-\frac{1}{2m_r}\left[\frac{1}{r}\frac{d}{dr}\left(r\frac{d}{dr}\right)-\frac{l^2}{r^2}\right]R_l(r)+\mathcal{V}(r)R_l(r)=ER_l(r). \tag{A.136}$$

Since we are interested in the low energy property, we can take $l=0$ component. Then, the Schrödinger equation reduces to

$$\left(\frac{d^2}{dr^2}+\frac{1}{r}\frac{d}{dr}+p^2-2m_r\mathcal{V}(r)\right)R_0(r)=0, \tag{A.137}$$

the solutions of which are the Bessel functions of the first and the second kinds.

At $r<r_0$, the general solution to this radial equation is

$$R_0(r)=AJ_0(\sqrt{p^2+2m_rV_0}\cdot r)+BN_0(\sqrt{p^2+2m_rV_0}\cdot r), \tag{A.138}$$

while at $r>r_0$, we have

$$R_0(r)=CJ_0(pr)+DN_0(pr). \tag{A.139}$$

Since the wavefunction should be analytic at the origin, $B=0$. Also, from (A.108), we can write the wavefunction at $r>r_0$ as

$$R_0(r)=\cos\delta_0(p)J_0(pr)-\sin\delta_0(p)N_0(pr). \tag{A.140}$$

Thus, R_0 is given by

$$R_0(r)=\begin{cases}AJ_0(\sqrt{p^2+2m_rV_0}\cdot r) & \text{for } r<r_0\\ \cos\delta_0(p)J_0(pr)-\sin\delta_0(p)N_0(pr) & \text{for } r>r_0.\end{cases} \tag{A.141}$$

Requiring that the two pieces of $R_0(r)$ be smoothly connected, we match the logarithmic derivative at $r = r_0$, which yields the condition

$$\sqrt{p^2 + 2m_r V_0}\frac{J_0'(\sqrt{p^2 + 2m_r V_0}\cdot r_0)}{J_0(\sqrt{p^2 + 2m_r V_0}\cdot r_0)} = p\frac{\cos\delta_0(p)J_0'(pr_0) - \sin\delta_0(p)N_0'(pr_0)}{\cos\delta_0(p)J_0(pr_0) - \sin\delta_0(p)N_0(pr_0)}. \tag{A.142}$$

Solving for $\tan\delta_0(p)$, we obtain

$$\tan\delta_0(p) = \frac{\sqrt{p^2 + 2m_r V_0}\frac{J_0'(\sqrt{p^2 + 2m_r V_0}\cdot r_0)}{J_0(\sqrt{p^2 + 2m_r V_0}\cdot r_0)}J_0(pr_0) - pJ_0'(pr_0)}{\sqrt{p^2 + 2m_r V_0}\frac{J_0'(\sqrt{p^2 + 2m_r V_0}\cdot r_0)}{J_0(\sqrt{p^2 + 2m_r V_0}\cdot r_0)}N_0(pr_0) - pN_0'(pr_0)}. \tag{A.143}$$

Using $J_0'(x) = -J_1(x)$ and $N_0'(x) = -N_1(x)$, this expression becomes

$$\tan\delta_0(p) = \frac{\sqrt{p^2 + 2m_r V_0}J_1(\sqrt{p^2 + 2m_r V_0}\cdot r_0)J_0(pr_0) - pJ_0(\sqrt{p^2 + 2m_r V_0}\cdot r_0)J_1(pr_0)}{\sqrt{p^2 + 2m_r V_0}J_1(\sqrt{p^2 + 2m_r V_0}\cdot r_0)N_0(pr_0) - pJ_0(\sqrt{p^2 + 2m_r V_0}\cdot r_0)N_1(pr_0)}. \tag{A.144}$$

Taking the low energy limit $p \to 0$, we have

$$\begin{aligned}\lim_{p\to 0}\tan\delta_0(p) &= \frac{\sqrt{2m_r V_0}J_1(\sqrt{2m_r V_0}\cdot r_0) - pJ_0(\sqrt{2m_r V_0}\cdot r_0)pr_0/2}{\sqrt{2m_r V_0}J_1(\sqrt{2m_r V_0}\cdot r_0)2/\pi\cdot(\ln(pr_0/2)+\gamma) + pJ_0(\sqrt{2m_r V_0}\cdot r_0)2/\pi pr_0} \\ &= \frac{1+\mathcal{O}(p)}{2/\pi\cdot(\ln(pr_0/2)+\gamma) + J_0(\sqrt{2m_r V_0}\cdot r_0)2/\pi r_0\sqrt{2m_r V_0}J_1(\sqrt{2m_r V_0}\cdot r_0)} \\ &= \frac{1+\mathcal{O}(p)}{2/\pi\cdot(\ln(pa/2)+\gamma)},\end{aligned} \tag{A.145}$$

where

$$a = r_0\exp\left(\frac{J_0(\sqrt{2m_r V_0}\cdot r_0)}{\sqrt{2m_r V_0}\cdot r_0 J_1(\sqrt{2m_r V_0}\cdot r_0)}\right). \tag{A.146}$$

If $m_r V_0 r_0^2$ is small, the scattering length reduces to

$$a \sim r_0 e^{1/m_r V_0 r_0^2}. \tag{A.147}$$

The t-matrix is

$$\begin{aligned}
T(\mathbf{k},\mathbf{p}) &= \int d^2r e^{-i\mathbf{k}\cdot\mathbf{r}}\mathcal{V}(\mathbf{r})\Psi_{\mathbf{p}}(\mathbf{r}) \\
&= AV_0\int_0^{2\pi}d\theta\int_0^{r_0}drre^{-ikr\cos\theta}J_0(\sqrt{p^2+2m_rV_0}\cdot r) \\
&= \frac{\cos\delta_0(p)J_0(pr_0)-\sin\delta_0(p)N_0(pr_0)}{J_0(\sqrt{p^2+2m_rV_0}\cdot r_0)}2\pi V_0\int_0^{r_0}drrJ_0(kr)J_0(\sqrt{p^2+2m_rV_0}\cdot r) \\
&= \frac{\cos\delta_0(p)J_0(pr_0)-\sin\delta_0(p)N_0(pr_0)}{J_0(\sqrt{p^2+2m_rV_0}\cdot r_0)}2\pi V_0\frac{r_0}{k^2-p^2-2m_rV_0} \\
&\quad\cdot\left(kJ_0(\sqrt{p^2+2m_rV_0}\cdot r_0)J_1(kr_0)-\sqrt{p^2+2m_rV_0}J_0(kr_0)J_1(\sqrt{p^2+2m_rV_0}\cdot r_0)\right) \\
&= \frac{(\cos\delta_0(p)J_0(pr_0)-\sin\delta_0(p)N_0(pr_0))\,2\pi V_0r_0}{k^2-p^2-2m_rV_0} \\
&\quad\cdot\left(kJ_1(kr_0)-\sqrt{p^2+2m_rV_0}J_0(kr_0)\frac{J_1(\sqrt{p^2+2m_rV_0}\cdot r_0)}{J_0(\sqrt{p^2+2m_rV_0}\cdot r_0)}\right).
\end{aligned} \tag{A.148}$$

The zero energy limit of the t-matrix is then

$$\begin{aligned}
\lim_{k,p\to0}T(\mathbf{k},\mathbf{p}) &= \lim_{p\to0}\left(1-\tan\delta_0(p)N_0(pr_0)\right)\frac{\pi r_0}{m_r}\sqrt{2m_rV_0}\frac{J_1(\sqrt{2m_rV_0}\cdot r_0)}{J_0(\sqrt{2m_rV_0}\cdot r_0)} \\
&= \lim_{p\to0}\left(1-\frac{\ln(pr_0/2)+\gamma}{\ln(pa/2)+\gamma}\right)\frac{\pi r_0}{m_r}\sqrt{2m_rV_0}\frac{J_1(\sqrt{2m_rV_0}\cdot r_0)}{J_0(\sqrt{2m_rV_0}\cdot r_0)} \\
&= -\lim_{p\to0}\frac{\ln(a/r_0)}{\ln(pr_0/2)}\frac{\pi r_0}{m_r}\sqrt{2m_rV_0}\frac{J_1(\sqrt{2m_rV_0}\cdot r_0)}{J_0(\sqrt{2m_rV_0}\cdot r_0)} \\
&= 0.
\end{aligned} \tag{A.149}$$

Thus, for a square well potential in two dimensions, the t-matrix approaches zero in the low energy limit, in contrast to the three dimensional result where the low energy t-matrix generally approaches a nonzero value.

When $m_rV_0r_0^2$ is small, the low energy t-matrix is

$$\lim_{k,p\to0}T(\mathbf{k},\mathbf{p}) \sim -\frac{1}{m_rV_0r_0^2\ln(pr_0/2)}\frac{\pi r_0}{m_r}\sqrt{2m_rV_0}\frac{\sqrt{2m_rV_0}\cdot r_0}{2} = -\frac{\pi}{m_r\ln(pr_0/2)}, \tag{A.150}$$

which clearly shows that the t-matrix logarithmically approaches zero in the low energy limit.

Since the t-matrix is equivalent to the ladder approximation in the effective interaction, the effective interaction in the ladder approximation in two dimensions also approaches zero in the low energy limit.

A.6 Example: contact interaction

In ultracold atomic physics, one often approximates the two-body potential by a delta-function contact interaction $\mathcal{V}(\mathbf{r}) = g\delta(\mathbf{r})$, neglecting the large momentum behavior and only focusing on the low energy physics. A useful feature of the contact interaction is that the Fourier transform does not depend on the momentum $\mathcal{V}(\mathbf{p}) = g$.

To correctly deal with a contact interaction, we must be careful with our treatment of the large momentum. In this section, we derive properties of the scattering t-matrix in a contact interaction.

The t-matrix satisfies the equation (A.19), which is

$$\begin{aligned} T(\mathbf{p}', \mathbf{p}) &= g + g \int \frac{d^d k}{(2\pi)^d} \frac{1}{(p^2 - k^2)/2m_r} T(\mathbf{k}, \mathbf{p}) \\ &= g + g \int \frac{d^d k}{(2\pi)^d} \frac{1}{(p^2 - k^2)/2m_r} g \\ &\qquad + g \int \frac{d^d k}{(2\pi)^d} \frac{1}{(p^2 - k^2)/2m_r} g \int \frac{d^d k'}{(2\pi)^d} \frac{1}{(p^2 - k'^2)/2m_r} g + \cdots \\ &= g \sum_{n=0}^{\infty} \left(\int \frac{d^d k}{(2\pi)^d} \frac{1}{(p^2 - k^2)/2m_r} g \right)^n \\ &= \left(\frac{1}{g} - \int \frac{d^d k}{(2\pi)^d} \frac{1}{(p^2 - k^2)/2m_r} \right)^{-1}. \end{aligned} \tag{A.151}$$

Introducing a high momentum cutoff Λ for three and two dimensions, and a low momentum cutoff λ for two dimensions, the inverse of the zero-energy t-matrix is

$$\frac{1}{T(0,0)} = \frac{1}{g} + \int \frac{d^d k}{(2\pi)^d} \frac{2m_r}{k^2} = \begin{cases} 1/g + m_r \Lambda/\pi^2 & \text{for three dimensions} \\ 1/g + m_r \ln(\Lambda/\lambda)/\pi & \text{for two dimensions.} \end{cases} \tag{A.152}$$

The large momentum (ultraviolet) divergences due to Λ in the right hand sides are not a significant concern, since this will simply act as a renormalization of the bare coupling g. The low momentum (infrared) divergence in two dimensions due to λ is a result of a generic feature in two dimensions that the t-matrix vanishes in the low energy limit.

Appendix B

Derivation of Green's functions

We derive the Green's function (3.20) for the bosons with the isotropic Rashba-Dresselhaus spin-orbit coupling. The equations of motion for $\psi_{-,\mathbf{p}}$ and $\psi_{+,\mathbf{p}}$ in Heisenberg representation are

$$\begin{aligned} i\frac{\partial}{\partial t}\psi_{-,\mathbf{p}}(t) &= \left(\frac{p^2+\kappa^2}{2m}-\mu\right)\psi_{-,\mathbf{p}}(t) - \frac{\kappa}{m}(p_x\psi_{-,\mathbf{p}}(t) + ip_y\psi_{+,\mathbf{p}}(t)) \\ &\quad + \frac{g}{2V}N_0\left(4\psi_{-,\mathbf{p}}(t) + 2\psi^\dagger_{-,2\mathbf{p}_0-\mathbf{p}}(t)\right) \\ &\quad + \frac{g}{2V}\sum_{\substack{\mathbf{p}_1+\mathbf{p}_2=\mathbf{p}_3+\mathbf{p} \\ \mathbf{p}_i\neq\mathbf{p}_0}}\left(2\psi^\dagger_{-,\mathbf{p}_3}(t)\psi_{-,\mathbf{p}_2}(t)\psi_{-,\mathbf{p}_1}(t) + 2\psi^\dagger_{+,\mathbf{p}_3}(t)\psi_{+,\mathbf{p}_2}(t)\psi_{-,\mathbf{p}_1}(t)\right) \\ &= \left(\frac{p^2+\kappa^2}{2m}-\mu-\frac{\kappa}{m}p_x+2gn_0\right)\psi_{-,\mathbf{p}}(t) - i\frac{\kappa}{m}p_y\psi_{+,\mathbf{p}}(t) + gn_0\psi^\dagger_{-,2\mathbf{p}_0-\mathbf{p}}(t) \\ &\quad + \frac{g}{2V}\sum_{\substack{\mathbf{p}_1+\mathbf{p}_2=\mathbf{p}_3+\mathbf{p} \\ \mathbf{p}_i\neq\mathbf{p}_0}}\left(2\psi^\dagger_{-,\mathbf{p}_3}(t)\psi_{-,\mathbf{p}_2}(t)\psi_{-,\mathbf{p}_1}(t) + 2\psi^\dagger_{+,\mathbf{p}_3}(t)\psi_{+,\mathbf{p}_2}(t)\psi_{-,\mathbf{p}_1}(t)\right) \end{aligned} \tag{B.1}$$

$$\begin{aligned} -i\frac{\partial}{\partial t}\psi^\dagger_{-,\mathbf{p}}(t) &= \left(\frac{p^2+\kappa^2}{2m}-\mu-\frac{\kappa}{m}p_x+2gn_0\right)\psi^\dagger_{-,\mathbf{p}}(t) + i\frac{\kappa}{m}p_y\psi^\dagger_{+,\mathbf{p}}(t) + gn_0\psi_{-,2\mathbf{p}_0-\mathbf{p}}(t) \\ &\quad + \frac{g}{2V}\sum_{\substack{\mathbf{p}_1+\mathbf{p}_2=\mathbf{p}_3+\mathbf{p} \\ \mathbf{p}_i\neq\mathbf{p}_0}}\left(2\psi^\dagger_{-,\mathbf{p}_1}(t)\psi^\dagger_{-,\mathbf{p}_2}(t)\psi_{-,\mathbf{p}_3}(t) + 2\psi^\dagger_{-,\mathbf{p}_1}(t)\psi^\dagger_{+,\mathbf{p}_2}(t)\psi_{+,\mathbf{p}_3}(t)\right) \end{aligned} \tag{B.2}$$

and

$$\begin{aligned} i\frac{\partial}{\partial t}\psi_{+,\mathbf{p}}(t) &= \left(\frac{p^2+\kappa^2}{2m}-\mu\right)\psi_{+,\mathbf{p}}(t)+\frac{\kappa}{m}(p_x\psi_{+,\mathbf{p}}(t)+ip_y\psi_{-,\mathbf{p}}(t))+\frac{g}{2V}N_0 2\psi_{+,\mathbf{p}}(t) \\ &\quad+\frac{g}{2V}\sum_{\substack{\mathbf{p}_1+\mathbf{p}_2=\mathbf{p}_3+\mathbf{p}\\ \mathbf{p}_i\neq\mathbf{p}_0}}\left(2\psi^\dagger_{+,\mathbf{p}_3}(t)\psi_{+,\mathbf{p}_2}(t)\psi_{+,\mathbf{p}_1}(t)+2\psi^\dagger_{-,\mathbf{p}_3}(t)\psi_{+,\mathbf{p}_2}(t)\psi_{-,\mathbf{p}_1}(t)\right) \\ &= \left(\frac{p^2+\kappa^2}{2m}-\mu+\frac{\kappa}{m}p_x+gn_0\right)\psi_{+,\mathbf{p}}(t)+i\frac{\kappa}{m}p_y\psi_{-,\mathbf{p}}(t) \\ &\quad+\frac{g}{2V}\sum_{\substack{\mathbf{p}_1+\mathbf{p}_2=\mathbf{p}_3+\mathbf{p}\\ \mathbf{p}_i\neq\mathbf{p}_0}}\left(2\psi^\dagger_{+,\mathbf{p}_3}(t)\psi_{+,\mathbf{p}_2}(t)\psi_{+,\mathbf{p}_1}(t)+2\psi^\dagger_{-,\mathbf{p}_3}(t)\psi_{+,\mathbf{p}_2}(t)\psi_{-,\mathbf{p}_1}(t)\right) \end{aligned} \tag{B.3}$$

$$\begin{aligned} -i\frac{\partial}{\partial t}\psi^\dagger_{+,\mathbf{p}}(t) &= \left(\frac{p^2+\kappa^2}{2m}-\mu+\frac{\kappa}{m}p_x+gn_0\right)\psi^\dagger_{+,\mathbf{p}}(t)-i\frac{\kappa}{m}p_y\psi^\dagger_{-,\mathbf{p}}(t) \\ &\quad+\frac{g}{2V}\sum_{\substack{\mathbf{p}_1+\mathbf{p}_2=\mathbf{p}_3+\mathbf{p}\\ \mathbf{p}_i\neq\mathbf{p}_0}}\left(2\psi^\dagger_{+,\mathbf{p}_1}(t)\psi^\dagger_{+,\mathbf{p}_2}(t)\psi_{+,\mathbf{p}_3}(t)+2\psi^\dagger_{-,\mathbf{p}_1}(t)\psi^\dagger_{+,\mathbf{p}_2}(t)\psi_{-,\mathbf{p}_3}(t)\right) \end{aligned} \tag{B.4}$$

Then,

$$\begin{aligned} &i\frac{\partial}{\partial t_1}G_{11}(\mathbf{p};t_1,t_2)=\delta(t_1-t_2)+\langle T\frac{\partial\psi_{-,\mathbf{p}}(t_1)}{\partial t_1}\psi^\dagger_{-,\mathbf{p}}(t_2)\rangle \\ &=\delta(t_1-t_2)+\left(\frac{p^2+\kappa^2}{2m}-\mu-\frac{\kappa}{m}p_x+2gn_0\right)G_{11}(\mathbf{p};t_1,t_2) \\ &-i\frac{\kappa}{m}p_yG_{31}(\mathbf{p};t_1,t_2)+n_0gG_{21}(\mathbf{p};t_1,t_2)-i\frac{g}{2V}\sum_{\substack{\mathbf{p}_1+\mathbf{p}_2=\mathbf{p}_3+\mathbf{p}\\ \mathbf{p}_i\neq\mathbf{p}_0}} \\ &\langle T\left(2\psi^\dagger_{-,\mathbf{p}_3}(t_1)\psi_{-,\mathbf{p}_2}(t_1)\psi_{-,\mathbf{p}_1}(t_1)\psi^\dagger_{-,\mathbf{p}}(t_2)+2\psi^\dagger_{+,\mathbf{p}_3}(t_1)\psi_{+,\mathbf{p}_2}(t_1)\psi_{-,\mathbf{p}_1}(t_1)\psi^\dagger_{-,\mathbf{p}}(t_2)\right)\rangle. \end{aligned} \tag{B.5}$$

Including the Hartree-Fock energy, this becomes

$$\begin{aligned} i\frac{\partial}{\partial t_1}G_{11}(\mathbf{p};t_1,t_2) &= \delta(t_1-t_2)+\left(\frac{p^2+\kappa^2}{2m}-\mu-\frac{\kappa}{m}p_x+g(2n_0+2n_-+n_+)\right)G_{11}(\mathbf{p};t_1,t_2) \\ &\quad-i\frac{\kappa}{m}p_yG_{31}(\mathbf{p};t_1,t_2)+gn_0G_{21}(\mathbf{p};t_1,t_2). \end{aligned} \tag{B.6}$$

Similarly,

$$
\begin{aligned}
&i\frac{\partial}{\partial t_1}G_{33}(\mathbf{p};t_1,t_2) = \delta(t_1-t_2) + \left(\frac{p^2+\kappa^2}{2m} - \mu + \frac{\kappa}{m}p_x + gn_0\right) G_{33}(\mathbf{p};t_1,t_2) \\
&+ i\frac{\kappa}{m}p_y G_{31}(\mathbf{p};t_1,t_2) - i\frac{g}{2V}\sum_{\substack{\mathbf{p}_1+\mathbf{p}_2=\mathbf{p}_3+\mathbf{p} \\ \mathbf{p}_i\neq\mathbf{p}_0}} \\
&\langle T\left(2\psi^\dagger_{+,\mathbf{p}_3}(t_1)\psi_{+,\mathbf{p}_2}(t_1)\psi_{+,\mathbf{p}_1}(t_1)\psi^\dagger_{+,\mathbf{p}}(t_2) + 2\psi^\dagger_{-,\mathbf{p}_3}(t_1)\psi_{+,\mathbf{p}_2}(t_1)\psi_{-,\mathbf{p}_1}(t_1)\psi^\dagger_{+,\mathbf{p}}(t_2)\right)\rangle \\
&\sim \delta(t_1-t_2) + \left(\frac{p^2+\kappa^2}{2m} - \mu + \frac{\kappa}{m}p_x + g(n_0+n_-+2n_+)\right) G_{33}(\mathbf{p};t_1,t_2) + i\frac{\kappa}{m}p_y G_{31}(\mathbf{p};t_1,t_2).
\end{aligned}
\tag{B.7}
$$

And

$$
\begin{aligned}
&-i\frac{\partial}{\partial t_1}G_{22}(\mathbf{p};t_1,t_2) = \delta(t_1-t_2) - \langle T\frac{\partial\psi^\dagger_{-,\mathbf{p}'}(t_1)}{\partial t_1}\psi_{-,\mathbf{p}'}(t_2)\rangle \\
&= \delta(t_1-t_2) + \left(\frac{p'^2+\kappa^2}{2m} - \mu - \frac{\kappa}{m}p'_x + 2gn_0\right) G_{22}(\mathbf{p};t_1,t_2) \\
&+ i\frac{\kappa}{m}p'_y G_{42}(\mathbf{p};t_1,t_2) + gn_0 G_{12}(\mathbf{p};t_1,t_2) + \frac{g}{2V}\sum_{\substack{\mathbf{p}_1+\mathbf{p}_2=\mathbf{p}_3+\mathbf{p}' \\ \mathbf{p}_i\neq\mathbf{p}_0}} \\
&\langle T\left(2\psi^\dagger_{-,\mathbf{p}_1}(t_1)\psi^\dagger_{-,\mathbf{p}_2}(t_1)\psi_{-,\mathbf{p}_3}(t_1)\psi_{-,\mathbf{p}'}(t_2) + 2\psi^\dagger_{-,\mathbf{p}_1}(t_1)\psi^\dagger_{+,\mathbf{p}_2}(t_1)\psi_{+,\mathbf{p}_3}(t_1)\psi_{-,\mathbf{p}'}(t_2)\right)\rangle \\
&\sim \delta(t_1-t_2) + \left(\frac{p'^2+\kappa^2}{2m} - \mu - \frac{\kappa}{m}p'_x + g(2n_0+2n_-+n_+)\right) G_{22}(\mathbf{p};t_1,t_2) \\
&\qquad + i\frac{\kappa}{m}p'_y G_{42}(\mathbf{p};t_1,t_2) + gn_0 G_{12}(\mathbf{p};t_1,t_2).
\end{aligned}
\tag{B.8}
$$

Similarly,

$$
\begin{aligned}
-i\frac{\partial}{\partial t_1}G_{44}(\mathbf{p};t_1,t_2) = \delta(t_1-t_2) + \left(\frac{p'^2+\kappa^2}{2m} - \mu + \frac{\kappa}{m}p'_x + g(n_0+n_-+2n_+)\right) G_{44}(\mathbf{p};t_1,t_2) \\
- i\frac{\kappa}{m}p'_y G_{24}(\mathbf{p};t_1,t_2).
\end{aligned}
\tag{B.9}
$$

Similar relations hold for the time-dependence of the off-diagonal Green's functions, and in the end, we obtain the following equation of motion for the matrix Green's function.

$$
\delta(t_1-t_2)I = \begin{pmatrix}
i\frac{\partial}{\partial t_1} - A & -gn_0 & i\frac{\kappa}{m}p_y & 0 \\
-gn_0 & -i\frac{\partial}{\partial t_1} - C & 0 & -i\frac{\kappa}{m}p'_y \\
-i\frac{\kappa}{m}p_y & 0 & i\frac{\partial}{\partial t_1} - B & 0 \\
0 & i\frac{\kappa}{m}p'_y & 0 & -i\frac{\partial}{\partial t_1} - D
\end{pmatrix} \mathbf{G}(\mathbf{p};t_1,t_2),
\tag{B.10}
$$

where

$$A = \frac{p^2 - 2\kappa p_x + \kappa^2}{2m} - \mu + g(2n_0 + 2n_- + n_+) = \frac{(\mathbf{p} - \mathbf{p}_0)^2}{2m} - \mu + g(2n_0 + 2n_- + n_+) \tag{B.11}$$

$$B = \frac{p^2 + 2\kappa p_x + \kappa^2}{2m} - \mu + g(n_0 + n_- + 2n_+) = \frac{(\mathbf{p} + \mathbf{p}_0)^2}{2m} - \mu + g(n_0 + n_- + 2n_+) \tag{B.12}$$

$$C = \frac{p'^2 - 2\kappa p'_x + \kappa^2}{2m} - \mu + g(2n_0 + 2n_- + n_+) = \frac{(\mathbf{p}' - \mathbf{p}_0)^2}{2m} - \mu + g(2n_0 + 2n_- + n_+) \tag{B.13}$$

$$D = \frac{p'^2 + 2\kappa p'_x + \kappa^2}{2m} - \mu + g(n_0 + n_- + 2n_+) = \frac{(\mathbf{p}' + \mathbf{p}_0)^2}{2m} - \mu + g(n_0 + n_- + 2n_+). \tag{B.14}$$

In terms of frequencies

$$\mathbf{G}(\mathbf{p}; t_1, t_2) = \int \frac{dz}{2\pi} \mathbf{G}(\mathbf{p}, z) e^{-iz(t_1 - t_2)}, \tag{B.15}$$

the equations of motion become

$$I = \begin{pmatrix} z - A & -gn_0 & i\frac{\kappa}{m} p_y & 0 \\ -gn_0 & -z - C & 0 & -i\frac{\kappa}{m} p'_y \\ -i\frac{\kappa}{m} p_y & 0 & z - B & 0 \\ 0 & i\frac{\kappa}{m} p'_y & 0 & -z - D \end{pmatrix} \mathbf{G}(\mathbf{p}, z). \tag{B.16}$$

Inverting this equation gives the equation (3.20).

Appendix C

Absence of population imbalance in a normal state

In this appendix, we prove that there is no population imbalance in a normal state of bosons with Rashba-Dresselhaus spin-orbit coupling considered in the section 3.4.

In this section we introduce separate chemical potentials μ_- and μ_+ for the bases $(-)$ and $(+)$, respectively, to determine if there is a spontaneous population imbalance. We prove that there is no spontaneous population imbalance by seeing that the second derivative of the Ginzburg-Landau free energy with respect to the population imbalance is positive.

The reduced Hamiltonian within the Hartree-Fock approximation is, as in (3.66),

$$\mathcal{H}_{\mathrm{HF}} = -Vg\left(n_-^2 + n_+^2 + n_- n_+\right) + \sum_{\mathbf{p}\neq\boldsymbol{\kappa}} \begin{pmatrix} \psi_{-,\mathbf{p}}^\dagger & \psi_{+,\mathbf{p}}^\dagger \end{pmatrix} \begin{pmatrix} A & -i\frac{\kappa}{m}p_y \\ i\frac{\kappa}{m}p_y & B \end{pmatrix} \begin{pmatrix} \psi_{-,\mathbf{p}} \\ \psi_{+,\mathbf{p}} \end{pmatrix}. \tag{C.1}$$

where

$$A = \frac{(\mathbf{p}-\boldsymbol{\kappa})^2}{2m} - \mu_- + g(2n_- + n_+), \qquad B = \frac{(\mathbf{p}+\boldsymbol{\kappa})^2}{2m} - \mu_+ + g(n_- + 2n_+). \tag{C.2}$$

To diagonalize the Hamiltonian, we write

$$\begin{pmatrix} \psi_{-,\mathbf{p}} \\ \psi_{+,\mathbf{p}} \end{pmatrix} = \begin{pmatrix} v_{\alpha,1} & v_{\beta,1} \\ v_{\alpha,2} & v_{\beta,2} \end{pmatrix} \begin{pmatrix} \psi_{\alpha,\mathbf{p}} \\ \psi_{\beta,\mathbf{p}} \end{pmatrix}, \tag{C.3}$$

where $\mathbf{v}_\alpha \equiv \begin{pmatrix} v_{\alpha,1} \\ v_{\alpha,2} \end{pmatrix}$ and $\mathbf{v}_\beta \equiv \begin{pmatrix} v_{\beta,1} \\ v_{\beta,2} \end{pmatrix}$ are the normalized eigenvectors of $\begin{pmatrix} A & -i\frac{\kappa}{m}p_y \\ i\frac{\kappa}{m}p_y & B \end{pmatrix}$, whose

eigenvalues are

$$\xi_\alpha = \frac{p^2+\kappa^2}{2m} - \frac{\mu_- + \mu_+}{2} + \frac{3}{2}g(n_- + n_+) - \sqrt{\left(-\frac{\kappa}{m}p_x - \frac{\mu_- - \mu_+}{2} + \frac{g}{2}(n_- - n_+)\right)^2 + \left(\frac{\kappa}{m}p_y\right)^2} \tag{C.4}$$

$$\xi_\beta = \frac{p^2+\kappa^2}{2m} - \frac{\mu_- + \mu_+}{2} + \frac{3}{2}g(n_- + n_+) + \sqrt{\left(-\frac{\kappa}{m}p_x - \frac{\mu_- - \mu_+}{2} + \frac{g}{2}(n_- - n_+)\right)^2 + \left(\frac{\kappa}{m}p_y\right)^2}. \tag{C.5}$$

By an explicit calculation, one can derive

$$\begin{aligned}\begin{pmatrix} v_{\alpha,1} \\ v_{\alpha,2} \end{pmatrix} &= C_\alpha \begin{pmatrix} -\frac{\kappa p_x}{m} - \frac{\mu_- - \mu_+}{2} - \frac{g}{2}\Delta n - \sqrt{\left(-\frac{\kappa p_x}{m} - \frac{\mu_- - \mu_+}{2} - \frac{g}{2}\Delta n\right)^2 + \frac{\kappa^2 p_y^2}{m^2}} \\ i\frac{\kappa}{m}p_y \end{pmatrix} \\ &\equiv C_\alpha \begin{pmatrix} \gamma_1 - \sqrt{\gamma_1^2+\gamma_2^2} \\ -i\gamma_2 \end{pmatrix} \end{aligned} \tag{C.6}$$

$$\begin{aligned}\begin{pmatrix} v_{\beta,1} \\ v_{\beta,2} \end{pmatrix} &= C_\beta \begin{pmatrix} -\frac{\kappa p_x}{m} - \frac{\mu_- - \mu_+}{2} - \frac{g}{2}\Delta n + \sqrt{\left(-\frac{\kappa p_x}{m} - \frac{\mu_- - \mu_+}{2} - \frac{g}{2}\Delta n\right)^2 + \frac{\kappa^2 p_y^2}{m^2}} \\ i\frac{\kappa}{m}p_y \end{pmatrix} \\ &\equiv C_\beta \begin{pmatrix} \gamma_1 + \sqrt{\gamma_1^2+\gamma_2^2} \\ -i\gamma_2 \end{pmatrix}, \end{aligned} \tag{C.7}$$

where $\Delta n \equiv n_+ - n_-$ as before, and C_α and C_β are normalization constants which satisfy

$$C_\alpha^2 = \frac{\sqrt{\gamma_1^2+\gamma_2^2}+\gamma_1}{2\gamma_2^2\sqrt{\gamma_1^2+\gamma_2^2}}, \qquad C_\beta^2 = \frac{\sqrt{\gamma_1^2+\gamma_2^2}-\gamma_1}{2\gamma_2^2\sqrt{\gamma_1^2+\gamma_2^2}}. \tag{C.8}$$

Since the Hamiltonian is diagonalized in the basis $(\psi_{\alpha,\mathbf{p}}, \psi_{\beta,\mathbf{p}})$, the number of particles in the states ψ_α and ψ_β, with momentum $\mathbf{p}$, are $f_B(\xi_\alpha(\mathbf{p}))$ and $f_B(\xi_\beta(\mathbf{p}))$ respectively, where $f_B(x) = 1/(e^{\beta x}-1)$ is the Bose distribution function. Then, the number of particles in the states $(-)$ and $(+)$ with momentum $\mathbf{p}$ is

$$\langle \psi_{-,\mathbf{p}}^\dagger \psi_{-,\mathbf{p}} \rangle = |v_{\alpha,1}|^2 f_B(\xi_\alpha(\mathbf{p})) + |v_{\beta,1}|^2 f_B(\xi_\beta(\mathbf{p})) \tag{C.9}$$

$$\langle \psi_{+,\mathbf{p}}^\dagger \psi_{+,\mathbf{p}} \rangle = |v_{\alpha,2}|^2 f_B(\xi_\alpha(\mathbf{p})) + |v_{\beta,2}|^2 f_B(\xi_\beta(\mathbf{p})). \tag{C.10}$$

Therefore,

$$\begin{aligned} n_- &= \frac{1}{V}\sum_{\mathbf{p}}\langle\psi^\dagger_{-,\mathbf{p}}\psi_{-,\mathbf{p}}\rangle = \frac{1}{V}\sum_{\mathbf{p}}\left(|v_{\alpha,1}|^2 f_B(\xi_\alpha(\mathbf{p})) + |v_{\beta,1}|^2 f_B(\xi_\beta(\mathbf{p}))\right) \\ &= \frac{1}{V}\sum_{\mathbf{p}}\left(C_\alpha^2\left(\gamma_1 - \sqrt{\gamma_1^2+\gamma_2^2}\right)^2 f_B(\xi_\alpha(\mathbf{p})) + C_\beta^2\left(\gamma_1 + \sqrt{\gamma_1^2+\gamma_2^2}\right)^2 f_B(\xi_\beta(\mathbf{p}))\right) \\ &= \frac{1}{V}\sum_{\mathbf{p}}\left(\frac{\sqrt{\gamma_1^2+\gamma_2^2}-\gamma_1}{2\sqrt{\gamma_1^2+\gamma_2^2}} f_B(\xi_\alpha(\mathbf{p})) + \frac{\sqrt{\gamma_1^2+\gamma_2^2}+\gamma_1}{2\sqrt{\gamma_1^2+\gamma_2^2}} f_B(\xi_\beta(\mathbf{p}))\right), \end{aligned} \tag{C.11}$$

and similarly,

$$n_+ = \frac{1}{V}\sum_{\mathbf{p}}\left(\frac{\sqrt{\gamma_1^2+\gamma_2^2}+\gamma_1}{2\sqrt{\gamma_1^2+\gamma_2^2}} f_B(\xi_\alpha(\mathbf{p})) + \frac{\sqrt{\gamma_1^2+\gamma_2^2}-\gamma_1}{2\sqrt{\gamma_1^2+\gamma_2^2}} f_B(\xi_\beta(\mathbf{p}))\right). \tag{C.12}$$

These equations determine n_- and n_+ self-consistently.

In order to investigate the possibility of spontaneous population imbalance, we consider the Ginzburg-Landau free energy as a function of population imbalance, and ask whether $\mu_- = \mu_+$ with $n_- = n_+$ is a minimum or a local maximum.

The Helmholtz free energy density is

$$\begin{aligned} \mathcal{F} =& \mu_- n_- + \mu_+ n_+ - g\left(n_-^2 + n_+^2 + n_- n_+\right) \\ &+ \frac{1}{\beta V}\sum_{\mathbf{p}}\ln\left(1 - e^{-\beta\xi_\alpha(\mathbf{p})}\right) + \frac{1}{\beta V}\sum_{\mathbf{p}}\ln\left(1 - e^{-\beta\xi_\beta(\mathbf{p})}\right). \end{aligned} \tag{C.13}$$

In order to regard this free energy as a function of a population imbalance, we define the population imbalance ϕ by

$$n_- = \frac{n}{2} + \phi, \qquad\qquad n_+ = \frac{n}{2} - \phi, \tag{C.14}$$

and regard μ_- and μ_+ as functions of ϕ. Then, taking derivatives of (C.11) and (C.12) with respect to ϕ, one can derive

$$\left.\frac{\partial\mu_-}{\partial\phi}\right|_{\phi=0} = -\left.\frac{\partial\mu_+}{\partial\phi}\right|_{\phi=0}. \tag{C.15}$$

Using this relation, one obtains

$$\left.\frac{\partial^2\mathcal{F}}{\partial\phi^2}\right|_{\phi=0} = -2\left.\frac{\partial\mu_-}{\partial\phi}\right|_{\phi=0}, \tag{C.16}$$

where

$$\left.\frac{\partial \mu_-}{\partial \phi}\right|_{\phi=0} = \\ -g + 2\left[\frac{1}{V}\sum_{\mathbf{p}} \frac{p_y^2}{p_\perp^3}\left(-f_B(\xi_\alpha(\mathbf{p})) + f_B(\xi_\beta(\mathbf{p}))\right) + \frac{1}{V}\sum_{\mathbf{p}} \frac{p_x^2}{p_\perp^2}\left(f_B'(\xi_\alpha(\mathbf{p})) + f_B'(\xi_\beta(\mathbf{p}))\right)\right]^{-1} < 0. \tag{C.17}$$

Therefore

$$\left.\frac{\partial^2 \mathcal{F}}{\partial \phi^2}\right|_{\phi=0} > 0, \tag{C.18}$$

which implies that $\mu_- = \mu_+$ with $n_- = n_+ = n/2$ is a minimum and there is no spontaneous population imbalance.

Appendix D

T-matrix for bosons

We derive the t-matrix for bosons (4.21). Our starting point is the set of Bethe-Salpeter equations (4.7). Explicitly writing out $\mathcal{V}^{(i)}$s, the Bethe-Salpeter equations are

$$
\begin{aligned}
\Gamma^{\alpha\alpha}_{\alpha\alpha}(\mathbf{p},\mathbf{p}';\mathbf{q}) &= \frac{g_{aa}}{4} + \frac{g_{bb}}{4}e^{i(\phi_1+\phi_2-\phi_3-\phi_4)} + \frac{g_{ab}}{4}\frac{(e^{i\phi_1}+e^{i\phi_2})(e^{-i\phi_3}+e^{-i\phi_3})}{2} \\
&- \int \frac{d^3k}{(2\pi)^3}\left[\frac{g_{aa}}{4} + \frac{g_{bb}}{4}e^{i(\phi_1+\phi_2-\phi_5-\phi_6)} + \frac{g_{ab}}{4}\frac{(e^{i\phi_1}+e^{i\phi_2})(e^{-i\phi_5}+e^{-i\phi_6})}{2}\right]\frac{\Gamma^{\alpha\alpha}_{\alpha\alpha}(\mathbf{k},\mathbf{p}';\mathbf{q})}{\epsilon_-(\frac{\mathbf{q}}{2}-\mathbf{k})+\epsilon_-(\frac{\mathbf{q}}{2}+\mathbf{k})} \\
&- \int \frac{d^3k}{(2\pi)^3}\left[\frac{g_{aa}}{4} + \frac{g_{bb}}{4}e^{i(\phi_1+\phi_2-\phi_5-\phi_6)} - \frac{g_{ab}}{4}\frac{(e^{i\phi_1}+e^{i\phi_2})(e^{-i\phi_5}+e^{-i\phi_6})}{2}\right]\frac{\Gamma^{\alpha\alpha}_{\beta\beta}(\mathbf{k},\mathbf{p}';\mathbf{q})}{\epsilon_+(\frac{\mathbf{q}}{2}-\mathbf{k})+\epsilon_+(\frac{\mathbf{q}}{2}+\mathbf{k})} \\
&- \int \frac{d^3k}{(2\pi)^3}\left[\frac{g_{aa}}{4} - \frac{g_{bb}}{4}e^{i(\phi_1+\phi_2-\phi_5-\phi_6)} - \frac{g_{ab}}{4}\frac{(e^{i\phi_1}+e^{i\phi_2})(e^{-i\phi_5}-e^{-i\phi_6})}{2}\right]\frac{\sqrt{2}\Gamma^{\alpha\alpha}_{\alpha\beta}(\mathbf{k},\mathbf{p}';\mathbf{q})}{\epsilon_+(\frac{\mathbf{q}}{2}-\mathbf{k})+\epsilon_-(\frac{\mathbf{q}}{2}+\mathbf{k})}, \\
\Gamma^{\alpha\alpha}_{\beta\beta}(\mathbf{p},\mathbf{p}';\mathbf{q}) &= \frac{g_{aa}}{4} + \frac{g_{bb}}{4}e^{i(\phi_1+\phi_2-\phi_3-\phi_4)} - \frac{g_{ab}}{4}\frac{(e^{i\phi_1}+e^{i\phi_2})(e^{-i\phi_3}+e^{-i\phi_3})}{2} \\
&- \int \frac{d^3k}{(2\pi)^3}\left[\frac{g_{aa}}{4} + \frac{g_{bb}}{4}e^{i(\phi_1+\phi_2-\phi_5-\phi_6)} - \frac{g_{ab}}{4}\frac{(e^{i\phi_1}+e^{i\phi_2})(e^{-i\phi_5}+e^{-i\phi_6})}{2}\right]\frac{\Gamma^{\alpha\alpha}_{\alpha\alpha}(\mathbf{k},\mathbf{p}';\mathbf{q})}{\epsilon_-(\frac{\mathbf{q}}{2}-\mathbf{k})+\epsilon_-(\frac{\mathbf{q}}{2}+\mathbf{k})} \\
&- \int \frac{d^3k}{(2\pi)^3}\left[\frac{g_{aa}}{4} + \frac{g_{bb}}{4}e^{i(\phi_1+\phi_2-\phi_5-\phi_6)} + \frac{g_{ab}}{4}\frac{(e^{i\phi_1}+e^{i\phi_2})(e^{-i\phi_5}+e^{-i\phi_6})}{2}\right]\frac{\Gamma^{\alpha\alpha}_{\beta\beta}(\mathbf{k},\mathbf{p}';\mathbf{q})}{\epsilon_+(\frac{\mathbf{q}}{2}-\mathbf{k})+\epsilon_+(\frac{\mathbf{q}}{2}+\mathbf{k})} \\
&- \int \frac{d^3k}{(2\pi)^3}\left[\frac{g_{aa}}{4} - \frac{g_{bb}}{4}e^{i(\phi_1+\phi_2-\phi_5-\phi_6)} + \frac{g_{ab}}{4}\frac{(e^{i\phi_1}+e^{i\phi_2})(e^{-i\phi_5}-e^{-i\phi_6})}{2}\right]\frac{\sqrt{2}\Gamma^{\alpha\alpha}_{\alpha\beta}(\mathbf{k},\mathbf{p}';\mathbf{q})}{\epsilon_+(\frac{\mathbf{q}}{2}-\mathbf{k})+\epsilon_-(\frac{\mathbf{q}}{2}+\mathbf{k})},
\end{aligned}
\tag{D.1}
$$

and

$$\frac{1}{\sqrt{2}}\Gamma^{\alpha\alpha}_{\alpha\beta}(\mathbf{p},\mathbf{p}';\mathbf{q}) = \frac{g_{aa}}{4} - \frac{g_{bb}}{4}e^{i(\phi_1+\phi_2-\phi_3-\phi_4)} + \frac{g_{ab}}{4}\frac{(e^{i\phi_1}-e^{i\phi_2})(e^{-i\phi_3}+e^{-i\phi_3})}{2}$$
$$-\int\frac{d^3k}{(2\pi)^3}\left[\frac{g_{aa}}{4} - \frac{g_{bb}}{4}e^{i(\phi_1+\phi_2-\phi_5-\phi_6)} + \frac{g_{ab}}{4}\frac{(e^{i\phi_1}-e^{i\phi_2})(e^{-i\phi_5}+e^{-i\phi_6})}{2}\right]\frac{\Gamma^{\alpha\alpha}_{\alpha\alpha}(\mathbf{k},\mathbf{p}';\mathbf{q})}{\epsilon_-(\frac{\mathbf{q}}{2}-\mathbf{k})+\epsilon_-(\frac{\mathbf{q}}{2}+\mathbf{k})}$$
$$-\int\frac{d^3k}{(2\pi)^3}\left[\frac{g_{aa}}{4} - \frac{g_{bb}}{4}e^{i(\phi_1+\phi_2-\phi_5-\phi_6)} - \frac{g_{ab}}{4}\frac{(e^{i\phi_1}-e^{i\phi_2})(e^{-i\phi_5}+e^{-i\phi_6})}{2}\right]\frac{\Gamma^{\alpha\alpha}_{\beta\beta}(\mathbf{k},\mathbf{p}';\mathbf{q})}{\epsilon_+(\frac{\mathbf{q}}{2}-\mathbf{k})+\epsilon_+(\frac{\mathbf{q}}{2}+\mathbf{k})}$$
$$-\int\frac{d^3k}{(2\pi)^3}\left[\frac{g_{aa}}{4} + \frac{g_{bb}}{4}e^{i(\phi_1+\phi_2-\phi_5-\phi_6)} - \frac{g_{ab}}{4}\frac{(e^{i\phi_1}-e^{i\phi_2})(e^{-i\phi_5}-e^{-i\phi_6})}{2}\right]\frac{\sqrt{2}\Gamma^{\alpha\alpha}_{\alpha\beta}(\mathbf{k},\mathbf{p}';\mathbf{q})}{\epsilon_+(\frac{\mathbf{q}}{2}-\mathbf{k})+\epsilon_-(\frac{\mathbf{q}}{2}+\mathbf{k})}. \tag{D.2}$$

Changing $\mathbf{p}$ to $-\mathbf{p}$ in (D.2) corresponds to interchanging ϕ_1 and ϕ_2 in the right hand side. Thus,

$$\frac{1}{\sqrt{2}}\Gamma^{\alpha\alpha}_{\alpha\beta}(-\mathbf{p},\mathbf{p}';\mathbf{q}) = \frac{g_{aa}}{4} - \frac{g_{bb}}{4}e^{i(\phi_1+\phi_2-\phi_3-\phi_4)} - \frac{g_{ab}}{4}\frac{(e^{i\phi_1}-e^{i\phi_2})(e^{-i\phi_3}+e^{-i\phi_3})}{2}$$
$$-\int\frac{d^3k}{(2\pi)^3}\left[\frac{g_{aa}}{4} - \frac{g_{bb}}{4}e^{i(\phi_1+\phi_2-\phi_5-\phi_6)} - \frac{g_{ab}}{4}\frac{(e^{i\phi_1}-e^{i\phi_2})(e^{-i\phi_5}+e^{-i\phi_6})}{2}\right]\frac{\Gamma^{\alpha\alpha}_{\alpha\alpha}(\mathbf{k},\mathbf{p}';\mathbf{q})}{\epsilon_-(\frac{\mathbf{q}}{2}-\mathbf{k})+\epsilon_-(\frac{\mathbf{q}}{2}+\mathbf{k})}$$
$$-\int\frac{d^3k}{(2\pi)^3}\left[\frac{g_{aa}}{4} - \frac{g_{bb}}{4}e^{i(\phi_1+\phi_2-\phi_5-\phi_6)} + \frac{g_{ab}}{4}\frac{(e^{i\phi_1}-e^{i\phi_2})(e^{-i\phi_5}+e^{-i\phi_6})}{2}\right]\frac{\Gamma^{\alpha\alpha}_{\beta\beta}(\mathbf{k},\mathbf{p}';\mathbf{q})}{\epsilon_+(\frac{\mathbf{q}}{2}-\mathbf{k})+\epsilon_+(\frac{\mathbf{q}}{2}+\mathbf{k})}$$
$$-\int\frac{d^3k}{(2\pi)^3}\left[\frac{g_{aa}}{4} + \frac{g_{bb}}{4}e^{i(\phi_1+\phi_2-\phi_5-\phi_6)} + \frac{g_{ab}}{4}\frac{(e^{i\phi_1}-e^{i\phi_2})(e^{-i\phi_5}-e^{-i\phi_6})}{2}\right]\frac{\sqrt{2}\Gamma^{\alpha\alpha}_{\alpha\beta}(\mathbf{k},\mathbf{p}';\mathbf{q})}{\epsilon_+(\frac{\mathbf{q}}{2}-\mathbf{k})+\epsilon_-(\frac{\mathbf{q}}{2}+\mathbf{k})}, \tag{D.3}$$

which turns out to be useful in solving the set of Bethe-Salpeter equations.

The key to solving this set of equations is to construct the quantities

$$X(\mathbf{p},\mathbf{p}';\mathbf{q}) \equiv \frac{1}{4}\left(\Gamma^{\alpha\alpha}_{\alpha\alpha}(\mathbf{p},\mathbf{p}';\mathbf{q}) + \Gamma^{\alpha\alpha}_{\beta\beta}(\mathbf{p},\mathbf{p}';\mathbf{q}) + \Gamma^{\alpha\alpha}_{\alpha\beta}(\mathbf{p},\mathbf{p}';\mathbf{q})/\sqrt{2} + \Gamma^{\alpha\alpha}_{\alpha\beta}(-\mathbf{p},\mathbf{p}';\mathbf{q})/\sqrt{2}\right),$$
$$Y(\mathbf{p},\mathbf{p}';\mathbf{q})e^{i(\phi_1+\phi_2-\phi_3-\phi_4)}$$
$$\equiv \frac{1}{4}\left(\Gamma^{\alpha\alpha}_{\alpha\alpha}(\mathbf{p},\mathbf{p}';\mathbf{q}) + \Gamma^{\alpha\alpha}_{\beta\beta}(\mathbf{p},\mathbf{p}';\mathbf{q}) - \Gamma^{\alpha\alpha}_{\alpha\beta}(\mathbf{p},\mathbf{p}';\mathbf{q})/\sqrt{2} - \Gamma^{\alpha\alpha}_{\alpha\beta}(-\mathbf{p},\mathbf{p}';\mathbf{q})/\sqrt{2}\right),$$
$$Z(\mathbf{p},\mathbf{p}';\mathbf{q}) \equiv \frac{1}{2}\frac{\Gamma^{\alpha\alpha}_{\alpha\alpha}(\mathbf{p},\mathbf{p}';\mathbf{q}) - \Gamma^{\beta\beta}_{\alpha\alpha}(\mathbf{p},\mathbf{p}';\mathbf{q})}{(e^{i\phi_1}+e^{i\phi_2})(e^{-i\phi_3}+e^{-i\phi_4})} = \frac{1}{2}\frac{\Gamma^{\alpha\alpha}_{\alpha\beta}(\mathbf{p},\mathbf{p}';\mathbf{q})/\sqrt{2} - \Gamma^{\alpha\alpha}_{\alpha\beta}(-\mathbf{p},\mathbf{p}';\mathbf{q})/\sqrt{2}}{(e^{i\phi_1}-e^{i\phi_2})(e^{-i\phi_3}+e^{-i\phi_4})}. \tag{D.4}$$

The last equation can be verified by looking at the Bethe-Salpeter equations. Constructing X, Y, and Z from the Bethe-Salpeter equations (D.1)-(D.3), we obtain

$$X(\mathbf{p},\mathbf{p}';\mathbf{q}) = \frac{g_{aa}}{4}\left[1 - \int\frac{d^3k}{(2\pi)^3}\right.$$
$$\left.\times\left(\frac{\Gamma^{\alpha\alpha}_{\alpha\alpha}(\mathbf{k},\mathbf{p}';\mathbf{q})}{\epsilon_-(\frac{\mathbf{q}}{2}-\mathbf{k})+\epsilon_-(\frac{\mathbf{q}}{2}+\mathbf{k})} + \frac{\Gamma^{\alpha\alpha}_{\beta\beta}(\mathbf{k},\mathbf{p}';\mathbf{q})}{\epsilon_+(\frac{\mathbf{q}}{2}-\mathbf{k})+\epsilon_+(\frac{\mathbf{q}}{2}+\mathbf{k})} + \frac{\sqrt{2}\Gamma^{\alpha\alpha}_{\alpha\beta}(\mathbf{k},\mathbf{p}';\mathbf{q})}{\epsilon_+(\frac{\mathbf{q}}{2}-\mathbf{k})+\epsilon_-(\frac{\mathbf{q}}{2}+\mathbf{k})}\right)\right], \tag{D.5}$$

$$Y(\mathbf{p},\mathbf{p}';\mathbf{q}) = \frac{g_{bb}}{4}\left[1 - \int \frac{d^3k}{(2\pi)^3}\frac{1}{e^{i(\phi_5+\phi_6-\phi_3-\phi_4)}}\right.$$
$$\left.\times\left(\frac{\Gamma^{\alpha\alpha}_{\alpha\alpha}(\mathbf{k},\mathbf{p}';\mathbf{q})}{\epsilon_-(\frac{\mathbf{q}}{2}-\mathbf{k})+\epsilon_-(\frac{\mathbf{q}}{2}+\mathbf{k})} + \frac{\Gamma^{\alpha\alpha}_{\beta\beta}(\mathbf{k},\mathbf{p}';\mathbf{q})}{\epsilon_+(\frac{\mathbf{q}}{2}-\mathbf{k})+\epsilon_+(\frac{\mathbf{q}}{2}+\mathbf{k})} - \frac{\sqrt{2}\Gamma^{\alpha\alpha}_{\alpha\beta}(\mathbf{k},\mathbf{p}';\mathbf{q})}{\epsilon_+(\frac{\mathbf{q}}{2}-\mathbf{k})+\epsilon_-(\frac{\mathbf{q}}{2}+\mathbf{k})}\right)\right], \quad \text{(D.6)}$$

and

$$Z(\mathbf{p},\mathbf{p}';\mathbf{q}) = \frac{g_{ab}}{8}\left[1 - \int \frac{d^3k}{(2\pi)^3}\left(\frac{e^{-i\phi_5}+e^{-i\phi_6}}{e^{-i\phi_3}+e^{-i\phi_4}}\frac{\Gamma^{\alpha\alpha}_{\alpha\alpha}(\mathbf{k},\mathbf{p}';\mathbf{q})}{\epsilon_-(\frac{\mathbf{q}}{2}-\mathbf{k})+\epsilon_-(\frac{\mathbf{q}}{2}+\mathbf{k})}\right.\right.$$
$$\left.\left.-\frac{e^{-i\phi_5}+e^{-i\phi_6}}{e^{-i\phi_3}+e^{-i\phi_4}}\frac{\Gamma^{\alpha\alpha}_{\beta\beta}(\mathbf{k},\mathbf{p}';\mathbf{q})}{\epsilon_+(\frac{\mathbf{q}}{2}-\mathbf{k})+\epsilon_+(\frac{\mathbf{q}}{2}+\mathbf{k})} - \frac{e^{-i\phi_5}-e^{-i\phi_6}}{e^{-i\phi_3}+e^{-i\phi_4}}\frac{\sqrt{2}\Gamma^{\alpha\alpha}_{\alpha\beta}(\mathbf{k},\mathbf{p}';\mathbf{q})}{\epsilon_+(\frac{\mathbf{q}}{2}-\mathbf{k})+\epsilon_-(\frac{\mathbf{q}}{2}+\mathbf{k})}\right)\right]. \quad \text{(D.7)}$$

We can see that the right hand sides of (D.5), (D.6), and (D.7) do not depend on $\mathbf{p}$. Thus, X, Y, and Z do not depend on their first argument and we can write $X(\mathbf{k},\mathbf{p}';\mathbf{q}) = X(\mathbf{p}';\mathbf{q})$, etc. Inverting (D.4), the t-matrices can be written in terms of X, Y, and Z as

$$\begin{aligned}
\Gamma^{\alpha\alpha}_{\alpha\alpha}(\mathbf{k},\mathbf{p}';\mathbf{q}) &= X(\mathbf{p}';\mathbf{q}) + Y(\mathbf{p}';\mathbf{q})e^{i(\phi_5+\phi_6-\phi_3-\phi_4)} + Z(\mathbf{p}';\mathbf{q})(e^{i\phi_6}+e^{i\phi_5})(e^{-i\phi_3}+e^{-i\phi_4}) \\
\Gamma^{\alpha\alpha}_{\beta\beta}(\mathbf{k},\mathbf{p}';\mathbf{q}) &= X(\mathbf{p}';\mathbf{q}) + Y(\mathbf{p}';\mathbf{q})e^{i(\phi_5+\phi_6-\phi_3-\phi_4)} - Z(\mathbf{p}';\mathbf{q})(e^{i\phi_6}+e^{i\phi_5})(e^{-i\phi_3}+e^{-i\phi_4}) \\
\frac{1}{\sqrt{2}}\Gamma^{\alpha\alpha}_{\alpha\beta}(\mathbf{k},\mathbf{p}';\mathbf{q}) &= X(\mathbf{p}';\mathbf{q}) - Y(\mathbf{p}';\mathbf{q})e^{i(\phi_5+\phi_6-\phi_3-\phi_4)} + Z(\mathbf{p}';\mathbf{q})(e^{i\phi_6}-e^{i\phi_5})(e^{-i\phi_3}+e^{-i\phi_4}).
\end{aligned} \quad \text{(D.8)}$$

Using (D.8), all the t-matrices in the equations (D.5), (D.6), and (D.7) can be written in terms of X, Y, and Z. After arranging terms, from (D.5) we obtain

$$\begin{aligned}
&X(\mathbf{p}';\mathbf{q}) \\
&\left[\frac{4}{g_{aa}} + \int \frac{d^3k}{(2\pi)^3}\left(\frac{1}{\epsilon_-(\frac{\mathbf{q}}{2}-\mathbf{k})+\epsilon_-(\frac{\mathbf{q}}{2}+\mathbf{k})} + \frac{1}{\epsilon_+(\frac{\mathbf{q}}{2}-\mathbf{k})+\epsilon_+(\frac{\mathbf{q}}{2}+\mathbf{k})} + \frac{2}{\epsilon_+(\frac{\mathbf{q}}{2}-\mathbf{k})+\epsilon_-(\frac{\mathbf{q}}{2}+\mathbf{k})}\right)\right] \\
&+ Y(\mathbf{p}';\mathbf{q})e^{-i(\phi_3+\phi_4)} \\
&\int \frac{d^3k}{(2\pi)^3}\left(\frac{e^{i(\phi_5+\phi_6)}}{\epsilon_-(\frac{\mathbf{q}}{2}-\mathbf{k})+\epsilon_-(\frac{\mathbf{q}}{2}+\mathbf{k})} + \frac{e^{i(\phi_5+\phi_6)}}{\epsilon_+(\frac{\mathbf{q}}{2}-\mathbf{k})+\epsilon_+(\frac{\mathbf{q}}{2}+\mathbf{k})} - \frac{2e^{i(\phi_5+\phi_6)}}{\epsilon_+(\frac{\mathbf{q}}{2}-\mathbf{k})+\epsilon_-(\frac{\mathbf{q}}{2}+\mathbf{k})}\right) \\
&+ Z(\mathbf{p}';\mathbf{q})(e^{-i\phi_3}+e^{-i\phi_4}) \\
&\int \frac{d^3k}{(2\pi)^3}\left(\frac{e^{i\phi_5}+e^{i\phi_6}}{\epsilon_-(\frac{\mathbf{q}}{2}-\mathbf{k})+\epsilon_-(\frac{\mathbf{q}}{2}+\mathbf{k})} - \frac{e^{i\phi_5}+e^{i\phi_6}}{\epsilon_+(\frac{\mathbf{q}}{2}-\mathbf{k})+\epsilon_+(\frac{\mathbf{q}}{2}+\mathbf{k})} - \frac{2(e^{i\phi_5}-e^{i\phi_6})}{\epsilon_+(\frac{\mathbf{q}}{2}-\mathbf{k})+\epsilon_-(\frac{\mathbf{q}}{2}+\mathbf{k})}\right) \\
&= 1.
\end{aligned} \quad \text{(D.9)}$$

Defining

$$f(\tilde{q}/2) \equiv$$
$$\frac{\pi}{m\kappa}\int\frac{d^3k}{(2\pi)^3}\left[\frac{1}{\epsilon_-(\frac{\mathbf{q}}{2}+\mathbf{k})+\epsilon_-(\frac{\mathbf{q}}{2}-\mathbf{k})}+\frac{1}{\epsilon_+(\frac{\mathbf{q}}{2}+\mathbf{k})+\epsilon_+(\frac{\mathbf{q}}{2}-\mathbf{k})}+\frac{2}{\epsilon_-(\frac{\mathbf{q}}{2}+\mathbf{k})+\epsilon_+(\frac{\mathbf{q}}{2}-\mathbf{k})}-\frac{4m}{k^2}\right]$$
$$g(\tilde{q}/2) \equiv$$
$$-\frac{\pi}{m\kappa}\int\frac{d^3k}{(2\pi)^3}\left[\frac{\cos(\phi_5-\phi_6)}{\epsilon_-(\frac{\mathbf{q}}{2}+\mathbf{k})+\epsilon_-(\frac{\mathbf{q}}{2}-\mathbf{k})}+\frac{\cos(\phi_5-\phi_6)}{\epsilon_+(\frac{\mathbf{q}}{2}+\mathbf{k})+\epsilon_+(\frac{\mathbf{q}}{2}-\mathbf{k})}-\frac{2\cos(\phi_5-\phi_6)}{\epsilon_-(\frac{\mathbf{q}}{2}+\mathbf{k})+\epsilon_+(\frac{\mathbf{q}}{2}-\mathbf{k})}\right]$$
$$h_1(\tilde{\mathbf{q}}/2) \equiv$$
$$\frac{\pi}{m\kappa}\int\frac{d^3k}{(2\pi)^3}\left[\frac{e^{i(\phi_5+\phi_6)}}{\epsilon_-(\frac{\mathbf{q}}{2}+\mathbf{k})+\epsilon_-(\frac{\mathbf{q}}{2}-\mathbf{k})}+\frac{e^{i(\phi_5+\phi_6)}}{\epsilon_+(\frac{\mathbf{q}}{2}+\mathbf{k})+\epsilon_+(\frac{\mathbf{q}}{2}-\mathbf{k})}-\frac{2e^{i(\phi_5+\phi_6)}}{\epsilon_-(\frac{\mathbf{q}}{2}+\mathbf{k})+\epsilon_+(\frac{\mathbf{q}}{2}-\mathbf{k})}\right]$$
$$h_2(\tilde{\mathbf{q}}/2) \equiv$$
$$\frac{\pi}{2m\kappa}\int\frac{d^3k}{(2\pi)^3}\left[\frac{e^{i\phi_5}+e^{i\phi_6}}{\epsilon_-(\frac{\mathbf{q}}{2}+\mathbf{k})+\epsilon_-(\frac{\mathbf{q}}{2}-\mathbf{k})}-\frac{e^{i\phi_5}+e^{i\phi_6}}{\epsilon_+(\frac{\mathbf{q}}{2}+\mathbf{k})+\epsilon_+(\frac{\mathbf{q}}{2}-\mathbf{k})}-\frac{2(e^{i\phi_5}-e^{i\phi_6})}{\epsilon_-(\frac{\mathbf{q}}{2}+\mathbf{k})+\epsilon_+(\frac{\mathbf{q}}{2}-\mathbf{k})}\right], \tag{D.10}$$

the equation (D.9) becomes

$$1 = X(\mathbf{p}';\mathbf{q})\left(\frac{4}{g_{aa}}+\int\frac{d^3k}{(2\pi)^3}\frac{4m}{k^2}+\frac{m\kappa}{\pi}f(\tilde{q}/2)\right)+Y(\mathbf{p}';\mathbf{q})e^{-i(\phi_3+\phi_4)}\frac{m\kappa}{\pi}h_1(\tilde{\mathbf{q}}/2)$$
$$+Z(\mathbf{p}';\mathbf{q})(e^{-i\phi_3}+e^{-i\phi_4})\frac{2m\kappa}{\pi}h_2(\tilde{\mathbf{q}}/2). \tag{D.11}$$

Introducing the free field scattering lengths by

$$\frac{1}{g_{ij}} = \frac{m}{4\pi a_{ij}} - \int\frac{d^3k}{(2\pi)^3}\frac{m}{k^2}, \tag{D.12}$$

we obtain

$$\frac{\pi}{m\kappa} = X(\mathbf{p}';\mathbf{q})\left(\frac{1}{\kappa a_{aa}}+f(\tilde{q}/2)\right)+Y(\mathbf{p}';\mathbf{q})e^{-i(\phi_3+\phi_4)}h_1(\tilde{\mathbf{q}}/2)+4Z(\mathbf{p}';\mathbf{q})\frac{e^{-i\phi_3}+e^{-i\phi_4}}{2}h_2(\tilde{\mathbf{q}}/2). \tag{D.13}$$

Similarly, from (D.6) and (D.7), we obtain

$$\frac{\pi}{m\kappa}e^{-i(\phi_3+\phi_4)} = X(\mathbf{p}';\mathbf{q})h_1^*(\tilde{\mathbf{q}}/2)+Y(\mathbf{p}';\mathbf{q})e^{-i(\phi_3+\phi_4)}\left(\frac{1}{\kappa a_{bb}}+f(\tilde{q}/2)\right)$$
$$+4Z(\mathbf{p}';\mathbf{q})\frac{e^{-i\phi_3}+e^{-i\phi_4}}{2}h_2^*(\tilde{\mathbf{q}}/2), \tag{D.14}$$
$$\frac{\pi}{m\kappa}\frac{e^{-i\phi_3}+e^{-i\phi_4}}{2} = X(\mathbf{p}';\mathbf{q})h_2^*(\tilde{\mathbf{q}}/2)+Y(\mathbf{p}';\mathbf{q})e^{-i(\phi_3+\phi_4)}h_2(\tilde{\mathbf{q}}/2)$$
$$+4Z(\mathbf{p}';\mathbf{q})\frac{e^{-i\phi_3}+e^{-i\phi_4}}{2}\left(\frac{1}{2\kappa a_{ab}}+\frac{f(\tilde{q}/2)-g(\tilde{q}/2)}{2}\right). \tag{D.15}$$

From (D.13), (D.14), and (D.15), we obtain the following matrix equation:

$$
\begin{aligned}
&\frac{\pi}{m\kappa}\begin{pmatrix} 1 \\ e^{-i(\phi_3+\phi_4)} \\ \frac{e^{-i\phi_3}+e^{-i\phi_4}}{2} \end{pmatrix} \\
&= \begin{pmatrix} f(\frac{\tilde{q}}{2})+\frac{1}{\kappa a_{aa}} & h_1(\tilde{\mathbf{q}}/2) & h_2(\tilde{\mathbf{q}}/2) \\ h_1^*(\tilde{\mathbf{q}}/2) & f(\frac{\tilde{q}}{2})+\frac{1}{\kappa a_{bb}} & h_2^*(\tilde{\mathbf{q}}/2) \\ h_2^*(\tilde{\mathbf{q}}/2) & h_2(\tilde{\mathbf{q}}/2) & \frac{1}{2}\left(f(\frac{\tilde{q}}{2})-g(\frac{\tilde{q}}{2})+\frac{1}{\kappa a_{ab}}\right) \end{pmatrix} \begin{pmatrix} X(\mathbf{p}';\mathbf{q}) \\ Y(\mathbf{p}';\mathbf{q})e^{-i(\phi_3+\phi_4)} \\ 4Z(\mathbf{p}';\mathbf{q})\frac{e^{-i\phi_3}+e^{-i\phi_4}}{2} \end{pmatrix} \\
&\equiv M \begin{pmatrix} X(\mathbf{p}';\mathbf{q}) \\ Y(\mathbf{p}';\mathbf{q})e^{-i(\phi_3+\phi_4)} \\ 4Z(\mathbf{p}';\mathbf{q})\frac{e^{-i\phi_3}+e^{-i\phi_4}}{2} \end{pmatrix}. \qquad \text{(D.16)}
\end{aligned}
$$

Then, from (D.8), we finally obtain the expression for the t-matrix

$$
\begin{aligned}
\Gamma^{\alpha\alpha}_{\alpha\alpha}(\mathbf{p},\mathbf{p}';\mathbf{q}) &= \begin{pmatrix} 1 & e^{i(\phi_1+\phi_2)} & \frac{e^{i\phi_1+i\phi_2}}{2} \end{pmatrix} \begin{pmatrix} X(\mathbf{p}';\mathbf{q}) \\ Y(\mathbf{p}';\mathbf{q})e^{-i(\phi_3+\phi_4)} \\ 4Z(\mathbf{p}';\mathbf{q})\dfrac{e^{-i\phi_3}+e^{-i\phi_4}}{2} \end{pmatrix} \\
&= \frac{\pi}{m\kappa}\begin{pmatrix} 1 & e^{i(\phi_1+\phi_2)} & \frac{e^{i\phi_1+i\phi_2}}{2} \end{pmatrix} \mathcal{M}^{-1} \begin{pmatrix} 1 \\ e^{-i(\phi_3+\phi_4)} \\ \dfrac{e^{-i\phi_3}+e^{-i\phi_4}}{2} \end{pmatrix}, \qquad \text{(D.17)}
\end{aligned}
$$

which is (4.21).

Appendix E

The coefficients of the Ginzburg-Landau free energy

We outline here the derivation of the Ginzburg-Landau free energy (5.32) from the free energy $\mathcal{F}_{\rm GL}(\Delta,\phi)$, Eq. (5.29). Since Δ always appears squared in the equations, odd powers of Δ do not occur in the free energy. To find the coefficients of Δ^2 and Δ^4, we set $\phi=0$, and expand $\mathcal{F}_{\rm GL}(\Delta,0)$ in powers of Δ^2. Taking the derivative of the number equation for blue particles (5.31) with respect to Δ^2, we see that μ_b (here allowed to differ from μ_r) does not depend on Δ^2. Differentiating the number equation for red particles (5.30), we obtain

$$\left.\frac{\partial\mu_r}{\partial\Delta^2}\right|_0 = -\frac{c_2}{c_1}, \tag{E.1}$$

where the subscript 0 denotes the derivative at $\Delta=\phi=0$, and

$$c_1 = -\frac{1}{V}\sum_{\mathbf{k}} f'(\xi^0_{\mathbf{k}}), \tag{E.2}$$

$$c_2 = \frac{1}{V}\sum_{\mathbf{k}}\left(\frac{\tanh\beta\xi^0_{\mathbf{k}}/2}{4(\xi^0_{\mathbf{k}})^2}+\frac{f'(\xi^0_{\mathbf{k}})}{2\xi^0_{\mathbf{k}}}\right). \tag{E.3}$$

Note that both c_1 and c_2 are positive. Then

$$\left.\frac{\partial\mathcal{F}_{\rm GL}(\Delta,0)}{\partial\Delta^2}\right|_0 = -\frac{1}{U}-\frac{1}{V}\sum_{\mathbf{k}}\frac{\tanh\beta\xi^0_{\mathbf{k}}/2}{2\xi^0_{\mathbf{k}}}, \tag{E.4}$$

$$\frac{1}{2}\left.\frac{\partial^2\mathcal{F}_{\rm GL}(\Delta,0)}{\partial(\Delta^2)^2}\right|_0 = b+\frac{(c_2)^2}{c_1}, \tag{E.5}$$

where

$$b = \frac{1}{V}\sum_{\mathbf{k}}\left(\frac{\tanh\beta\xi^0_{\mathbf{k}}/2}{8(\xi^0_{\mathbf{k}})^3}+\frac{f'(\xi^0_{\mathbf{k}})}{4(\xi^0_{\mathbf{k}})^2}\right) > 0. \tag{E.6}$$

We similarly derive the coefficients of ϕ, ϕ^2, ϕ^3, and ϕ^4:

$$\left.\frac{\partial \mathcal{F}_{\mathrm{GL}}(0,\phi)}{\partial \phi}\right|_0 = 0, \tag{E.7}$$

$$\frac{1}{2}\left.\frac{\partial^2 \mathcal{F}_{\mathrm{GL}}(0,\phi)}{\partial \phi^2}\right|_0 = 3\left(\frac{1}{c_1} - U_H\right), \tag{E.8}$$

$$\frac{1}{6}\left.\frac{\partial^3 \mathcal{F}_{\mathrm{GL}}(0,\phi)}{\partial \phi^3}\right|_0 = \frac{\kappa_1}{(c_1)^3}, \tag{E.9}$$

$$\frac{1}{24}\left.\frac{\partial^4 \mathcal{F}_{\mathrm{GL}}(0,\phi)}{\partial \phi^4}\right|_0 = \frac{3}{4(c_1)^4}\left(3\frac{(\kappa_1)^2}{c_1} - \kappa_2\right), \tag{E.10}$$

where

$$\kappa_1 = \frac{1}{V}\sum_{\mathbf{k}} f''(\xi^0_{\mathbf{k}}), \qquad\qquad \kappa_2 = -\frac{1}{V}\sum_{\mathbf{k}} f'''(\xi^0_{\mathbf{k}}). \tag{E.11}$$

Finally, the coefficients of $\phi\Delta^2$ and $\phi^2\Delta^2$ are

$$\left.\frac{\partial^2 \mathcal{F}_{\mathrm{GL}}(\Delta,\phi)}{\partial\phi\partial\Delta^2}\right|_{\Delta=\phi=0} = -2\frac{c_2}{c_1}, \tag{E.12}$$

$$\frac{1}{2}\left.\frac{\partial^3 \mathcal{F}_{\mathrm{GL}}(\Delta,\phi)}{(\partial\phi)^2\partial\Delta^2}\right|_{\Delta=\phi=0} = \frac{c_2\kappa_1}{(c_1)^3} + \frac{1}{(c_1)^2}\left(\frac{1}{V}\sum_{\mathbf{k}}\frac{f''(\xi^0_{\mathbf{k}})}{2\xi^0_{\mathbf{k}}} - 4b\right) \equiv c_5. \tag{E.13}$$

Therefore, the Ginzburg-Landau free energy up to fourth order in the order parameters is

$$\begin{aligned}\mathcal{F}_{\mathrm{GL}}(\Delta,\phi) &= \left(-\frac{1}{U} - \frac{1}{V}\sum_{\mathbf{k}}\frac{\tanh\beta\xi^0_{\mathbf{k}}/2}{2\xi^0_{\mathbf{k}}}\right)\Delta^2 + \left(b + \frac{(c_2)^2}{c_1}\right)\Delta^4 \\ &\quad + 3\left(\frac{1}{c_1} - U_H\right)\phi^2 + \frac{\kappa_1}{(c_1)^3}\phi^3 + \frac{3}{4(c_1)^4}\left(3\frac{(\kappa_1)^2}{c_1} - \kappa_2\right)\phi^4 - 2\frac{c_2}{c_1}\phi\Delta^2 + c_5\phi^2\Delta^2 \\ &\equiv a\Delta^2 + \left(b + \frac{(c_2)^2}{c_1}\right)\Delta^4 + 3\left(\frac{1}{c_1} - U_H\right)\phi^2 + c_3\phi^3 + c_4\phi^4 - 2\frac{c_2}{c_1}\Delta^2\phi + c_5\Delta^2\phi^2.\end{aligned} \tag{E.14}$$

Note that the c_i and b are all positive. Also, since U_H is negative, the coefficient of ϕ^2 is positive.

Appendix F

Population imbalance above the Bose condensation temperature

We derive the condition for the homogeneous state with population balance to be stable in a Bose mixture, which is used in the section 5.5. Although the three-component ultracold Fermi gas can form three types of molecules, the basic physics of the instability toward inhomogeneous states can be captured by considering a two-component Bose system.

We derive the Ginzburg-Landau free energy of a system of two species of bosons, a and b, as a function of their population imbalance at fixed total number $N = N_a + N_b$. With $a_{\mathbf{k}}$ and $b_{\mathbf{k}}$ the annihilation operators of bosons a and b of momentum $\mathbf{k}$, the Hamiltonian is

$$H - \mu_a N_a - \mu_b N_b = \sum_{\mathbf{k}} \left(\frac{k^2}{2m} - \mu_a \right) a^\dagger_{\mathbf{k}} a_{\mathbf{k}} + \sum_{\mathbf{k}} \left(\frac{k^2}{2m} - \mu_b \right) b^\dagger_{\mathbf{k}} b_{\mathbf{k}} + \frac{U_0}{2V} \sum_{\mathbf{k},\mathbf{k}',\mathbf{q}} \left(a^\dagger_{\mathbf{k}+\mathbf{q}} a^\dagger_{\mathbf{k}'-\mathbf{q}} a_{\mathbf{k}'} a_{\mathbf{k}} + b^\dagger_{\mathbf{k}+\mathbf{q}} b^\dagger_{\mathbf{k}'-\mathbf{q}} b_{\mathbf{k}'} b_{\mathbf{k}} \right) + \frac{U_1}{V} \sum_{\mathbf{k},\mathbf{k}',\mathbf{q}} a^\dagger_{\mathbf{k}+\mathbf{q}} b^\dagger_{\mathbf{k}'-\mathbf{q}} b_{\mathbf{k}'} a_{\mathbf{k}}, \quad \text{(F.1)}$$

where $U_0 = 4\pi a_0/m$ and $U_1 = 4\pi a_1/m$ are the s-wave interaction strength between the same type and between different types of bosons, and a_0 and a_1 are the corresponding scattering lengths.

We assume a sufficiently high temperature that neither system is condensed. In the Hartree-Fock approximation, we obtain

$$H - \mu_a N_a - \mu_b N_b \approx \sum_{\mathbf{k}} \left(\xi_{a,\mathbf{k}} + 2U_0 \frac{N_a}{V} + U_1 \frac{N_b}{V} \right) a^\dagger_{\mathbf{k}} a_{\mathbf{k}} + \sum_{\mathbf{k}} \left(\xi_{b,\mathbf{k}} + 2U_0 \frac{N_b}{V} + U_1 \frac{N_a}{V} \right) b^\dagger_{\mathbf{k}} b_{\mathbf{k}} - \frac{U_0}{V} \left(N_a^2 + N_b^2 \right) - \frac{U_1}{V} N_a N_b, \quad \text{(F.2)}$$

where $\xi_{a,\mathbf{k}} \equiv k^2/2m - \mu_a$ and $\xi_{b,\mathbf{k}} \equiv k^2/2m - \mu_b$. The number of particles N_a and N_b satisfies the

self-consistent equations,

$$N_a = \sum_{\mathbf{k}} g\left(\xi_{a,\mathbf{k}} + 2U_0 n_a + U_1 n_b\right) \tag{F.3}$$

$$N_b = \sum_{\mathbf{k}} g\left(\xi_{b,\mathbf{k}} + 2U_0 n_b + U_1 n_a\right), \tag{F.4}$$

where $g(x) = 1/(e^{\beta x} - 1)$ is the Bose distribution function, and $n_a = N_a/V$ and $n_b = N_b/V$. Then the thermodynamic potential is

$$\begin{aligned}\frac{\Omega}{V} = -U_0\left(n_a^2 + n_b^2\right) - U_1 n_a n_b + \frac{1}{\beta V}\sum_{\mathbf{k}} \ln\left\{1 - \exp\left(-\beta\left(\xi_{a,\mathbf{k}} + 2U_0 n_a + U_1 n_b\right)\right)\right\} \\ + \frac{1}{\beta V}\sum_{\mathbf{k}} \ln\left\{1 - \exp\left(-\beta\left(\xi_{b,\mathbf{k}} + 2U_0 n_b + U_1 n_a\right)\right)\right\},\end{aligned} \tag{F.5}$$

and the Helmholtz free energy is

$$\frac{F}{V} = \frac{\Omega}{V} + \mu_a n_a + \mu_b n_b. \tag{F.6}$$

The condition for the stability of the homogeneous state is found by expanding the Helmholtz free energy in terms of the deviation of the number of particles from the homogeneous state. We write the deviation of the numbers of particles from the balanced case as

$$\varphi = n_a - \frac{n}{2} = -\left(n_b - \frac{n}{2}\right); \tag{F.7}$$

then

$$\left.\frac{\partial}{\partial\varphi}\frac{F}{V}\right|_{\varphi=0} = 0 \tag{F.8}$$

$$\left.\frac{\partial^2}{\partial\varphi^2}\frac{F}{V}\right|_{\varphi=0} = 2\left(2U_0 - U_1 - \frac{1}{G}\right), \tag{F.9}$$

where

$$G = \frac{1}{V}\sum_{\mathbf{k}} g'\left(\frac{k^2}{2m} - \mu_0 + 2U_0\frac{n}{2} + U_1\frac{n}{2}\right) < 0, \tag{F.10}$$

and the homogeneous chemical potential μ_0 is determined by

$$\frac{n}{2} = \frac{1}{V}\sum_{\mathbf{k}} g\left(\frac{k^2}{2m} - \mu_0 + 2U_0\frac{n}{2} + U_1\frac{n}{2}\right). \tag{F.11}$$

The homogeneous state is stable if and only if $\partial^2(F/V)/\partial\varphi^2 > 0$. Since $G < 0$, we immediately conclude that when $2U_0 > U_1$, as in the present system, the homogeneous state is always stable

at $T > T_{\rm BEC}$. [For $2U_0 < U_1$, one finds $G \to 0^-$ as $T \to \infty$, and $G \to -\infty$ as T approaches $T_{\rm BEC}$ from above, implying a phase transition from the homogeneous to an inhomogeneous state at $T > T_{\rm BEC}$. The transition temperature increases with increasing $U_1 - 2U_0$. As $U_1 \to 2U_0$ from above, the transition temperature approaches $T_{\rm BEC}$ from above.]

Since the interaction is the same as that between identical and different molecules in the BEC limit of three-component ultracold fermions, the result derived here implies that the system is homogeneous above the condensation temperature.

Appendix G

Expansion of $\Gamma_{rg}(\mathbf{q},\omega_q)^{-1}$ in (5.65)

The expansion of $\Gamma_{rg}(\mathbf{q},\omega_q)^{-1}$ in (5.65) can be explicitly carried out using Eq. (5.60), with the result of Eq. (5.65), $-\Gamma_{rg}(\mathbf{q},\omega_q)^{-1} \approx Z\omega_q - \gamma q^2$, where

$$Z = \int \frac{d^3k}{(2\pi)^3} \left(\frac{\tanh(\beta_c E_{\mathbf{k}}/2)}{2E_{\mathbf{k}}} + f'(E_{\mathbf{k}}) \right) \frac{\xi_{\mathbf{k}}}{2E_{\mathbf{k}}^2} \tag{G.1}$$

and

$$\begin{aligned}\gamma = \int \frac{d^3k}{(2\pi)^3} \frac{1}{2mE_{\mathbf{k}}^7} \Bigg[& \left\{ \xi_{\mathbf{k}}^2 \Delta_{pg}^2 \frac{k^2}{3m} + \frac{1}{8}\xi_{\mathbf{k}} E_{\mathbf{k}}^2 \left(2\xi_{\mathbf{k}}^2 - \Delta_{pg}^2\right) \right. \\ & \left. + \frac{k^2}{24m}\left(\Delta_{pg}^2 - \xi_{\mathbf{k}}^2\right)\left(E_{\mathbf{k}}^2 + \xi_{\mathbf{k}}^2\right) \right\} \left(\tanh\frac{\beta_c E_{\mathbf{k}}}{2} + 2E_{\mathbf{k}} f'(E_{\mathbf{k}}) \right) \\ & + \left\{ \frac{\xi_{\mathbf{k}} \Delta_{pg}^2 E_{\mathbf{k}}^2}{4} + \frac{k^2}{12m}\left(2\xi_{\mathbf{k}}^4 - \xi_{\mathbf{k}}^2\Delta_{pg}^2 + \Delta_{pg}^4\right) \right\} E_{\mathbf{k}}^2 f''(E_{\mathbf{k}}) + \frac{k^2}{18m}\xi_{\mathbf{k}}^2 \Delta_{pg}^2 E_{\mathbf{k}}^3 f'''(E_{\mathbf{k}}) \Bigg]. \end{aligned} \tag{G.2}$$

In this appendix, we derive the relations (G.1) and (G.2). We first obtain some useful formulae on the summation of Matsubara frequencies. We then use the formula to derive the desired relations.

G.1 Matsubara sum

Fermionic Matsubara frequencies are defined by $\omega_n = i\pi(2n+1)/\beta$. The residue of a complex function $g(z)$ at a pole c of order n is

$$Res(g,c) = \frac{1}{(n-1)!} \lim_{z\to c} \frac{d^{n-1}}{dz^{n-1}}((z-c)^n g(z)). \tag{G.3}$$

We consider the integral in the complex z-plane along the contour C in Figure G.1, which is deformed as in the figure. The most basic formula is

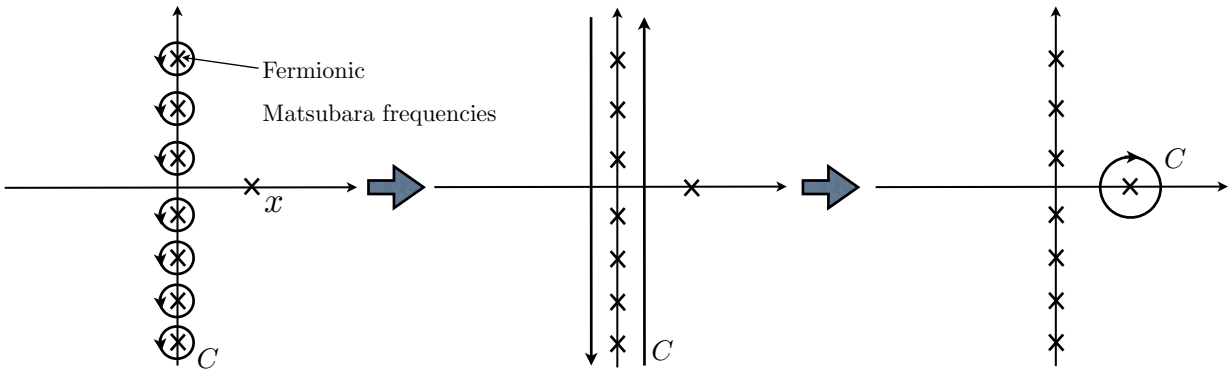

Figure G.1: Deformation of the contour C in the complex z plane.

$$\frac{1}{\beta}\sum_n \frac{1}{\omega_n - x} = \lim_{\eta\to+0}\frac{1}{\beta}\sum_n \frac{e^{\omega_n\eta}}{\omega_n - x} = -\frac{1}{2\pi i}\lim_{\eta\to+0}\int_C dz \frac{e^{z\eta}}{z-x}\frac{1}{e^{\beta z}+1}$$
$$= \lim_{\eta\to+0} Res\left(\frac{e^{z\eta}}{z-x}\frac{1}{e^{\beta z}+1}, x\right) = f(x), \tag{G.4}$$

where $f(x) = 1/(e^{\beta x}+1)$ is the Fermi distribution function. The formula is true for both positive and negative x. More complicated formulae are derived similarly:

$$\frac{1}{\beta}\sum_n \frac{1}{(\omega_n - x)^2} = -\frac{1}{2\pi i}\lim_{\eta\to+0}\int_C dz \frac{e^{z\eta}}{(z-x)^2}\frac{1}{e^{\beta z}+1} = -\beta\frac{e^{\beta x}}{(e^{\beta x}+1)^2} = f'(x) \tag{G.5}$$

$$\frac{1}{\beta}\sum_n \frac{1}{(\omega_n - x)^3} = -\frac{1}{2\pi i}\lim_{\eta\to+0}\int_C dz \frac{e^{z\eta}}{(z-x)^3}\frac{1}{e^{\beta z}+1} = \frac{1}{2}f''(x) \tag{G.6}$$

$$\frac{1}{\beta}\sum_n \frac{1}{(\omega_n - x)^4} = -\frac{1}{2\pi i}\lim_{\eta\to+0}\int_C dz \frac{e^{z\eta}}{(z-x)^4}\frac{1}{e^{\beta z}+1} = \frac{1}{6}f'''(x), \tag{G.7}$$

and some combinations:

$$\frac{1}{\beta}\sum_n \frac{1}{\omega_n - x}\cdot\frac{1}{\omega_n + x} = \frac{1}{\beta}\sum_n\left(\frac{1}{\omega_n - x} - \frac{1}{\omega_n + x}\right)\frac{1}{2x} = \frac{1}{2x}(f(x) - f(-x)) = -\frac{1}{2x}\tanh\frac{\beta x}{2} \tag{G.8}$$

$$\frac{1}{\beta}\sum_n \frac{1}{\omega_n - x}\cdot\frac{1}{(\omega_n + x)^2} = \frac{1}{\beta}\sum_n\left(\frac{1}{\omega_n - x} - \frac{1}{\omega_n + x}\right)\frac{1}{\omega_n + x}\cdot\frac{1}{2x}$$
$$= -\left(\frac{1}{2x}\right)^2\tanh\frac{\beta x}{2} - \frac{1}{2x}\cdot f'(-x) \tag{G.9}$$

$$\frac{1}{\beta}\sum_n \frac{1}{\omega_n - x}\cdot\frac{1}{(\omega_n + x)^3} = \frac{1}{\beta}\sum_n\left(\frac{1}{\omega_n - x} - \frac{1}{\omega_n + x}\right)\frac{1}{(\omega_n + x)^2}\cdot\frac{1}{2x}$$
$$= -\left(\frac{1}{2x}\right)^3\tanh\frac{\beta x}{2} - \left(\frac{1}{2x}\right)^2 f'(-x) - \frac{1}{2x}\cdot\frac{1}{2}f''(-x). \tag{G.10}$$

G.2 Derivation of coefficients

Now we derive the coefficients of the expansion of $-\Gamma_{rg}(\mathbf{q},\omega_q)^{-1}$. Taking the lowest order in the frequency and momenta, we expand as

$$\begin{aligned}-\Gamma_{rg}(\mathbf{q},\omega_q)^{-1} &= \frac{1}{U}+\int\frac{d^3p}{(2\pi)^3}\frac{1}{\beta_c}\sum_{\omega_p}\mathcal{G}_r(p)\mathcal{G}_g(q-p)\\ &\approx \int\frac{d^3p}{(2\pi)^3}\frac{1}{\beta_c}\sum_{\omega_p}\mathcal{G}_r(p)\left\{\frac{\partial}{\partial z}\mathcal{G}_g(\mathbf{k},z)\Big|_{k=-p}\omega_q+\nabla_{\mathbf{k}}\mathcal{G}_g(\mathbf{k},z)|_{k=-p}\cdot\mathbf{q}\right.\\ &\qquad\left.+\frac{1}{2}\sum_{ij}\frac{\partial^2}{\partial k_i\partial k_j}\mathcal{G}_g(\mathbf{k},z)\Big|_{k=-p}q_iq_j\right\}. \qquad \text{(G.11)}\end{aligned}$$

Since

$$\mathcal{G}_g(\mathbf{k},z)=\frac{1}{2}\cdot\frac{1+\xi_{\mathbf{k}}/E_{\mathbf{k}}}{z-E_{\mathbf{k}}}+\frac{1}{2}\cdot\frac{1-\xi_{\mathbf{k}}/E_{\mathbf{k}}}{z+E_{\mathbf{k}}}, \qquad \text{(G.12)}$$

the derivatives are

$$\frac{\partial}{\partial z}\mathcal{G}_g(\mathbf{k},z)=-\frac{1}{2}\cdot\frac{1+\xi_{\mathbf{k}}/E_{\mathbf{k}}}{(z-E_{\mathbf{k}})^2}-\frac{1}{2}\cdot\frac{1-\xi_{\mathbf{k}}/E_{\mathbf{k}}}{(z+E_{\mathbf{k}})^2} \qquad \text{(G.13)}$$

$$\frac{\partial}{\partial k_i}\mathcal{G}_g(\mathbf{k},z)=\left(\frac{1+\xi_{\mathbf{k}}/E_{\mathbf{k}}}{(z-E_{\mathbf{k}})^2}-\frac{1-\xi_{\mathbf{k}}/E_{\mathbf{k}}}{(z+E_{\mathbf{k}})^2}\right)\frac{\xi_{\mathbf{k}}}{E_{\mathbf{k}}}\frac{k_i}{2m}+\left(\frac{1}{z-E_{\mathbf{k}}}-\frac{1}{z+E_{\mathbf{k}}}\right)\frac{\Delta_{pg}^2}{E_{\mathbf{k}}^3}\frac{k_i}{2m}. \qquad \text{(G.14)}$$

Since the derivative of $\mathcal{G}_g(\mathbf{k},z)$ with respect to k_i is odd in k_i, the linear term in $\mathbf{q}$ in (G.11) is zero after integrating over $\mathbf{p}$. Similarly, quadratic terms with $i\neq j$ are zero. Thus we have

$$-\Gamma_{rg}(\mathbf{q},\omega_q)^{-1}\approx\int\frac{d^3p}{(2\pi)^3}\frac{1}{\beta_c}\sum_{\omega_p}\mathcal{G}_r(p)\left\{\frac{\partial}{\partial z}\mathcal{G}_g(\mathbf{k},z)\Big|_{k=-p}\omega_q+\frac{1}{2}\sum_i\frac{\partial^2}{\partial k_i^2}\mathcal{G}_g(\mathbf{k},z)\Big|_{k=-p}q_i^2\right\}. \qquad \text{(G.15)}$$

The second derivative of $\mathcal{G}_g(\mathbf{k},z)$ with respect to k_i is

$$\begin{aligned}\frac{\partial^2}{\partial k_i^2}\mathcal{G}_g(\mathbf{k},z) &= \left(\frac{1}{z-E_{\mathbf{k}}}-\frac{1}{z+E_{\mathbf{k}}}\right)\left(\frac{\Delta_{pg}^2}{2E_{\mathbf{k}}^3}\frac{1}{m}-\frac{3\Delta_{pg}^2\xi_{\mathbf{k}}}{2E_{\mathbf{k}}^5}\left(\frac{k_i}{m}\right)^2\right)\\ &\quad+\frac{1}{(z-E_{\mathbf{k}})^2}\left(\frac{\xi_{\mathbf{k}}}{2E_{\mathbf{k}}}\frac{1}{m}+\frac{\Delta_{pg}^2}{2E_{\mathbf{k}}^3}\left(\frac{k_i}{m}\right)^2+\frac{3}{2}\frac{\Delta_{pg}^2\xi_{\mathbf{k}}}{E_{\mathbf{k}}^4}\left(\frac{k_i}{m}\right)^2\right)\\ &\quad-\frac{1}{(z+E_{\mathbf{k}})^2}\left(\frac{\xi_{\mathbf{k}}}{2E_{\mathbf{k}}}\frac{1}{m}+\frac{\Delta_{pg}^2}{2E_{\mathbf{k}}^3}\left(\frac{k_i}{m}\right)^2-\frac{3}{2}\frac{\Delta_{pg}^2\xi_{\mathbf{k}}}{E_{\mathbf{k}}^4}\left(\frac{k_i}{m}\right)^2\right)\\ &\quad+\left(\frac{1+\xi_{\mathbf{k}}/E_{\mathbf{k}}}{(z-E_{\mathbf{k}})^3}+\frac{1-\xi_{\mathbf{k}}/E_{\mathbf{k}}}{(z+E_{\mathbf{k}})^3}\right)\frac{\xi_{\mathbf{k}}^2}{E_{\mathbf{k}}^2}\left(\frac{k_i}{m}\right)^2. \qquad \text{(G.16)}\end{aligned}$$

Therefore, we have

$$\int \frac{d^3p}{(2\pi)^3}\mathcal{G}_r(\mathbf{p})\ \frac{\partial^2}{\partial k_x^2}\mathcal{G}_g(\mathbf{k},z)\bigg|_{k=-p} = \int \frac{d^3p}{(2\pi)^3}\mathcal{G}_r(\mathbf{p})\ \frac{\partial^2}{\partial k_y^2}\mathcal{G}_g(\mathbf{k},z)\bigg|_{k=-p} = \int \frac{d^3p}{(2\pi)^3}\mathcal{G}_r(\mathbf{p})\ \frac{\partial^2}{\partial k_z^2}\mathcal{G}_g(\mathbf{k},z)\bigg|_{k=-p}, \tag{G.17}$$

and thus

$$\begin{aligned}-\Gamma_{rg}(\mathbf{q},\omega_q)^{-1} &\approx \int \frac{d^3p}{(2\pi)^3}\frac{1}{\beta_c}\sum_{\omega_p}\mathcal{G}_r(p)\left\{\frac{\partial}{\partial z}\mathcal{G}_g(\mathbf{k},z)\bigg|_{k=-p}\omega_q + \frac{1}{2}\frac{\partial^2}{\partial k_x^2}\mathcal{G}_g(\mathbf{k},z)\bigg|_{k=-p}q^2\right\}\\ &= \int \frac{d^3p}{(2\pi)^3}\frac{1}{\beta_c}\sum_{\omega_p}\mathcal{G}_r(p)\left\{\frac{\partial}{\partial z}\mathcal{G}_g(\mathbf{k},z)\bigg|_{k=-p}\omega_q + \frac{1}{6}\nabla^2\mathcal{G}_g(\mathbf{k},z)\bigg|_{k=-p}q^2\right\},\end{aligned} \tag{G.18}$$

and the expansion coefficients are

$$Z = \int \frac{d^3p}{(2\pi)^3}\frac{1}{\beta_c}\sum_{\omega_p}\mathcal{G}_r(p)\ \frac{\partial}{\partial z}\mathcal{G}_g(\mathbf{k},z)\bigg|_{k=-p} \tag{G.19}$$

$$\gamma = -\int \frac{d^3p}{(2\pi)^3}\frac{1}{\beta_c}\sum_{\omega_p}\mathcal{G}_r(p)\ \frac{1}{6}\nabla_2\mathcal{G}_g(\mathbf{k},z)\bigg|_{k=-p}. \tag{G.20}$$

Using Matsubara formulae derived in the previous section, we obtain

$$\begin{aligned}Z &= -\int \frac{d^3p}{(2\pi)^3}\frac{1}{\beta_c}\sum_{\omega_p}\left(\frac{1}{2}\cdot\frac{1+\xi_{\mathbf{p}}/E_{\mathbf{p}}}{\omega_p - E_{\mathbf{p}}} + \frac{1}{2}\cdot\frac{1-\xi_{\mathbf{p}}/E_{\mathbf{p}}}{\omega_p + E_{\mathbf{p}}}\right)\left(\frac{1}{2}\cdot\frac{1+\xi_{\mathbf{p}}/E_{\mathbf{p}}}{(-\omega_p - E_{\mathbf{p}})^2} + \frac{1}{2}\cdot\frac{1-\xi_{\mathbf{p}}/E_{\mathbf{p}}}{(-\omega_p + E_{\mathbf{p}})^2}\right)\\ &= -\frac{1}{4}\int \frac{d^3p}{(2\pi)^3}\frac{1}{\beta_c}\sum_{\omega_p}\left\{\left(\frac{1}{(\omega_p - E_{\mathbf{p}})^3} + \frac{1}{(\omega_p + E_{\mathbf{p}})^3}\right)\frac{\Delta_{pg}^2}{E_{\mathbf{p}}^2} + \frac{1}{\omega_p - E_{\mathbf{p}}}\frac{1}{(\omega_p + E_{\mathbf{p}})^2}\left(1 + \frac{\xi_{\mathbf{p}}}{E_{\mathbf{p}}}\right)^2\right.\\ &\qquad\left. + \frac{1}{\omega_p + E_{\mathbf{p}}}\frac{1}{(\omega_p - E_{\mathbf{p}})^2}\left(1 - \frac{\xi_{\mathbf{p}}}{E_{\mathbf{p}}}\right)^2\right\}\\ &= -\frac{1}{4}\int \frac{d^3p}{(2\pi)^3}\left\{\left(f''(E_{\mathbf{p}}) + f''(-E_{\mathbf{p}})\right)\frac{\Delta_{pg}^2}{2E_{\mathbf{p}}^2} - \left(\frac{\tanh(\beta_c E_{\mathbf{p}}/2)}{4E_{\mathbf{p}}^2} + \frac{f'(-E_{\mathbf{p}})}{2E_{\mathbf{p}}}\right)\left(1 + \frac{\xi_{\mathbf{p}}}{E_{\mathbf{p}}}\right)^2\right.\\ &\qquad\left. + \left(\frac{\tanh(\beta_c E_{\mathbf{p}}/2)}{4E_{\mathbf{p}}^2} + \frac{f'(E_{\mathbf{p}})}{2E_{\mathbf{p}}}\right)\left(1 - \frac{\xi_{\mathbf{p}}}{E_{\mathbf{p}}}\right)^2\right\}.\end{aligned} \tag{G.21}$$

Since $f'(-x) = f'(x)$ and $f''(-x) = -f''(x)$, we finally obtain

$$Z = \int \frac{d^3p}{(2\pi)^3}\left\{\left(\frac{\tanh(\beta_c E_{\mathbf{p}}/2)}{4E_{\mathbf{p}}^2} + \frac{f'(-E_{\mathbf{p}})}{2E_{\mathbf{p}}}\right)\frac{\xi_{\mathbf{p}}}{E_{\mathbf{p}}}\right\}, \tag{G.22}$$

which is exactly (G.1).

The expression for γ can be obtained similarly:

$$
\begin{aligned}
\gamma = {} & \frac{1}{12}\int \frac{d^3p}{(2\pi)^3}\frac{1}{\beta_c}\sum_{\omega_p}\left(\frac{1+\xi_{\mathbf{p}}/E_{\mathbf{p}}}{\omega_p - E_{\mathbf{p}}} + \frac{1-\xi_{\mathbf{p}}/E_{\mathbf{p}}}{\omega_p + E_{\mathbf{p}}}\right) \\
& \left\{\left(\frac{1}{\omega_p + E_{\mathbf{p}}} - \frac{1}{\omega_p - E_{\mathbf{p}}}\right)\left(\frac{\Delta_{pg}^2}{2E_{\mathbf{p}}^3}\frac{3}{m} - \frac{3\Delta_{pg}^2\xi_{\mathbf{p}}}{2E_{\mathbf{p}}^5}\frac{p^2}{m^2}\right) - \frac{1}{(\omega_p + E_{\mathbf{p}})^2}\left(\frac{\xi_{\mathbf{p}}}{2E_{\mathbf{p}}}\frac{3}{m} + \left(1 + \frac{3\xi_{\mathbf{p}}}{E_{\mathbf{p}}}\right)\frac{\Delta_{pg}^2}{2E_{\mathbf{p}}^3}\frac{p^2}{m^2}\right)\right. \\
& \left. + \frac{1}{(\omega_p - E_{\mathbf{p}})^2}\left(\frac{\xi_{\mathbf{p}}}{2E_{\mathbf{p}}}\frac{3}{m} + \left(1 - \frac{3\xi_{\mathbf{p}}}{E_{\mathbf{p}}}\right)\frac{\Delta_{pg}^2}{2E_{\mathbf{p}}^3}\frac{p^2}{m^2}\right) + \left(\frac{1+\xi_{\mathbf{p}}/E_{\mathbf{p}}}{(\omega_p + E_{\mathbf{p}})^3} + \frac{1-\xi_{\mathbf{p}}/E_{\mathbf{p}}}{(\omega_p - E_{\mathbf{p}})^3}\right)\frac{\xi_{\mathbf{p}}^2}{E_{\mathbf{p}}^2}\frac{p^2}{m^2}\right\} \\
= {} & \frac{1}{12}\int \frac{d^3p}{(2\pi)^3}\left(1 + \frac{\xi_{\mathbf{p}}}{E_{\mathbf{p}}}\right)\left\{\left(-\frac{1}{2E_{\mathbf{p}}}\tanh\frac{\beta_c E_{\mathbf{p}}}{2} - f'(E_{\mathbf{p}})\right)\left(\frac{\Delta_{pg}^2}{2E_{\mathbf{p}}^3}\frac{3}{m} - \frac{3\Delta_{pg}^2\xi_{\mathbf{p}}}{2E_{\mathbf{p}}^5}\frac{p^2}{m^2}\right)\right. \\
& + \left(\frac{\tanh(\beta_c E_{\mathbf{p}}/2))}{(2E_{\mathbf{p}})^2} + \frac{f'(E_{\mathbf{p}})}{2E_{\mathbf{p}}}\right)\left(\frac{\xi_{\mathbf{p}}}{2E_{\mathbf{p}}}\frac{3}{m} + \left(1 + \frac{3\xi_{\mathbf{p}}}{E_{\mathbf{p}}}\right)\frac{\Delta_{pg}^2}{2E_{\mathbf{p}}^3}\frac{p^2}{m^2}\right) \\
& + \frac{1}{2}f''(E_{\mathbf{p}})\left(\frac{\xi_{\mathbf{p}}}{2E_{\mathbf{p}}}\frac{3}{m} + \left(1 - \frac{3\xi_{\mathbf{p}}}{E_{\mathbf{p}}}\right)\frac{\Delta_{pg}^2}{2E_{\mathbf{p}}^3}\frac{p^2}{m^2}\right) \\
& \left. - \left(\frac{\tanh(\beta_c E_{\mathbf{p}}/2)}{(2E_{\mathbf{p}})^3} + \frac{f'(E_{\mathbf{p}})}{(2E_{\mathbf{p}})^2} - \frac{f''(E_{\mathbf{p}})}{4E_{\mathbf{p}}}\right)\left(1 + \frac{\xi_{\mathbf{p}}}{E_{\mathbf{p}}}\right)\frac{\xi_{\mathbf{p}}^2}{E_{\mathbf{p}}^2}\frac{p^2}{m^2} + \frac{1}{6}f'''(E_{\mathbf{p}})\left(1 - \frac{\xi_{\mathbf{p}}}{E_{\mathbf{p}}}\right)\frac{\xi_{\mathbf{p}}^2}{E_{\mathbf{p}}^2}\frac{p^2}{m^2}\right\} \\
& + (\text{terms obtained by taking } E_{\mathbf{p}} \to -E_{\mathbf{p}})\,. \qquad \text{(G.23)}
\end{aligned}
$$

After arranging terms, we obtain (G.2).

Bibliography

[1] T. Ozawa and G. Baym, "Stability of ultracold atomic Bose condensates with Rashba spin-orbit coupling against quantum and thermal fluctuations," `arXiv:1203.6367`.

[2] T. Ozawa and G. Baym, "Ground-state phases of ultracold bosons with Rashba-Dresselhaus spin-orbit coupling," *Phys. Rev. A* **85**, 013612 (2012).

[3] T. Ozawa and G. Baym, "Renormalization of interactions of ultracold atoms in simulated Rashba gauge fields," *Phys. Rev. A* **84**, 043622 (2011).

[4] T. Ozawa and G. Baym, "Population imbalance and pairing in the BCS-BEC crossover of three-component ultracold fermions," *Phys. Rev. A* **82**, 063615 (2010).

[5] G. Baym and T. Ozawa, "Two-slit diffraction with highly charged particles: Niels Bohr's consistency argument that the electromagnetic field must be quantized," *Proceedings of the National Academy of Sciences (USA)* **106**, 3035–3040 (2009).

[6] L. D. Landau and E. M. Lifshitz, *Mechanics*. Butterworth-Heinemann, 1976.

[7] K. W. Madison, F. Chevy, W. Wohlleben, and J. Dalibard, "Vortex formation in a stirred Bose-Einstein condensate," *Phys. Rev. Lett.* **84**, 806–809 (2000).

[8] J. R. Abo-Shaeer, C. Raman, J. M. Vogels, and W. Ketterle, "Observation of vortex lattices in Bose-Einstein condensates," *Science* **292**, 476–479 (2001).

[9] N. Cooper, "Rapidly rotating atomic gases," *Advances in Physics* **57**, 539–616 (2008).

[10] A. L. Fetter, "Rotating trapped Bose-Einstein condensates," *Rev. Mod. Phys.* **81**, 647–691 (2009).

[11] J. Bardeen, L. N. Cooper, and J. R. Schrieffer, "Microscopic theory of superconductivity," *Phys. Rev.* **106**, 162–164 (1957).

[12] J. Bardeen, L. N. Cooper, and J. R. Schrieffer, "Theory of superconductivity," *Phys. Rev.* **108**, 1175–1204 (1957).

[13] A. J. Leggett, *Quantum Liquids: Bose Condensation and Cooper Pairing in Condensed-Matter Systems*. Oxford, 2006.

[14] A. J. Leggett, "Diatomic molecules and cooper pairs,", in *Modern Trends in the Theory of Condensed Matter*, A. Pekalski and R. Przystawa, eds. Springer-Verlag, Berlin, 1980.

[15] P. Nozières and S. Schmitt-Rink, "Bose condensation in an attractive fermion gas: From weak to strong coupling superconductivity," *Journal of Low Temperature Physics* **59**, 195–211 (1985).

[16] M. Greiner, C. A. Regal, and D. S. Jin, "Emergence of a molecular Bose—Einstein condensate from a Fermi gas," *Nature (London)* **426**, 537–540 (2003).

[17] M. Bartenstein, A. Altmeyer, S. Riedl, S. Jochim, C. Chin, J. H. Denschlag, and R. Grimm, "Crossover from a molecular Bose-Einstein condensate to a degenerate Fermi gas," *Phys. Rev. Lett.* **92**, 120401 (2004).

[18] M. W. Zwierlein, C. A. Stan, C. H. Schunck, S. M. F. Raupach, A. J. Kerman, and W. Ketterle, "Condensation of pairs of fermionic atoms near a Feshbach resonance," *Phys. Rev. Lett.* **92**, 120403 (2004).

[19] M. W. Zwierlein, J. R. Abo-Shaeer, A. Schirotzek, C. H. Schunck, and W. Ketterle, "Vortices and superfluidity in a strongly interacting Fermi gas," *Nature (London)* **435**, 1047–1051 (2005).

[20] W. E. Lamb and M. O. Scully, "The photoelectric effect without photons,", in *Polarization, Matière et Rayonnement (Jubilee Volume in honor of Alfred Kastler)*, pp. 363–369. Presses Universitaires de France, Paris, 1969.

[21] W. E. Lamb, "Anti-photon," *Applied Physics B: Lasers and Optics* **60**, 77–84 (1995).

[22] Y. Aharonov and D. Rohrlich, *Quantum Paradoxes: Quantum Theory for the Perplexed.* WILEY-VCH Verlag GmbH & Co., 2005.

[23] A. Tonomura, J. Endo, T. Matsuda, T. Kawasaki, , and H. Ezawa, "Demonstration of single - electron buildup of an interference pattern," *American Journal of Physics* **57**, 117–120 (1989).

[24] Y.-J. Lin, R. L. Compton, A. R. Perry, W. D. Phillips, J. V. Porto, and I. B. Spielman, "Bose-Einstein condensate in a uniform light-induced vector potential," *Phys. Rev. Lett.* **102**, 130401 (2009).

[25] Y.-J. Lin, R. L. Compton, K. Jiménez-García, J. V. Porto, and I. B. Spielman, "Synthetic magnetic fields for ultracold neutral atoms," *Nature (London)* **462**, 628–632 (2009).

[26] Y.-J. Lin, R. L. Compton, K. Jimnez-Garca, W. D. Phillips, J. V. Porto, and I. B. Spielman, "A synthetic electric force acting on neutral atoms," *Nature Physics* **7**, 531–534 (2011).

[27] Y.-J. Lin, K. Jiménez-García, and I. B. Spielman, "Spin-orbit-coupled Bose-Einstein condensates," *Nature (London)* **471**, 83–86 (2011).

[28] R. A. Williams, L. J. LeBlanc, K. Jiménez-García, M. C. Beeler, A. R. Perry, W. D. Phillips, and I. B. Spielman, "Synthetic partial waves in ultracold atomic collisions," *Science* **335**, 314–317 (2012).

[29] Z. Fu, P. Wang, S. Chai, L. Huang, and J. Zhang, "Bose-Einstein condensate in a light-induced vector gauge potential using 1064-nm optical-dipole-trap lasers," *Phys. Rev. A* **84**, 043609 (2011).

[30] M. Aidelsburger, M. Atala, S. Nascimbène, S. Trotzky, Y.-A. Chen, and I. Bloch, "Experimental realization of strong effective magnetic fields in an optical lattice," *Phys. Rev. Lett.* **107**, 255301 (2011).

[31] L. J. LeBlanc, K. Jiménez-García, R. A. Williams, M. C. Beeler, A. R. Perry, W. D. Phillips, and I. B. Spielman, "Observation of a superfluid Hall effect," `arXiv:1201.5857`.

[32] M. V. Berry, "Quantal phase factors accompanying adiabatic changes," *Proc. R. Soc. Lond. A* **392**, 45–57 (1984).

[33] J. Dalibard, F. Gerbier, G. Juzeliūnas, and P. Öhberg, "*Colloquium* : Artificial gauge potentials for neutral atoms," *Rev. Mod. Phys.* **83**, 1523–1543 (2011).

[34] I. B. Spielman, "Raman processes and effective gauge potentials," *Phys. Rev. A* **79**, 063613 (2009).

[35] É. I. Rashba, "Properties of semiconductors with an extremum loop I. cyclotron and combinational resonance in a magnetic field perpendicular to the plane of the loop," *Fizika Tverdogo Tela* **2**, 1224 – 1238 (1960). [Sov. Phys. Solid State **2**, 1109 (1960)].

[36] G. Dresselhaus, "Spin-orbit coupling effects in zinc blende structures," *Phys. Rev.* **100**, 580–586 (1955).

[37] R. Winkler, *Spin-Orbit Coupling Effects in Two-Dimensional Electron and Hole Systems.* Springer, 2003.

[38] J. Schliemann, J. C. Egues, and D. Loss, "Nonballistic spin-field-effect transistor," *Phys. Rev. Lett.* **90**, 146801 (2003).

[39] J. Ruseckas, G. Juzeliūnas, P. Öhberg, and M. Fleischhauer, "Non-Abelian gauge potentials for ultracold atoms with degenerate dark states," *Phys. Rev. Lett.* **95**, 010404 (2005).

[40] S.-L. Zhu, H. Fu, C.-J. Wu, S.-C. Zhang, and L.-M. Duan, "Spin Hall effects for cold atoms in a light-induced gauge potential," *Phys. Rev. Lett.* **97**, 240401 (2006).

[41] X.-J. Liu, M. F. Borunda, X. Liu, and J. Sinova, "Effect of induced spin-orbit coupling for atoms via laser fields," *Phys. Rev. Lett.* **102**, 046402 (2009).

[42] G. Juzeliūnas, J. Ruseckas, and J. Dalibard, "Generalized Rashba-Dresselhaus spin-orbit coupling for cold atoms," *Phys. Rev. A* **81**, 053403 (2010).

[43] D. L. Campbell, G. Juzeliūnas, and I. B. Spielman, "Realistic Rashba and Dresselhaus spin-orbit coupling for neutral atoms," *Phys. Rev. A* **84**, 025602 (2011).

[44] T.-L. Ho and S. Zhang, "Bose-Einstein condensates with spin-orbit interaction," *Phys. Rev. Lett.* **107**, 150403 (2011).

[45] A. Jacob, P. Öhberg, G. Juzeliūnas, and L. Santos, "Cold atom dynamics in non-Abelian gauge fields," *Applied Physics B: Lasers and Optics* **89**, 439–445 (2007).

[46] H. Zhai, "Spin-orbit coupled quantum gases," *Int. J. of Mod. Phys. B* **26**, 1230001 (2012).

[47] T. D. Stanescu, B. Anderson, and V. Galitski, "Spin-orbit coupled Bose-Einstein condensates," *Phys. Rev. A* **78**, 023616 (2008).

[48] W. Cong-Jun, I. Mondragon-Shem, and Z. Xiang-Fa, "Unconventional Bose-Einstein condensations from spin-orbit coupling," *Chinese Physics Letters* **28**, 097102 (2011).

[49] C. Wang, C. Gao, C.-M. Jian, and H. Zhai, "Spin-orbit coupled spinor Bose-Einstein condensates," *Phys. Rev. Lett.* **105**, 160403 (2010).

[50] C.-M. Jian and H. Zhai, "Paired superfluidity and fractionalized vortices in systems of spin-orbit coupled bosons," *Phys. Rev. B* **84**, 060508 (2011).

[51] S.-K. Yip, "Bose-Einstein condensation in the presence of artificial spin-orbit interaction," *Phys. Rev. A* **83**, 043616 (2011).

[52] Y. Zhang, L. Mao, and C. Zhang, "Mean-field dynamics of spin-orbit coupled Bose-Einstein condensates," *Phys. Rev. Lett.* **108**, 035302 (2012).

[53] S. Gopalakrishnan, A. Lamacraft, and P. M. Goldbart, "Universal phase structure of dilute Bose gases with Rashba spin-orbit coupling," *Phys. Rev. A* **84**, 061604 (2011).

[54] R. Barnett, S. Powell, T. Graß, M. Lewenstein, and S. Das Sarma, "Order by disorder in spin-orbit-coupled Bose-Einstein condensates," *Phys. Rev. A* **85**, 023615 (2012).

[55] E. J. Mueller, T.-L. Ho, M. Ueda, and G. Baym, "Fragmentation of Bose-Einstein condensates," *Phys. Rev. A* **74**, 033612 (2006).

[56] A. Fetter and J. D. Walecka, *Quantum Theory of Many-Particle Systems*. Dover, New York, 2003.

[57] T. D. Lee and C. N. Yang, "Many-body problem in quantum mechanics and quantum statistical mechanics," *Phys. Rev.* **105**, 1119–1120 (1957).

[58] T. D. Lee, K. Huang, and C. N. Yang, "Eigenvalues and eigenfunctions of a Bose system of hard spheres and its low-temperature properties," *Phys. Rev.* **106**, 1135–1145 (1957).

[59] M. Holzmann and G. Baym, "Condensate superfluidity and infrared structure of the single-particle Green's function: The Josephson relation," *Phys. Rev. B* **76**, 092502 (2007).

[60] M. Holzmann and G. Baym, "Condensate density and superfluid mass density of a dilute Bose-Einstein condensate near the condensation transition," *Phys. Rev. Lett.* **90**, 040402 (2003).

[61] J. P. Vyasanakere and V. B. Shenoy, "Bound states of two spin-$\frac{1}{2}$ fermions in a synthetic non-abelian gauge field," *Phys. Rev. B* **83**, 094515 (2011).

[62] J. P. Vyasanakere, S. Zhang, and V. B. Shenoy, "Bcs-bec crossover induced by a synthetic non-abelian gauge field," *Phys. Rev. B* **84**, 014512 (2011).

[63] M. Gong, S. Tewari, and C. Zhang, "Bcs-bec crossover and topological phase transition in 3d spin-orbit coupled degenerate fermi gases," *Phys. Rev. Lett.* **107**, 195303 (2011).

[64] Z.-Q. Yu and H. Zhai, "Spin-orbit coupled fermi gases across a feshbach resonance," *Phys. Rev. Lett.* **107**, 195305 (2011).

[65] H. Hu, L. Jiang, X.-J. Liu, and H. Pu, "Probing anisotropic superfluidity in atomic fermi gases with rashba spin-orbit coupling," *Phys. Rev. Lett.* **107**, 195304 (2011).

[66] L. Han and C. A. R. Sá de Melo, "Evolution from bcs to bec superfluidity in the presence of spin-orbit coupling," *Phys. Rev. A* **85**, 011606 (2012).

[67] P. Nozières, in *Bose-Einstein Condensation*, A. Griffin, D. W. Snoke, and S. Stringari, eds. Cambridge Univ. Press, Cambridge, 1995.

[68] G. Baym and C. J. Pethick, "Ground-state properties of magnetically trapped bose-condensed rubidium gas," *Phys. Rev. Lett.* **76**, 6–9 (1996).

[69] C. Honerkamp and W. Hofstetter, "Ultracold fermions and the SU(N) Hubbard model," *Phys. Rev. Lett.* **92**, 170403 (2004).

[70] C. Honerkamp and W. Hofstetter, "BCS pairing in Fermi systems with N different hyperfine states," *Phys. Rev. B* **70**, 094521 (2004).

[71] M. A. Cazalilla, A. F. Ho, and M. Ueda, "Ultracold gases of ytterbium: ferromagnetism and Mott states in an SU(6) Fermi system," *New Journal of Physics* **11**, 103033 (2009).

[72] A. V. Gorshkov, M. Hermele, V. Gurarie, C. Xu, P. S. Julienne, J. Ye, P. Zoller, E. Demler, M. D. Lukin, and A. M. Rey, "Two-orbital SU(N) magnetism with ultracold alkaline-earth atoms," *Nature Physics* **6**, 289 – 295 (2010).

[73] S. Taie, Y. Takasu, S. Sugawa, R. Yamazaki, T. Tsujimoto, R. Murakami, and Y. Takahashi, "Realization of a SU(2) × SU(6) system of fermions in a cold atomic gas," *Phys. Rev. Lett.* **105**, 190401 (2010).

[74] A. Rapp, G. Zaránd, C. Honerkamp, and W. Hofstetter, "Color superfluidity and "baryon" formation in ultracold fermions," *Phys. Rev. Lett.* **98**, 160405 (2007).

[75] A. Rapp, W. Hofstetter, and G. Zaránd, "Trionic phase of ultracold fermions in an optical lattice: A variational study," *Phys. Rev. B* **77**, 144520 (2008).

[76] F. Wilczek, "Two-orbital $SU(N)$ magnetism with ultracold alkaline-earth atoms," *Nature Physics* **3**, 375 – 376 (2007).

[77] K. Maeda, G. Baym, and T. Hatsuda, "Simulating dense QCD matter with ultracold atomic boson-fermion mixtures," *Phys. Rev. Lett.* **103**, 085301 (2009).

[78] A. Modawi and A. Leggett, "Some properties of a spin-1 fermi superfluid: Application to spin-polarized ^{6}Li," *Journal of Low Temperature Physics* **109**, 625–639 (1997).

[79] P. F. Bedaque and J. P. D ' Incao, "Superfluid phases of the three-species fermion gas," *Annals of Physics* **324**, 1763 – 1768 (2009).

[80] T. Paananen, J.-P. Martikainen, and P. Törmä, "Pairing in a three-component Fermi gas," *Phys. Rev. A* **73**, 053606 (2006).

[81] T. Paananen, P. Törmä, and J.-P. Martikainen, "Coexistence and shell structures of several superfluids in trapped three-component Fermi mixtures," *Phys. Rev. A* **75**, 023622 (2007).

[82] H. Zhai, "Superfluidity in three-species mixtures of Fermi gases across Feshbach resonances," *Phys. Rev. A* **75**, 031603 (2007).

[83] G. Catelani and E. A. Yuzbashyan, "Phase diagram, extended domain walls, and soft collective modes in a three-component fermionic superfluid," *Phys. Rev. A* **78**, 033615 (2008).

[84] L. He, M. Jin, and P. Zhuang, "Superfluidity in a three-flavor Fermi gas with SU(3) symmetry," *Phys. Rev. A* **74**, 033604 (2006).

[85] R. W. Cherng, G. Refael, and E. Demler, "Superfluidity and magnetism in multicomponent ultracold fermions," *Phys. Rev. Lett.* **99**, 130406 (2007).

[86] T. B. Ottenstein, T. Lompe, M. Kohnen, A. N. Wenz, and S. Jochim, "Collisional stability of a three-component degenerate Fermi gas," *Phys. Rev. Lett.* **101**, 203202 (2008).

[87] J. H. Huckans, J. R. Williams, E. L. Hazlett, R. W. Stites, and K. M. O'Hara, "Three-body recombination in a three-state Fermi gas with widely tunable interactions," *Phys. Rev. Lett.* **102**, 165302 (2009).

[88] V. Efimov, "Energy levels arising from resonant two-body forces in a three-body system," *Physics Letters B* **33**, 563 – 564 (1970).

[89] V. Efimov, "Energy levels of three resonantly interacting particles," *Nuclear Physics A* **210**, 157 – 188 (1973).

[90] E. Braaten and H.-W. Hammer, "Universality in few-body systems with large scattering length," *Physics Reports* **428**, 259 – 390 (2006).

[91] E. Braaten and H.-W. Hammer, "Efimov physics in cold atoms," *Annals of Physics* **322**, 120 – 163 (2007).

[92] S. Floerchinger, R. Schmidt, S. Moroz, and C. Wetterich, "Functional renormalization for trion formation in ultracold fermion gases," *Phys. Rev. A* **79**, 013603 (2009).

[93] S. Moroz, S. Floerchinger, R. Schmidt, and C. Wetterich, "Efimov effect from functional renormalization," *Phys. Rev. A* **79**, 042705 (2009).

[94] S. Floerchinger, R. Schmidt, and C. Wetterich, "Three-body loss in lithium from functional renormalization," *Phys. Rev. A* **79**, 053633 (2009).

[95] T. Luu and A. Schwenk, "Three-fermion problems in optical lattices," *Phys. Rev. Lett.* **98**, 103202 (2007).

[96] P. Naidon and M. Ueda, "Possible Efimov trimer state in a three-hyperfine-component lithium-6 mixture," *Phys. Rev. Lett.* **103**, 073203 (2009).

[97] E. Braaten, H.-W. Hammer, D. Kang, and L. Platter, "Three-body recombination of ^{6}Li atoms with large negative scattering lengths," *Phys. Rev. Lett.* **103**, 073202 (2009).

[98] T. Kraemer, M. Mark, P. Waldburger, J. G. Danzl, C. Chin, B. Engeser, A. D. Lange, K. Pilch, A. Jaakkola, H.-C. Nägerl, and R. Grimm, "Evidence for Efimov quantum states in an ultracold gas of caesium atoms," *Nature (London)* **440**, 315 – 318 (2006).

[99] V. M. Galitskii, "The energy spectrum of a non-ideal Fermi gas," *Zh. Eksp. Teor. Fiz.* **34**, 151 – 162 (1958). [Sov. Phys.—JETP 7, 104 (1958)].

[100] J.-P. Martikainen, J. J. Kinnunen, P. Törmä, and C. J. Pethick, "Induced interactions and the superfluid transition temperature in a three-component Fermi gas," *Phys. Rev. Lett.* **103**, 260403 (2009).

[101] M. Y. Kagan and A. V. Chubukov, "Possibility of a superf luid transition in a slightly nonideal fermi gas with repulsion," *Pis'ma Zh. Eksp. Teor. Fiz.* **47**, 525–528 (1988). [JETP Lett. **47**, 614 (1988)].

[102] T. Hatsuda, M. Tachibana, N. Yamamoto, and G. Baym, "New critical point induced by the axial anomaly in dense QCD," *Phys. Rev. Lett.* **97**, 122001 (2006).

[103] N. Yamamoto, M. Tachibana, T. Hatsuda, and G. Baym, "Phase structure, collective modes, and the axial anomaly in dense QCD," *Phys. Rev. D* **76**, 074001 (2007).

[104] G. Baym, T. Hatsuda, M. Tachibana, and N. Yamamoto, "The axial anomaly and the phases of dense QCD," *Journal of Physics G: Nuclear and Particle Physics* **35**, 104021 (2008).

[105] Y. Nambu and G. Jona-Lasinio, "Dynamical model of elementary particles based on an analogy with superconductivity. I," *Phys. Rev.* **122**, 345–358 (1961).

[106] Y. Nambu and G. Jona-Lasinio, "Dynamical model of elementary particles based on an analogy with superconductivity. II," *Phys. Rev.* **124**, 246–254 (1961).

[107] T. Hatsuda and T. Kunihiro, "QCD phenomenology based on a chiral effective Lagrangian," *Physics Reports* **247**, 221 – 367 (1994).

[108] H. Abuki, G. Baym, T. Hatsuda, and N. Yamamoto, "Nambu–Jona-Lasinio model of dense three-flavor matter with axial anomaly: The low temperature critical point and BEC-BCS diquark crossover," *Phys. Rev. D* **81**, 125010 (2010).

[109] D. S. Petrov, C. Salomon, and G. V. Shlyapnikov, "Weakly bound dimers of fermionic atoms," *Phys. Rev. Lett.* **93**, 090404 (2004).

[110] R. Haussmann, "Crossover from BCS superconductivity to Bose-Einstein condensation: A self-consistent theory," *Zeitschrift fr Physik B Condensed Matter* **91**, 291–308 (1993).

[111] C. A. R. Sá de Melo, M. Randeria, and J. R. Engelbrecht, "Crossover from BCS to Bose superconductivity: Transition temperature and time-dependent Ginzburg-Landau theory," *Phys. Rev. Lett.* **71**, 3202–3205 (1993).

[112] P. Pieri, L. Pisani, and G. C. Strinati, "BCS-BEC crossover at finite temperature in the broken-symmetry phase," *Phys. Rev. B* **70**, 094508 (2004).

[113] H. Hu, P. D. Drummond, and X.-J. Liu, "Universal thermodynamics of strongly interacting Fermi gases," *Nature Physics* **3**, 469–472 (2007).

[114] K. Levin, Q. Chen, C.-C. Chien, and Y. He, "Comparison of different pairing fluctuation approaches to BCS—BEC crossover," *Annals of Physics* **325**, 233 – 264 (2010).

[115] R. Haussmann, *Self-consistent Quantum-Field Theory and Bosonization for Strongly Correlated Electron Systems*. Springer, Berlin, 1999.

[116] N. Bohr and L. Rosenfeld *Mat.-fys. Medd. Dansk Vid. Selsk.* **12**, (1933). [Translated from German (1996) Niels Bohr Collected Works, Zur Frage der Messbarkeit der elektromagnetischen Feldgrössern, ed Kalckar J (Amsterdam, North—Holland), 7, p 123.].

[117] N. Bohr and L. Rosenfeld, "Field and charge measurements in quantum electrodynamics," *Phys. Rev.* **78**, 794–798 (1950).

[118] Y. Aharonov and D. Bohm, "Significance of electromagnetic potentials in the quantum theory," *Phys. Rev.* **115**, 485–491 (1959).

[119] P. Grangier, G. Roger, and A. Aspect, "Experimental evidence for a photon anticorrelation effect on a beam splitter: A new light on single-photon interferences," *Europhysics Letters* **1**, 173 (1986).

[120] T. Pfau, S. Spälter, C. Kurtsiefer, C. R. Ekstrom, and J. Mlynek, "Loss of spatial coherence by a single spontaneous emission," *Phys. Rev. Lett.* **73**, 1223–1226 (1994).

[121] M. S. Chapman, T. D. Hammond, A. Lenef, J. Schmiedmayer, R. A. Rubenstein, E. Smith, and D. E. Pritchard, "Photon scattering from atoms in an atom interferometer: Coherence lost and regained," *Phys. Rev. Lett.* **75**, 3783–3787 (1995).

[122] M. O. Scully, B.-G. Englert, and H. Walther, "Quantum optical tests of complementarity," *Nature (London)* **351**, 111–116 (1991).

[123] W. H. Furry and N. F. Ramsey, "Significance of potentials in quantum theory," *Phys. Rev.* **118**, 623–626 (1960).

[124] S. Olariu and I. I. Popescu, "The quantum effects of electromagnetic fluxes," *Rev. Mod. Phys.* **57**, 339–436 (1985).

[125] A. Stern, Y. Aharonov, and Y. Imry, "Phase uncertainty and loss of interference: A general picture," *Phys. Rev. A* **41**, 3436–3448 (1990).

[126] R. Schuster, E. Buks, M. Heiblum, D. Mahalu, V. Umansky, and H. Shtrikman, "Phase measurement in a quantum dot via a double-slit interference experiment," *Nature (London)* **385**, 417–420 (1997).

[127] E. Buks, R. Schuster, M. Heiblum, D. Mahalu, and V. Umansky, "Dephasing in electron interference by a 'which-path' detector," *Nature (London)* **391**, 871–874 (1998).

[128] D.-I. Chang, G. L. Khym, K. Kang, Y. Chung, H.-J. Lee, M. Seo, M. Heiblum, D. Mahalu, and V. Umansky, "Quantum mechanical complementarity probed in a closed-loop Aharonov-Bohm interferometer," *Nature Physics* **4**, 205–209 (2008).

[129] X. Calmet, M. Graesser, and S. D. H. Hsu, "Minimum length from quantum mechanics and classical general relativity," *Phys. Rev. Lett.* **93**, 211101 (2004).

[130] L. Landau and R. Peierls, "Erweiterung des unbestimmtheitsprinzips fr die relativistische quantentheorie," *Zeitschrift fr Physik A Hadrons and Nuclei* **69**, 56–69 (1931).

[131] G. Compagno and F. Persico, "Limits of the measurability of the local quantum electromagnetic-field amplitude," *Phys. Rev. A* **57**, 1595–1603 (1998).

[132] V. Hnizdo, "Comment on "limits of the measurability of the local quantum electromagnetic-field amplitude"," *Phys. Rev. A* **60**, 4191–4195 (1999).

[133] L. G. P. Saavedra, "Quantum control, entanglement and noise in the seminal Bohr and Rosenfeld paper on electromagnetic field measurements," *AIP Conf. Proc.* **734**, 75–78 (2004).

[134] W. K. Wootters and W. H. Zurek, "Complementarity in the double-slit experiment: Quantum nonseparability and a quantitative statement of Bohr's principle," *Phys. Rev. D* **19**, 473–484 (1979).

[135] G. Jaeger, A. Shimony, and L. Vaidman, "Two interferometric complementarities," *Phys. Rev. A* **51**, 54–67 (1995).

[136] B.-G. Englert, "Fringe visibility and which-way information: An inequality," *Phys. Rev. Lett.* **77**, 2154–2157 (1996).

[137] V. Jacques, E. Wu, F. Grosshans, F. Treussart, P. Grangier, A. Aspect, and J.-F. Roch, "Delayed-choice test of quantum complementarity with interfering single photons," *Phys. Rev. Lett.* **100**, 220402 (2008).

[138] K. G. Wilson, "Confinement of quarks," *Phys. Rev. D* **10**, 2445–2459 (1974).

[139] L. H. Ford, "Electromagnetic vacuum fluctuations and electron coherence," *Phys. Rev. D* **47**, 5571–5580 (1993).

[140] H.-P. Breuer and F. Petruccione, "Destruction of quantum coherence through emission of bremsstrahlung," *Phys. Rev. A* **63**, 032102 (2001).

[141] J. Hough, S. Rowan, and B. S. Sathyaprakash, "The search for gravitational waves," *Journal of Physics B: Atomic, Molecular and Optical Physics* **38**, S497 (2005).

[142] A. Peres and N. Rosen, "Quantum limitations on the measurement of gravitational fields," *Phys. Rev.* **118**, 335–336 (1960).

[143] H. P. Yuen, "Contractive states and the standard quantum limit for monitoring free-mass positions," *Phys. Rev. Lett.* **51**, 719–722 (1983).

[144] M. Ozawa, "Measurement breaking the standard quantum limit for free-mass position," *Phys. Rev. Lett.* **60**, 385–388 (1988).

[145] C. M. Caves, K. S. Thorne, R. W. P. Drever, V. D. Sandberg, and M. Zimmermann, "On the measurement of a weak classical force coupled to a quantum-mechanical oscillator. i. issues of principle," *Rev. Mod. Phys.* **52**, 341–392 (1980).

[146] V. B. Braginsky, M. L. Gorodetsky, F. Y. Khalili, A. B. Matsko, K. S. Thorne, and S. P. Vyatchanin, "Noise in gravitational-wave detectors and other classical-force measurements is not influenced by test-mass quantization," *Phys. Rev. D* **67**, 082001 (2003).

[147] S. Baharian, "Low-energy scattering theory in two dimensions." Private note.

[148] J. J. Sakurai, *Modern Quantum Mechanics*. Addison-Wesley, 1994.

[149] S. T. Beliaev, "Energy spectrum of a non-ideal Bose gas," *Zh. Eksp. Teor. Fiz.* **34**, 433 – 446 (1958). [Sov. Phys.—JETP 7, 299 (1958)].

[150] C.-c. Chang and R. Friedberg, "t matrix in hard-core two-body scattering in three and two dimensions," *Phys. Rev. A* **49**, 913–920 (1994).

[151] A. A. Abrikosov, L. P. Gorkov, and I. E. Dzyaloshinski, *Methods of Quantum Field Theory in Statistical Physics*. Dover, New York, 1975.

[152] L. D. Landau and E. M. Lifshitz, *Quantum Mechanics*. Butterworth-Heinemann, 1977.

[153] G. Baym, *Lectures on Quantum Mechanics*. Westview Press, 1974.